europhysics
conference
abstracts

20th EPS Conference on Controlled Fusion and Plasma Physics

Lisboa, 26–30 July 1993

Editors: J. A. Costa Cabral, M. E. Manso, F. M. Serra,
F. C. Schüller

Contributed Papers, Part IV

Published by: European Physical Society

Series Editor: Prof. K. Bethge, Frankfurt/M

Managing Editor: G. Thomas, Genève

Volume 17C
Part IV

europhysics
conference
abstracts

20th EPS Conference on Controlled Fusion and Plasma Physics

LISBOA, 26-30 JULY 1993

Editors: J.A.Costa Cabral, M.E. Manso, F.M. Serra,
F.C. Schüller

CONTRIBUTED PAPERS, PART IV

Published by :	The European Physical Society	VOLUME
Series Editor:	Prof. K. Bethge, Frankfurt/M	17C
Managing Editor:	G. Thomas, Genève.	Part IV

TOPICS 7-8

20th EPS Conference on Controlled Fusion and Plasma Physics

LISBOA, 26-30 JULY 1993

Editors: J.A.C. Cabral, M.E. Manso, F.M. Serra, F.C. Schüller

CONTRIBUTED PAPERS, PART IV

EUROPHYSICS CONFERENCE ABSTRACTS is published by the European Physical Society, c 1993

The Proceedings may be purchased from "Centro de Fusão Nuclear" of "Instituto Superior Técnico", Av. Rovisco Pais, 1096 Lisboa Codex, Portugal.

PREFACE

The 20th EPS Conference on Controlled Fusion and Plasma Physics is Organized, on behalf of the European Physical Society (EPS), by "Sociedade Portuguesa de Física" (SPF) and "Centro de Fusão Nuclear" (CFN) of "Instituto Superior Técnico" (IST) of the Lisbon Technical University.

The Programme, Format and Schedule of the Conference were determined by its International Programme Committee, which also selected the Plenary and Topical Invited Lectures.

The International Programme Committee has also made the selection of the submitted one-page abstracts. Some of these abstracts, of outstanding quality, have been selected, for both poster and oral presentation of the corresponding four-page papers.

In the odd years the Conference is essentially related with Controlled Fusion Research and it has a reduced format. Therefore, the IPC has only been able to accept for conference presentation about 435 abstracts from the almost 620 received.

The Conference Format is: 9 Review Lectures of 45 minutes, 18 Topical Lectures of 30 minutes, 24 Oral Presentations of Contributred Papers of 20 minutes, 4 poster sessions with about 110 posters each and a Special Evening Public Lecture.

Lisboa, June 1993 The Editors

Acknowledgements:

The Conference Organizers acknowledge the financial support of the following Agencies and Institutions:

- Junta Nacional de Investigação Científica e Tecnologica
- Commission of the European Communities
- Fundação Calouste Gulbenkian
- Instituto Superior Técnico
- Câmara Municipal de Lisboa
- Banco Comercial de Lisboa

PROGRAMME COMMITTEE:

F. C. Schüller (Chairman) ..... Netherlands
K. Lackner (Chairman Innsbruck Conference)..... Germany
F. W. Sluijter (Chairman Plasma Phys. Division EPS)..... Netherlands
J. A. Costa Cabral (Chairman Local Org. Committee)..... Portugal
R. Bartiromo..... Italy
C. De Michelis..... France
J.R.Drake..... Sweden
F. Engelmann..... Germany
O. S. Pavlichenko..... Russia
J. Stöckel..... Tchekoslovakia
P. R. Thomas..... United Kingdom
J. Winter..... Germany
H..Wobig..... Germany

LOCAL ORGANIZING COMMITTEE:

C. M. Ferreira..... .....(General Secretary SPF, IST)
C. F. Varandas..... (President CFN, IST)

J. A. Costa Cabral.....(Chairman LOC, IST)
M. E. Manso.....(Secretary, IST)
F. Serra..... (Vice-Secretary, IST)
A.Moreira.....(IST)
A.Praxedes.....(IST)
H. Fernandes.....(IST)
A.Silva.....(IST)
A.Soares.....(IST)

CONTENTS

LIST OF TITLES
PART I
Topic 1: Tokamaks

Poster no — Volume/Page
Title
Authors

Poster no / Title / Authors — Volume/Page

Poster no Volume/Page
Title
Authors

Poster no Volume/Page
Title
Authors

Poster no Volume/Page
Title
Authors

Poster no / Title / Authors — Volume/Page

Poster no
Title
Authors

Volume/Page

Topic 2: Stellarators

Poster no
Title
Authors

Volume/Page

Topic 3: Alternative Confinement Schemes

Poster no — Volume/Page
Title
Authors

Topic 4: Plasma Edge Physics

Poster no — Volume/Page
Title
Authors

Poster no — Volume/Page
Title
Authors

Poster no
Title
Authors

Volume/Page

Poster no
Title
Authors

Volume/Page

Poster no — Volume/Page
Title
Authors

Topic 5: Heating and Current Drive

Poster no — Volume/Page
Title
Authors

Poster no
Title
Authors

Volume/Page

Poster no
Title
Authors

Volume/Page

Poster no
Title
Authors

Volume/Page

Poster no
Title
Authors

Volume/Page

Topic 6: Diagnostics

Poster no
Title
Authors

Volume/Page

Poster no
Title
Authors

Volume/Page

Topic 7: Inertial Confinement Fusion

Poster no
Title
Authors
Volume/Page

Topic 8: General Plasma Theory

Poster no
Title
Authors

Volume/Page

Poster no
Title
Authors

Volume/Page

Poster no
Title
Authors

Volume/Page

Poster no — Volume/Page
Title
Authors

Contributed Papers received during Printing

Poster no | Volume/Page
Title
Authors

6-44 IV-1517
Study of plasmas turbulence in the T-10 and tuman-3 tokamaks by reflectometer with cross-detection
Bulanin V.V., Korneev D.O., Dreval V.V.

6-45 IV-1521
X-ray vision technique for proton and alpha-particle diagnostics
Kiptilyj V.G.

Topic 7

Inertial Confinement Fusion

VLASOV-MAXWELL SIMULATIONS OF SIMULTANEOUS STIMULATED RAMAN FORWARD AND BACKWARD SCATTERING

P. Bertrand[1], A. Ghizzo[1], S.J. Karttunen[2], T.J.H. Pättikangas[2], R.R.E. Salomaa[3] and M. Shoucri[4]

[1]Université de Nancy–I, L.P.M.I.-C.N.R.S. URA 835, France
[2]Nuclear Engineering Laboratory, Technical Research Centre of Finland, Finland
[3]Department of Technical Physics, Helsinki University of Technology, Finland
[4]Centre Canadien de Fusion Magnétique, Tokamak de Varennes, IREQ, Canada

1. Introduction

In stimulated Raman scattering (SRS), an electromagnetic pump wave decays into a scattered wave and a plasma wave. In long nearly uniform plasmas, the electrostatic fields may reach large amplitudes and thus trap and accelerate electrons to high energies. In laser fusion, even a small number of energetic electrons can cause severe preheating and thus prevent the efficient compression of the fuel capsule. In magnetic fusion, the beat wave process [1] or SRS [2] in the microwave region can be applied to current drive in tokamaks. In current drive, collisionless fast electrons are beneficial.

Both in Raman forward (SRS-F) and backward scattering (SRS-F), the electron plasma waves travel forwards but their phase velocities can differ considerably. In most laser-plasma experiments, SRS-B dominates over SRS-F because of its larger gain. In well-underdense high-temperature plasmas, however, the Landau damping strongly limits SRS-B, which allows the growth of SRS-F [3,4]. In some cases, solely SRS-F is excited [5]. The parameters corresponding to reactor-grade laser-plasma experiments and to SRS current drive in fusion reactors lie in an intermediate region where both processes can occur simultaneously [4].

The coupled mode theory predicts that in a homogeneous plasma slab, SRS-B and SRS-F, and correspondingly the respective plasma waves, are localized in spatially distinct regions: SRS-B in the front and SRS-F in the rear part of the plasma slab [4]. The phase velocity of the SRS-B plasma wave is lower and closer to the electron thermal velocity than the phase velocity of the SRS-F plasma wave. The intense SRS-B plasmon can interact with a fairly large number of bulk electrons which get trapped into the plasma wave. If the amplitude of the SRS-F plasma wave is so large that the trapping regions of the two plasma waves overlap in velocity space, a large number of ultrafast electrons may be created. The role of SRS-B is to extract bulk electrons which are further accelerated by SRS-F. Note that the two wavepackets can be spatially separate — the overlapping of the trapping regions has to occur only in the velocity space.

2. Vlasov–Maxwell Simulations of Simultaneous SRS-B and SRS-F

We apply a nonperiodic Eulerian Vlasov code which solves the relativistic Vlasov and Maxwell equations for plane waves propagating in a bounded 1D electron plasma in a fixed ion background. The noiseless Eulerian code makes possible very precise diagnostics of the electric fields and envelopes [5].

We consider a homogeneous plasma slab of length L surrounded by a void. An electromagnetic pump wave is launched at $x = 0$ into the system with a frequency $\omega_0 = 2.36\omega_p$ (i.e. $n/n_{cr} = 0.18$) and with an amplitude $v_0/c = 0.1$, where v_0 is the quiver velocity. The length of the system is $L = 188c/\omega_p$. The initial electron distribution function is Maxwellian at $T_e = 10$ keV. These parameters are in the optimum operating region for simultaneous SRS-B and SRS-F [4]. The steep density gradient at the entrance of the plasma provides an initial perturbation for the forward Raman instability. On the other hand, a small initial sinusoidal perturbation ($\delta n/n = 0.019$) is introduced into the plasma to set on the SRS-B instability.

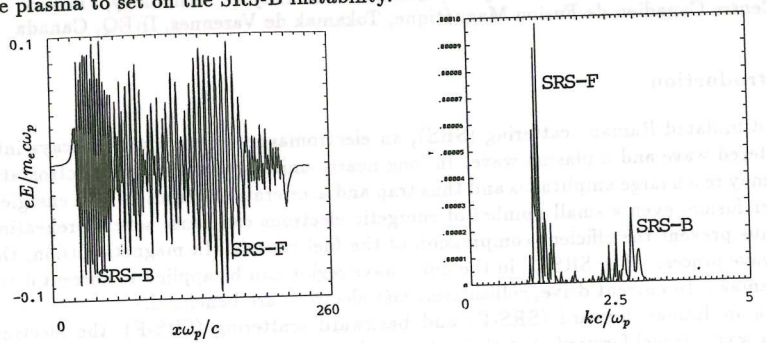

Fig. 1 *Electrostatic field* $eE/m_e c\omega_p$ *and* k*–spectrum at* $\omega_p t = 300$.

The frequencies and the wavenumbers are calculated from the phase matching conditions and the dispersion relations. The wavenumbers of the plasma waves are $k_F\lambda_D = 0.18$ and $k_B\lambda_D = 0.38$. The linear Landau damping of the plasma wave excited by SRS-B is strong, $\Gamma_B/\omega_p = 0.049$, in contrast to the wave excited by SRS-F, which is almost undamped. The phase velocities (momenta) of the plasma waves are $v_{phB} = 0.45c$ ($p_{phB} = 0.50m_e c$) and $v_{phF} = 0.82c$ ($p_{phF} = 1.42m_e c$).

Figure 1 displays the electrostatic field generated by SRS and the corresponding wavenumber spectrum at $\omega_p t = 300$. In the total electrostatic field, the two main components corresponding to SRS-B and SRS-F are very clearly seen, because they are spatially separated and their wavelengths differ considerably. At $\omega_p t = 300$, the saturation effects, wave-wave and wave-particle interactions play a role, and the electrostatic spectrum has broadened considerably.

The phase-space plot of Fig. 2 illustrates the electron response to the electrostatic field. The solid line corresponds to the separatrix momentum of an marginally trapped electron. At the rear end of the plasma, the electrostatic field becomes weaker and, therefore, the decoupled energetic electrons are streaming freely. Figure 2 shows also two distribution functions corresponding to spatial averages over the regions $26.5 \leq x\omega_p/c \leq 50$ and $120.5 \leq x\omega_p/c \leq 144$, respectively. In the front part, the dominant wave-particle interaction is due to the SRS-B plasma wave. A plateau is formed in the distribution function around $\gamma_{phB} - 1 = 0.11$, where γ_{phB} is the Lorentz factor at v_{phB}. In the centre of the plasma, the plateau appears around $\gamma_{phF} - 1 = 0.75$, which can be seen from the second distribution function. As the separatrices in the phase-space plot

show, the trapping region extends from $\gamma - 1 = 0.2$ to about 2.0, which agrees well with the observed plateau.

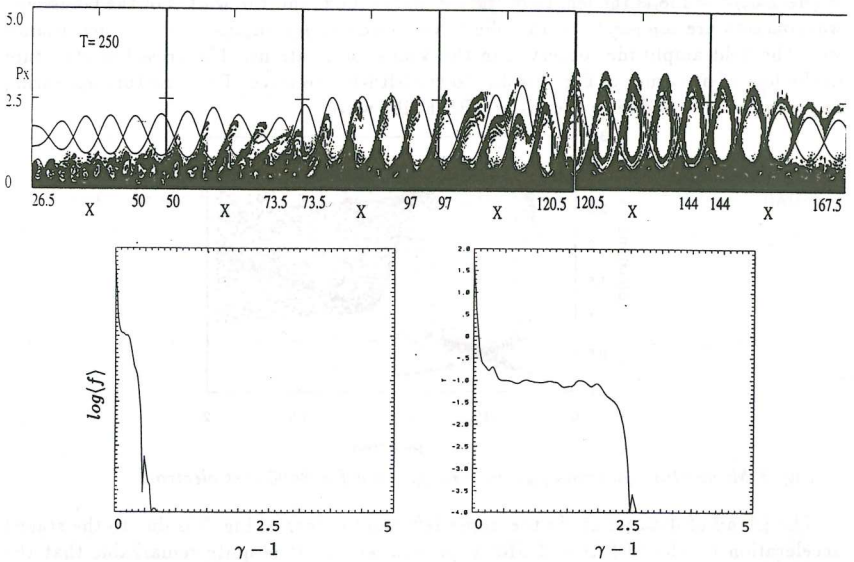

Fig. 2 *Phase space plot (x-p) of the electron distribution function at* $\omega_p t = 250$ *and space averaged electron distributions.*

The important feature in the distribution functions in Fig. 2 is that the level of the plateau is only one order of magnitude smaller in the SRS-B dominated region than in the SRS-F region. This demonstrates that the amount of fast electrons generated by SRS can be drastically increased, when both the backward and forward electrostatic components are simultaneously present even though they are not spatially overlapping. We have also run simulations where SRS-B is suppressed due to a higher temperature or smaller initial amplitude. Then the fast electron tail is at several orders of magnitude lower level than the tail in Fig. 2.

3. Test Particle Simulations

To understand the behaviour of an individual electron, we have studied the staged acceleration of electrons by test particle simulations in spatially separated fields which resemble the plasma waves generated by SRS-B and SRS-F. We have solved numerically the equations of motion of an electron in the two-component electrostatic field $E = \sum_{i=F,B} E_i(x) \cos(k_i x - \omega_i t + \varphi_i)$, where Gaussian envelopes $E_i(x) = E_i \exp[-(x-x_0)^2/w^2]$ are assumed. The test particles have the initial momentum p_{in} at $x = 0$, and the final momentum p_{out} at $x = L$ is calculated.

Figure 3 shows the final momentum $p_{out}/m_e c$ for an ensemble of test electrons having

an even distribution of initial momenta $p_{in}/m_e c$. For each calculated electron trajectory, the field phases have been chosen randomly. The fields are centred at $L/4$ and $3L/4$, where $L\omega_p/c = 188$ is the length of the simulation box, and the widths of the Gaussians wavepackets are $w_{B,F}\omega_p/c = 15$. We have chosen $eE_{B,F}/m_e\omega_p c = 0.1$ in accordance with the field amplitudes observed in the Vlasov simulations. The cross-like structure in the lower left corner of Fig. 3 is due to the SRS-B like wave. The structure appearing at $p_{in}/m_e c > 0.7$ is due to the faster SRS-F like wave.

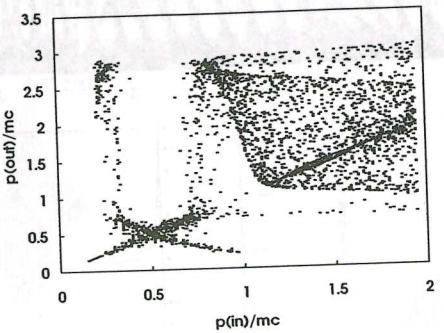

Fig. 3 *Momentum patterns $p_{out}/m_e c$ vs $p_{in}/m_e c$ for 3600 test electrons.*

The island of data points in the upper left-hand corner of Fig. 3 is due to the staged acceleration by the SRS-B and SRS-F plasma waves. It is quite remarkable that the electrons with $p_{in}/m_e c \approx 0.3$ are directly accelerated to $p_{out}/m_e c \approx 2 \ldots 3$. SRS-B alone would produce only particles up to about $p_{out}/m_e c < 1$. On the other hand, even at fusion temperatures there is only a negligible amount of particles present in the thermal distribution at $p_{in}/m_e c > 0.7$, which momentum is required for an efficient single-step acceleration by SRS-F. Thus the synergy between SRS-B and SRS-F leads to an unanticipated amount of very fast electrons.

4. Conclusions

In conclusion, our Vlasov and test particle simulations show that simultaneous SRS-B and SRS-F are able to produce superhot electrons in the MeV-range. The SRS-B plasma wave preaccelerates a large number of electrons from the bulk of the distribution. These are then further accelerated by the faster SRS-F plasma wave. An essential feature in this two-stage process is that SRS-B and SRS-F are spatially localized and separated. SRS-B occurs near the front region and SRS-F deeper inside the plasma slab. In reactor-grade laser-fusion experiments, the simultaneous occurrence of SRS-B and SRS-F and the consequent fast electrons make the prevention of SRS particularly important.

[1] B.I. Cohen et al., Nucl. Fusion **28** (1988) 1519.
[2] S.J. Karttunen et al., Nucl. Fusion **31** (1991) 1079.
[3] K. Estabrook and W.L. Kruer, Phys. Fluids **26** (1983) 1892.
[4] S.J. Karttunen and R.R.E. Salomaa, Laser Part. Beams **10** (1992) 75.
[5] P. Bertrand et al., Phys. Fluids B **2** (1990) 1028.

On modulated instability in collisional plasmas

S.V. Vladimirov*

Theor. Physik I, Ruhr-Universität-Bochum, D-44721 Bochum, Germany

We consider a strongly collisional plasma, where the effective collision frequency ν_{eff} is not only much larger than the characteristic frequency $\Delta\omega$ of the modulational perturbations, but also is larger in the presence of significantly stronger inequality:

$$|\Delta\omega| \ll \nu_{\text{eff}}^{(\text{eq})} = \frac{m_e}{m_i}\nu_{\text{eff}}. \tag{1}$$

Here, $m_{e(i)}$ is the electron (ion) mass. The characteristic frequency $\nu_{\text{eff}}^{(\text{eq})}$ defines the time of equalization of the electron and ion temperatures; thus the inequality (1) means that for the time of modulational instability development (or for the period of modulations) the electron and ion temperatures have time to equalize each other. This problem arises, for instance, when investigating plasma heating by strong laser radiation, which is relevant for inertial confinement fusion schemes [1].

We start our investigation with the hydrodynamic equations that can be obtained from the kinetic equation with Landau collision integral [2]. We consider that, in general, among all the characteristic frequencies of the problem, only the frequencies of the modulated perturbations are in the hydrodynamical regime $|\Delta\omega| \ll \nu_{\text{eff}}$. The other frequencies correspond to the regime of rare collisions. In calculating the latter quantities, we use a collisionless approximation. Thus we have the following equations for the electron (ion) $\mathbf{v}^{(e,i)}$ velocities:

$$m_{e,i}n_{e,i}(\partial t + \mathbf{v}^{(e,i)}\cdot\nabla)v_j^{(e,i)} = -\nabla_j n_{e,i}T_{e,i} - \nabla_l \pi_{lj}^{(e,i)} \mp e n_{e,i}(E_j + [\mathbf{v}^{(e,i)}\times\mathbf{B}]_j/c) \pm R_j, \tag{2}$$

where we assume that the ions have the charge e. The equations (2) are completed by the continuity equations for the electrons and ions as well as the equations of thermal balance

$$3n_{e,i}(\partial_t + \mathbf{v}^{(e,i)}\cdot\nabla)T_{e,i}/2 + n_{e,i}T_{e,i}\nabla\cdot\mathbf{v}^{(e,i)} = -\nabla\cdot\mathbf{q}^{(e,i)} - \pi_{lj}^{(e,i)}\nabla v_l^{(e,i)} + Q_{e,i}. \tag{3}$$

In Eqs.(3) the terms containing ∇nT describe the contribution from the pressure of electron and ion gases; $\pi_{lj}^{(e,i)}$ are the tensors of electron and ion viscosity:

$$\pi_{lj}^{(e)} = -0.73\frac{n_e T_e}{\nu_e}w_{lj}^{(e)}, \quad \pi_{lj}^{(i)} = -0.96\frac{n_i T_i}{\nu_i}w_{lj}^{(i)}, \tag{4}$$

---

* *Permanent address: Theory Department, General Physics Institute, 117942 Moscow, Russia*

where $w_{lj}^{(e,i)} = \nabla_j v_l^{(e,i)} + \nabla_l v_j^{(e,i)} - \frac{2}{3}\delta_{lj}\nabla \cdot \mathbf{v}^{(e,i)}$. Further, $\mathbf{R}$ is the friction forse between the electrons and ions:

$$\mathbf{R} = \mathbf{R_u} + \mathbf{R}_T = -0.51 n_e m_e \nu_e \mathbf{u} - 0.71 n_e \nabla T_e, \tag{5}$$

where the forse of relative friction $\mathbf{R_u}$ is defined for $\omega \ll \nu_e$ (we have $\nu_{\text{eff}} \simeq \nu_e$ in the case considered; let us note that if $\omega \gg \nu_e$ holds with, then $\mathbf{R_u} \simeq -n_e m_e \nu_e \mathbf{u}$, but in this case some questions arise on applicability of the hydrodynamical description). Finally, $\mathbf{q}^{(e,i)}$ in Eq.(2) is the heat flux:

$$\mathbf{q}^{(e)} = \mathbf{q}_{\mathbf{u}}^{(e)} + \mathbf{q}_T^{(e)} = 0.71 n_e T_e \mathbf{u} - 3.16 \frac{n_e T_e}{m_e \nu_e} \nabla T_e, \quad \mathbf{q}^{(i)} = -3.9 \frac{n_i T_i}{m_i \nu_i} \nabla T_i, \tag{6}$$

and

$$Q_e = -\mathbf{R} \cdot \mathbf{u} - Q_i, \quad Q_i = 3 \frac{m_e}{m_i} n_e \nu_e (T_e - T_i) \tag{7}$$

are the heating powers.

We solve the above equations by expanding in powers of the electric field $\mathbf{E}$. To investigate modulational instability, we have to take into consideration terms up to the third order in the fields, as well as interactions through virtual waves (which are perturbations of the pump electric field on the beat frequency $\Delta\omega$ and in general also the double frequency $2\omega_0$). Then we proceed with the following ansatz

$$\mathbf{E}_{\mathbf{k}\omega} = \mathbf{E}_0 \delta(\mathbf{k} - \mathbf{k}_0)\delta(\omega - \omega_0) + \mathbf{E}_1 \delta(\mathbf{k} - \mathbf{k}_1)\delta(\omega - \omega_1) + \delta\mathbf{E}_{\mathbf{k}\omega}, \tag{8}$$

where $\delta\mathbf{E}_{\mathbf{k}\omega}$ is the modulated perturbation of the pump fields $\mathbf{E}_{0(1)}$, $|\delta\mathbf{E}_{\mathbf{k}\omega}| \ll |\mathbf{E}_{0(1)}|$.

After linearising the corresponding equation for $\delta\mathbf{E}_{\mathbf{k}\omega}$, and using an analogous procedure for the complex conjugate fields $\mathbf{E}^*$, we have the following dispersion equation for the modulational instability (the analogous equation was obtained in [3]):

$$1 = \Sigma_0 |\mathbf{E}_0|^2 \left[\frac{(\mathbf{k}_0 \cdot (\Delta\mathbf{k} + \mathbf{k}_0))^2}{\mathbf{k}_0^2 |\Delta\mathbf{k} + \mathbf{k}_0|^2 \varepsilon^l_{\Delta k + k_0}} + \frac{(\mathbf{k}_0 \cdot (\Delta\mathbf{k} - \mathbf{k}_0))^2}{\mathbf{k}_0^2 |\Delta\mathbf{k} - \mathbf{k}_0|^2 \varepsilon^l_{\Delta k - k_0}} \right] + \Sigma_1 |\mathbf{E}_1|^2 \times$$

$$\left[\frac{|\mathbf{k}_1 \times (\Delta\mathbf{k} + \mathbf{k}_1)|^2 / \mathbf{k}_1^2 |\Delta\mathbf{k} + \mathbf{k}_1|^2}{(\varepsilon^t_{\Delta k + k_1} - (\Delta k + k_1)^2 c^2 / (\Delta\omega + \omega_1)} + \frac{|\mathbf{k}_1 \cdot (\Delta\mathbf{k} - \mathbf{k}_1)|^2 / \mathbf{k}_1^2 |\Delta\mathbf{k} - \mathbf{k}_1|^2}{(\varepsilon^t_{\Delta k - k_1} - (\Delta k - k_1)^2 c^2 / (\Delta\omega - \omega_1)} \right], \tag{9}$$

where $\varepsilon^{l(t)}_{\Delta k \pm k_{0(1)}}$ is the linear high frequency longitudinal (transversal) dielectric permittivity of a plasma, and $E_{0(1)}$ is the Langmuir (electromagnetic) pump field (we assume the plasma is underdense: $\omega_1 \gg \omega_{pe}$, where $\omega_{pe} = (4\pi n_0 e^2 / m_e)^{1/2}$ is the electron plasma frequency). The factors Σ in Eq.(9) are

$$\Sigma_0 = \frac{i}{5} \frac{1}{4\pi n_0 T_e} \frac{\nu_e |\Delta\mathbf{k}|^2 v_s^2}{\Delta\omega [(\Delta\omega)^2 - |\Delta\mathbf{k}|^2 v_s^2]}, \quad \Sigma_1 = \frac{\omega_{pe}^4}{\omega_1^4} \Sigma_0, \tag{10}$$

where $v_s = (10T_e/3m_i)^{1/2}$ is the speed of sound (under the assumption (1)).

First we consider the case of Langmuir pump ($E_1 = 0$). The instability is possible only for supersonic regime. Its rate is determined by

$$\gamma_0^{\rm mod} = \nu_e \frac{\sqrt{3}}{2} \left(\frac{|\Delta \mathbf{k}| v_{Te}}{\nu_e} \right)^{\frac{2}{3}} \left[\frac{4}{3} \frac{m_e}{m_i} \frac{\omega_{pe}}{\nu_e} \frac{|\mathbf{E}_0|^2}{4\pi n_0 T_e} A(|\mathbf{k}_0|, |\Delta \mathbf{k}|) \right]^{\frac{1}{3}}. \tag{12}$$

where $A(|\mathbf{k}_0|, |\Delta \mathbf{k}|) \simeq \frac{|\Delta \mathbf{k}|^3}{|\mathbf{k}_0|^3}$, if $|\Delta \mathbf{k}| \ll |\mathbf{k}_0|$,, and $A(|\mathbf{k}_0|, |\Delta \mathbf{k}|) \simeq \frac{|\mathbf{k}_0|}{|\Delta \mathbf{k}|}$, if $|\Delta \mathbf{k}| \gg |\mathbf{k}_0|$. The maximum weave vector of the modulated perturbations is determined by the diffusion condition $|\Delta \omega| \gg |\Delta \mathbf{k}|^2 v_{Te}^2 / \nu_e$ as well as by the assumption of supersonic motion $|\Delta \omega|^{\rm mod} \gg |\Delta \mathbf{k}| v_s$. Thus we have for the maximum rate

$$\gamma_{0,\max}^{\rm mod} = \frac{2}{5} \omega_{pe} \frac{|\mathbf{E}_0|^2}{4\pi n_0 T_e}. \tag{13}$$

The minimum wave vector of the modulated perturbations for this situation follows from the condition of supersonic motions as well; this value also determines an instability threshold (as a condition $|\Delta \mathbf{k}|_{\min} < |\Delta \mathbf{k}|_{\max}$):

$$\frac{|\mathbf{E}_0|^2}{4\pi n_0 T_e} > \frac{5}{2} \left(\frac{10}{3} \frac{m_e}{m_i} \right)^{\frac{1}{2}} \frac{|\mathbf{k}_0| v_{Te}}{\nu_e} \frac{\nu_e}{\omega_{pe}}. \tag{14}$$

Thus the modulational instability of a monochromatic Langmuir wave can develop sufficiently effective practically at all angles between the wave vectors of the pump wave and low-frequency modulations. We stress that for the case considered the instability thresholds arise even for a monochromatic pump. So the investigated situation qualitatively differs from the collisionless case, where there are no thresholds for a monochromatic Langmuir pump. The appearance of the thresholds in the "collisional" situation is closely connected with collisional damping of wave-satellites to the monochromatic pump wave.

For the electromagnetic pump ($E_0 = 0$) the instability is also supersonic. Its rate is

$$\gamma_1^{\rm mod} = \frac{1}{2} \nu_e \left(\frac{|\Delta \mathbf{k}| v_s}{\nu_e} \right)^{\frac{2}{3}} \left[\frac{1}{5} \frac{\omega_{pe}^4}{\omega_1^4} \frac{|\mathbf{E}_1|^2}{4\pi n_0 T_e} \right]^{\frac{1}{3}}. \tag{15}$$

The instability rate is increased on the entire interval of the allowed values of $|\Delta \mathbf{k}|$, whose maximum is also given by the diffusion condition. We have

$$\gamma_{1,\max}^{\rm mod} = \nu_e \frac{v_s}{v_{Te}} \left(\frac{1}{5} \frac{\omega_{pe}^4}{\omega_1^4} \frac{|\mathbf{E}_1|^2}{4\pi n_0 T_e} \right)^{\frac{1}{2}}. \tag{16}$$

By deriving (9) we have used an assumption $|\Delta \mathbf{k}| > \omega_{pe}^3 \nu_e / \omega_0^3 c$, which gives the minimum value for the wave vector of the modulated perturbations. So the following threshold arise:

$$\frac{|\mathbf{E}_1|^2}{4\pi n_0 T_e} 5\max\left\{\left(\frac{\omega_{pe}}{\omega_1}\right)^2\left(\frac{v_{Te}}{c}\right)^2, \left(\frac{3m_i}{10m_e}\right)^2\left(\frac{v_{Te}}{c}\right)^4\left(\frac{\omega_{pe}}{\omega_0}\right)^8\right\}. \quad (17)$$

It is worth comparing the modulated instability rate and threshold with other nonlinear processes taking place in strongly underdense laser plasmas. The most effective nonlinear process there is stimulated Raman backscattering (SRS) [1]. Its rate and threshold are

$$\gamma^{\mathrm{SRS}} = \omega_{pe}\left(\frac{\omega_{pe}}{\omega_1}\frac{|E_1|^2}{4\pi n_0 m_e c^2}\right)^{\frac{1}{2}}, \quad \gamma_{\mathrm{thr}}^{\mathrm{SRS}} = \frac{1}{2}\left(\frac{\omega_{pe}}{\omega_1}\right)^2 \nu_{\mathrm{eff}}. \quad (18)$$

Comparing (16) and (18), we have

$$\frac{\gamma^{\mathrm{mod}}}{\gamma^{\mathrm{SRS}}} = \frac{10m_e}{3m_i}\frac{\nu_e}{\omega_{pe}}\left(\frac{\omega_{pe}^3}{\omega_0^3}\frac{c^2}{v_{Te}^2}\right)^{\frac{1}{2}}. \quad (19)$$

For the typical laser plasma parameters ($\omega_0 \sim 10^{15}$rad/sec, $\omega_{pe} \sim 10^{14}$rad/sec, $\nu_e \sim 10^{12}$rad/sec, $v_{Te}/c \sim 10^{-2} - 10^{-1}$), the rate of the modulational instability is always less than the γ^{SRS}. But we note that the SRS is a resonant process occuring only in localized regions of the (inhomogeneous) plasma corona determined by corresponding energy and momentum matching conditions. The modulational instability is a non-resonant process (like filamentation of the laser light), and consequently no matching conditions are to be satisfied. Moreover if we compare the thresholds of the modulational instability and the SRS, we find $\gamma_{\mathrm{thr}}^{\mathrm{mod}}/\gamma_{\mathrm{thr}}^{\mathrm{SRS}} \sim 10^5(v_{Te}/c)^4$, this can be much less than unity, depending on plasma temperature. Thus the modulational instability can occur when the SRS is "switched off".

The considered case of relatively small instability rates (because of condition (1)) is useful to establish the instability threshold. It is also interesting to examine the case of larger rates, when inequality opposite to (1) takes place.

Acknowledgments. I would like to thank the Alexander von Humboldt Foundation for financial support, and M.Y.Yu for hospitality.

[1] W.L.Kruer, *Physics of Laser Plasma Interactions* (Addison-Wesley, Redwood Sity, CA, 1988); E.M.Campbell, Phys. Fluids B **4**, 3781 (1992)

[2] S.I.Braginskii, *Reviews of Plasma Physics*, edited by M.A.Leontovich (Consultants Bureau, N.Y., 1965), p.205; V.N.Tsytovich, *Theory of Turbulent Plasma* (Consultants Bureau, N.Y., 1977)

[3] L.Stenflo, Physica Scripta **T30**, 166 (1990); J. Atm. Terr. Physics **52**, 6 (1990)

EXPERIMENTAL STUDY OF ELECTRIC AND MAGNETIC FIELDS OF LASER PLASMA

A.V.Kabashin, P.I.Nikitin, V.I.Konov.
General Physics Institute of Russia Academy of Sciences,
Vavilov street 38, 117942, Moscow, Russia.

By now a great number of papers have been published reporting investigations of magnetic fields of laser plasma (e.g./1-5/). However in most papers only fields withing plasma or surrounding it ionization "aureole" were studied, i.e. fields withing conductive medium, where plasma magnetic fields penetrate by the processes of "diffusion" or "convection".

Only in few papers magnetic fields of overall plasma blob have been investigated. Resulting dipole moment of plasma was attained by departure of laser beam from a lens center /1/ or by oblique incidence of radiation on target surface /2,4,5/.

In this paper new method of magnetic field "splash" from laser plasma is proposed.

Considerable signals of magnetic field near the plasma (e.g. in region behind the target) have been observed for the first time under production of asymmetric contact of plasma ionization "aureole" with target surface. Significant currents along the target were also observed in such conditions.

In addition, structure of electric fields near laser plasma have been investigated.

For the first time investigation of magnetic fields in laser plasma was carried out by fiber-optical sensors based on Faraday effect in ferrite-garnet films and semimagnetic semiconductors /6,7/.

Experimental set up.

In our experiments plasma was produced by several lasers of different wavelengths: λ_1= 10.6 μm (1 μs), λ_2= 1.06 μm, λ_3= 0.53 μm (0.7, 3.5 ns). Radiation was focused in air or on various targets with the intensities of $I=5\cdot10^{9}$-10^{13} W/cm^2 at pressure P= (0.1-760) Torr.

Conductive copper targets with the thickness of 0.1 mm and dielectric 2 mm teflon targets with dimensions 33·33 mm^2.

were used in experiments.

Magnetic fields in different points behind and in front of the target and current along the target were detected by sensors D_{1-4} as shown in Fig.1. A segment of a central core of of a 50-Ω cable, which had a load resistance R=50 Ω, was used as a probe in measurements of electric potentials.

Magnetic fields under plasma production on conductive target.

1. First of all laser beam with symmetric distribution of the intensity I(x) over the focal spot (spot diameter ≈3 mm, $I=10^{10} W/cm^2$) was displaced along the surface of target with respect to its geometric center (Fig.1). By such displacement l_x only asymmetry in contact of ionization "aureole" with target surface was produced.

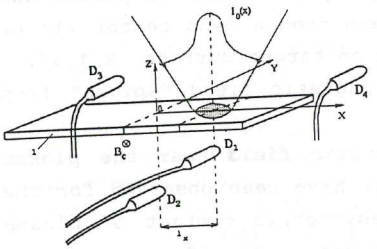

Fig.1 Experimental scheme

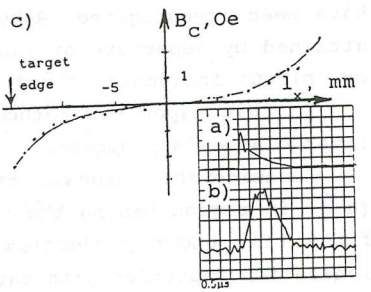

Fig.2 a) laser pulse, b) magnetic field, c) $B_c(l_x)$.

Experiments revealed the appearance of considerable magnetic field signals ($B_c \approx 2$-3 Oe) in all region behind the target under such displacement (Fig.2b). Direction of magnetic fields changed when the beam was displaced to different sides from the center. Direction of vector B_c was defined by the vector product [k, l_x], where k-wave vector of laser beam, l_x-vector from target center to the spot (Fig.1). Maximum amplitudes of signals were detected under the displacement of laser beam to target edges (Fig.2c).

Experiments also showed that as in /2,8/ plasma production by tandem pulses with variable delay results in considerable increase (20-40 times) of field amplitudes B_c.

2. To understand the influence of conductivity of aureole -target interface to magnetic field "splash", region of their contact was superposed from one edge by thin dielectric with the thickness of 0.1 mm (Fig.3).

Considerable magnetic fields behind the target were also observed under such superposition. Their direction was defined by vector product $-[k,m_x]$, where m_x-vector from target center to the edge of dielectric. Maximum amplitudes were attained when all region of contact with aureole from one side was superposed (Fig.3). However amplitudes decreased when dielectric superposed a part of laser spot.

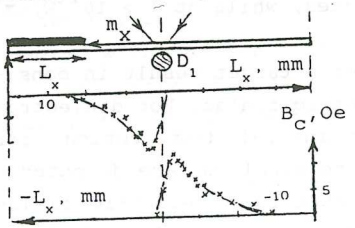

Fig.3 $B_c(L_x)$

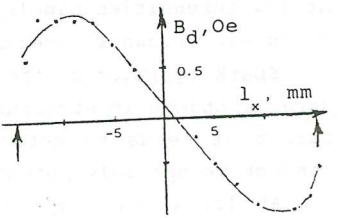

Fig.4 $B_d(l_x)$

Magnetic fields under plasma production on dielectric target.

Experiments in scheme Fig.1 were carried out using non-conductive targets of the same dimensions.

In this case magnetic fields B_d behind the target were also observed under the displacement of laser beam from target center. However their direction appeared to be directly opposite to the case of conductive target and was defined by the vector product $-[k,l_x]$. Temporal shape of signals was similar to the signal in Fig.2c, their amplitudes were maximum under certain displacement $l_{opt}<l_{max}$ (Fig.4).

Comparison of results for conductive and dielectric targets shows significant role of currents in contact aureole--target to generation of resulting dipole moment of plasma.

Eletric fields of laser plasma.

Spatial structure of electric field near laser spark in atmospheric air have been also investigated. For that purpose potentials along the spark axis were scanned by the probe.

Experiments revealed rather complicated distribution of electric potentials along Z-axis (Fig.5 b), that could be explained only by quadrupole configuration of volume charges in laser plasma. Such confi- guration may be composed e.g. by two dipoles in entrance d_1 and exit d_2 to the spark (Fig.5a).

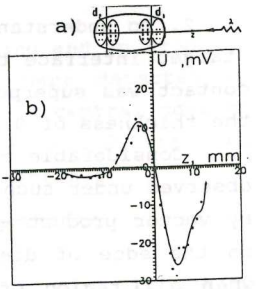

Fig.5 (U-signal from probe)

Relative contributions of dipoles d_1 and d_2 essentially depend on the intensity and wavelength of radiation. At low intensities dipole d_1 dominates, while at $I > 10^{11} W/cm^2$ d_2 is significantly predominant.

Spark ignition on the surface of a target result in considerable change in structure of electric fields. For dielectric target it leads to deformation of initial distribution, for conductive one only potentials due to dipole d_1 are detected.

At low intensities observed structure of electric fields could be explained by the mechanism, connected with gradients of electron pressure ∇N_e and temperature ∇T_e in plasma front. However dependencies at $I > 10^{13} W/cm^2$ show that in this conditions new nonlinear mechanisms take place.

Conclusions.

Asymmetry of contact of plasma aureole with target surface (or asymmetric conductivity in contact) result in magnetic field "splash" from laser plasma. Topology of such fields sufficiently differs for conductive and dielectric targets.

Quadrupole configuration of volume charges in laser plasma have been observed for the first time.

/1/ V.V.Korobkin, R.V.Serov, Sov. JETP lett 4, 103 (1966).
/2/ G.A.Askarjan et al., Sov. JETP lett 5, 93 (1967).
/3/ J.A.Stamper et al., Phys. Rev. Lett. 26, 1012 (1971).
/4/ V.V.Korobkin, S.L.Motylev, Sov. JETP lett 29, 700 (1979).
/5/ V.A.Gorbunov et al., Sov.J. Quant. Electr., 9, 130 (1982).
/6/ S.N.Baribin et al, Sens. and Act.A, 25-27, 767-774 (1991).
/7/ A.V.Kabashin, Abs.of Eurosensors-VI, San-Sebastian (1992).
/8/ V.I.Konov, P.I.Nikitin et.al., JETP Lett. 39, 609 (1984).

GENERATION OF MAGNETIC FIELDS AND POTENTIAL STRUCTURES IN VISCOUS LASER DRIVEN PLASMA.

A.N.Kochunov, A.V.Kabashin, P.I.Nikitin and A.V.Borovsky.
General Physics Institute of Russia Academy of Sciences,
Vavilov street 38, 117942, Moscow, Russia,

By now a great number of papers have been published reporting investigations of magnetic fields of laser plasma (e.g. /1-3/). Many mechanisms were mentioned for their explanation, including the most well known gradient mechanism, connected with the force of hydrodynamic pressure /3/.

In this paper theory of generation of spontaneous magnetic fields (SMF) in collisional viscous plasma under interaction with the field of monochromatic laser wave have been developed. In addition, mechanisms of generation of potential layers in laser plasma under the action of non-linear electromagnetic forces have been considered.

Initial equations.

Consider a model of plasma consisting of ions with mass m_i, charge e_z, and electrons with mass m_e and charge -e. We will base our analysis on the two-fluid hydrodynamics of plasma in an electromagnetic field. The equations for it in a 10-momentum approximation of Grad's method are:

$$\frac{\partial}{\partial t}n_e + \nabla \cdot n_e v_e = 0, \tag{1}$$

$$\frac{\partial}{\partial t}n_i + \nabla \cdot n_i v_i = 0, \tag{2}$$

$$m_e n_e \left(\frac{\partial}{\partial t}v_e + (v_e \cdot \nabla)v_e\right) = -\nabla p_e - e n_e \left(E + \frac{1}{c}[v_e \times B]\right) - m_e n_e \nu_{ei}^{p}(v_e - v_i) + \frac{\partial}{\partial r}\hat{\pi}_e , \tag{3}$$

$$m_i n_i \left(\frac{\partial}{\partial t}v_i + (v_i \cdot \nabla)v_i\right) = -\nabla p_i + e n_i \left(E + \frac{1}{c}[v_i \times B]\right) + m_e n_e \nu_{ei}^{p}(v_e - v_i) + \frac{\partial}{\partial r}\hat{\pi}_i , \tag{4}$$

where $n_{e,i}$, $v_{e,i}$, $p_{e,i}$ - densities, velocities and pressures of electrons and ions; E and B - electric and magnetic fields; $F_{\pi}^{e,i}$ - viscous forces which in the Grad's 10-momentum approach are:

$$F_{\pi}^{e,i} = \frac{\partial}{\partial r_j}\hat{\pi}_{(e,i)s} \tag{5}$$

Viscous tensor in (5) is defined by the expression:

$$\frac{\partial}{\partial t}\hat{\pi}_{e,sj} + \frac{\partial}{\partial r_k}v_{e,k}\hat{\pi}_{e,sj} + \hat{\pi}_{e,sl}\frac{\partial}{\partial r_l}v_{e,j} + \hat{\pi}_{e,lj}\frac{\partial}{\partial r_l}v_{e,s} - \frac{2}{3}\delta_{sj}\hat{\pi}_{e,lr}\frac{\partial}{\partial r_l}v_{e,r} + a\nu_{ei}^{p}\hat{\pi}_{e,sj} + \frac{4}{5}\nu_{ei}^{p}m_e n_e\left(v_{e,s}v_{e,j} - \frac{1}{3}\delta_{sj}v_e^2\right) - n_e T_e\left(\frac{\partial}{\partial r_s}v_{e,j} + \frac{\partial}{\partial r_j}v_{e,s} - \frac{2}{3}\delta_{sj}\nabla\cdot v_e\right) - \frac{e}{m_e c}B_r\left(e_{slr}\hat{\pi}_{e,jl} + e_{jlr}\hat{\pi}_{e,sl}\right) = 0. \tag{6}$$

Where $a=-\frac{6}{5}\left(1+\frac{1}{Z2^{1/2}}\right)$ is a constant. The expression for $\pi_{sj}^{i} = \hat{\pi}_{i,sj}$ is the same as for $\pi_{sj}^{e} = \hat{\pi}_{e,sj}$, only the superscript (e)→ (i). Further, the quasi neutral condition is assumed to be satisfied

$$n_e = Zn_i \tag{7}$$

Physical variables such as electric and magnetic fields and current density are assumed to contain slowly and fast varying temporal dependencies. So

$$B=<B>+\tilde{B}_1, \quad E=<E>+\tilde{E}_1, \quad J=<J>+\tilde{J}_1, \quad v=<v>, \quad n_e=<n_e>, \quad n_i=<n_i> \tag{8}$$

Generation of SMF by Rotational Part of Miller's Force.

For calculation of Miller's Force, let us consider eq.(3-4) in combination with Maxwell's equations /4/. Using representation (8), the slow current amplitude can be derived as:

$$\tilde{J}_1=(\omega_p^2/4\pi)\frac{\tilde{E}_1}{\nu_{ei}^{p}+i\omega} \tag{9}$$

From Maxwell's eq. we have:

$$\tilde{B}_1=(ic/\omega)[\nabla x\tilde{E}_1]. \tag{10}$$

Using (3),(4) and (8) it's easy to write the expression for Miller's force:

$$F_M = <-\frac{1}{c}[\tilde{J} \times \tilde{B}] - m_e n_e\left(\frac{\tilde{J}}{en_e}\cdot\nabla\right)\frac{\tilde{J}}{en_e}>, \tag{11}$$

Substituting (9) and (10) to (11), we obtain:

$$F_M=-(\omega_p^2/16\pi)\left\{\frac{\nabla(\tilde{E}_1\cdot\tilde{E}_1^*)}{(\nu_{ei}^{p2}+\omega^2)}\frac{\nu_{ei}^p}{\omega}\frac{Im[(\tilde{E}_1\cdot\nabla)\tilde{E}_1^*]}{(\nu_{ei}^{p2}+\omega^2)}\right\}. \qquad (12)$$

Taking the curl of Eq.(12), gives:

$$rot\left(\frac{F_M}{en_e}\right)=-(\omega_p^2/16\pi en_e)\ rot\left\{\frac{\nu_{ei}^p}{\omega}\frac{Im[(\tilde{E}_1\cdot\nabla)\tilde{E}_1^*]}{(\nu_{ei}^{p2}+\omega^2)}\right\} \qquad (13)$$

As a result we obtain the expression for the source produced by the rotational part of Miller´s force:

$$\frac{1}{c}\frac{\partial<B>}{\partial t}=\frac{c}{4\pi\sigma}\Delta<B>+\frac{1}{c}[\nabla x[vx<B>]]+\left[\nabla x\left(\frac{\nabla p_e}{en_e}-\frac{F_M}{en_e}\right)\right] \qquad (14)$$

Generation of SMF by viscous force.

From eq. (3),(4),(6), (8-10) we obtain /5/:

$$<\pi_{e,sj}>=\frac{\omega_p^2}{20\pi a\omega^2}\left\{\left\{\frac{2}{3}\delta_{sj}(\tilde{E}_1\cdot\tilde{E}_1^*)-(\tilde{E}_{1s}\tilde{E}_{1j}^*+\tilde{E}_{1s}^*\tilde{E}_{1j})\right\}-\right.$$

$$\left.-(\omega_B/\nu_{ei}^p a)\left\{\tilde{E}_{1j}[\tilde{E}_1^* x<b>]_s+\tilde{E}_{1s}[\tilde{E}_1^* x<b>]_j+\text{к.с.}\right\}\right\} \qquad (15)$$

Here $b=<B>/|<B>|$, $\omega_B=e<B>/m_e c$.

By using $\omega_B/\nu_{ei}^p a \ll 1$, it is easy to write the expression for the source of the SMF produced by the viscous force:

$$[\nabla x\left(\frac{F_\pi}{en_e}\right)]=-(\omega_p^2/20\pi aen_e)\cdot\frac{[\nabla x((\tilde{E}_1\cdot\nabla)\tilde{E}_1^*+(\tilde{E}_1^*\cdot\nabla)\tilde{E}_1)]}{(\nu_{ei}^{p2}+\omega^2)} \qquad (16)$$

As a result, the equation of generation of SMF by F_π is:

$$\frac{1}{c}\frac{\partial<B>}{\partial t}=\frac{c}{4\pi\sigma}\Delta<B>+\frac{\omega_p^2}{10\pi aen_e\omega^2}[\nabla x((\tilde{E}_1\cdot\nabla)\tilde{E}_1^*+(\tilde{E}_1^*\cdot\nabla)\tilde{E}_1)] \qquad (17)$$

Maximum magnetic fields could be expressed as: $B\simeq(\omega_p^2/\omega^2)\cdot 3{,}6\cdot 10^4\cdot I(W/см^2)/\nu$. For $I\simeq 10^{14}$ $W/см^2$, $\lambda=1{,}06$ μm ($T_e=100$ eV, $n_e\simeq 10^{20}$ $см^{-3}$), we obtain B≃0,1 MG.

Generation of potential structures in laser plasma.

Electron component in plasma is subjected to the action of lateral forces that give rise to charge separation. Forces of electromagnetic origin try to compensate them. From (3),(4) condition of balance of forces may be writen as follows:

$$E = \frac{\nabla P_e}{en_e} + \frac{\nabla T_e}{e} + \frac{F_M}{en_e} + \frac{F_\pi}{en_e} + \frac{1}{c}[V,B] + \ldots \quad (18)$$

For dipole moment of plasma volume $d = \int_v r\,\rho\,d^3r$ it is easy to obtain that:

$$d = \int r \cdot \frac{1}{4\pi}(\nabla E_{pot})\,d^3r = -\frac{1}{4\pi}\int_v E_{pot}\,d^3r \quad (19)$$

because $E_{pot} = 0$ outside plasma region.

Let us consider contribution of forses F_M and F_π of eq.(18) to integral (19) consequently.

1)Miller's force.

Substituting the expression for Miller's force (12) to (20), we obtain:

$$d_M = \frac{\omega_p^2}{e16\pi\omega^2 en}(P_{out} - P_{in}) \quad (20)$$

Or rewriting in numerical representation:

$$d(CGSE) = 2{,}48\ 10^{-11}\lambda^2\Delta P \quad (21)$$

Here ΔP- loss of radiation power in MW, λ-wavelength in μm

For Nd-glass and CO_2 lasers with the intensity of $I=10^{12}W/cm^2$ we obtain respectively: $d_m=10^{-10},10^{-8}$ CGSE.

2)Viscous force.

Using the the expressions for viscous force (5),(15), it is easy to obtain from (19):

$$d_s = -\frac{\omega_p^2}{120a\pi\omega^2 en}\int_v \frac{\partial}{\partial r_s}|E^2|\,d^3r = -0.11 d_M \quad (11)$$

Conclusions.

Generation of magnetic fields in collisional, viscous laser driven plasma have been considered. Apart from well known gradient, mechanisms connected with Miller's force and the force of electromagnetic viscosity have been obtained.

In addition, mechanisms of generation of potential structures in laser plasma have been considered.

/1/ V.V.Korobkin, R.V.Serov, Sov. JETP lett **4**, 103 (1966).
/2/ G.A.Askarjan et al., Sov. JETP lett **5**, 93 (1967).
/3/ J.A.Stamper et al., Phys. Rev. Lett. **26**, 1012 (1971).
/4/ H.Hora, Phys.of laser driven plasmas,J.Wiley & Sons (1981)
/5/ Y.M.Abdullaev et.al, Zh.Eksp.Teor.Fiz. 94, 133 (1988)

CHARGED PARTICLE AND PHOTON ACCELERATION BY WAKEFIELD PLASMA WAVES IN NON-UNIFORM PLASMAS

S.V.Bulanov*, V.I.Kirsanov*, F.Pegoraro**, and A.S.Sakharov*

* General Physics Institute of Russian Academy of Sciences, Moscow, Russia
** Dept. of Theoretical Physics, University of Turin, Turin, Italy

We discuss the acceleration of charged particles and the upshift of the frequency of short wave packets of laser radiation. The acceleration and the upshift are caused by wake plasma waves excited by a strong laser pulse in a non-uniform plasma. We show that unlimited acceleration of charged particles is possible for specific spatial dependencies of the plasma density. In this unlimited acceleration regime, particles have a fixed phase relationship with respect to the plasma wave, while their energy increases with time. When the wave breaking limit is approached and surpassed, the efficiency of the acceleration of the charged particles and of the frequency upshift of the photons can be increased significantly.

The acceleration of charged particles and the frequency upshift of short wavepackets of electromagnetic radiation takes place if they have the appropriate phase with respect to the the wake plasma wave [1,2]. In a plasma with a uniform background density the charged particles and the wavepackets leave eventually the phase interval where acceleration occurs. This restricts the value of particle energy gain and the increase of the packet frequency. In a non-uniform plasma the speed of propagation of a plasma wave and its wavelength, as well as the group velocity of the electromagnetic radiation, depend on position and it is thus possible to increase the time interval during which the charged particles or the electromagnetic wave packet remain in phase [3] (in this reference the amplitude of the plasma wave is taken to be spatially constant).

The relativistic equations of motion of an electron with momentum p in the field E of a one-dimensional electrostatic wake plasma wave can be written in the form

$$\frac{d}{dx}\left(\frac{\psi}{\omega_p}\right) = \frac{(m_e^2c^2+p^2)^{1/2}-p}{cp} - \frac{\omega_p^2}{2\omega_o^2 c}, \tag{1}$$

$$\frac{d}{dx}(m_e^2c^4+p^2c^2)^{1/2} = -eE, \tag{2}$$

where

$$\psi = \omega_p(t-t_o) = \omega_p\left(t - \int^x \frac{dx'}{v_g}\right) \tag{3}$$

is the phase of the plasma wave, with t_o the arrival time of the electromagnetic radiation with frequency $\omega_o \gg \omega_p$ and group velocity $v_g \approx c[1 - (\omega_p^2/2\omega_o^2)]$ at point x, and E depends on the phase ψ and on the coordinate x. In a uniform plasma, in the ultrarelativistic particle limit and for moderately strong plasma waves, the energy gain of the charged particles is given approximately by $\Delta\mathcal{E} = eEl_{acc}$ with $l_{acc} = 2(\lambda_p/2\pi)(\omega_o/\omega_p)^2$ the "acceleration length" over which the the particles remain in phase with the wave. This length is much greater than the wavelength $\lambda_p = 2\pi c/\omega_p$ since $(\omega_o/\omega_p)^2 \gg 1$. The energy of the accelerated particles exceeds the typical quiver energy of the electrons in the plasma wave by the same factor.

The above limit on the energy gain is due to the fact that the accelerated particles eventually escape from the phase interval in which the electric field of the plasma wave is accelerating. This loss of phase matching can also result from the non-uniformity of the plasma density which leads to a change of the plasma wavelength or from the change in the amplitude of the driving electromagnetic pulse due to self-focusing, defocusing, energy depletion, etc. In addition in a relativistically strong plasma wave the wavelength depends on the wave amplitude so that a change in the amplitude results in an increase or a decrease of the wavelength. However these same effects can also allow for an "unlimited acceleration" regime in which the final energy gain is determined only by the length of the plasma.

We consider a small amplitude plasma wave ($eE/\omega_p m_e c \ll 1$), in which case $E(x,t) = -\omega_p(x)^2 m_e F(\psi)/e$, with $F(\psi) = -(l\ |a_o|^2/4)\cos(\psi)$, l the length of the short laser pulse, and $a_o = eA_\perp/m_e c^2$ with $A_\perp$ thewave vector potential. By direct inspection we see that, for ultrarelativistic particles, Eqs. (1-3) admit a solution with unlimited acceleration at constant phase $\psi(x) = \psi(0)$ and energy $\mathcal{E}(x) = \mathcal{E}_o(x/\mathcal{L})^{1/3}$, if the density profile is chosen such that

$$\omega_p(x) = \omega_{po}\ (\mathcal{L}/x)^{1/3}, \tag{4}$$

and the non-uniformity scale length $\mathcal{L}$, the reference values of the plasma frequency ω_{po} and of the particle energy $\mathcal{E}_o$ are related by $\mathcal{L} = (c/3\omega_{po})(\omega_o/\omega_{po})^2\ \{\ [\psi(0)^2 + (c^2/\omega_o^2 F(\psi(0))^2)\ ]^{1/2} - \psi(0)\}$, and by $\mathcal{E}_o = 3m_e\mathcal{L}\ \omega_{po}^2\ F(\psi(0))$, with $F(\psi(0)) > 0$. The optimal acceleration rate occurs at $\psi(0) = \pi$ and has its maximum for a relatively small amplitude of the wake wave $E_m = (m_e/\sqrt{3}\pi e)(c\omega_{po}^2/\omega_o)$, corresponding to $\mathcal{L}$ of the order of l_{acc}. In this case

$$\mathcal{E}(x) \approx m_e c^2(\omega_o/\omega_{po})\ (x/l_{acc})^{1/3}. \tag{5}$$

Note that for relativistically strong wake plasma waves significantly larger acceleration rates can be produced, but in such a case particles remain at resonance with the plasma wave only for a limited time so that the final energy gain is limited. On the contrary in the case discussed above, even if the acceleration rate is smaller, the particle energy gain is in principle not limited in time. An unlimited particle acceleration regime is also possible in the case of a strongly non linear plasma wave, but it can be shown that unlimited energy gain can only be obtained at a small acceleration rate.

A second possibility of enhancing the efficiency of the acceleration of charged particles is to increase the value of the electric field in the plasma wave. The maximum field in a stationary plasma wave is given by $E = \sqrt{2}(m_e c\ \omega_p/e)\ (\omega_o/\omega_{po})$. For larger values the wave breaks and its structure becomes distorted and transient. The region where the wave breaks spreads towards the trailing edge of the driving laser pulse with a velocity of order $(c/2)(\omega_p/\omega_o)^2 \ll c$ so that a region with a regular structure can exist for a rather long time due to the relatively low value of this velocity. An estimate of the maximum wake field amplitude can be obtained by requiring that no wavebreaking occurs inside the laser pulse before the electrostatic potential in the pulse reaches its maximum amplitude. The corresponding value of the electric field $E = (m_e c\ \omega_p/e)(\omega_o/\omega_{po})^2$ is much bigger than the wave breakig value given before. In this case, the particle energy gain can scale as $(\omega_o/\omega_{po})^4 m_e c^2$.

If a short laser pulse, with central frequency $\omega_o \gg \omega_p$ interacts with a plasma wave propagating with phase velocity $v_{ph} \approx c$ and a wavelength much longer than the width of the pulse envelope, the energy of the pulse can either decrease or increase depending on their relative phase. In the first case the wavepacket can be used to amplify the plasma wave. In the second case it is the energy of the wavepacket that increases. In the geometrical optics approximation the number of photons is conserved and the increase of the pulse energy corresponds to the upshift of its frequency. This mechanism has been called "photon accelerator" in analogy to the process of particle acceleration. We denote by $\Omega = \Omega(\psi, x)$ the local electron plasma frequency, which includes the effect of the plasma wave on the background density and electron energy, and assume that its dependence on x is weaker than that on ψ. Then, with ϕ the electrostatic potential of the wake field, we have in lieu of Eqs (1) and (2)

$$\frac{d}{dx}\left(\frac{\psi}{\omega_p}\right) = \frac{\omega_p^2}{2k^2c^3\ \left[(1+\phi)^2\ -\ (\omega_p^2/\omega_o^2)\right]^{1/2}} - \frac{\omega_p^2}{2\ \omega_o^2\ c}, \qquad (6)$$

and

$$\frac{dk^2}{dx} = -\frac{\omega_p^3\,(1+\phi)\,(\partial\phi/\partial\psi)}{c^3\,\left[(1+\phi)^2\,-\,(\omega_p^2/\omega_o^2)\right]^{3/2}}. \tag{7}$$

In the wave breaking regime the denominators on the right hand sides approach zero as a consequence either of the decrease in the minimum value of $(1+\phi)^2$, or in the increase of the value of ω_p^2/ω_o^2. The latter case can occur when the plasma wave propagates in the direction of increasing plasma density. The solution of Eqs. (6) and (7) corresponding to unlimited frequency upshift is obtained to a density profile of the form

$$\omega_p(x) = \omega_p(0)\left(1+\frac{2x}{\mathcal{L}}\right)^{1/2}, \tag{8}$$

with inhomogeneity scale-length $\mathcal{L} = \psi_m[2c/\omega_p(0)]\,[\omega_o/\omega_p(0)]^2$ The frequency upshift of the wave packet is given by $\omega(x) = 4\omega_o(\omega_o/2)^{1/8}\,\{\mathcal{L}/[\mathcal{L}(\omega_o/\omega_{po})^2\Delta\phi - x]\}^{1/4}$. This solution is valid only until the photons reach $x = 0$. The maximum frequency of the accelerated photons is $\omega_{max} = 4\omega_o[\omega_o/\omega_p(0)]^{3/2}[2(\omega_o/\omega_{po})^2\Delta\phi]^{-1/8}$, however, due to the dependence of ω_{max} on $\Delta\phi$ this acceleration mechanism leads to a large frequency spread of the accelerated photons in the wave packet.

The scale of the plasma non-uniformity and of the particle and photon acceleration given above can be of the order of or much shorter than the laser pulse depletion length, except for the case of a relativistically strong plasma wave. As long as $(c/\omega_o) < l < (c/\omega_p)$, the distortion length due to the dispersion of the electromagnetic radiation can be either shorter or longer than the acceleration length.

In conclusion we have analyzed the role of the spatial non-uniformity of the parameters of the wake plasma wave. An appropriate choice of the plasma density profile is more convenient in the case of particle acceleration, as it is possible to achieve a regime of unlimited acceleration, while in the case of photons the acceleration scheme that exploits the increasing electron density of a breaking plasma wave is more advantageous.

1) T. Tajima and J.M. Dawson, Phys. Rev. Lett. **43**, 267 (1979).

2) S.C. Wilks, J.M. Dawson, W.B. Mori, T. Katsouleas and M.E. Jones, Phys. Rev. Lett. **62**, 2600 (1989).

3) B. Meerson, Phys. Lett. **A150**, 290 (1990).

LANGMUIR WAVE COLLAPSE WITH RIPPLED CRITICAL SURFACE IN LASER PRODUCED PLASMAS

FAIZ DAHMANI
Labo Fusion, CDTA/HCR. 2,Bd.Frantz Fanon BP1017
Alger-Gare, Algiers - ALGERIA

The Langmuir wave collapse in laser-produced plasmas is of great interest because of its great role in Langmuir turbulence kinetics, being the main mechanism of absorption of Langmuir oscillation energy. Collapse has recently been studied extensively both in numerical simulations and experiments.

In this work, experiments were conducted using a 1.06μm laser light at irradiances of 10^{14} - 5×10^{15} W/cm^2 on a flat gold target. The second harmonic emission from the plasma was collected at 90° of the incident laser beam onto a streak camera.

A typical result obtained at a laser intensity of 4×10^{15} W/cm^2 is shown in Fig.1(a). The analyzed spectrum [Fig.1(b)] shows the existence of two lines corresponding to two wavelengths λ_1 and λ_2. The second line shifts to the blue, whereas, the first one (λ_1) appears before the end of the process (L). A very important result was set up in these experiments; it's the apparition of a second and third burst which seem to be due to a broadening toward the end of the processes (L') and (L''), respectively, of other lines between λ_1 and λ_0 (λ_3), and λ_0 and λ_2 (λ_4). These lines; λ_3 and λ_4, originate from λ_1, broaden and shift toward the red with time, and eventually give rise to a continuum super-imposed on λ_1 and λ_2.

Since the second harmonic ($2\omega_o$) emission is collected perpendicularly to the laser propagation direction and then parallel to the laser field $\vec{E}_o$, a simple physical argument shows that the $2\omega_o$ emission arising from the beating of the laser ($\vec{k}_o \simeq 0$) with such a plasma wave will give zero emission in this direction. The plasma wave is a longitudinal oscillation where the electrons are vibrating in the direction of $\vec{k}_e$. The electron current associated with the transverse light wave is also in this direction. Thus, there is normally no current transverse to the laser axis and therefore no radiation in this configuration. The unique explanation of this phenomenon is an eventual nonplanar nature of the critical surface. Effectively, simple calculations showed that due to a rippling of the critical surface,[1] the effective incident angle of the laser light is changed from $\theta = 0^\circ$ to $\theta = 11^\circ$.

In the first phase of the temporal evolution, at laser intensities on the order of 5×10^{13} W/cm^2 (PDI's threshold) a decay instability develops generating a plasmon family (ω_e, $\vec{k}_e$) and ion-acoustic waves (ω_a, $\vec{k}_a$) near the critical surface and gives rise to λ_1 whose relative shift with respect to λ_o is : $(\lambda_1 - \lambda_o)/\lambda_o = (\sqrt{3}/2).C_s/C$ (C_s, C; ion sound and light speeds).

In a second phase of the temporal evolution, the effects of Langmuir weak turbulence appear with the decomposition of ω_e plasmons into ω_e' ones and give rise to a second line λ_2 such that : $(\lambda_2 - \lambda_1)/\lambda_o = \sqrt{3}\, C_s/C$.

This spectral line λ_2 undergoes the same effects as λ_1, i.e., the Doppler effect and the ponderomotive effects in $\langle(\vec{E} + \vec{E}_o)^2\rangle$ increasing in time three times larger than that for λ_1 ($\vec{E}$ is to the local electric field of the Langmuir wave)

These arguments are in perfect agreement with the experimental results presented in Fig.1. The split between λ_1 and λ_2, which equals $\sqrt{3}\ C_s/C$ is $\lambda_2 - \lambda_1 \simeq 8$Å. This leads in this instance to $C_s/C \simeq 8.6\times10^{-4}$, and hence $C_s \simeq 2.5\times10^7$ cm/sec, corresponding for gold targets having $Z/A \simeq 0.4$ to $T_e \simeq 1.6$ keV which is in very good agreement with the experimental value deduced from x-ray vacuum diodes ($T_e \simeq 1.4$ keV for 4×10^{15}W/cm^2),[2] and then to $v_e/C \simeq 8.3\times10^{-4}$ proving the existence of λ_2.

Furthermore, the average shifts observed correspond to the values of $W = \langle(\vec{E}+\vec{E}o)^2\rangle$, which for $E > E_o$, is the super-position of two effects $\langle\vec{E}_o\vec{E}\rangle$ and $\langle E^2\rangle$, the first one is generally negligible compared to the second one. During Landau damping, the expression in E^2 can no more bring its contribution to the spectrum of $2\omega_o$. It is supposed that the trapping effects in $\langle\vec{E}_o\vec{E}\rangle$ (nucleations) must dominate and therefore reconstitute the initial ray λ_1 in new rays λ_3 and λ_4 subjected as λ_1 to ponderomotive effects and broadenings L′ and L′′ characteristic of new sequences of collapse.

As far as the temporal evolution is concerned, these results are in good agreement with Cheung and Wong.[3,4] Effectively, the time duration of a collapse (supersonic evolution), τ_c, as measured in the experiments in Refs.3 and 4 is roughly $10^2\omega_{pi}^{-1}$ (ω_{pi} denotes the ion plasma frequency) and in the simulation results of Ref.5, when converted to physical units, give $\tau_c < (A/Z)(1836).\omega_{pe}^{-1} \simeq \sqrt{A}\ \omega_{pi}^{-1}$ which is generally smaller. Taking $\omega_{pe} \simeq \omega_o \simeq 2.83\times10^{14}$s^{-1}, $\omega_{pi} \simeq 0.9\times10^{12}$s^{-1} for the conditions of the present work (Z= 79, A= 179) and therefore $\tau_c \leq 10^2\omega_{pi}^{-1} \simeq 110$ps. This is in very good agreement with the observed streaked features

observed here (≤ 108ps).

In conclusion, lateral observations of ($2\omega_o$) emission from a laser-produced gold plasma at high laser intensities permits to, show experimentally the existence of processes linked with collapsing evolutions and their final damping by burnout with a rippled critical surface, to observe three sequences of collapse, which bring supporting evidence to Zakharov's theoretical works on Langmuir collapse, and to complete the works of Cheung and Wong of nonlinear evolution of collapsing plasmons.

REFERENCES:

[1] J.J.Thomson *et al.*, Phys.Fluids 21, 707 (1978).
[2] F.Dahmani, Phys.Fluids B4(7), 1943 (1992).
[3] P.Y.Lee and A.Y.Wong , Phys.Fluids 28, 1538 (1985).
[4] P.Y.Lee and A.Y.Wong, Phys.Rev.Lett.55, 1880 (1985).
[5] D.Russell *et al.*, Phys.Rev.Lett.60, 581 (1988).

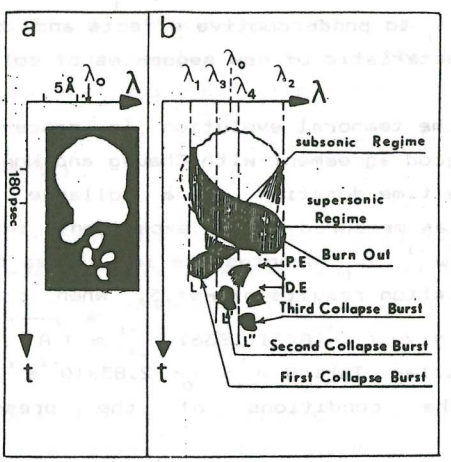

FIGURE 1

Critical Surface Behaviour Through Second Harmonic Spectra

A.H. Khalfaoui, S. Abdelli, T. Kerdja and D. Ghobrini
CDTA, 2 Bd Frantz Fanon, BP 1017, Alger-Gare, Algeria

Introduction

An experimental analysis is reported on visualisation of sidescattered second harmonic spectra originating from the critical surface of a plasma produced from a 1.06 μm Nd-Yag laser beam.

In an inhomogeneous plasma electromagnetic wave can be linearly converted by resonance absorption to an electrostatic plasma wave. This well known process takes place near the critical density when a p-polarized wave is obliquely incident on a plane target.

Observation and analysis show that, mainly two interaction processes contribute to the 2ω emission, resonant absorption, and the parametric decay instability[1] (PDI) in which the incident electromagnetic wave decay into a Langmuir wave and an ion acoustic wave just below n_c. Qualitatively, the latter possibility of exciting longitudinal oscillation arise at sufficiently high intensity of laser radiation energy flux, where certain thresholds need to be reached. The present results confirm these origins and extend the investigation to the coupling physics. Second harmonic radiation is emitted from such a system where at least one of the merging waves is a Langmuir wave and shifted in the presence of motion of the critical surface such as[2] $\omega_2 = 2\omega_o - 2(\vec{k}_o - \vec{k}_o z).\vec{u}$, $\vec{u}$ is the critical surface velocity and $\vec{k}_o$ is the wavenumber of the incident transverse wave. The shift relative to the nominal value of 2ω will be in the blue or red direction, depending on the sign of u.

The maximum value of the shift is attained when the pump wave is incident along the direction of divergence of the plasma, i.e., $\vec{k}_o = -k_o\vec{z}$ or $\Delta\omega = 4\omega_o u/c$. By monitoring these Doppler

The velocity of the critical surface can, thus, be calculated as $u = c\,\Delta\omega/4\omega$ where $\Delta\omega$ is the shift, c the speed of light and ω_o the pump frequency, e.g., at t = 0.21 nsec, $\Delta\lambda$ = 5 Å then $u = 1.4 \times 10^7$ cm/sec.

A later times, t > 0.03 nsec the intensity of the second harmonic increases further but with a stronger red shift, and hence the velocity changes sign. The bulk of photons reach n_c at arround 0.27 nsec whith $\vec{u}$ in the same direction as the incident beam, the plasma is being compressed.

Extending this analysis, several accelerations have been obtained by monitoring the shifts of the main peak at different fluxes Fig. 2. For incident beam intensity $I_o \leq 4 \times 10^{13}$ W/cm^2 the critical surface has a complex hydrodynamic behavior as the critical surface heads, first, toward the beam ($u<0$) before starting compression ($u>0$) and coming back in expansion again, with greater acceleration. For $I_o \simeq 10^{14}$ the critical surface motion is relatively more stable e.g. at $I_o = 3 \times 10^{14}$ it is constantly heading in the same direction as the incident beam.

Time resolved second harmonic spectra

In Fig. 3. the second harmonic optical density has a complex time evolution .

The observed oscillatory structure could shed a light on several phenomena of the coupling physics involved near the critical surface. It shoud be noted, first, that the oscillations are more prononced as the incident flux goes from $\simeq 10^{13}$ to $> 10^{14}$ W/cm^2.

The nonlinear process involved in the coupling of the longitudinal and transverse waves, inherently produces[3] very hot electrons at the phase matching points. These hot electrons are, virtualy collisionless at these densities, they quickly spread out and augment the hot spots dimensions to relatively large observable spatial scales.

This specific event depresses locally the plasma density below n_c postponing any new coupling in this particular zone. The spatial and time dispersion of the incident laser beam is such as to repeat the process, and hence the second harmonic will be

shifts of the second harmonic a resonable estimation of the critical surface behavior can be quantified.

Experimental arrangement

In the present experiment, a plasma was produced by focussing a Nd-Yag laser pulse of τ = o.7 nsec with a wavelength of λ = 1.064μm through a f/1.2 lens on a slab target of polyethylene $(CH_2)_n$.
The intensity range was such as $7x\ 10^{12} < I_o < 3x\ 10^{14}$ W/cm^2 with an incident angle $0 < \theta < 11.7^\circ$. The focal spot, receiving the 80 % of the incident energy, measured has a value d $\simeq$ 22 μm.
The sidescattered 2ω spectra were observed at about 45° with respect to the p-polarized incident beam. Using a 1200 lines/mm, and a one meter long spectrograph, coupled to a streak camera Imacon 675, the time evolution of the 2ω spectra have been recorded.
An image of the target is accurately focussed at the entrance slit of the spectrograph. The output plane of the spectrograph is then imaged on the entrance slit of the streak camera.
A microdensitometer has been used to measure the optical density from the spectrographic films with dynamic range of over two order of magnitude.

Critical surface dynamics

Fig. 1. shows a time evolution of a second harmonic optical density as a gaussian incident laser beam of $4x\ 10^{13}$ W/cm^2 impinges into the inhomogeneous plasma. To construct the evolution of the critical surface velocity the spectrum of the harmonic is recorded with a time resolution of 60 psec.
A typical time scan of the 2ω spectrum is, also, seen on the same figure on the photograph.
One of the main features of this spectral time evolution is the varying wavelength of the main peak. For $t \leq 0.03$ nsec the optical density has a growing Doppler blue shifted amplitude as more photons arrive to n_c indicating the motion of the critical density towards the beam, at times when the plasma starts its expansion.

generated from several emitting regions, in spatial motion, thereby producing an oscillatory spectrum. Several concequences of these cyclic events may have some effects on the integrity of both the laser beam[4] (filamentation) and the critical surface (rippling).

/1/.K. Tanaka et al., Phys. Fluids, 27, 2187 (1984).
/2/.N.G. Basov et al., Sov. Phys. JETP, 49, 1059 (1979).
/3/.P.D. Carter et al., Opt. Commun. 27, 423, (1978).
/4/.S. Abdelli et al., Laser and Particles Beams 10, 4, 629 (1992).

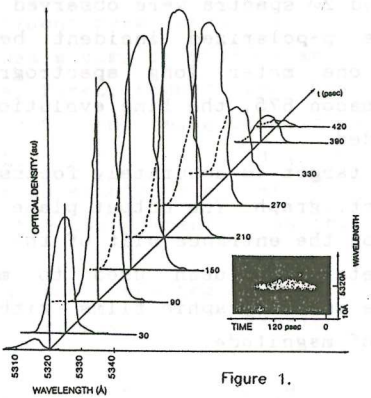

Figure 1.

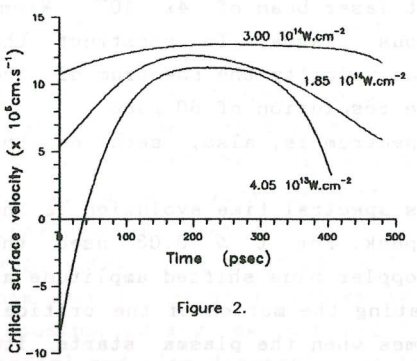

Figure 2.

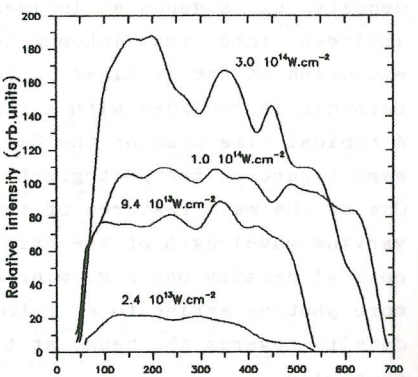

Figure 3.

Topic 8

General Plasma Theory

INDUCED SURFACE CURRENT EFFECT IN TOKAMAKS AND STELLARATORS

B. Lehnert
Alfvén Laboratory, Royal Institute of Technology
S-100 44 Stockholm, Sweden

Introduction

A problem of general interest in MHD theory is that of free-boundary modes in a plasma confined in equilibrium by a magnetic field $\mathbf{B}_o = \mathbf{B}_{jo} + \mathbf{B}_{co}$, i.e. when $\mathbf{B}_{jo}$ is due to the plasma volume current $\mathbf{j}_o = \text{curl}\, \mathbf{B}_{jo}/\mu_o$ and $\mathbf{B}_{co}$ is produced by steady currents in a set of external conductors. Thus curl $\mathbf{B}_{co} = 0$ in the plasma and in vacuo near its boundary. Often the field $\mathbf{B}_{co}$ is inhomogeneous and the motion of the plasma boundary then generates an induced surface current effect and a corresponding force on the plasma due to a related pressure unbalance. This contributes to the change in potential energy /1/. The induced surface current effect will here be discussed in connection with tokamaks and stellarators.

Basic Concepts

We restrict ourselves to incompressible motion for which the macroscopic time scale of the plasma perturbations becomes long as compared to the time for MHD signals to traverse the plasma body. In the unperturbed state $\nabla p_o = \mathbf{j}_o \times \mathbf{B}_o$ where the pressure p_o and the current density $\mathbf{j}_o$ vanish at the plasma boundary. For small displacements $\tilde{\boldsymbol{\xi}}$ the change in potential energy becomes $\delta W = \delta W_V + \delta W_S$ where /1/

$$\delta W_V = -\frac{1}{2}\iiint \tilde{\boldsymbol{\xi}} \cdot \tilde{\mathbf{F}}_V dV \tag{1}$$

$$\delta W_S = -\frac{1}{2}\iint \tilde{\boldsymbol{\xi}} \cdot (\tilde{\mathbf{f}}_{Sj} + \tilde{\mathbf{f}}_{Sc}) dS \equiv \delta W_{Sj} + \delta W_{Sc} = -\frac{1}{2}\iiint \tilde{\boldsymbol{\xi}} \cdot \tilde{\mathbf{F}}_S dV \tag{2}$$

$$\mu_o \tilde{\mathbf{F}}_V = \left\{ \text{curl}\left[(\mathbf{B}_o \cdot \nabla)\tilde{\boldsymbol{\xi}} \right] - \tilde{\mathbf{D}} \times \mathbf{B}_o \right\} \times \mathbf{B}_o + (\text{curl}\, \mathbf{B}_o) \times \left[(\mathbf{B}_o \cdot \nabla)\tilde{\boldsymbol{\xi}} \right] + \mu_o \tilde{\mathbf{D}} p_o \tag{3}$$

$$\tilde{\mathbf{D}} = \left[(\partial\tilde{\boldsymbol{\xi}}/\partial x) \cdot \nabla, (\partial\tilde{\boldsymbol{\xi}}/\partial y) \cdot \nabla, (\partial\tilde{\boldsymbol{\xi}}/\partial z) \cdot \nabla \right] \tag{4}$$

$$\mu_o(\tilde{\mathbf{f}}_{Sj} + \tilde{\mathbf{f}}_{Sc}) \equiv -\hat{\mathbf{n}} \left\{ (\mathbf{B}_{jo} + \mathbf{B}_{co}) \cdot \left[(\tilde{\boldsymbol{\xi}} \cdot \nabla)\mathbf{B}_{co} \right] \right\} \equiv \mu_o \tilde{\mathbf{f}}_S \tag{5}$$

$$\mu_o \tilde{\mathbf{F}}_S = \left\{ \text{curl}\left[(\tilde{\boldsymbol{\xi}} \cdot \nabla)\, \mathbf{B}_{co} \right] \right\} \times \mathbf{B}_o + \left\{ \left[\text{curl}\, (\tilde{\boldsymbol{\xi}} \times \mathbf{B}_o) \right] \cdot \nabla \right\} \mathbf{B}_{co} \tag{6}$$

Here $\hat{\mathbf{n}}$ is the outward directed normal of the plasma surface, V and S are the plasma volume and surface, $\tilde{\mathbf{F}}_V = \tilde{\mathbf{j}} \times \mathbf{B}_o + \mathbf{j}_o \times \tilde{\mathbf{B}} - \nabla \tilde{p}$ is the perturbation of the conventional plasma volume force, and $\tilde{\mathbf{f}}_S$ is the surface force due to the induced surface current effect, with $\tilde{\mathbf{F}}_S$ as

a corresponding volume force obtained from a formal rewriting of the surface integral into the volume integral of eq. (2). Moreover, the force $\tilde{\mathbf{f}}_S$ is transferred into a physical volume force $\tilde{\mathbf{G}}_S$ by "retarded" MHD signals propagating into the plasma /1/. The result is represented by an integro–differential equation

$$\rho_o (\partial^2 \tilde{\boldsymbol{\xi}}/\partial t^2) = \tilde{\mathbf{F}}_V(\tilde{\boldsymbol{\xi}}) + \tilde{\mathbf{G}}_S(\tilde{\boldsymbol{\xi}}) \qquad (7)$$

where ρ_o is the plasma mass density. This is a genuine eigenvalue equation for unrestricted displacements, taking all plasma forces into account. It is consistent with the starting points of the extended energy principle /2/, but not with its final formulation in which the contribution δW_S is being neglected. The latter and the corresponding term $\tilde{\mathbf{G}}_S$ in eq. (7) modify the eigenvalues and extremum values related to the total change δW in potential energy. The induced surface current effect is, of course, of equivalent importance also in the non-linear case of large displacements.

A crude estimate of the magnitude of the induced surface current effect is obtained from replacing all derivatives in eqs. (1) – (6) by equivalent characteristic lengths, i.e. $L_\xi = \tilde{\xi}/|\nabla\tilde{\xi}|$, $L_j = B_{jo}/|\nabla B_{jo}|$, $L_c = B_{co}/|\nabla B_{co}|$. We consider a toroidal system with the major and minor radii R and $\bar{a}$. When the wavelength spectrum of a perturbation includes large-scale parts for which L_ξ is comparable to a and L_c, the contribution δW_S cannot be neglected as compared to δW_V. This happens even in cases where the inhomogeneity of the external field $\mathbf{B}_{co}$ is rather small. It applies to ohmically heated low-beta tokamaks where $L_c \cong R$, $L_j \cong \bar{a}$ and $B_{jo}L_c/B_{co}L_j \leq 1$. It also applies to low-beta stellarators with an equivalent number of 2ι helical windings and a magnetic vacuum well of the order of one percent for which $L_c \cong \bar{a}B_{co}/B_{ho}(\iota - 1)$, i.e. when there is an average helical field strength $B_{ho} \cong 0.1\, B_{co}$ at the plasma surface.

Rigid Displacements in Toroidal Systems

We introduce a rectangular frame with z along the axis of a toroidal system, possibly having small deviations from exact axisymmetry. The external field $\mathbf{B}_{co} = \mathbf{B}_{cot} + \mathbf{B}_{cop}$ is assumed to have the toroidal and poloidal parts $\mathbf{B}_{cot}$ and $\mathbf{B}_{cop}$. The contribution δW_{Sj} from $\tilde{\mathbf{f}}_{Sj}$ in eqs. (2) and (5) represents an interaction between the total plasma current and the external field $\mathbf{B}_{co}$, whereas δW_{Sc} and $\tilde{\mathbf{f}}_{Sc}$ are due to the interaction between the induced surface current and $\mathbf{B}_{co}$. Rigid displacements $\tilde{\boldsymbol{\xi}} = \tilde{\boldsymbol{\xi}}_c = \underline{\text{const.}}$ yield $\tilde{\mathbf{F}}_V = 0$ and $\delta W_V = 0$ according to eqs. (1) and (3), i.e. $\delta W = \delta W_S$. Neglecting δW_S, as in conventional theory /2/, would thus lead to the paradoxical result of vanishing induced surface currents and $\delta W = 0$ for rigid plasma motion across an inhomogeneous external field $\mathbf{B}_{co}$.

For tokamaks axial (vertical) displacements $\tilde{\boldsymbol{\xi}}_c = \tilde{\xi}_c \mathbf{z}$ are of special interest. Then $(\tilde{\boldsymbol{\xi}}_c \cdot \nabla)\mathbf{B}_{co} = (\tilde{\boldsymbol{\xi}}_c \cdot \nabla)\mathbf{B}_{cop}$. The contribution δW_{Sj} for a "frozen-in" plasma body of finite size is similar to but not identical with that obtained from the simplified classical model, where the plasma is represented by a line current, and where a mirror-type component $\mathbf{B}_{cop}$ contributes to vertical stability /3/. However, there is also a contribution from

$$\delta W_{Sc} = (1/2\,\mu_o) \iiint \left[(\tilde{\xi}_c \cdot \nabla) \mathbf{B}_{co} \right]^2 dV \geq 0 \qquad (8)$$

In systems with a homogeneous imposed vertical field and no extra poloidal field, there is no vertical derivative of $\mathbf{B}_{co}$, i.e. $\delta W_S = 0$. More advanced systems with vertical inhomogeneities of $\mathbf{B}_{co}$ from additional sets of poloidal field coils will on the other hand be subject to an extra stabilizing effect due to eq. (8). This provides additional means for vertical position control of tokamaks with strongly elongated cross sections.

For low-beta stellarators the field $\mathbf{B}_{co}$ is inhomogeneous in all spatial directions. The contribution δW_{Sj} can be neglected since the current density $\mathbf{j}_o$ is then small in equilibrium. The contribution δW_{Sc} remains, and it is always stabilizing.

Non-Rigid Displacements in Toroidal Systems

The change δW_{Sc} in potential energy can in general be written as

$$\delta W_{Sc} = (1/4\,\mu_o) \iint u_S dS \qquad u_S = (\hat{\mathbf{n}} \cdot \tilde{\xi}) (\tilde{\xi} \cdot \nabla) B_{co}^2 \qquad (9)$$

Thus u_S becomes positive in regions of "good" magnetic curvature where B_{co}^2 increases in the direction of $\hat{\mathbf{n}}$, and negative in "bad" regions. The integrated effect of δW_{Sc} can therefore provide an additional stabilizing contribution in minimum-average-B geometry, when the displacements are coupled along the field lines in a collective mode. A particular case is that of the idealized low-beta isodynamic stellarator /4/ where the magnetic surfaces and the surfaces of the magnetic guiding centre drift coincide. Then there is even a local minimum-B well, $u_S > 0$ all over the plasma surface, and $\delta W_S \cong \delta W_{Sc} > 0$ for any displacement. This particular case demonstrates that the genuine eigenvalue equation (7) modifies the minimum (extremum) values of the potential energy change, as given by the extra contribution δW_S of eq. (2). Configurations which tend to approach this isodynamic limit belong to the Helias class of advanced stellarators /5/.

An example can finally be given on the external m = 1 kink mode in tokamaks. The minimizing eigenfunction of conventional MHD theory has earlier been deduced for a radial displacement $\xi_r = \xi_c \exp[i(m\theta - n\varphi - \omega t)]$ in a frame (r, θ, φ) with r as the distance from the magnetic axis of a tokamak with nearly circular plasma cross-section /6/. The first non-vanishing contribution from the work of the volume force $\tilde{\mathbf{F}}_V$ then becomes /6/

$$\delta W_V \cong (2\pi \bar{a} B_{\varphi o} \tilde{\xi}_c)^2 n \left[n - (1/q_a) \right] / \mu_o R \qquad (10)$$

where $B_{\varphi o}$ is the toroidal magnetic field strength at the magnetic axis and q_a the safety factor at the plasma surface. To get an indication of how this result is modified by the induced surface current effect, we introduce the contribution δW_S from the inhomogeneity of the toroidal field and of a superimposed magnetic octupole field having the moderate strength B_{oo} at the plasma surface. For the worst case n = 1 we then have $\delta W_{Sj} = 0$ and the total change in potential energy becomes

$$\delta W = (2\pi \bar{a} B_{\varphi o} \tilde{\xi}_c)^2 \left[(9/8) - (1/q_a) + (3/2)(RB_{oo}/\bar{a} B_{\varphi o})^2 \right] / \mu_o R \qquad (11)$$

corresponding to the stability condition

$$q_a > 1 / \left[1 + (1/8) + (3/2) (RB_{oo}/\bar{a} B_{\varphi o})^2 \right] \qquad (12)$$

The critical safety factor would then become reduced from $q_a = 1$ to $q_a = 8/9$ by the toroidal field inhomogeneity, and be further reduced by the octupole field. Needless to say, a rigorous determination of the critical q_a–values has to be made in terms of the eigenvalue equation (7) with the included force $\tilde{G}_S$.

Conclusions

For tokamaks, stellarators, and a number of other magnetic confinement schemes,

— MHD theory has to be revised by taking the induced surface current effect properly into account;

— there are several cases in which this effect is expected to provide new possibilities of stabilization and of lowering the critical safety factor.

References

/1/ B. Lehnert, Physica Scripta 10 (1974) 139; Plasma Phys. Contr. Fusion 33 (1991) 1757, 34 (1992) 1651 and 35 (1993, in press)

/2/ I.B. Bernstein, E.A. Frieman, M.D. Kruskal, R.M. Kulsrud, Proc. Roy. Soc. A 244 (1958) 17.

/3/ J.A. Wesson, Nuclear Fusion 18 (1978) 87.

/4/ D. Palumbo, Nuovo Cimento B 53 (1968) 507.

/5/ G. Grieger et al., Nuclear Fusion, Suppl. 2 (1989) 369.

/6/ J.P. Freidberg. Ideal Magnetohydrodynamics, Plenum Press, New York 1987, Ch. 9,.6.4.

MHD EQUILIBRIUM AND STABILITY OF DOUBLET CONFIGURATIONS

S. Medvedev*, L. Villard, L.M. Degtyarev*, A. Martynov*, R. Gruber** and F. Troyon

Centre de Recherches en Physique des Plasmas
Association EURATOM - Confédération Suisse,
Ecole Polytechnique Fédérale de Lausanne
21, Av. des Bains, CH-1007 Lausanne, Switzerland

* Keldysh Institute of Applied Mathematics, Russian Academy of Sciences, Miusskaya sq. 4, Moscow 135047, Russia

** R. Gruber, Gruppo Applicazione Scientifiche della Svizzera, Centro Svizzero di Calcolo Scientifico, Via Cantonale, CH-6928 Manno, Switzerland

1. The operational limits of tokamak configurations with single magnetic axis imposed by ideal MHD stability have been intensively studied in the last decade [1]. Much less efforts have been made to investigate plasmas with external separatrix [2]. On the other hand, plasmas with external separatrix are used in modern tokamaks to obtain better confinement. Doublet configurations with two magnetic axes and a separatrix inside the plasma may have different confinement properties than single axis tokamaks. Doublet tokamak configurations were tried experimentally [3] but were not studied in detail theoretically [4]. In order to determine the operational space of these configurations allowed by ideal MHD constraints, a package of equilibrium and stability codes has been developed with an appropriate treatment of the internal separatrix. Some stability results for $n = 0$ and $n = 1$ ideal MHD modes are presented.

2. The poloidal flux function $\psi(r,z)$ for an axisymmetric equilibrium magnetic field $B = \nabla\psi \times \nabla\phi + F(\psi)\nabla\phi$ satisfies the Grad-Shafranov equation:

$$\nabla \cdot \left(\frac{\nabla\psi}{r^2}\right) = -\frac{j_\phi}{r}, \qquad j_\phi = r\frac{dP}{d\psi} + \frac{1}{r}F\frac{dF}{d\psi}, \tag{1}$$

where $p(\psi)$ is the plasma pressure and $F(\psi)$ the toroidal flux function. To solve the equation one can prescribe the shape of the plasma boundary and the current density profile j_ϕ specifying either $dp/d\psi$ and $FdF/d\psi$ or $dp/d\psi$ and

$$I^*(\psi) = \frac{d}{d\psi}\left(\int_{S_\psi} j_\phi \, ds\right) \Big/ \frac{d}{d\psi}\left(\int_{S_\psi} ds\right). \tag{2}$$

The plasma domain is decomposed into three subdomains: two inside, and one outside the separatrix. In each subdomain a structured grid with quadrangular cells is introduced. We use a variational finite difference scheme that is the average of two finite element discretizations corresponding to two different triangularizations [5].

The mapping procedure is replaced with a grid adaptation scheme on magnetic surfaces $\psi = \text{const}$. This was already successfully used in a number of codes [5,6,7]. The iterative procedure combines grid adaptation and

Picard iterations on nonlinearity. The Grad-Shafranov equation with prescribed right-hand side is solved with an overrelaxation method. Then the hyperbolic x-point is determined and the separatrix is traced as $\psi = \psi_{x\text{-point}}$. In each of the subdomains a linear interpolation is used to match the grid points positions with magnetic surfaces. Flux functions $dp/d\psi$ and $FdF/d\psi$ or I^* are then updated on the new grid and the loop is repeated.

For code verification analytical solutions were used which are superpositions of Solev'ev and vacuum solutions :

$$\psi = \psi_0 - (r^2 - r_0^2)^2 + 4\alpha^2(r^2 - \sigma^2)z^2 + (a + br^2)\, z + c\cos(dz)\, r\, I_1(dr), \qquad (3)$$

$$dp/d\psi = 8(1 + \alpha^2), \qquad F\, dF/d\psi = -8\alpha^2\sigma^2.$$

In Fig. 1 the grid adapted to magnetic surfaces is shown for $\psi_0 = 0.6$, $r_0 = 1$, $\alpha = 0.6$, $\sigma = 0.3$, $a = 0$, $b = 0.1$, $c = 0.7$, $d = 2$. The external boundary is chosen to coincide with the external separatrix.

A convergence rate N^{-2} (N is the number of points in one direction) is achieved for the coordinates of magnetic surfaces and those of the magnetic axes. With grid packing near the separatrix the same rate can be reached for the x-point position also.

For characteristic up-down symmetric equilibria with $N_\psi = 64$, $N_\theta = 64$, (N_ψ, N_θ – number of points in radial and poloidal directions) inside separatrix and $N_\psi = 32$, $N_\theta = 64$ outside, 15 iterations are needed to reach an accuracy of 10^{-5} in ψ variations over the adapted grid. It takes 20 s on NEC SX-3/22 at 240 Mflops.

3. A variational formulation of the linearized ideal MHD equations is used for the stability code. The potential energy representation is based on the following displacement vector representation [8]:

$$\vec{\xi} = X\frac{\vec{D}\times\vec{B}}{B^2} + Y\frac{\vec{B}\times\nabla\psi}{B^2} + Z\frac{\vec{B}}{B^2}, \qquad (4)$$

where $\vec{B} = \nabla\psi \times \vec{D}$.

Flux coordinates (ψ,θ,ϕ) in each subdomain and finite hybrid elements are used to avoid spectral pollution [9]. The poloidal coordinate is not fixed by a choice of the Jacobian but is defined by the equilibrium grid. Some further modifications were introduced to improve code convergence: "spectral shift" elimination [9] and numerical destabilization correction [10]. In the vacuum region between the plasma and the conducting wall a "pseudodisplacement" approach [11] is used.

Inverse iteration and a direct matrix solver are used to find the eigenvalues. The solver is based on the PAMERA code [12] modified to treat connectivity conditions between subdomains and to exploit the banded structure of matrix blocks. The connectivity conditions at the x-point are written as $X = \xi \cdot \nabla\psi = 0$.

For grid dimensions inside $N_{\psi 1} = 128$, $N_{\theta 1} = 128$, $N_{\psi 2} = 128$, $N_{\theta 2} = 128$ and outside separatrix $N_{\psi 3} = 32$, $N_{\theta 3} = 256$ the computation of one eigenvalue takes 70s at 900 Mflops on a NEC SX-3.

4. In Fig. 2 the adapted grid is shown for an up-down symmetric equilibrium with vacuum (or pressureless currentless plasma) outside

separatrix. Note that the angle between separatrix branches is $\pi/2$ at the x-point. Stability of n = 0 and n = 1 external modes was computed for such type of equilibria. For n = 0 two unstable modes are present when the conducting wall is far from the plasma. The most unstable mode corresponds to displacements of upper and lower parts of the plasma in opposite directions (Fig. 3a). The mode with lower increment corresponds to mainly vertical displacement of the whole plasma (Fig. 3b). The distance wall-plasma boundary needed to stabilize n = 0 modes is about equal to the plasma minor radius for a wall shape similar to the external boundary. This distance is close to the value needed to stabilize a single axis plasma inside the separatrix taken alone (the elongation is 1.5 for the case considered).

Limiting β-values against n = 1 external mode were also computed for the case $I^*(\psi) = 1-\psi$, $q_o = 1.05$, aspect ratio of internal plasma 4.2, elongation of internal plasma 3.0. First, the ballooning marginally stable pressure profile was computed. Then $dp/d\psi$ was scaled to get n = 1 external mode stability. At marginal n = 1 stability we get $g \equiv \beta\, a\, B_o/\mu_o I_p = 3.5$. The limiting β -value against external n = 1 mode is barely effected by the presence of the mantle. Let us note that there are two unstable n = 1 modes with different increments even for an up-down symmetric doublet plasma corresponding to a single unstable mode in a single domain plasma. The two modes differ mainly in mode structure outside separatrix.

5. The validity of the developed codes was demonstrated with various convergence studies, checking against analytical solutions and benchmarking with other codes. Stability criteria for high-n ballooning and localized Mercier modes were implemented. Automatic pressure profile optimization against ballooning mode stability can also be performed. Preliminary studies of doublet configuration stability have shown that both n = 0 and n = 1 external modes are not more unstable than for a single plasma with nested mangetic surfaces and half the elongation. Future work should investigate doublet β-limits and n = 0 stability in more detail including the effect of up-down asymmetry.

Acknowledgement: This work was partly supported by the Swiss National Science Foundation.

References

1. F. Troyon et al., Plasma Phys. and Contr. Fusion **26** (1984) 209.
2. A. Roy and F. Troyon, 17th EPS Conf. on Contr. Fusion and Plasma Heating, Amsterdam, June 1990, **14B, Part II** (1990) 958.
3. J.C. Wesley et al., Proceedings of 8th IAEA Conf. on Plasma Physics and Contr. Fusion, Brussels 1980, **1** (1980) 35.
4. T.S. Wang, F.J. Helton, Comput. Phys. Commun. **24** (1981) 255.
5. L.M. Degtyarev, V.V. Drozdov, Computer Phys. Reports **2** (1985) 342.
6. D.E. Shumaker, J. Comput. Phys. **53** (1984) 456.
7. S. Semenzato, R. Gruber, H.P. Zehrfeld, Comput. Phys. Reports **1** (1984) 389.
8. F. Wysocki, R.C. Grimm, J. Comp. Phys. **66** (1986) 225.
9. R. Gruber, J. Comput. Phys. **26** (1978) 379.
   R. Gruber, J. Rappaz, Finite element methods in ideal linear magnetohydrodynamics. (Springer series in computational physics, Springer, 1985).
10. L.M. Degtyarev, S.Yu. Medvedev, Comput. Phys. Commun. **43** (1986) 29.
11. R. Gruber et al., Comput. Phys. Commun. **24** (1981) 363.
12. R. Gruber et al., Phys. Reports **207** (1991) 167.

Fig.1. Up-down asymmetric equilibrium with grid adapted to magnetic surfaces. Corresponds to the analytic solution Eq.(3).

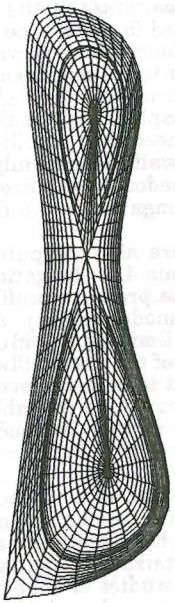

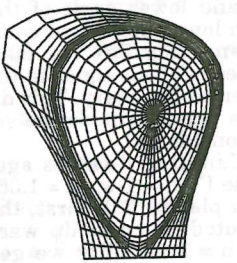

Fig.2. Up-down symmetric equilibrium with grid adapted to magnetic surfaces. The region outside separatrix is pressureless and currentless.

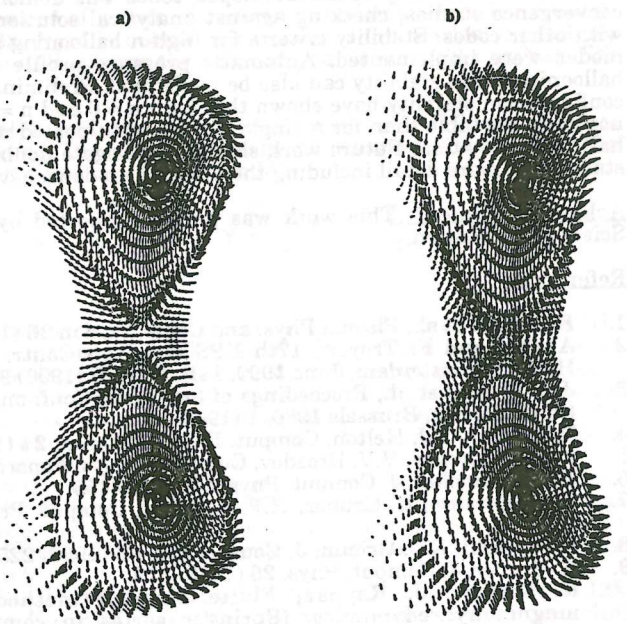

Fig.3. Displacement fields of n=0 modes for a wall far from plasma boundary; (a) most unstable mode, $\omega^2/\omega_A^2 = -10^{-2}$; (b) lower growth rate mode, $\omega^2/\omega_A^2 = -0.5\ 10^{-2}$.

IDEAS IN TOKAMAK CONCEPT IMPROVEMENT

W. A. Cooper and F. Troyon
Centre de Recherches en Physique des Plasmas,
Association Euratom-Confédération Suisse,
Ecole Polytechnique Fédérale de Lausanne,
Lausanne, Switzerland

It is experimentally observed that the transport properties of tokamak devices improve with the transformer-induced toroidal plasma current. For configurations in the parameter range of the ITER (International Tokamak Experimental Reactor) device, however, the toroidal current requirements predicted become very large ($25MA$). Steady state operation is impossible and disruption phenomena triggered by these currents could cause severe damage to the vacuum vessel and other systems of the device. It would be thus of great interest to devise a way to relax the toroidal currents needs without degrading the confinement properties. One possible approach that we propose here is the use of external helical windings to sustain a significant fraction of the edge rotational transform. The tokamak, however, ceases to be axisymmetric and becomes a three-dimensional (3D) configuration.

We consider here a circular cross section tokamak with finite toroidal current on which we impose a $L = 3$ external helical field to produce a triangular deformation of the plasma that rotates toroidally. The application of $L = 1$ or $L = 2$ components, or combinations thereof could also be considered. But we have decided to limit the scope of the study so far to $L = 3$ components motivated by the fact that this class of field only alters the external region of the plasma. The bulk of the plasma where the pressure concentrates remains essentially a conventional tokamak. The basic configuration has 8 periods and an aspect ratio $A = 10$, large enough to permit comparisons with analytic calculations. The plasma boundary is prescribed as

$$R = R_{00}(1) + R_{10}(1)cosu + \delta cos(u - Nv) + \delta cos(u - 3Nv), \quad (1)$$

$$Z = R_{10}(1)sinu + \delta sin(u - Nv) - \delta sin(u - 3Nv), \quad (2)$$

where $R_{00}(1) = 10$, $R_{10}(1) = 1$, $\delta = -0.055$ and $N = 8$. We use the VMEC equilibrium code [1] to compute 3D equilibria that selfconsistently model tokamaks with externally applied helical fields. This code imposes nested magnetic flux surfaces on the configurations investigated. The coordinate system is (s, u, v) where $0 \leq s \leq 1$ is the radial variable, $0 \leq u \leq 2\pi$ is the poloidal angle and $0 \leq v \leq 2\pi/N$ is the toroidal angle. The magnetic axis is at $s = 0$ and the plasma boundary is at $s = 1$. In order to calculate 3D tokamak equilibria, we must prescribe two surface functions. One is the pressure profile given by

$$p(s) = p(0)(1 - s - 0.5s^2 + 0.5s^4). \quad (3)$$

This choice makes the pressure gradients relatively weak in the outer region dominated by the stellarator fields. The toroidal plasma current enclosed within each flux surface

s is prescribed as

$$2\pi J(s) = \frac{8}{15}[2\pi J(0)]\left(s - \frac{2}{3}s^3 + \frac{1}{5}s^5\right). \quad (4)$$

The normalised toroidal current shown in the results is defined as $J(1)R_{10}(1)/\Phi(1)$, where $2\pi\Phi$ is the toroidal magnetic flux. The rotational transform profiles for a tokamak at $\beta^* = 1.55\%$ and normalised toroidal current equal to 0.0433 are shown for a case of an external $L = 3$ helical field ($\delta = -0.055$) and for the axisymmetric case ($\delta = 0$) in Fig. 1. This example illustrates the point that the bulk plasma is basically a conventional tokamak, while the stellarator fields provide the rotational transform support in the near force-free plasma edge. We define $\beta^* = (V \int d^3x p^2)^{1/2} / \int d^3x (B^2/2)$, where V is the plasma volume.

The TERPSICHORE package of codes [2] has been employed to investigate the Mercier, the ballooning and the global external ideal magnetohydrodynamic (MHD) stability properties of the 3D tokamaks under consideration. Within the parameter ranges that we have explored, the ballooning modes yield more restrictive criteria on local stability than the Mercier modes. The stability calculations are performed in the Boozer magnetic coordinate system [3] and the parallel current density is calculated to consistently satisfy the condition of charge conservation [4]. For the ballooning calculations, the spectrum of modes in the Boozer coordinate system includes poloidal mode numbers m upto 60. Nevertheless, we find that this is insufficient to correctly converge ballooning eigenstructures in the outer edge of the plasma where the stellarator fields dominate when the Shafranov shift approaches and exceeds 50% of the minor radius for cases with $\beta^* > 1.5\%$. Upto 84 mode pairs are employed to determine the stability to $n = 1$ modes. An axisymmetric conducting wall is placed at 3 times the average minor radius to simulate a wall at infinity. We find that for the configuration examined, the coupling between different toroidal modes within the $n = 1$ family [2] is weak. The calculations are performed on 48, 56, 68 and 96 radial intervals within the plasma. The number of interval in the vacuum region corresponds to 1/4 that within the plasma. The convergence is quadratic in the mesh size. In Fig. 2, we show the converged eigenvalue for $n = 1$ external modes as a function of the normalised toroidal current. Each curve corresponds to different values of the parameter β^*, ranging from 0.99% to 3.22%. The stability results we have obtained are summarised in Fig. 3. The dotted curve in the figure constitutes the Shafranov shift equal to half the minor radius in the normalised toroidal current and β^* parameter space. The domain above this curve corresponds to Shafranov shifts that are smaller and that below to shifts that are larger. Two regions of stable ballooning operation are obtained. In the high current region, the ballooning stability limits improve with increasing current This property characterises typical operation in the first stability regime of a conventional tokamak. The region is limited from above in the figure by the emergence of the $q = 1$ surface from the magnetic axis. In the lower current ballooning stable region, we find that for fixed β^*, the stability properties improve with decreasing plasma current. This would characterise operation in a second stable regime. However, as the current decreases, the Shafranov shift becomes increasingly large, leading eventually to convergence difficulties in the equilibrium and stability computations. The external $n = 1$ global ideal modes yield a more restrictive limit than the ballooning modes, as shown by the solid curve in Fig. 3. For $\beta^* > 1.5\%$, the limit imposed by the external modes is closely aligned with

a Shafranov shift of half the minor radius. The stable domain lies below the curve. One important difference with the conventional tokamak second stability operation is that a second stable window for the $n = 1$ modes is demonstrated here with a wall far from the plasma [5].

In conclusion, we have investigated the ideal MHD stability limits of a tokamak device of aspect ratio 10 and circular cross section on which we have superimposed a $L = 3$ external helical field to reduce the plasma current required to sustain the rotational transform at the edge of the plasma at finite β. We have demonstrated that the helical fields and the plasma current combine to permit access to the tokamak second stable regime, where not only the ballooning modes but also the $n = 1$ external modes are stabilised. For values of $\beta^* > 1.5\%$, the limit imposed by the $n = 1$ modes almost coincides with a Shafranov shift of half the minor radius.

REFERENCES

[1] S. P. Hirshman and O. Betancourt, *J. Comput. Phys.* **96** (1991) 99.
[2] D. V. Anderson, W. A. Cooper, R. Gruber, S. Merazzi and U. Schwenn, *Int. J. Supercomp. Appl.* **4** (1990) 34; W. A. Cooper, G. Y. Fu R. Gruber, S. Merazzi, U. Schwenn, D. V. Anderson, *Proc. Joint Varenna – Lausanne Int. Workshop on Theory of Fusion Plasmas* (Editrice Compositori, Bologna) (1990) 655.
[3] A. H. Boozer, *Physics Fluids* **23** (1980) 904.
[4] J. Nührenberg, R. Zille, *Proc. Joint Varenna – Lausanne Int. Workshop on Theory of Fusion Plasmas* (Editrice Compositori, Bologna) (1988) 3.
[5] S. C. Jardin, A. Bhattacharjee, A. Bondeson, M. S. Chance, S. C. Cowley et al., *Proc. 14th Int. Conf. Plasma Phys. Contr. Nucl. Fusion* IAEA-CN-56/D-4-13, Würzburg, FRG 1992.

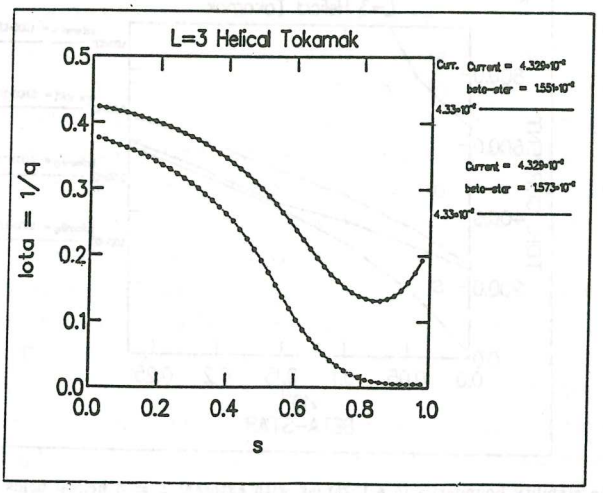

Figure 1: The rotational transform profiles in tokamaks with external $L = 3$ helical windings (upper curve, $\delta = -0.055$) and without them (lower curve, $\delta = 0$). The normalised toroidal current is 0.0433 and $\beta^* = 1.55\%$ in both cases.

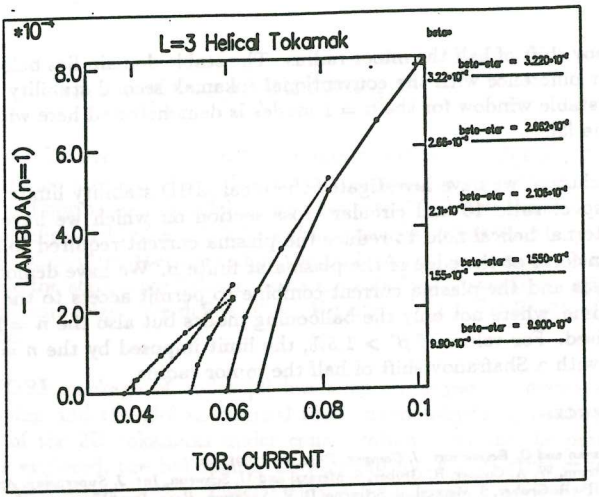

Figure 2: The converged eigenvalue of external $n = 1$ modes with conducting wall at infinity for a tokamak with $L = 3$ helical windings as a function of the normalised toroidal current. The curves correspond to values of the parameter β^* of 0.99%, 1.55%, 2.106%, 2.662% and 3.22% from low current to high current.

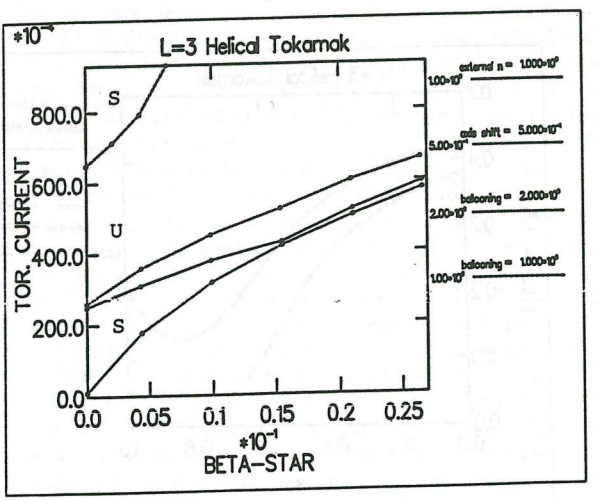

Figure 3: The stability boundaries in a tokamak with external $L = 3$ helical fields in the parameter space of normalised toroidal current versus β^*. The dashed curve that bounds the upper left hand corner constitutes the first ballooning stable domain. The region below the other dashed curve constitutes the second ballooning stable domain. The region below the solid curve is stable to $n = 1$ external modes. The domain above the dotted curve has a Shafranov shift smaller than half the minor radius.

A MULTIPLE TIMESCALE APPROACH APPLIED TO TAYLOR'S THEORY

J. W. Edenstrasser & M. M. M. Kassab*)
Institute for Theoretical Physics, University of Innsbruck, Austria.

Abstract

A multiple timescale derivative expansion is applied to Taylor's theory of plasma relaxation to the state of minimum magnetic energy, in particular to investigate his famous conjecture concerning the helicity conservation $K = \int \mathbf{A}.\mathbf{B}\, d\tau = const.$ *for a 'slightly imperfect' plasma. The invariance properties of the helicity integral K are investigated on the ideal MHD (Alfvén), collision, and resistive diffusion timescales. On the ideal MHD timescale it is found, just as expected, that K is an invariant of motion for each single flux tube. On the collision timescale Taylor's conjecture that only the overall K is an invariant of motion is explicitly proven. Finally, for the resistive diffusion timescale it turns out that – in accordance with Taylor and Woltjer – the time derivative is proportional to the resistivity apart from an additional contribution arising from the MHD fluctuation spectrum.*

INTRODUCTION

Many theories have been presented to describe plasma relaxation processes, the most famous of which, however, is the one presented by J.B.Taylor [1,2]. Taylor's theory states that, after an initial violently unstable phase the plasma relaxes, under the topological constraint of helicity conservation $K = \int \mathbf{A}.\mathbf{B}\, d\tau = \text{constant}$, into a quiescent, grossly stable state of minimum magnetic energy. Since for an ideal plasma, the magnetic field lines are frozen to the plasma, i.e., each field line maintains its own identity, Taylor concluded that K represents an infinity of topological constraints, in the sense that K is conserved for each flux tube. Furthermore, he concluded that for a 'slightly nonideal' plasma, in the sense that the topological properties of the field lines are no longer preserved, the global K is the only topological invariant of motion.

In spite of the success of Taylor's theory, there remain some important questions to be answered. First of all, what does a *'slightly imperfect'* plasma mean and what are the dominant physical processes which destroy the infinity of ideal MHD (IMHD) invariants of motion preserving the overall K as the only one and furthermore what are the corresponding timescales. In this paper, we answer this question on the basis of the multiple timescale approach presented by J.W.Edenstrasser [3]. The invariance property or the time evolution of the helicity integral K is investigated on the IMHD (Alfvén), on the collision, and on the resistive diffusion timescale.

*) *On leave from the Dept. of Eng. Physics, Cairo University.*

BASIC EQUATIONS

Following Ref.[3] we consider the three timescales $\tau_0 = \tau(\text{Alfvén})$, $\tau_1 = \tau(\text{collision})$, and $\tau_2 = \tau(\text{resistive diffusion})$, satisfying for a present–day large fusion device the ordering $\tau_0 \ll \tau_1 \ll \tau_2$, and apply the following multiple timescale derivative expansion scheme :

$$Q = \sum_{n=0} \delta^n Q_n(\mathbf{x},t_0,t_1,t_2) \ , \quad \frac{\partial}{\partial t} = \sum_{n=0} \delta^n \frac{\partial}{\partial t_n}, \quad \text{and} \quad \delta := \frac{\tau_0}{\tau_1}, \tag{1}$$

where Q stands for any dimensionless physical quantity. This expansion scheme is then applied to the dimensionless Maxwell's equations

$$\text{curl } \mathbf{B} = \mathbf{J} + L\frac{\partial \mathbf{E}}{\partial t}, \ \text{div } \mathbf{B} = 0, \ \text{curl } \mathbf{E} = -\frac{\partial \mathbf{B}}{\partial t}, \ \text{div } \mathbf{E} = L^{-1} q$$
$$\mathbf{E} = -\frac{\partial \mathbf{A}}{\partial t} - \nabla X, \ q = n_i - n_e, \ L := (v_a/c)^2 \simeq O(\delta^2), \tag{2}$$

and to Ohms' law, whereupon we obtain for each order of the expansion parameter δ a separate set of equations . For example, the equations for Ohm's law read

$$\mathbf{E}_0 = -\mathbf{U}_0 \times \mathbf{B}_0 \quad (3) \qquad \mathbf{E}_1 = -\left[\mathbf{U}_0 \times \mathbf{B}_1 + \mathbf{U}_{1x} \times \mathbf{B}_0 + \left\{\frac{\delta_e}{\delta_i}\right\}^{\frac{1}{2}}(1/a_e)(\nabla P_{e0}/n_0)\right] \quad (4)$$

$$\mathbf{E}_2 = -\Big[\ \mathbf{U}_0 \times \mathbf{B}_2 + \mathbf{U}_{1x} \times \mathbf{B}_1 + \left\{\frac{\delta_e}{\delta_i}\right\}^{\frac{1}{2}}(n_{e1}/n_0)\{\mathbf{U}_{1x} \times \mathbf{B}_0 + \left\{\frac{\delta_e}{\delta_i}\right\}^{\frac{1}{2}}(1/a_e)(\nabla P_{e0}/n_0)\}$$
$$+ \mathbf{U}_{2x} \times \mathbf{B}_0 + \left\{\frac{\delta_e}{\delta_i}\right\}[(1/a_e)\ ((\nabla \cdot \Pi_{i1} + \nabla P_{i1})/n_0) - \Lambda_e \langle \mathbf{V} \rangle_e]\Big], \quad \text{with}$$
$$\mathbf{U}_{nx} = \left\{\left\{\frac{\delta_e}{\delta_i}\right\}^{\frac{1}{2}}\right\}^n (n_{in}/n_0)(\ \mathbf{U}_{in} - \mathbf{U}_0\ ) \quad \text{and} \quad \langle \mathbf{V} \rangle_e = -\eta_0 \mathbf{J}_0. \tag{5}$$

For non standard notations the reader is referred to Ref.[3].

Boundary Conditions

(a) At the magnetic flux surface $\Psi = \Psi_0 + \delta\Psi_1 + \delta^2\Psi_2 = \text{const.}$

$$(\mathbf{B}_0 + \delta\mathbf{B}_1 + \delta^2\mathbf{B}_2)\cdot\nabla(\Psi_0 + \delta\Psi_1 + \delta^2\Psi_2) = 0, \tag{6.a}$$
$$(\mathbf{B}_0 + \delta\mathbf{B}_1 + \delta^2\mathbf{B}_2)\cdot(d\mathbf{s}_0 + \delta d\mathbf{s}_1 + \delta^2 d\mathbf{s}_2) = 0. \tag{6.b}$$

(b) At the perfect conducting wall surrounding the plasma:

$$\mathbf{B}_n \cdot d\mathbf{S} = 0 \ \ \& \ \mathbf{U}_{in} \cdot d\mathbf{S} = 0 \ \ \& \ \mathbf{U}_{en} \cdot d\mathbf{S} = 0 \ . \tag{6.c}$$

THE INVARIANCE OF THE LOCAL HELICITY ON THE ALFVEN TIMESCALE

According to our expansion scheme we can write the local helicity K for each single flux tube in the form

$$K^\Psi = \int_{\Psi} (\mathbf{A}_0 + \delta\mathbf{A}_1 + \delta^2\mathbf{A}_2)\cdot(\mathbf{B}_0 + \delta\mathbf{B}_1 + \delta^2\mathbf{B}_2)\ (d\tau_0 + \delta d\tau_1 + \delta^2 d\tau_2), \tag{7}$$

where $d\tau = (d\tau_0 + \delta\, d\tau_1 + \delta^2\, d\tau_2)$ is a volume element enclosed between two neighbouring magnetic surfaces $\Psi = \Psi_0 + \delta\Psi_1 + \delta^2\Psi_2 = \text{const.}$, created by the magnetic field $\mathbf{B}_0 + \delta\mathbf{B}_1 + \delta^2\mathbf{B}_2$. The application of the multiple timescale expansion [3] then

yields in leading order the time evolution of the local K on the IMHD timescale

$$\frac{\partial K^{\Psi}}{\partial t}_0 = \int A_0 \cdot \frac{\partial B_0}{\partial t}_0 d\tau_0 + \int B_0 \cdot \frac{\partial A_0}{\partial t}_0 d\tau_0 + \int (A_0 \cdot B_0) \frac{\partial \tau_0}{\partial t_0} . \quad (8)$$

Making use of the zero–order Maxwell's equations and zero–order Ohm's law we obtain

$$\frac{\partial K^{\Psi}}{\partial t}_0 = \int A_0 \times E_0 \cdot ds_0 - 2\int B_0 \cdot E_0 d\tau_0 + \int B_0 . \nabla X_0 \, d\tau_0 + \int (A_0 \cdot B_0) \, U_0 \cdot ds_0 \equiv 0 . \quad (9)$$

This means that for the IMHD timescale we have obtained the result of Taylor, i.e., that K is conserved for each single flux tube. If we assume that the plasma is surrounded by a rigid, perfectly conducting wall so that the plasma boundary is identical with the outermost magnetic surface, then naturally also the overall K taken over the whole plasma volume is an invariant of motion.

THE INVARIANCE OF THE GLOBAL "K" ON THE COLLISION TIMESCALE

First, we will investigate the time evolution of the local K for a single flux tube. The next order in our expansion scheme yields for the time derivative on the collision timescale the expression

$$\begin{aligned} \frac{\partial K^{\Psi}}{\partial t}_1 = & \oint A_0 \times E_0 \cdot ds_1 - 2 \int B_0 \cdot E_0 \, d\tau_1 + \int B_0 \cdot \nabla X_0 \, d\tau_1 + \oint A_0 \times E_1 \cdot ds_0 - \\ & 2\int B_0 \cdot E_1 \, d\tau_0 + \int B_0 \cdot \nabla X_1 \, d\tau_0 + \oint A_1 \times E_0 \cdot ds_0 - 2\int B_1 \cdot E_0 \, d\tau_0 + \\ & \int B_1 \cdot \nabla X_0 \, d\tau_0 + \int (A_0 \cdot B_0)\left(\frac{\partial \tau_0}{\partial t_1} + \frac{\partial \tau_1}{\partial t_0}\right) + \int (A_0 \cdot B_1 + A_1 \cdot B_0) \frac{\partial \tau_0}{\partial t_0} . \end{aligned} \quad (10)$$

We now perform the time average over the Alfvén scale ,assume that the plasma behaves along the field lines like a polytropic medium, i.e., that $\nabla P_{e0}/n_0$ can be considered as the gradient of a function of n_0, $\nabla P_{e0}/n_0 = \nabla f(n_0)$, and finally arrive after some tedious manipulations at the following surface integrals taken at the zero–order surface $\Psi_0 = \text{const.}$

$$\left\langle \frac{\partial K^{\Psi}}{\partial t}_1 \right\rangle_{\tau_0} = \left\langle \oint [\frac{\partial A_0}{\partial t}_1 \times A_0] \cdot ds_0 + \left\{\frac{\delta_e}{\delta_i}\right\}^{\frac{1}{2}} \oint \frac{n_{i1}}{n_0} U_{i1} (A_0 \cdot B_0) \cdot ds_0 - \oint (A_0 \cdot B_0) B_1 \cdot ds_0 \right\rangle_{\tau_0} \neq 0 \quad (11)$$

Thus, we conclude that the *local K is* on the collision timescale *no more an invariant of motion*, whereby the violation is essentially due to the radial first order electrical, magnetic and ion particle fluxes. On the other hand, from the boundary conditions (6) we further conclude, that the *global K remains an invariant of motion* Thus we have explicitly proven that Taylor's famous conjecture is valid for the collision timescale .

EVOLUTION OF THE GLOBAL "K" ON THE RESISTIVE DIFFUSION SCALE

Due to the resistivity the magnetic field lines no longer preserve its topological properties, so that it is meaningless to investigate K for each flux surface. In this

section we investigate the global K taken over the whole plasma volume and first obtain

$$\frac{\partial K^w}{\partial t}_2 = \oint \mathbf{A}_0 \times \mathbf{E}_2 \cdot d\mathbf{S} - 2\int \mathbf{B}_0 \cdot \mathbf{E}_2 \, d\tau + \int \mathbf{B}_0 \cdot \nabla X_2 \, d\tau + \oint \mathbf{A}_1 \times \mathbf{E}_1 \cdot d\mathbf{S} - 2\int \mathbf{B}_1 \cdot \mathbf{E}_1 \, d\tau + \int \mathbf{B}_1 \cdot \nabla X_1 \, d\tau + \oint \mathbf{A}_2 \times \mathbf{E}_0 \cdot d\mathbf{S} - 2\int \mathbf{B}_2 \cdot \mathbf{E}_0 \, d\tau + \int \mathbf{B}_2 \cdot \nabla X_0 \, d\tau \qquad (12)$$

Now we assume that all zero order quantities are independent from t_0, i.e., that the plasma has on the Alfvèn timescale already relaxed to the zero–order equilibrium and that the first order quantities have a harmonic t_0–dependence and then perform the time averages over the IMHD and collision timescales, leading us to the final result

$$\langle \frac{\partial K^w}{\partial t} \rangle_{\tau_{0,1}} = \langle \oint \mathbf{A}_1 \times \mathbf{E}_1 \, d\mathbf{S} - 2\int \mathbf{B}_1 \cdot \mathbf{E}_1 \, d\tau \rangle - \left\{\frac{\delta_e}{\delta_i}\right\} \Lambda_e \langle \oint \mathbf{A}_0 \times \eta_0 \mathbf{J}_0 \, d\mathbf{S} + \int \mathbf{B}_0 \cdot \eta_0 \mathbf{J}_0 \, d\tau \rangle_{\tau_{0,1}} \qquad (13)$$

The first two terms in Eq.(13) represent the contribution arising from the MHD fluctuation spectrum, whereas the third term is the one found by Centen [4], and finally the fourth one represents the well known result found by Woltjer [5]. This means, that on the resistive diffusion timescale $\langle \frac{\partial K}{\partial t} \rangle$ is proportional to the resistivity η_0, apart from an additional fluctuation term.

SUMMARY

A multiple timescale approach has been applied to investigate the invariance of the helicity K in Taylors relaxation theory. On the IMHD timescale the known results were reproduced. At the collision timescale we have proven Taylor's conjecture concerning the local and overall helicity for a 'slightly nonideal' plasma. On the resistive timescale we have not only found the known proportionality between the time dependence of K and the resistivity, but have furthermore shown the contribution arising from the IMHD fluctuation spectrum and the one arising from the time evolution on the collision timescale.

REFERENCES

(1) J.B.Taylor, Phys. Rev. Lett. 33, 1139 (1974).

(2) J.B.Taylor, Proc. of the Third Topical Conf. on Pulsed High Beta Plasmas, ed. by D.E.Evans, Pergammon Press, 1976, p. 59.

(3) J.W.Edenstrasser, Proc. Intern. Workshop on Plasma Physics, Pichl, 1992, Austria

(4) P.G.M.Centen, Ph.D.thesis,1984, University of Eindhoven,The Netherlands.

(5) L.Woltjer, Rev. Mod. Phys., 32, 914 (1960).

This work was supported in part by the Austrian Science Foundation (FWF) under contract P 8105 – PHY

PLASMA RELAXATION and CURRENT REVERSE in TOKAMAK

V.I. Petviashvili

Russian Research Center Kurchatov Institute, Moscow,123182

ABSTRACT: Turbulent relaxation of a plasma is described in terms of Lyapunov theory of stability of dissipative systems. The turbulence itself is supposed to disappear at the end of relaxation, when stable state is reached. The state corresponds to the minimum of Lyapunov functional L proposed in [1]. The relaxed equilibrium states are found with the considerable pressure maximum inside the plasma. They correspond to Tokamak or toroidal pinch type of configuration. Arnold's restriction of equivalent vorticity is needed to have minimal L for tokamaks.

1.The tenet of turbulent relaxation in plasma devices was advanced by J.B.Taylor [2]. According to it, the turbulence, reconnecting magnetic field lines, changes plasma equilibrium structurally, directing it to the relaxed state. Turbulence ceases at the relaxed state because the state is stable. The relaxed states obtained in [2] are force -free, with zero pressure.

We show here that Lyapunov's functional L, proposed in [1] for ideal plasma, can be used for description of turbulent relaxation. The relaxed states obtained are of Tokamak or toroidal pinch type, with rather high pressure in the center. These are well organized structures, with minimal freedom in distribution of parameters. The similarity of L with free energy in thermodynamics can be seen: The state with minimal L is stable.

The simple way to obtain L is to assume incompressibility of plasma flow. This allows to apply Arnold's theorem about foliation of phase space of vector functions satisfying the freezing-in equation. This imposes reasonable restriction on variations, so the minimum of L on the Arnold's leaf may give

tokamak
-type configuration. As was shown in [1] the minimum of L with no restrictions on variations gives toroidal pinch configurations only.

2.We start from MHD equations for incompressible plasma:

$$\rho(\partial_t \underline{v}+\underline{v}\cdot\nabla\underline{v})=-\nabla p+\underline{j}\times\underline{B}; \quad \underline{j}=\nabla\times\underline{B}/4\pi; \qquad (1)$$

$$\partial_t\rho+\underline{v}\cdot\nabla\rho=0; \quad \nabla\cdot\underline{v}=0 ; \qquad (2)$$

$$\partial_t\underline{B}=\nabla\times(\underline{v}\times\underline{B})+\nabla\times\underline{T}; \quad \nabla\cdot\underline{B}=0 ; \qquad (3)$$

$\underline{T}$ is the operator of turbulent dissipation, which may include the α-effect of turbulent dynamo theory and turbulent viscozity. Introducing the vector -potential $\underline{A}$ we obtain from (3):

$$\partial_t\underline{A}+\nabla(\underline{v}\cdot\underline{A})=\underline{v}\times\underline{B}+\underline{T} ; \quad \underline{B}=\nabla\times\underline{A} . \qquad (4)$$

Arbitrary potential vector function here is chosen in a way to make $\underline{A}$ frozen in plasma, along with $\underline{B}$, if $\underline{T}=0$. The density of helicity h is frozen as well then, satisfying the equation of continuity, the consequence of (3,4):

$$\partial_t h+\underline{v}\cdot\nabla h=0 ; \quad h=\underline{A}\cdot\underline{B}; \quad \text{if } \underline{T}=0. \qquad (5)$$

We take L as a sum of integrals of motion of (1-5), when $\underline{T}=0$

$$L=E+I_f; \quad E=\int(\rho v^2/2+B^2/8\pi)d^3\underline{x}; \quad I_f=\int f(h)d^3\underline{x} ; \qquad (6)$$

Here E is energy, I_f is helicity integral, f is arbitrary function [1]. The plasma equilibrium is stable if it corresponds to the extremum point $\delta L=0$ and minimum condition $\delta^2L>0$ is fulfield. Equation for extremum of (6) is:

$$\underline{j}+2f'\underline{B}=\underline{A}\times\nabla f'; \quad \underline{v}=0; \quad f'=d_h f. \qquad (7)$$

We have from (1,7):

$$\nabla p=\underline{j}\times\underline{B}; \quad \underline{B}\cdot\nabla h=0; \quad \underline{A}\cdot\underline{j}=-2f'h. \quad p=\int hf''dh=hf'-f+\text{const}. \qquad (8)$$

This means that p, $h=\underline{A}\cdot\underline{B}$ and $\underline{A}\cdot\underline{j}$ are constants on magnetic surfaces. These last conditions select from the set of general equilibrium states (first eq.(8)) very small subset satisfying (7) which are stable if $\delta^2L>0$. If $\nabla f'=0$ the current is parallel to $\underline{B}$ and p=0 (force -free equilibrium [2]). The function f(h) alone determines distribution of p and $\underline{B}$ by (7) along with proper boundary conditions.

3. If $\underline{T}\neq 0$ we have from (1-4) and (7):

$$d_tL=\int(\underline{j}+2f'\underline{B}-\underline{A}\times\nabla f')\cdot\underline{T}\, d^3\underline{x}; \quad d_tL|_e=0, \quad L|_e=\text{const}. \qquad (9)$$

Index e here means substitution of extremum (7). The boundary effects are neglected here. In the vicinity of extremum (7) energy is decreasing and helicity integral I_f is growing. The rate of change depends not only on scales of turbulence but on

orientation of the vector $\underline{T}$ too. In view of (9) the states (7) can be attractors if other conditions of Lyapunov stability

$$d_t L \le 0; \quad L>L_e \Rightarrow \delta^2 L>0. \qquad (10)$$

are fulfilled in vicinity of them. For the simplest model

$$\underline{T} \approx -\delta\underline{A}/\tau; \quad \delta\underline{A}=\underline{A}-\underline{A}_e; \quad \tau>0, \qquad (11)$$

($\underline{A}_e$ is the solution of (7), τ is time of turbulent relaxation) where the vanishing of turbulence at extremum is assumed, we have from (9):

$$d_t L \approx -\delta^2 L/\tau; \qquad (12)$$

This indicates the condition for point (7) to be attractor: it should be the minimum of L i.e. the inequality $\delta^2 L>0$ is needed. Similar conditions can be derived for more complex forms of $\underline{T}$.

4.The last stability condition (10) will be considered here. From (6,7) we obtain:

$$\delta^2 L=\int(\rho\delta v^2/2+\delta B^2/8\pi+f'h_2+f''h_1^2/2)d^3\underline{x} >0, \qquad (13)$$

where

$$h_1=\underline{A}\cdot\delta\underline{B}+\underline{B}\cdot\delta\underline{A}; \quad h_2=\delta\underline{A}\cdot\delta\underline{B}; \quad \delta\underline{B}=\nabla\times\delta\underline{A};$$

The necessary condition for positivly definiteness of (13) for arbitrary $\delta\underline{A}$ is $f''>0$. This can not be met in Tokamak -type solutions of (7) [1]. In this case (13) can be positive only for the restricted set of $\delta\underline{A}$. One consequence of freeze -in equations (3,4) may serve as the natural restriction. According to [3] variations of $\underline{A},\underline{B}$ for arbitrary $\underline{v}$ and time t are located on a certain leaves, invariant relative (3,4), if $\underline{T}=0$. Arnold proposed to look for minima of Lyapunov functional on the leaf. Small variations in this case have the form [3]:

$$\delta\underline{B}=\underline{B}_1+\underline{B}_2+0(\xi^3); \quad \underline{B}_1=\nabla\times(\underline{\xi}\times\underline{B}); \quad \underline{B}_2=\nabla\times(\underline{\xi}\times\underline{B}_1)/2; \quad \nabla\cdot\underline{\xi}=0; \qquad (14)$$

where $\underline{\xi}(\underline{x})$ is arbitrary vector function, meaning virtual displacement. After this it follows from (5) that

$$\delta h=h_1+h_2+0(\xi^3); \quad h_1=-\underline{\xi}\cdot\nabla h; \quad h_2=-\underline{\xi}\cdot\nabla h_1/2, \qquad (15)$$

and this gives: $h(\underline{x})+\delta h \cong h(\underline{x}+\underline{\xi})$. Substituting (14,15) into (13) we obtain the reduced condition of stability:

$$\delta^2 L_\xi \ge W>0; \quad W[\underline{\xi}]=\int(B_1^2/2+\underline{B}\cdot\underline{B}_2)d^3\underline{x}/4\pi, \qquad (16)$$

the index ξ here means that variation is carried on Arnold's invariant leaf. W coincides with potential energy in energetical principle of linearized equations of incompressible MHD. So equilibrium states in Tokamaks to be attractors require to satisfy (7,8) and be stable in linear approximation.

5.The condition that current density is 0 at the boundary of plasma can be satisfied if

$$f'|_b=0; \quad \nabla f'|_b=0 \qquad (17)$$

at the boundary. This follows from (7). The parallel current changes direction in the periphery of plasma into solutions of (7) with such f [4]. The reversed current amounts from few to 30% of direct current. The upper limit is reached when direct current is close to bootstrap current.

The reverse current may occur in experiments when external toroidal electric field is put off. Generation of reversed current in the plasma periphery may improve plasma confinement in Tokamaks.

6.The safety factor and absolute value of helicity are growing in Tokamaks and decrease in toroidal pinches from plasma center to the boundary. In the toroidal pinch -type solutions f can not satisfy (17) because of this. So the parallel current is not exactly 0 at the boundary of them.

In the pinch-type solutions of (7), with sufficiently high pressure in the center, the toroidal current may not change direction when toroidal magnetic field is reversed near the boundary. The favorable feature of the pinches is: L may be minimal in toroidal pinches without any restriction on $\delta\underline{A}$. That means (13) may be positively definite for some f with $f''>0$.

Making plasma configuration close to some solution of eq.(7), which satisfy (16) or last inequality (10)), may improve the confinement of thermal energy.

REFERENCES

1.V.A. Gordin,V.I. Petviashvili//Sov.Phis.JETP,1989,v.68,p.988.
2.J.B. Taylor//Phys. Rev. Lett., 1974. v.33. p.1139.
3.V.I. Arnold//J. Appl. Math. Mech., 1965, v.29, p.1002.
4.V.I. Petviashvili//Sov. Phys. JETP Lett., 1993, v.57, № 2.

Pressure and Inductance Effects on the Vertical Stability of Shaped Tokamaks

D. J. Ward, A. Bondeson, F. Hofmann,
Centre de Recherches en Physique des Plasmas,
Association Euratom–Confédération Suisse, EPFL, Lausanne

In previous work [1] it was shown that the combination of triangularity and high β_p is strongly stabilizing for axisymmetric modes in highly elongated ($2.5 < \kappa < 3.0$) tokamak plasmas. The effect of pressure in dee shaped plasmas reduces the driving energy of the instability. In contrast, in an inverse-dee pressure is highly destabilizing. In a pure ellipse pressure has a negligible effect on the free space growth rate, but is somewhat stabilizing in the presence of a resistive or ideal wall. The purpose of the present note is to extend the study of shape and profile effects to cross-sections of moderate elongation in the range $1.6 \leq \kappa \leq 2$.

The primary results from Ref. [1] are shown in Fig. 1. Here an upper limit on the growth rate of the vertical instability is specified (such an upper limit is imposed by limitations of the active feedback system), and we find that the stability boundary in terms of the operational parameters l_i and β_p is very nearly linear. This boundary defines a region of stability (toward low l_i and high β_p) for a given shape of the plasma cross section. This stability boundary is nearly independent of the details of the current profile, and also independent of the aspect ratio if the boundary is plotted in terms of l_i vs. $\epsilon\beta_p$. We see from Fig. 1 that the slope of this boundary increases strongly with increasing triangularity, and decreases with increasing elongation.

Here we present some first results from a comprehensive study of the effects of triangularity, pressure, and profile effects in moderately shaped ($\kappa = 1.6$–2.0) tokamak plasmas surrounded by a resistive wall. These results again show the stabilizing effect of triangularity and pressure.

The resistive wall stability calculations are performed using the NOVA-W [2] stability code with equilibria calculated using the CHEASE equilibrium code [3]. For the cases shown in Figs. 2 & 3, the resistive wall is specified to be conformal to the plasma shape, and to be at a distance from the plasma at the midplane of 1.4 times the plasma minor radius, $d = 1.4a$. The resistive wall has a ratio of resistivity to wall thickness of $\eta/\delta_w = 4 \times 10^{-5}\Omega$.

The plasma–vacuum boundary is specified as

$$R/a = A + \cos(\theta + \delta \sin\theta + \lambda \sin 2\theta) \quad , \quad Z/a = \kappa \sin\theta \tag{1}$$

where κ is the elongation, δ is the triangularity, and λ is a squareness parameter (used in some of the cases shown in Fig. 1). The following definitions are used for the poloidal beta, $\beta_p \equiv (4/\mu_0 I_p^2 R_0) \int_{pl} p \, d^3x$, and internal inductance, $l_i \equiv (2/\mu_0^2 I_p^2 R_0) \int_{pl} B_p^2 \, d^3x$.

Figure 2 shows results for equilibria with elongation $\kappa = 1.8$ for several different values of triangularity ranging from $\delta = 0$ to $\delta = 0.5$. The resistive wall growth rate γ (in s^{-1}) is plotted vs. β_p. For each value of triangularity two pressure profile specifications are used: one peaked, with pressure peaking factors $PPF \approx 3.3$, and one relatively flat, with $PPF \approx 2$. The same current profile is specified for all cases in this figure yielding $l_i \approx 0.75$.

Figure 2 shows the stabilizing effect of high β_p in all cases except for the pure ellipse with a peaked pressure profile. This stabilizing effect increases strongly with triangularity. Only at very low values of β_p do the high-triangularity equilibria have higher

Figure 1

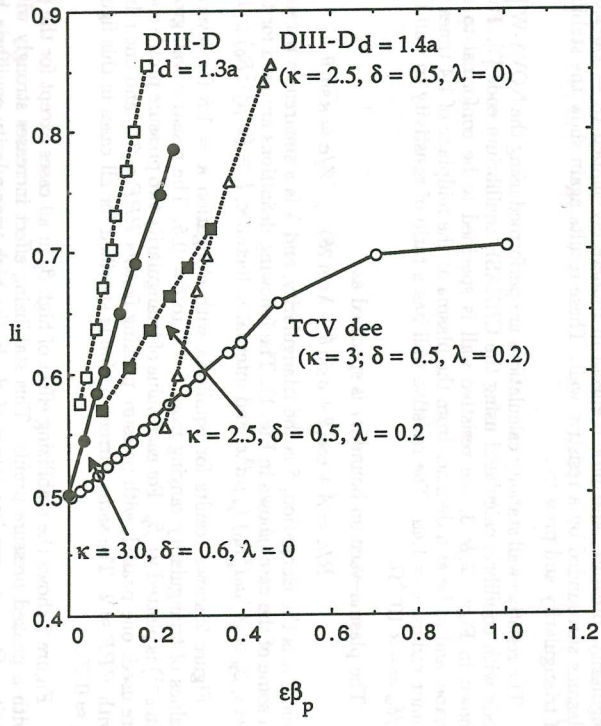

Figure 2

(1)-> flat pressure profile
(2)-> peaked pressure profile

κ = 1.8 d / a = 1.4

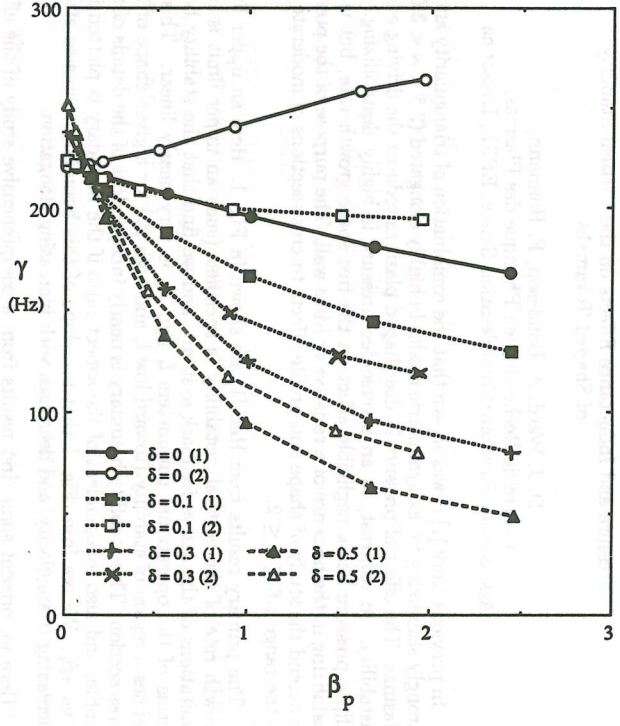

growth rates than those at lower triangularity. Here, at $\beta_p = 0$, the $\delta = 0.5$ equilibria have growth rates higher than those at $\delta = 0$ by about 15%. Furthermore, the shape of the pressure profile has only a modest influence on the stability. The stabilization by pressure and positive triangularity is somewhat stronger for the broader pressure profiles.

Figure 3 shows results for the same shapes and wall but with a narrower current profile, so that $l_i \approx 0.95$. Here, the growth rates are higher than in Fig. 2 (note the difference in the scale) owing to the reduced coupling of the current profile to the wall. For the low-triangularity cases there is a much larger increase in the growth rates as the inductance is increased than for the high-triangularity cases. In fact, the growth rates at $\beta_p = 0$ for the $\delta = 0$ equilibria almost double in magnitude as l_i is increased from $l_i \approx 0.75$ to $l_i \approx 0.95$, whereas the growth rates for the $\delta = 0.5$ equilibria increase by only about 20%. Note that for this high-inductance current profile, the higher-triangularity cases are more stable than the low-triangularity cases for all values of β_p.

We find that the results for cases with higher elongation ($\kappa = 2$) give the same trends, but naturally with higher growth rates. One clear conclusion is that with any nonzero triangularity the most unstable equilibria are those with $\beta_p = 0$. Therefore, low-pressure operation gives the most restrictive conditions on the vertical stability for a given configuration. We consider now these zero-pressure cases and the variation of growth rate with respect to the resistive wall distance.

Figure 4 shows how the growth rate varies with respect to the normalized distance d/a of the resistive wall for various values of triangularity and with $\beta_p = 0$. We see that for the cases with the broader current profiles ($l_i \approx 0.75$) the growth rates for equilibria with different triangularities are quite similar, with the high-triangularity cases being slightly more unstable. However, equilibria with narrower current profiles ($l_i \approx 0.95$) show a much greater variation in growth rate with respect to the amount of triangularity, and the high-triangularity cases are more stable. In fact, the curves for $\delta = 0.5$ are fairly close in magnitude for the broad and narrow current profiles, as mentioned above. The curves are shown for both the $\kappa = 1.8$ and the $\kappa = 2$ equilibria. At zero triangularity the $\kappa = 1.8$ equilibria with $l_i \approx 0.95$ have growth rates quite close to those of the $\kappa = 2$ equilibria with $l_i \approx 0.71$, whereas at triangularity $\delta = 0.5$ the growth rates for the $\kappa = 1.8$ cases remain well below those for the $\kappa = 2$ cases for the broad and narrow current profiles.

CONCLUSION

The combination of high triangularity and high β_p is strongly stabilizing for the vertical instability in tokamak plasmas surrounded by a resistive wall. For narrow current profiles triangularity is stabilizing even at $\beta_p = 0$. Only with broader current profiles at very low values of β_p do the high-triangularity cases have larger growth rates than the low-triangularity cases (and only by about 10–15% at zero pressure). Also, the variation in resistive wall growth rate with respect to changes in the internal inductance is much smaller at high triangularity. We conclude, therefore, that high triangularity is generally beneficial for vertical stability in elongated tokamak plasmas.

[1] D. J. Ward, A. Bondeson, and F. Hofmann, LRP 468/92, CRPP-EPFL, Lausanne (December 1992). To appear in Nucl. Fusion **33** (1993) #5 or #6.

[2] D. J. Ward, S. C. Jardin, and C. Z. Cheng, J. Comput. Phys. **104** (1993) 221.

[3] H. Lütjens, A. Bondeson, and A. Roy, Comput. Phys. Commun. **69** (1992) 287.

Figure 3

(1)-> flat pressure profile
(2)-> peaked pressure profile

$\kappa = 1.8$ $\quad d / a = 1.4$

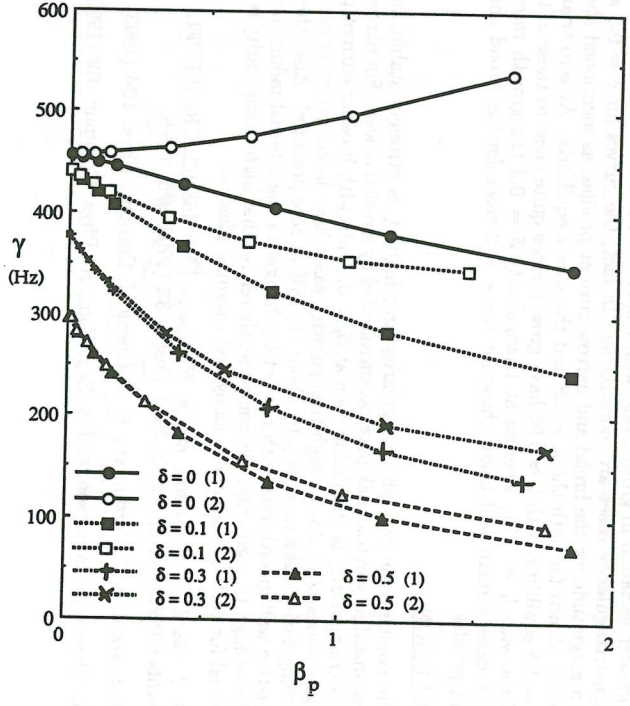

Figure 4

Growth rate vs. wall distance for $\beta\rho = 0$

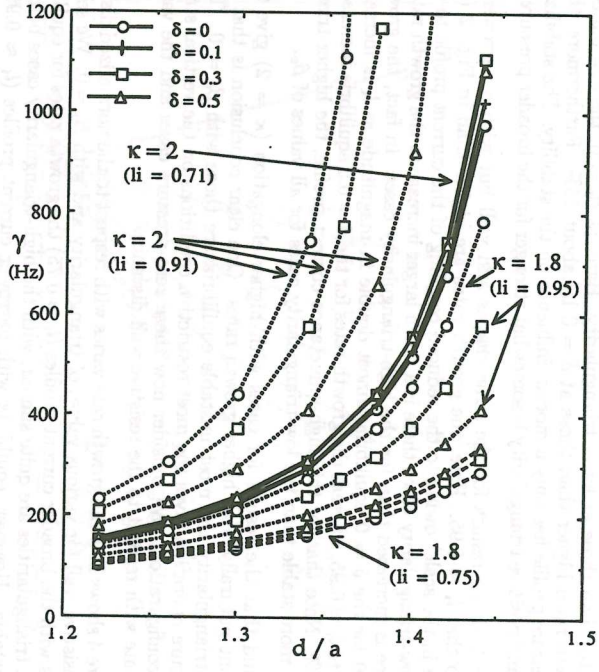

PROBABILITY OF ACCESSING THE MULTIPLE SATURATED STATES IN THE RESISTIVE INTERCHANGE INSTABILITY

L. Garcia
Universidad Carlos III and Asociación Euratom-Ciemat, Madrid, Spain
B.A. Carreras and V.E. Lynch
Oak Ridge National Laboratory, Oak Ridge, USA

Poloidal flows at the edge of a tokamak play a critical role in the overall plasma confinement. A poloidal shear flow in a plasma confined by a sheared magnetic field has, in general, a strong stabilizing effect [1]. Linear stability theory shows this stabilizing effect for many plasma instabilities. One might expect that the shear flow would have a similar effect on a nonlinear stability. A general scaling model developed by Biglari et al. [2] shows that when the shearing frequency dominates over the diffusive time scale, fluctuation levels should be reduced. However, numerical and analytical studies of long-wavelength drift wave turbulence and resistive pressure-gradient-driven turbulence show that the effect of a pure shear poloidal flow is much weaker [3, 4] than predicted by the scaling model.

In the case of resistive interchange modes, the effect of the poloidal flow in the nonlinear stability regime depends on the radial structure of the flow. At a given rational surface, the effect of a sheared poloidal flow, $V_\theta' \neq 0$, is very weak, while the effect of a curvature flow, $V_\theta'' \neq 0$, is strong, and produces a reduction of the fluctuation level [4, 5].

The saturation level of the fluctuations is computed numerically by time evolution of the equations describing the instability with an initial value approach. By changing the initial perturbation, different saturated states can be reached. They are associated with different dominant wave number in the spectrum. In a previous paper, we have investigated the existence of multiple saturated states, and the effect of an external poloidal flow on the probability of accessing these states [6]. The calculations included only modes resonant at the $q = 1.5$ singular surface, and most of them were restricted to the 9/6 sub-helicity because of the large number of calculations required.

In this paper, we study the probability of accessing the multiple saturated states for the full 3/2 helicity. We use for the calculations the same equilibrium parameters as in Ref. [7]. The presence of an external flow can induce Kelvin-Helmholtz type instabilities for relatively low beta values. This seems to be the case for the low-m modes with the equilibrium parameters used in our calculations. To separate this effect, we employ a simplified electrostatic model in the numerical calculations.

The basic geometry is a periodic cylinder with minor radius a and length $L = 2\pi R_0$. We use cylindrical coordinates r, θ, and $z \equiv R_0\zeta$. The model consists of the momentum balance equation, and the density evolution equation,

$$\frac{\rho_m}{B_0}\frac{\partial \tilde{U}}{\partial t} = -\frac{\rho_m}{B_0}\vec{V}\cdot\vec{\nabla}\tilde{U} - \frac{B_0}{\eta}\nabla_\parallel^2\Phi + T_e\frac{d\Omega_0}{dr}\frac{1}{r}\frac{\partial \tilde{n}_e}{\partial\theta} + \frac{\rho_m}{B_0}\mu\nabla_\perp^2\tilde{U},$$

$$\frac{\partial \tilde{n}_e}{\partial t} = -\vec{V}\cdot\vec{\nabla}\tilde{n}_e - \frac{dn_0}{dr}\tilde{V}_r + \chi_\perp\nabla_\perp^2\tilde{n}_e.$$

Here, n_e is the electron density, $\vec{V}$ is the fluid velocity, U is the z-component of the vorticity,

T_e is the electron temperature, and $\rho_m = m_i n_0$ is the mass density.

The velocity is given in terms of a stream function Φ/B_0, $\vec{V} = V_0(r)\hat{\theta} + \left(\vec{\nabla}\Phi \times \hat{z}\right)/B_0$. Here, V_0 is the equilibrium poloidal flow velocity. The velocity stream function is trivially related to the electrostatic potential $-\Phi$. The derivative parallel to the magnetic field, $\nabla_\parallel$, is defined as $\nabla_\parallel = \partial/\partial\zeta - (1/q)\partial/\partial\theta$.

The driving term of the resistive interchange instability is the pressure gradient in the bad curvature region ($d\Omega_0/dr > 0$). The second term on the right-hand-side of the momentum balance equation is the field line bending term, which is stabilizing. The resistivity weakens this term and allows the instability to grow.

The potential and density perturbations are written as a Fourier expansion

$$\tilde{f}(r,\theta,\zeta) = \sum_{m,n}\left[f^{+}_{mn}(r)\cos(m\theta + n\zeta) + f^{-}_{mn}(r)\sin(m\theta + n\zeta)\right].$$

The initial perturbation for each potential component is a Gaussian centered at the rational surface with a given amplitude. The amplitude of each mode (m; n) is a constant C_0 multiplied by a random number between 0 and 1. The phase of each mode is a random number between 0 and 2π. For the cases shown here, $C_0 = 0.1B_0a^2\tau_R$, where τ_R is the resistive time.

We begin by studying the case without external poloidal flow. The nonlinear evolution of 13 different initial conditions leads to the same final saturated state (Fig. 1). At the time $t = 0.01\tau_R$, there are shoulders in the evolution curves of the potential fluctuations. Each of these shoulders is dominated by one of the fastest-growing modes, $m = 21$ to $m = 30$. The higher fluctuation levels are associated with lower mode numbers. The presence of these high-m finite amplitudes has a stabilizing effect on the low-m modes [6]. The linear growth rate of the $m = 3$ mode is 310 (in resistive units), and it is reduced to values between 100 to 160, depending on the dominant mode in the shoulder.

To study the effect of an external shear flow, we have used the poloidal velocity profile $V_0(x) = \lambda\tanh(x/L_E)$. For this profile, $V_0'(0) = \lambda/L_E$. For $\lambda = 500a/\tau_R$ and $L_E = 0.1a$, and 40 random initial conditions, we have calculated the probability of reaching the various final states. This sample size gives us an statistical error of 16% in our probability estimate. As shown in Ref. 4, the level of fluctuations for a given dominant mode does not change with increasing V_0'. However, when $\tau_R V_0'$ is varied between 0 and 5000, the probability of accessing each final state changes significantly. This can be seen in Fig. 2, where we have used the dominant mode in the saturated state spectrum as a label for this particular

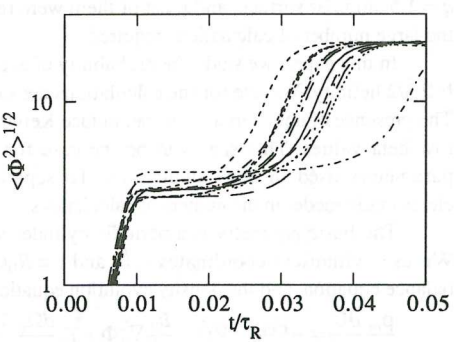

Fig. 1. Time evolution of the rms potential fluctuations for 13 random cases without equilibrium flow. A logarithmic scale is used to show the shoulders in the evolution.

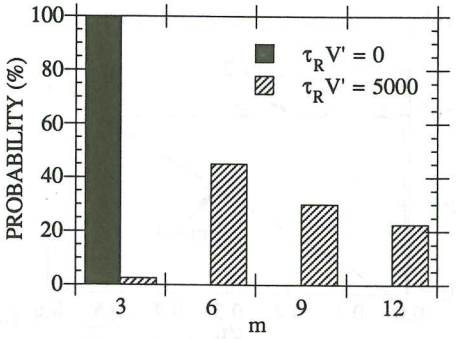

Fig. 2. Probability distribution of accessing different saturated final states for two values of the external flow shear.

final state. As $\tau_R V_0'$ increases from 0 to 5000, the most likely final state goes from m = 3 to m = 6. The nonlinear evolution of some of the 40 cases can be seen in Fig. 3. Depending on the initial conditions, the instability evolves to some intermediate states (shoulders) or it goes directly to the final saturation state. When V_0' is increased, the number of linearly unstable modes is decreased [4]. The first shoulder is dominated, in general, by one of the fastest-growing modes, m = 12 to m = 18 for $\lambda = 500a/\tau_R$.

By weighting the saturation levels with the probability that they will be accessed, we can see that increasing the shear in the flow decreases the weighted averaged fluctuation level. This result agrees with the scaling model results [2] , and it contradicts previous results [6] in which the magnetic flux evolution was taken into account. The presence of an external flow breaks the symmetry of the eddies associated with the resistive interchange fluctuations. This induces a nonlinear modification of the poloidal flow profile. The value of the shear of the poloidal flow at saturation increases with respect to the externally applied shear. The higher fluctuations levels are associated with higher shear flows.

To study the effect of the flow curvature, $V_0''(0) \neq 0$, we use the following profile for the equilibrium poloidal flow:

$$V_0(x) = \frac{r}{r_s}\overline{V}_0 \exp\left(-x^2/2L_E^2\right).$$

In these calculations, $L_E = 0.1a$. A factor r/r_s is included to reduce the V_0' induced by the cylindrical geometry effects. By using this external flow profile it has been shown [4, 5] that there is a reduction in the saturation level. We have done statistical calculations of the distribution of final states by using samples of 40 cases for $\tau_R\overline{V}_0/a = 6\times10^3$ and 9×10^3. For these values of the curvature flow, the number of linearly unstable modes is slightly reduced with respect to the case without flow, and the fastest growing modes have similar mode number. The consequence is that the effect of the external flow on the probability of accessing the first steady state (first shoulder) in the evolution is very weak. However, as V_0'' increases, the

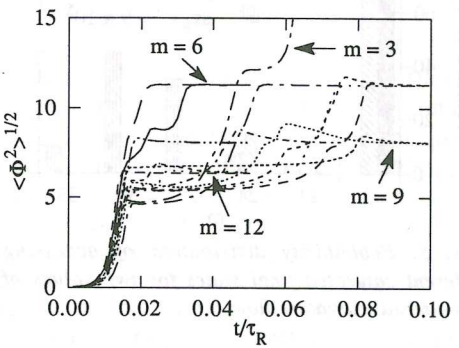

Fig. 3. Time evolution of the potential fluctuations for different random cases with $\tau_R V_0'$ = 5000.

linear growth rate is reduced, and the $m = 3$ mode can be completely stabilized by the presence of the high-m amplitude in the first steady state. If this is the case, all of the low-m modes are stabilized, and the first steady state is the final saturation state.

The dominant modes in the first steady state go from $m = 21$ to $m = 33$. For the case with $\tau_R \overline{V}_0 / a = 6 \times 10^3$, the $m = 3$ mode is completely stabilized when the dominant mode is $m = 21$ or $m = 24$. The evolution of the $m = 3$ in a case dominated in the first shoulder by $m = 27$ can be seen in Fig. 4. The growth rate of the $m = 3$ mode during the first steady state phase is 9. For the case with $\tau_R \overline{V}_0 / a = 9 \times 10^3$, all of the low-$m$ modes are stabilized in the first (and final) steady state phase. This implies that there is an abrupt change in the probability of accessing the final saturated states (Fig. 5), and in the weighted averaged fluctuation level. The effect is thus much stronger than in the case of shear flow, and it has similarities with the experimental data showing a strong surge of the poloidal flow, and a decrease in the fluctuation level in high confinement mode (H-mode) discharges.

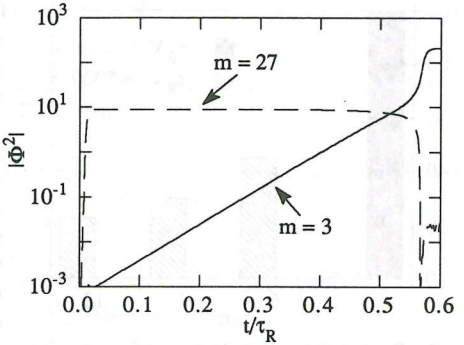

Fig. 4. Time evolution of the potential fluctuations of the m =3 and m = 27 modes for a case with $\tau_R \overline{V}_0 / a = 6 \times 10^3$.

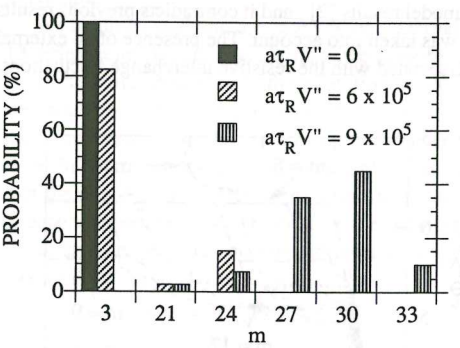

Fig. 5. Probability distribution of accessing different saturated final states for two values of the external curvature flow.

REFERENCES

[1] T. Chiueh, P.W. Terry, P.H. Diamond, J.E. Sedlak, Phys. Fluids **29** (1986) 231.
[2] H. Biglari, P.H. Diamond, P.W. Terry, Phys. Fluids B **2** (1990) 1.
[3] B.A. Carreras, et al., Phys. Fluids B **4** (1992) 3115.
[4] B.A. Carreras, V.E. Lynch, L. Garcia, P.H. Diamond, submitted to Phys. Fluids.
[5] L. Garcia, et al., in Proc. 14th Int. Conf. on Plasma Physics and Controlled Nuclear Fusion Research, Würzburg, 1992 (IAEA, Vienna, in press), paper D-4-6.
[6] B.A. Carreras, V.E. Lynch, L. Garcia, submitted to Phys. Fluids.
[7] B.A. Carreras, L. Garcia, P.H. Diamond, Phys. Fluids **30** (1986) 1388.

A MECHANISM FOR THE FAST MHD EVENTS IN SHEAR REVERSAL REGIMES OF TORE-SUPRA

D.Edery, A-L.Pecquet, P.Cristofani, J-P Morera, E.Joffrin, P.Lecoustey, M.Talvard, J-C Vallet, D.Van Houtte
Association Euratom-CEA sur la fusion contrôlée, C.E.Cadarache,13108 Saint Paul lez Durance France

Introduction

In the Tokamak, internal disruptions are generally observed when q=1 magnetic surface penetrates into the plasma. In this regime the internal kink mode m=1, n=1 is basic in the triggering of the instability[1]. However in enhanced confinement regimes (PEP, monsters,LHEP) although the poloidal β goes beyond the kink limit, no violent instability occurs. Recently improved regimes with shear reversal profiles have been achieved on TORE-SUPRA in ohmic and ICR heated discharges with central pellet injection. In these experiments a new kind of sawtooth has been observed. In particular,these sawteeth are localized in an annular region around the inversion radius.

In the following we present a theoretical model which attempts to explain the mechanism of appearence of this kind of sawteeth.

Theoretical model

Enhanced regimes are characterized by nonmonotonic q(r) profiles with large pressure gradients on the reversal shear radius r_1 where the minimum of q, q_{min} is almost 1. The high pressure gradient and the smallness of the quantity $\Delta q=q_{min}-1$ make these profiles very sensitive to the linear internal kink mode [2]. The accessibility to regimes without sawteeth should then be possible only if some saturation mechanism could be invoked. In fact, after its linear growth the internal kink mode will develop non linearly towards a saturated helical state with helicity 1 [2,3]. The magnetic topology of this accessible 3D equilibrium is constituted by tangent kinked magnetic surfaces which are compressed together at the reversal shear radius.In addition this compressional effect is located in the region of bad curvature of the Tokamak.Consequently all these effects allow to interpret the new sawteeth behaviour as resulting from destabilization of the ballooning mode.

Before analyzing the ballooning mode stability, we recall the main properties of the linear and nonlinear kink mode in the particular case of nonmonotonic q profiles. The linear kink mode is unstable if Δq is less than a critical value Δq_c at which the equilibrium is marginally stable [2] and which depends on the strength of the toroidal potential energy of the mode [1]. The nonlinear evolution of the kink mode takes place within a narrow layer of width $\Delta r_1/r_1=(r_1/R)^{2/3}$, leaving the outer region unchanged. The achieved helical state must satisfy the nonlinear equilibrium equation for the helical flux Ψ:

$$\Delta\Psi = J(\Psi) \tag{1}$$

with solution:

$$\frac{d\Psi}{dr} = \frac{2(q_{min}-1)}{q''(r_1)} (f(x)+g(\theta))^{1/2} \tag{2}$$

where $x = r_0 - r_1$, r_0 is the radial coordinate in the axisymmetric configuration and θ is the poloidal angle. The radial coordinate r in the non linear topology is given by:

$$\frac{\partial r_0}{\partial r} = (f(x) + g(\theta))^{+1/2} \tag{3}$$

The two functions f(x) and $g(\theta)$ result from the matching of the inner and outer solutions at the boundary of the nonlinear layer. In fact $\frac{\partial r}{\partial r_0}$ represents the local deformation in r_0, θ, of the original magnetic surfaces measured on the unperturbed coordinate system and depends on the strenght of the kink potential energy [2].

In the unperturbed equilibrium case one has $\frac{\partial r_0}{\partial r} = 1$.

In the kinked equilibrium case one has $(\frac{\partial r_0}{\partial r})_{max} = 1 + r_1/R$. (4)

We now study the stability of the nonlinear equilibrium with respect to the ballooning mode. In toroidal geometry the instability condition for a localized perturbation is written [4] $\partial W < 0$

$$\partial W = \int | \nabla_\perp \nabla_{//} \phi |^2 - \int 2\mu_0 \frac{dp}{dr} \vec{\xi}^* . \vec{\nabla} r \, \vec{\xi} . \vec{\kappa} \tag{5}$$

where, $\vec{\xi} = (\vec{B} \times \vec{\nabla}\phi)/B^2$ is the ballooning displacement, ϕ is the perturbation of the electric field potential $\vec{\kappa} = \nabla_{//}(\vec{B}/B)$ is the curvature of the field lines and $\frac{dp}{dr}$ is the local pressure gradient in the helical topology. In the case of circular plasmas and large aspect ratio, minimization of the energy integral(5) leads to the explicit instability condition for the ballooning mode:

$$\frac{1}{4}\frac{\partial r_0}{\partial r} (\frac{\partial r_0}{\partial r} + 3)\alpha^2 - (\frac{\partial r_0}{\partial r} - 1) < 0 \tag{6}$$

where $\alpha = \frac{2\mu_0 R q^2}{B^2} (-\frac{dp}{dr_0})$ is the ballooning pressure gradient parameter in the unperturbed equilibrium. Hence the nonlinear kinked equilibrium is unstable with respect to the ballooning mode if the pressure gradient α is less than the critical value

$$\alpha_c = 2[(\frac{\partial r_0}{\partial r} - 1) / \frac{\partial r_0}{\partial r}(3 + \frac{\partial r_0}{\partial r})]^{1/2} \tag{7}$$

Using (4) in formula (7), one gets for α_c the approximation:

$$\alpha_c = (r_1/R)^{1/2} \tag{8}$$

The ballooning mode is then destabilized if the local pressure gradient takes its values within the interval [0, $(r_1/R)^{1/2}$] (Fig1).
We now propose the following mechanism for the triggering of the sawtooth crash.

Just before the sawtooth rise the local pressure gradient is relatively small in comparison with α_c. At this step the ballooning mode is marginally unstable.

During the sawtooth rise the pressure gradient increases locally on the inversion radius up to values of order of r_1/R.These values are now large enough to destabilize the ballooning mode which ultimately triggers the crash.

Experimental analysis and theoretical comparison

High velocity pellets are injected in low current Tore-Supra discharges (Ip=0.88MA, Bt=3.8T, $ne(0)=4.10^{19}m^{-3}$, q(a)=5.5). Prior to the pellet injection, 2MW of ICRH power are applied to preheat the plasma [5]. A transient period (250ms) of enhanced confinement is obtained corresponding to peaked density and pressure profiles (Fig 3) as measured by Thomson scattering. In such conditions the bootstrap current represents 20% of the total current. The polarimetry shows a slight variation of the central q value which starts from 0.98 before injection and reaches 1.02 during the enhanced confinement phase (Fig 4a). In comparison soft X-ray signals exhibit different behaviours. Before the pellet injection, the inversion radius is located at 13.5cm, the relative amplitude of the crash, function of the radius is plotted on Fig 4b. One observes a typical value of 12% in the center. During the enhanced confinement phase the inversion radius moves towards the plasma outside (25cm). Associated to polarimetry, these above observations tend to demonstrate that the current profile should be hollow. In such condition the sawteeth are only localized near the inversion radius as shown on Fig 5 which gives the time evolution of central and near rinv soft X-ray signals. No sawteeth are visible on the central chord except one at t=7.97s which terminates the enhanced confinement phase. This is probably due to the flattening of the q profile.

Now both theory and experiment have found that the observed instability during the enhanced confinement regime in TS is localized at the vicinity of the reversal shear radius within a layer of width $\Delta r_1=r_1(r_1/R)^{2/3}=5cm$ (Fig 2).
Moreover the pressure gradient calculated on the inversion radius from the measured averaged profiles is $\alpha_{exp}=0.05$ and is included within the theoretical instability domain [0, $(r_1/R)^{1/2}$] (Fig 1).

In conclusion, a theoretical model has been presented which can explain the fast MHD activity in shear reversal regimes obtained on Tore-Supra.This model is well supported by experimental data and probably could be applied in other Tokamaks during regimes with nonmonotonic profiles.

Reference
[1] MN Bussac,R.Pellat,D.Edery,JL.Soulé PRL35,1638(1975)
[2] Avinash,RJ.Hastie,JB.Taylor,SC.Cowley PRL59,23(1987)
[3]MN.Bussac,R.Pellat PRL60(1987)
[4]C.Mercier Plasma Physics21-589(1979)
[5]A.Géraud et al this conference(Lisboa 1993)

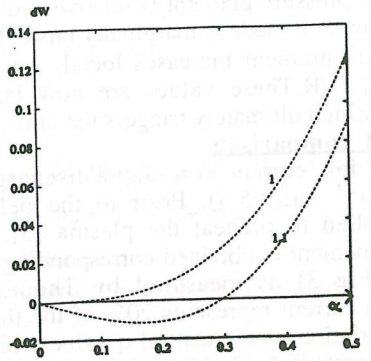

Fig.1- Stability diagram for the Ballooning mode Axisymmetric equilibrium : (1.) Helical 3D equilibrium : (1.1) ($\alpha = 2\mu_0 R q^2/B^2(-dP/dr)$ is the pressure gradient parameter)

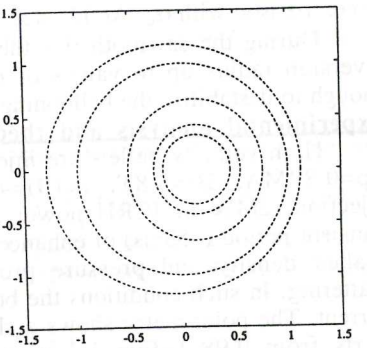

Fig.2- Magnetic topology of the helical 3D equilibrium

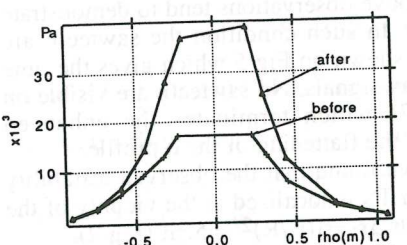

Fig 3 pressure profile variation during pellet injection

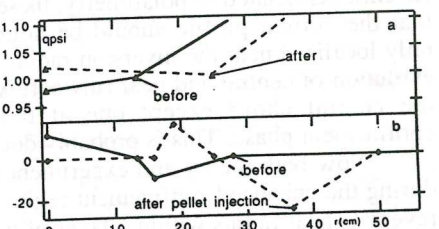

Fig 4 -a:estimated current profile -b:relative sawtooth amplitude

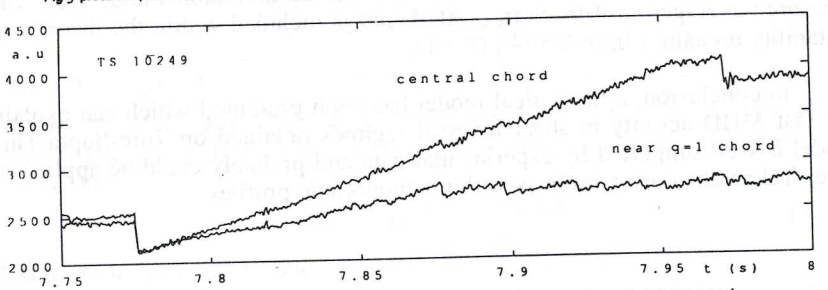

Fig 5 localized sawteeth during shear reversal

LOCKED MODE STABILITY IN PLASMAS WITH SHAPED CROSS-SECTIONS

R Fitzpatrick, R J Hastie, P S Haynes, T C Hender, T J Martin,
A W Morris and C M Roach
AEA Technology, Fusion, Culham, Abingdon, Oxfordshire,
OX14 3DB, UK (UKAEA/Euratom Fusion Association).

Introduction Experiments on COMPASS–C [1], JET [2] and DIII–D [3] have demonstrated that error fields can drive large locked modes. In particular, the poloidal mode number $m = 2$ and toroidal mode number $n = 1$ component of field errors can drive large islands at $q = 2$. The processes governing the formation of these locked modes are reasonably well understood theoretically [4]. It is predicted, and observed experimentally, that there is a threshold error field above which a locked mode island is driven, and below which very little tearing occurs (ie. no locked mode island is formed). As the machine size increases, this threshold error field decreases for a fixed density, or for a fixed error field there is a increase in the threshold density below which locked modes occur. The effects of machine size are confirmed by comparison of COMPASS–C, DIII–D and JET data. Extrapolation to ITER (EDA, $R = 7.75$m) shows the expected error field threshold in ohmic operation with $\bar{n}_e \simeq 2 \times 10^{19}\mathrm{m}^{-3}$ is very low $[B_{r_{2,1}}/B_T \sim \mathcal{O}(10^{-5})]$. The theoretical understanding of the formation of error field driven locked modes is based largely on the infinite aspect ratio circular flux surface calculations. For quantitative predictions of error field thresholds in devices such as ITER, it is important to understand the effects of finite aspect ratio, plasma shaping, and high β. Such effects are discussed in this paper.

Theory Background A threshold above which error fields will give rise to locked modes occurs for the following reason. In general, the plasma at the rational surface (r_s), where the field error is resonant, flows relative to the static error field. This relative flow has the effect of screening the field error. Despite this, there is a small amount of reconnection at r_s, driven by the field error, which gives rise to a braking torque on the plasma (near r_s). This braking torque is opposed by a viscous torque which tries to maintain the plasma rotation. This balance of torques causes the amount of driven reconnection to be a highly nonlinear function of the field error amplitude (or plasma density). As the field error amplitude is increased, there is a critical threshold above which the locking torque slows the plasma, increasing the driven reconnection and thus further increasing the torque and slowing the plasma. Eventually, this leads to the plasma flow near r_s ceasing completely and the error field driving a fully reconnected island.

In a toroidal system, the electromagnetic torque applied at a rational surface (r_j) is

$$T_\phi(r_j) = 2n\pi^2 R_0 |\psi_j|^2 \mathrm{Im}(r_j \Delta_j) \qquad (1)$$

where ψ_j is the reconnected poloidal flux at r_j, Δ_j is the jump in the ratio of the small to large Newcomb solutions at r_j, and R_0 is the major radius. To evaluate the torque it

is necessary to calculate ψ_j, and to invoke a layer theory to fix the value (and parameter dependence) of Δ_j.

In a vacuum, the helical flux interior to a set of conductors generating an error field may be written as

$$\psi_{vac}(r,\theta,\phi) = \sum_m I_m Q_m(r,\theta,\phi) \tag{2}$$

where the basis functions Q_m are obtained from an aspect ratio expansion of the standard toroidal ring functions which are well behaved as $r \to 0$. Thus the I_m may be regarded as a set of idealised error field currents. In the presence of plasma, the error field gives rise to a toroidal tearing mode relation

$$(\boldsymbol{\Delta} - \boldsymbol{E})\boldsymbol{\psi} = \sum_m I_m \boldsymbol{C}^m \tag{3}$$

where for a system of J rational surfaces, $\boldsymbol{\Delta}$ and $\boldsymbol{E}$ are $J \times J$ matrices, and $\boldsymbol{\psi}$ and $\boldsymbol{C}^m$ are J element column vectors. Here, $\boldsymbol{\psi}$ is the vector of the reconnected fluxes and $\boldsymbol{\Delta}$ is a diagonal matrix of elements $r_j\Delta_j$. The quantities $\boldsymbol{E}$ and $\boldsymbol{C}^m$ are evaluated with an aspect ratio, beta and shaping expansion using the T7 code. In the simplest case the driven layer dispersion relation is given by

$$r_j\Delta_j \simeq -i(\omega - \omega_j)\tau_j \tag{4}$$

where ω is the angular frequency of the error field, ω_j is the angular frequency of a naturally growing mode at $r = r_j$ and τ_j is a typical reconnection timescale at $r = r_j$. From Eqs (1), (3) and (4) the torque is given by

$$T_\phi(r_j) \simeq \frac{2n\pi^2 R_0}{(\omega - \omega_j)\tau_j}\left\{\sum_m I_m C_j^m\right\}^2 \tag{5}$$

in the physical limit where $|\omega - \omega_j|\tau_j \gg 1$. Hence the parameter dependence of the torque at $r = r_j$ may be determined from examination of the coefficients C_j^m. Physically an increase in torque will be manifested as an increase in density threshold for locking, or equivalently as a reduced minimum error field for locking at a given density.

Results Figure 1 shows the various components in an aspect ratio, beta and shaping expansion of C_1^2, (which gives the torque at surface 1, $q = 2$ in this case, due to the $m = 2$ 'error field' current I_2). The current profile here is $J_\phi \propto (1 - (r/a)^2)^\nu$ with a central $q_0 = 1.05$, and the pressure profile is $P \propto (1 - (r/a)^2)^2$. Here the ellipticity parameter (E_a) is related to the elongation by $b/a = (1 + E_a)/(1 - E_a)$ and the poloidal β_p is defined as $\beta_p = \mu_0 q_a^2 P_0/(\epsilon B_0)^2$ where $\epsilon = a/R$. The jumps in the toroidally coupled (ϵ) terms at $q_a = 3$ in Fig. 1 are related to toroidal coupling to the (stable) $m = 3$ external kink mode and similarly the jump at $q_a = 4$ is related to elliptic coupling to the $m = 4$ kink mode. It can be seen from Fig. 1 that the torque increases with increasing ϵ, β_p and E_a. Thus as the elongation (or ϵ or β_p) is increased at fixed q_a the minimum error field to induce locked modes will decrease. Experiments in COMPASS–D are in progress to examine the effects of plasma shape on error field thresholds [5].

In the above the effect of a pure $m = 2$, $n = 1$ field error has been considered. In general of course field errors due to coil misalignments, winding errors or current feeds

will give rise to a broad error field spectrum. Figure 2 shows how the torque at $q = 2$ varies with q_a for the same equilibrium as Fig. 1 with $\epsilon = 0.2$ and $E_a = 0.2$. In this case the error field currents (I_2, I_3, I_4) have relative signs representative of a field error due to an outboard midplane dipole. From Fig. 2 it can be seen that there are sharp increments in the torque at $q_a = 3$ and 4. These are partly due to couplings to external kink modes (discussed above) but are dominantly due to the loss of coupled torque as the $q = 3$ and 4 surfaces leave the plasma. Such a staircase like increment in critical density (and therefore torque) with q_a has been observed in JET experiments [2]. In the JET experiments the dominant error was due to turn–to–turn transitions of the winding in the vertical field coils and has a qualitatively similar spectrum to that used in Fig. 2.

An outstanding issue experimentally is the considerable amplification of the field error which is observed in larger tokamaks; for example in JET the observed locked mode has an $m = 2$ $n = 1$ radial field at $q = 2$ which is 60 times larger than the calculated vacuum error field [2]. An amplification of the vacuum error field of 2 to 3 is expected due to the requirement of maintaining force balance [4]. The observed amplifications however are not explicable by this mechanism. A possible explanation is a change in natural stability of the plasma due to mode locking:– since following locking tearing can occur at all surfaces and the wall no longer acts as an ideal conductor. Calculations however show under this mechanism locking does not cause a significant change in mode stability, except for $q_a \lesssim 3$ – eg. for $q_a = 4$ and the current profiles used in Figs. 1 and 2, the increase in $\Delta'_{q=2}$ is about 2 when tearing can occur at all surfaces, for JET like parameters.

Summary The effects of toroidicity, plasma shape and pressure on the threshold for error field locked modes have been studied. It is found that for an $m = 2$ error field the threshold for locked modes decreases with increasing ϵ, E and β. Electromagnetic torque can also be applied at $q = 2$ by sideband coupling to $m = 3$, 4 etc components of an error field. If q_a is decreased then these sideband coupled torques are abruptly lost when the surfaces at which they are resonant leave the plasma. This result explains the abrupt changes in threshold density at integer q_a (=3,4) observed in JET experiments [2].

Acknowledgement We thank Dr G Fishpool for many useful conversations. This work was jointly funded by the UK Department of Trade and Industry and EURATOM.

References

[1] T.C.Hender et al, Nucl Fusion **32** (1992) 2091.

[2] G.M.Fishpool and P.S.Haynes, JET pre–print JET–P(93)05.

[3] J.T.Scoville, R.J.LaHaye et al, Nucl Fusion **31** (1991) 875 and
R.J.LaHaye, A.W.Hyatt and J.T.Scoville, Nucl Fusion **32** (1992) 2119.

[4] R.Fitzpatrick in Theory of Fusion Plasmas (Varenna – Lausanne workshop, 1992) in press.

[5] A.W.Morris et al, 'Error Field Studies and Plasma Velocity Measurements in Shaped Plasma on COMPASS–D', this conf.

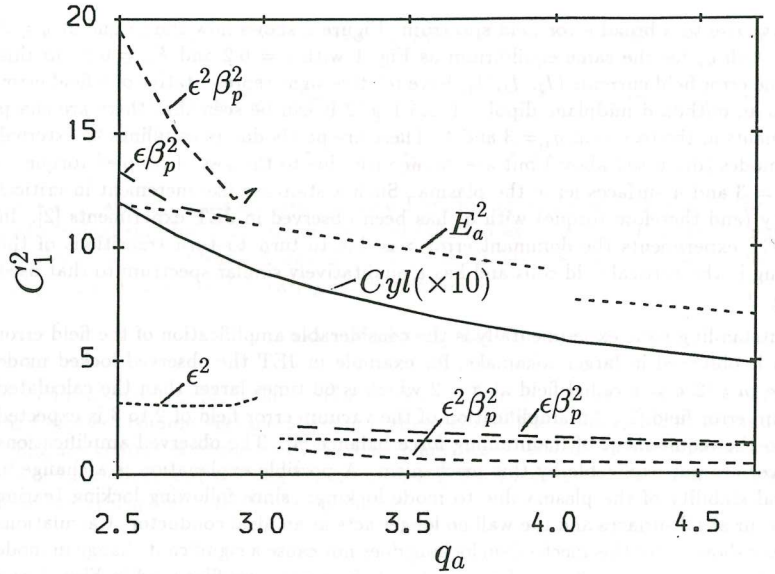

Fig. 1 Variation of various components of C_1^2 with edge-q (q_a) in an inverse aspect ratio (ϵ), elongation (E_a) and poloidal-β (β_p) expansion.

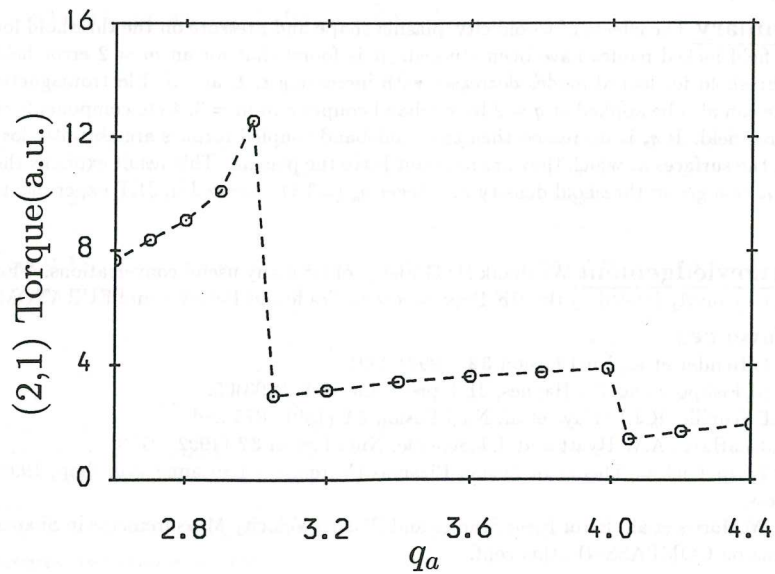

Fig. 2 Variation of (2,1) Torque with edge-q (q_a) for an error field spectrum representative of an outboard midplane dipole error.

Theory for small growth rates of the tearing mode in a sheet pinch

W. Barbulla and E. Rebhan
Institut für Theoretische Physik, Heinrich-Heine-Universität Düsseldorf, Universitätsstr. 1, D-4000 Düsseldorf, Federal Republic of Germany

Abstract: In the theory of tearing modes, analytical expressions for the growth rate γ are only known for large values $\gamma >> 1/\tau_R$. However, since resistive instabilities cannot be externally suppressed, they will be rather observed at small growth rates. In this paper, the described gap in the tearing theory is closed. The expressions obtained for small growth rates are as simple as the ones for large growth rates but differ from them appreciably. Their good quality was confirmed by numerical solution of the full tearing equations. In addition, an implicit analytical formula is presented that bridges the gap between small and large growth rates.

Introduction In the usual tearing theory it is assumed that the growth rate γ lies between the typical rates for resistive and ideal MHD processes, $1/\tau_R << \gamma << 1/\tau_A$ (τ_A = Alfvén time, τ_R = resistive time). In addition, the magnetic Reynolds number $S = \tau_R/\tau_A$ is assumed to be large. Accordingly, the limit $\gamma \to 0$ lies outside the realm of the usual theory. However, since practically tearing instabilities are triggered by slow changes of plasma parameters and cannot be suppressed, they will never be observed at higher growth rates. In the contrary, immediately after the threshold of instability is passed over there will occur a transition into neighboring or distant bifurcational equilibria with tearing structure. In the study of tearing bifurcations and the related dynamical processes it is just the limit of small growth rates that matters and bears the seed of the bifurcating structure in it.

Basic equations We consider an incompressible resistive plasma and neglect the heating caused by resistivity. The geometry of the equilibrium plasma will be restricted to a sheet. The equilibrium values of the magnetic field, the plasma velocity and the resistivity are then given by

$$\vec{B}_0 = \psi_0'(x)\vec{e}_y + B_{0z}\vec{e}_z, \quad \vec{v}_0 = 0, \quad \eta_0 = \eta_0(x), \tag{1}$$

where ψ_0 and η_0 are related by $\eta_0'\psi_0'' = -\eta_0\psi_0'''$ or $\eta_0 = const/\psi_0''$ equivalently. The stability equations for $\gamma \to 0$ are the same as the ones that were investigated[1] for $\gamma >> 1/\tau_A$ and are

$$\psi'' - k^2\psi - \frac{F_0''}{F_0}\psi = \left(\frac{\gamma}{\eta_0} - \frac{F_0''}{F_0}\right)(\psi + F_0\xi) \tag{2}$$

$$\xi'' - k^2\xi = (\frac{S}{\gamma})^2 F_0 \left(\frac{\gamma}{\eta_0} - \frac{F_0''}{F_0}\right)(\psi + F_0\xi). \tag{3}$$

where $\psi(x)$ is a flux function for the perturbational magnetic field and ξ is the plasma shift. They are subject to the boundary conditions $|\psi| \to |\xi| \to 0$ for $|x| \to \infty$.

Asymptotic perturbation theory Equations (2)-(3) can be solved by the means of an asymptotic perturbation theory. Since $S/\gamma >> 1$, according to (3) $\xi(x)$ must satisfy almost everywhere the approximate "exterior equation" $\psi + F_0\xi = 0$ except for a very thin "resistive sheet" in which $\xi''(x)$ becomes large. Outside this sheet, ψ satisfies

$$\psi'' - k^2\psi - \frac{F_0''}{F_0}\psi = 0. \tag{4}$$

Within the resistive sheet, eqs. (2)-(3) can be approximated in the usual manner by the sheet equations

$$\psi'' = \left(k^2 + \frac{\gamma}{\eta_0}\right)\hat{\psi} + \left(\frac{\gamma F_0}{\eta_0} - F_0''\right)\xi \tag{5}$$

$$\xi'' = \left(\frac{S}{\gamma}\right)^2 \left(\frac{\gamma F_0}{\eta_0} - F_0''\right)(\hat{\psi} + F_0\xi). \tag{6}$$

where $\hat{\psi} = const.$ It suffices to expand the coefficients up to linear terms in the distance $s = x - x_0$ from the singular point x_0 only. In the symmetric case ($F(x-x_0) = -F(x_0-x)$), F_0 and F_0'' vanish simultaneously at x_0 whence

$$F_0(x) = F_0'(x_0)s \ , \ F_0''(x) = F_0'''(x_0)s,$$

and equations (5)–(6) are approximated by

$$\psi'' = \left[k^2 + \frac{\gamma}{\eta_0}\left(1 - \frac{\eta_0'}{\eta_0}s\right)\right]\hat{\psi} + \left(\frac{\gamma F_0'}{\eta_0} - F_0'''\right)s\xi \tag{7}$$

$$\xi'' = \left(\frac{S}{\gamma}\right)^2 F_0' \left(\frac{\gamma F_0'}{\eta_0} - F_0'''\right)\left(\frac{\hat{\psi}}{F_0'}s + \xi s^2\right), \tag{8}$$

all quantities with subscript like F_0' being understood as values at x_0. Rewriting (8) in the form

$$\xi'' = A(Bs + \xi s^2)$$

with

$$A = \left(\frac{S}{\gamma}\right)^2 F_0' \left(\frac{\gamma F_0'}{\eta_0} - F_0'''\right) \ , \ B = \frac{\hat{\psi}}{F_0'} \tag{9}$$

and substituting

$$\xi = A^{\frac{1}{4}}B\chi_s \ , \ s = A^{-\frac{1}{4}}y, \tag{10}$$

we obtain

$$\chi_s''(y) = y + y^2\chi_s. \tag{11}$$

The growth rate can be obtained as usual by dividing (7) through $\hat{\psi}$ and integrating over the resistive layer. Using $\int_{-s_+}^{s_+} sds = 0$, $\Delta s = 2s_+$ and the definition

$$\Delta'(s_+) =: \frac{\psi'(x_0 + s_+)}{\psi(x_0 + s_+)} - \frac{\psi'(x_0 - s_+)}{\psi(x_0 - s_+)} = \Delta'(0) + \frac{\Delta''(0)}{2} \tag{12}$$

the result is

$$\begin{aligned}\Delta'(0) &= \left(k^2+\frac{\gamma}{\eta_0}-\frac{\Delta''(0)}{2}\right)\Delta s+\frac{1}{\hat{\psi}}\left(\frac{\gamma F_0'}{\eta_0}-F_0'''\right)\int_{-s_+}^{s_+}\xi s ds-\frac{\gamma\eta_0'}{\eta_0^2}\int_{-s_+}^{s_+}s ds \\ &= A^{-\frac{1}{4}}\left[\left(k^2+\frac{\gamma}{\eta_0}-\frac{\Delta''(0)}{2}\right)\Delta y+\frac{B}{\hat{\psi}}\left(\frac{\gamma F_0'}{\eta_0}-F_0'''\right)I_s\right],\end{aligned}$$

where

$$I_s=\int_{-y_+}^{y_+} y\chi_s dy \quad \text{and} \quad \Delta y = 2y_+,$$

the integral extending from the left hand boundary y_- to the right hand boundary y_+ of the resistive sheet and being independent of all parameters of the problem.

The exterior equation (4) can be used to calculate $\Delta''(0)$. The expansion of the exterior solution $\psi(x)$ around the singular point x_0 yields

$$\psi(x)=\psi(x_0)+\psi'(x_0)s+\frac{1}{2}\psi''(x_0)s^2+\ldots \quad \text{and} \quad \psi'(x)=\psi'(x_0)+\psi''(x_0)s\ldots$$

both to the left and to the right of the singular point. From this, with (4) we get

$$\frac{\psi'(x)}{\psi(x)}=\frac{\psi'(x_0)}{\psi(x_0)}+\left[k^2+\frac{F_0'''}{F_0'}-\left(\frac{\psi'(x_0)}{\psi(x_0)}\right)^2\right]s.$$

Making use of the symmetry around x_0, from this we get

$$\Delta'(s_+)=\Delta'(0)+(k^2+\frac{F_0'''}{F_0'})\Delta s-\frac{1}{\psi(x_0)^2}\left((\psi')^2(x_0^+)+(\psi')^2(x_0^-)\right)\Delta s.$$

It can be shown that the last term can be neglected whence we obtain

$$\Delta''(0)=2(k^2+\frac{F_0'''}{F_0'}). \tag{13}$$

Inserting this in (13), with the definitions (9) we finally obtain the result

$$\Delta'(0)=\left(\frac{\gamma}{S}\right)^{\frac{1}{2}}\frac{(\Delta y+I_s)\frac{\gamma}{\eta_0}-\frac{F_0'''}{F_0'}(\Delta y+I_s)}{\left[F_0'^2\left(\frac{\gamma}{\eta_0}-\frac{F_0'''}{F_0'}\right)\right]^{\frac{1}{4}}}. \tag{14}$$

(14) is an implicit formula for evaluating γ and is valid for $\gamma \to 0$ as well as for $\gamma >> 1/\tau_R$. In the latter case, the terms in the numerator of the right hand side of (14) that are free of γ can be neglected against the γ/η-term, and one obtains the well known result[1)]

$$\gamma=(S|F_0'|)^{\frac{2}{5}}\eta_0^{\frac{3}{5}}\left(\frac{\Delta'(0)}{\Delta y+I_s}\right)^{\frac{4}{5}}. \tag{15}$$

A good approximation for $I=\Delta y+I_s$ is obtained by setting $y_\pm=\pm\infty$ which delivers $I=2\pi\Gamma(3/4)\Gamma(1/4)=2.1236..$.

For small γ, the terms containing γ/η_0 can be neglected in (14) and we obtain the result

$$\gamma = S|F_0'|\left(-\frac{F_0'''}{F_0'}\right)^{\frac{1}{2}}\left(\frac{\Delta'(0)}{\frac{F_0'''}{F_0'}(\Delta y + I_s)}\right)^2 \tag{16}$$

that shows a completely different potential dependence of γ on S and Δ'. The dashed curves in Fig. 1 show the dependence of γ on Δ' for fixed S according to (15) and (16), evaluated for the simple equilibrium profile

$$F_0(x) = \tanh(\lambda x). \tag{17}$$

The full curve was obtained by evaluating (14) and shows the smooth transition between the two potential laws. It differs only invisibly from the curves obtained by a numerical evaluation of the full equations (2)–(3). Fig. 2 shows the corresponding results obtained for the dependence of γ on S for given Δ'. It is seen that γ becomes independent of S which means that for small growth rates the dynamics is determined by ideal MHD effects, the resistivity playing only the role of a trigger.

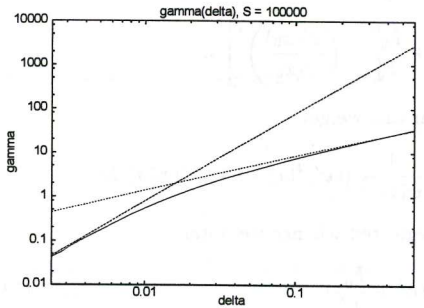

Fig. 1

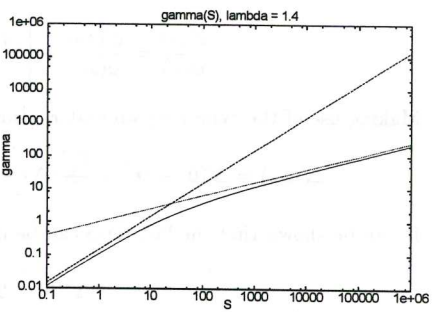

Fig. 2

[1] H. P. Furth, J. Killeen, M. N. Rosenbluth, Phys. Fluids 6, 459 (1963)

On MHD Description of Semicollisional Modes in Tokamaks

B. N. Kuvshinov*
FOM-Instituut voor Plasmafysica, "Rijnhuizen",
Nieuwegein, the Netherlands

In the high-temperature regimes relevant to present day fusion experiments with confined toroidal plasmas, the ion Larmor radius ρ_i can significantly exceed the characteristic scales of the plasma motion. Examples of such a situation are the so-called semicollisional modes [1], which occur when the plasma resistivity becomes so small that ρ_i is larger than the resistive layer width. Semicollisional modes are believed to be described properly only with the help of kinetic theory. Recently Zakharov and Rogers [2] have claimed that these modes can also be investigated within the framework of MHD. Having introduced a two-fluid MHD model they have obtained results which are suprisingly in agreement with those found from kinetic theory [3]. The primary goal of the present report is to reveal the origin of this agreement.

We are starting with the assumption that the ion Larmor radius is small enough so that the MHD approach is valid. The momentum equation and the equation for diffusion of generalized ion momentum in the ion fluid have the form (magnetic drift effects are neglected here)

$$\varrho \frac{d\mathbf{V}}{dt} = \mathbf{j} \times \mathbf{B} - \nabla p, \tag{1}$$

$$\frac{\partial}{\partial t}(\mathbf{B} + \frac{M}{e} \nabla \times \mathbf{V}) = \nabla \times [\mathbf{V} \times \mathbf{B}] - \nabla \times [(d_e^2 \frac{\partial}{\partial t} + D) \nabla \times \mathbf{B}], \tag{2}$$

$d_e = c/\omega_{pe}$ is the electron inertial skin depth, ω_{pe} is the plasma frequency, $D = c^2/(4\pi\sigma)$ is the diffusion coefficient for magnetic field, $\mathbf{V}$ is the mass plasma velocity and the other notations are standard. We omit the factors c and 4π in equations, but keep them in the definitions of the characteristic parameters. We consider the isothermal plasma model, i.e. suppose the adiabatic index to be equal to unity. Then the plasma pressure evolution equation is given by

$$dp/dt = -p \ \nabla \cdot \mathbf{V}. \tag{3}$$

Eqs. (1) - (3) are a closed set of equations which constitutes the starting point for the analysis. It differs from the standard set of resistive one-fluid MHD equations only in two points. Firstly, the skin depth in Eq. (2) is renormalized due to electron inertia. Secondly, in the left hand side of Eq. (2) a term appears which accounts for the Hall effect.

First of all we consider the small oscillations of a slab plasma immersed in a straight uniform magnetic field. The linear perturbation has the form $\boldsymbol{\xi}(\mathbf{r}) = \boldsymbol{\xi} \exp(-i\omega t + i\mathbf{kr})$,

*Also at Russian Scientific Center "Kurchatov Institute", Moscow, Russia

ω is the oscillation frequency, $\boldsymbol{\xi}$ is the perturbed plasma displacement, $(\partial\boldsymbol{\xi}/\partial t = \mathbf{V})$, $\mathbf{k}$ is the wave vector, $\mathbf{r}$ is the space coordinate. A further simplification is the omission of plasma resistivity and electron inertia effects. In this approximation Eqs. (1) - (3) become after linearization

$$-\omega^2\boldsymbol{\xi} = c_s^2\nabla(\nabla\cdot\boldsymbol{\xi}) + C_A^2\{\frac{\partial^2\boldsymbol{\xi}_\perp}{\partial z^2} + \nabla_\perp(\nabla_\perp\cdot\boldsymbol{\xi}_\perp) + i\frac{\omega}{\Omega_{Bi}}[(\nabla(\nabla\cdot\boldsymbol{\xi}) - \Delta\boldsymbol{\xi})\times\mathbf{e}_z]\}. \quad (4)$$

Here $c_s^2 = p_0/\varrho_0$, $C_A^2 = \mathbf{B}_0^2/(4\pi\varrho_0)$ is the Alfvén velocity, $\mathbf{e_z}$ is the unit vector along $\mathbf{B}_0$. Zero subscripts mark equilibrium quantities, the subscript "$\perp$" denotes the direction perpendicalar to $\mathbf{B}_0$. From Eq. (4) the following dispersion relation can be obtained

$$\{\omega^2(1-\frac{k_\perp^2c_s^2}{\omega^2-k_z^2c_s^2}) - k^2C_A^2\}(\omega^2-k_z^2C_A^2) - \frac{\omega^2}{\Omega_{Bi}^2}k_z^2k^2C_A^4(1-\frac{k_\perp^2c_s^2}{\omega^2-k_z^2c_s^2}) = 0, \quad (5)$$

where k_z is the longitudinal component of the wave vector and Ω_{Bi} is the ion cyclotron frequency. For tokamaks the Alfvén waves straighten along the magnetic field lines are typical, so that $k_\perp \gg k_z \simeq 1/R$ and $\omega \ll k_\perp C_A$, where R is the large tokamak radius. In addition we suppose $\omega \gg k_z c_s$ (i.e. we neglect the coupling of Alfvén waves with ion sound waves). Then Eq. (5) is reduced to

$$\omega^2 = k_z^2C_A^2(1+k_\perp^2\rho_s^2), \quad (6)$$

where $\rho_s^2 = c_s/\Omega_{Bi}$ is the ion sound Larmor radius. The dispersion of Alvfen waves is determined by the factor $k_\perp\rho_s$. Usual Alfvén wave converts to "semicollisional" one when this factor exeeds unity. To consider the case $k_\perp\rho_s > 1$ in the frame of MHD one could suppose $T_i \ll T_e$ in order to satisfy the inequality $k_\perp\rho_i < 1$. However, as will be shown below, the fluid model remains valid even when this inequality is violated, $k_\perp\rho_i > 1$.

Let us consider a cylindrical tokamak and suppose that $\boldsymbol{\xi}(\mathbf{r}) = \boldsymbol{\xi}(a)\exp(\gamma t + im\theta - in\zeta)$ (single helicity approximation), where θ and ζ are the poloidal and toroidal angles in a flux coordinate system, a is the radial coordinate. In the region near to the rational surface with $q = m/n$, q being the safety factor, the perturbation exibits singular behavior and the radial derivatives of the perturbed quantities are large in comparison with θ- and ζ-derivatives. This circumstance enables one to simplify significantly the starting equations. We neglect equilibrium pressure gradient effects and the coupling with the ion sound wave. Projection of Eq. (1) along $\mathbf{b}_0\times\nabla a$ with $\mathbf{b}_0 = \mathbf{B}_0/|\mathbf{B}_0|$, gives a relation for the perturbed magnetic field $\tilde{\mathbf{B}}$,

$$\tilde{\mathbf{B}}\cdot\mathbf{B}_0 = 0. \quad (7)$$

This condition means that we may introduce the perturbed poloidal flux ψ such that $\tilde{\mathbf{B}}$ will be proportional to $\mathbf{b}_0\times\nabla\psi$. From Eqs. (2), (7) it follows that two components of $\boldsymbol{\xi}_\perp$ can be expressed in terms of a single scalar quantity Φ,

$$\boldsymbol{\xi}\cdot\nabla a = [\mathbf{b}_0\times\nabla a]\cdot\nabla\Phi + \frac{\gamma}{\Omega_{Bi}}\frac{d\Phi}{da}, \qquad \eta = -\frac{d\Phi}{da}, \quad (8)$$

where $\eta = \boldsymbol{\xi}\cdot[\mathbf{b}_0\times\nabla a]$. The parallel component of $\boldsymbol{\xi}$ is found from the projection of Eq. (1) along $\mathbf{b}_0$ and from Eq. (8),

$$\boldsymbol{\xi}\cdot\mathbf{b}_0 = \frac{c_s^2}{\gamma\Omega_{Bi}}\,\mathbf{b}_0\cdot\nabla\frac{d^2\Phi}{da^2}. \quad (9)$$

Using the above relations one can write the vorticity equation (rotation of Eq. (1) projected along $\mathbf{b}_0$) and ∇a–component of Eq. (2) in the form

$$\hat{\gamma}^2 \frac{d^2\Phi}{dx^2} = -x\frac{d^2\psi}{dx^2}, \qquad \psi - \lambda_e^2 \frac{d^2\psi}{dx^2} = x(\Phi - \lambda_s^2 \frac{d^2\Phi}{dx^2}). \tag{10}$$

Here $x = m(a-a_r)/a_r$, $\lambda_s = m\rho_s/a_r$, $\lambda_e^2 = m(d_e^2 + D/\gamma)/a_r^2$, $\hat{\gamma} = \gamma/\omega_A$, $\omega_A = C_A S/(qR)$, and $S = d\ln q/d\ln a$.

Equations (10) coincide with those obtained by Zakharov and Rogers [2] except for the renormalization of the coefficients due to drift effects, which have been taken into account in Ref. [2]. Now we will show that the MHD resistive-layer equations are identical to the equations derived by Pegoraro and Schep [3] in the frame of kinetic formalism. To prove this fact one should compare the exact kinetic ion response (i.e. the relation between the perturbed ion density and the perturbed electric potential) and the ion response calculated with the help of MHD model. Projecting Eq. (2) along ∇a and expressing η through $\tilde{n}_i$ ($\tilde{n}_i$ is proportional to $\nabla \cdot \mathbf{V}$) we come to

$$\frac{1}{n_0}\frac{d^2\tilde{n}_i}{da^2} - \frac{1}{\rho_i^2}\frac{\tilde{n}}{n_0} + \frac{e}{T_i}\frac{d^2\varphi}{da^2} = 0. \tag{11}$$

The perturbed ion density $\tilde{n}_i$ obtained from the linearized Vlasov equation for the modes with $\omega > k_\parallel c_s$ is given by [4]

$$\frac{\tilde{n}_i}{n_0} = -\left[1 - \exp(\rho_i^2\Delta_\perp)\, I_0(-\rho_i^2\Delta_\perp)\right]\frac{e\varphi}{T_i}, \tag{12}$$

I_0 is the modified Bessel function of the first kind and $\Delta_\perp$ stands for the Laplassian. The transition from the kinetic ion response (Eq. (12)) to the MHD ion response (Eq. (11)) involves the substitution (remember that in the singular layer $\Delta_\perp \simeq d^2/da^2$)

$$1 - \exp(-z)\, I_0(z) \longrightarrow \frac{z}{1+z}. \tag{13}$$

This, however, is just the Padé approximation that has been introduced by Pegoraro and Schep [3].

We see that there is no difference between MHD and approximate kinetic [3] approaches. Both approaches are based on assumption (13) and, hence, give the same result. Indeed, using the Fourier transformation of Eqs. (10),

$$\frac{d}{dk}\left[\frac{k^2}{1+\lambda_e^2k^2}\frac{df}{dk}\right] - \frac{\hat{\gamma}^2k^2}{1+\lambda_s^2k^2}\, f = 0, \tag{14}$$

where $f = (1+k^2)\,\Phi_k$, and carrying out the standard asymptotic matching procedure one comes to the relations initially derived by Pegoraro and Schep [3]

$$\frac{P^2(\nu)\,Q(\nu)}{P^2(-\nu)\,Q(-\nu)} = \left(\frac{2\lambda_s^2}{\hat{\gamma}\lambda_e}\right)^{2\nu}. \tag{15}$$

Here

$$P(\nu) = \Gamma(-\nu)\Gamma(-1/4+\nu), \qquad Q(\nu) = 1 + \frac{1}{8}\frac{C_1}{C_2}\frac{\hat{\gamma}^2}{\lambda_s^3}\frac{\Gamma^2(-1/4-\nu/2)}{\Gamma^2(5/4-\nu/2)}, \tag{16}$$

$\nu = (1/4 + \hat{\gamma}^2/\lambda_s^2)^{1/2}$ (Eq. (15) is valid for $\nu < 1$). The value C_2/C_1 is determined from the solution in the ideal region (see Ref. [3] for details),

$$\frac{C_2}{C_1} = \begin{cases} -\lambda_H, & m = 1 \\ \pi m/\Delta', & m \geq 2, \end{cases} \tag{17}$$

λ_H and Δ' are the standard parameters in the theory of $m = 1$ kink mode [5] and tearing mode [6] respectively. In the limit $\hat{\gamma} \ll \lambda_s$ Eq.(15) can be significantly simplified. It then becomes

$$1 - \frac{\pi}{2}\frac{\hat{\gamma}^3}{\lambda_e \lambda_s^2} - \frac{C_2}{C_1}\frac{\hat{\gamma}}{\lambda_e \lambda_s} = 0. \tag{18}$$

The cubic equation (18) describes three branches of oscillations. In the limit $C_2/C_1 \to 0$ it means $\hat{\gamma}^3 = (2/\pi)\lambda_e \lambda_s^2$. For small, but finite C_2/C_1 ($\lambda_e^{2/3}\lambda_s^{1/3} < \lambda_H < \lambda_s$) we have $\hat{\gamma}^2 = (2/\pi)\lambda_H \lambda_s$. Finally, if $C_2/C_1 \to \infty$ Eq. (18) becomes $\hat{\gamma} = (\Delta'/\pi m)\lambda_e \lambda_s$. These instabilities are the semicollisional analogues of resistive kink, ideal $m = 1$ kink and tearing mode respectively.

We have demonstrated, that the MHD model properly describes semicollisional modes in tokamaks even if the characteristic width of the singular layer is less then the ion Larmor radius. Moreover, the MHD treatment is identical to the Padé approximation in the kinetic approach. This fact is not suprising. The above analysis shows that the "semicollisional" effect is intrinsically the fluid one. It simply means that at small scales not $\mathbf{B}$, but $\mathbf{B} + (M/e)\nabla \times \mathbf{V}$ becomes the frozen-in quantity. Obviously the kinetic theory is not necessarily required to describe such an effect. We conclude, that investigation of semicollisional modes in more realistic configurations also can be done on the basis of the MHD model.

Acknowledgements—I wish to thank prof. T. J. Schep for discussions and for editing the manuscript.

This work was performed as part of the research programme of the association agreement of Euroatom and the "Stichting voor Fundamenteel Onderzoek der Materie" (FOM) with financial support from the "Nederlandse Organisatie voor Wetenschappelijk Onderzoek" (NWO) and Euroatom.

References

[1] J. F. Drake and Y. C. Lee, Phys. Fluids **20**, 1341 (1977).

[2] L. Zakharov and B. Rogers, Phys. Fluids **B4**, 3285 (1992).

[3] F. Pegoraro and T. J. Schep, Plasma Phys. Contr. Fusion **28**, 647 (1986).

[4] A. B. Mikhailovskii, Theory of Plasma Instabilities, Vol. 2. Consultants' Bureau (1974).

[5] B. Coppi, R. Galvao, R. Pellat, M. N. Rosenbluth and P. H. Rutherford, Sov. J. Plasma Phys. **2**, 533 (1976).

[6] H. P. Furth, J. Killeen, and M. N. Rosenbluth, Phys. Fluids **6**, 459 (1963).

THE LINEAR THRESHOLD OF THE INTERNAL KINK MODE

G. Fogaccia[1] and F. Romanelli

Associazione EURATOM-ENEA sulla Fusione, Centro Ricerche Energia Frascati,
C. P. 65- 00044, Frascati, Rome (Italy)

The stability of the internal kink mode is usually described within the context of the ideal MHD model following the first work by Bussac et al.[1]. Toroidal effects, associated to the coupling of the dominant m=1 component to the m=2 and m=0 components of the eigenfunction, yield a stabilizing effect. Therefore the mode turns out to be stable for $\beta_p<\beta_{pc}$, where β_p is defined as

$$\beta_p=-\frac{R_0^2}{r_1^4}\int_0^{r_1} r^2\,\beta'\,dr \qquad (1)$$

with q the safety factor, $q(r_1)=1$, $\beta=2p/B^2$, p the pressure, B the toroidal magnetic field, R_0 the major radius and β_{pc} a coefficient which depends only on the current density profile. In the original Bussac paper, β_{pc} was approximately evaluated for a parabolic current density profile, obtaining $\beta_{pc}\approx 0.3$. It has been recently pointed out [2] that the value 0.3 tends to overestimate the threshold and that a more realistic estimate yields β_{pc} around 0.1. However, the ideal MHD model is inadequate to fully account for the physical effects relevant for a relatively weak instability as the internal kink mode. In particular, perpendicular compressibility of the thermal trapped and barely circulating particles can produce a significant stabilizing effect [3] which can determine, in situation of pratical interest, the actual stability of the internal kink mode.

The stability of the system is described by the ideal MHD model

$$-\omega^2\xi=\delta j\times B+j\times\delta B-\nabla\cdot\delta p \qquad (2)$$

with $\delta j=\nabla\times\delta B$ and $\delta B=\nabla\times(\xi\times B)$. The pressure tensor is expressed as $\delta p=\delta p_\perp I+(\delta p_\parallel-\delta p_\perp)bb$, where I is the unit matrix, b the unit vector in the direction of the equilibrium magnetic field, and the thermal ion and electron pressure contribution can be splitted into a convective and a compressional part: $\delta p_{j\perp}=-\xi_\perp\nabla\cdot p_{j\perp}+(m/2)\int d^3v v_\perp^2\, H_j$ and $\delta p_{j\parallel}=-\xi_\perp\nabla\cdot p_{j\parallel}+m\int d^3v v_\parallel^2 H_j$. The compressional contribution is evaluated by solving the drift kinetic equation

$$v_\parallel b\cdot\nabla H_j-i(\omega-\omega_{dj})H_j=-i(\omega-\omega^*_{Tj})\,\frac{\omega_{dj}}{\omega}\,\frac{e_j\phi}{T_j}\,F_{Mj} \qquad (3)$$

where ϕ is the electrostatic potential related to the perpendicular displacement by $\nabla\phi=i\omega(Bx\xi_\perp)$, $\omega^*Tj=-i(T_j/e_jB)(bx\nabla lnF_{Mj})\cdot\nabla$, $\omega_{dj}=-iv_{dj}\cdot\nabla$, v_{dj} is the magnetic drift velocity and the velocity space variables are the energy per unit mass $E=v^2/2$ and the magnetic moment $\mu=v_\perp^2/2B$.
The usual variational procedure is followed here, which corresponds to successive minimization of the energy functional, order by order in $\varepsilon=r_1/R_0$. The energy functional is obtained by multiplying Eq.(2) by ξ^* and integrating over the volume and it is given by

$$D(\xi)=\delta I+\delta W_{MHD}+\delta W_{kc} \qquad (4)$$

where the first term $\delta I=-(1/2)\omega^2\int d\tau\rho|\xi|^2$ is the kinetic energy functional, which is zero for marginally stable modes; the second term is the usual MHD contribution

$$\delta W_{MHD}=(1/2)\int d\tau[\, B^2|\nabla\cdot\xi_\perp+2\xi_\perp\cdot\kappa|^2-2(\xi_\perp\cdot\nabla p)(\xi_\perp^*\cdot\kappa)+|\delta B_\perp|^2-\xi_\perp^*\cdot(J_\parallel bx\delta B)]$$

and the last term is the compressional contribution given by $\delta W_{kc}=-(1/2)\int d\tau[\delta p_\perp{}^c\nabla\cdot\xi_\perp^*-(\delta p_\parallel{}^c-\delta p_\perp{}^c)(\xi_\perp^*\cdot\kappa)]$ (the superscript c refers to the compressional terms). In the MHD case such a contribution is given by $\delta W_{kc}=5/3\int d\tau|(\nabla\cdot\xi)|^2$ and can be set to zero by a proper choice of the parallel displacement. In the present analysis this term is evaluated by solving Eq(3). The minimization of the energy functional $D(\xi)$ in leading order ($\delta W_{MHD}{}^{(0)}$) and in the next one ($\delta W_{MHD}{}^{(2)}$) is satisfied by a displacement $\xi(r,\theta,\phi)=\xi_0(r,\theta,\phi)+\varepsilon\xi_1(r,\theta,\phi)+...$ such that $\nabla\cdot\xi_{\perp 0}=0$ and $\nabla\cdot\xi_{\perp 1}=-2\xi_{\perp 0}\cdot\kappa$, ($r$, θ, ϕ being the usual radial, poloidal and toroidal variables, and κ the equilibrium magnetic field curvature). Then at the lowest order the effect of perpendicular comressibility is minimized by a perpendicular displacement such that $\nabla\cdot\xi_{\perp 1}=-2\xi_{\perp 0}\cdot\kappa$.

In the limit $1-q(r)=O(1)$ inside the $q=1$ surface, $\xi_{\perp 0}$ is a rigid displacement with $\xi_{r0}(r)=\xi_0 e^{i(m\theta-n\phi)}$ for $r<r_1$ and $\xi_{r0}(r)=0$ for $r_1<r<a$. Therefore by using the eigenfunction corresponding to the rigid displacement and by solving Eq.(3) with the ordering $\omega_{dj},\omega^*Tj<<\omega<<\omega_{bi}=\varepsilon^{1/2}v_{ti}/qR_0$ to calculate pressure compressional terms, δW_{kc} can be evaluated exactly as the hot particle contribution in Ref.[4]. The most important contribute to δW_{kc} comes from the trapped particles. Equation (3) yields $b\cdot\nabla H_j=0$, i.e. $H_j=H_{jo}\, e^{iq\theta}$ with the quantity H_{jo} determined by orbit averaging the next order equation, yielding $H_{jo}=<\xi_\perp\cdot\kappa e^{iq\theta}>$, where $<...>$ denotes bounce average. By considering a parabolic pressure profile $p(r)=p_0(1-r^2/r_0{}^2)$, the final expression for δW_{kc} turns out to be $\delta W_{kc}\equiv 2\pi R_0(r_1B_0|\xi_{0l}/R_0)^2\cdot(3/4)(2\varepsilon)^{1/2}\mu_1(r_0{}^2/R_0{}^2)\beta_p$ with $\mu_1=2\int_0^1 d\lambda\lambda[2E(\lambda)-K(\lambda)]^2/K(\lambda)\approx 0.55$ and $E(\lambda)$, $K(\lambda)$ the complete elliptic integrals. Note that the compressional effects appear only at the fourth order in ε.
Following Ref.[1], the minimized functional can finally be written at the fourth order in the following form

$$-3\pi\,(1-q(0))\,(\beta_p^2-\beta_{pc}^2)+\frac{3}{4}(2\varepsilon)^{1/2}\mu_1\frac{r_0^2}{r_1^2}\beta_p=0 \qquad (5)$$

If the compressional contribution is neglected, the usual instability criterion $\beta_p>\beta_{pc}$ is recovered. However, for small values of β_{pc}, the instability condition becomes

$$\beta_p>\frac{3}{4}(2\varepsilon)^{1/2}\,\mu_1\,\frac{r_0^2}{r_1^2}\,\frac{1}{3\pi(1-q(0))} \qquad (6)$$

Therefore for q(0) approaching unity the stabilizing effect associated to compressibility may dominate over the effect of toroidal coupling.

The above calculation fails for $1-q(0)=O(\varepsilon)$. Following Ref.[5], the mode stability in this case is described by the integro-differential equation for $\xi_{r0}(r)$, (the subscript r will drop for simplicity):

$$\frac{d}{dx}\left[x^3(\delta q^2+3\gamma^2/\omega_A^2)\frac{d\xi_0}{dx}\right]+\alpha(x)x^2\Lambda_1\int_0^1\alpha(x)x^2\xi_0dx-\beta_K x^{3/2}\xi_0=0 \qquad (7)$$

where $x=r/r_1$, $\delta q(x)=1-q(x)$, $\gamma=-i\omega$ is the growth rate, $\omega_A=v_A/(3^{1/2}r_1q'R_0)$ with v_A the Alfvèn velocity, $\alpha(x)=(2R_0/r_1B_0^2)dp/dx$, $\Lambda_1=(C_1+3)/(1-C_1)$ with $C_1=(x\,d\xi_1^{(m=2)}/dx)/x_1^{(m=2)}|_{x=1}$ and finally the term β_K related to the compressional contribution is $\beta_K(x)=(15/8\pi)(p(x)/B_0^2)(2r_1/R_0)^{1/2}(\mu_1+\mu_2)$. The numerical coefficient μ_2, resulting from orbit averages for circulating particles, is given by $\mu_2=2\int_0^1 d\lambda[2E(\lambda)-(2-\lambda^2)K(\lambda)]^2/\lambda^6K(\lambda)$. Note that for ultra flat q profiles, both for trapped and for passing ions, the contributions to eingevalue equation (7) are $O(\varepsilon^{1/2})$ with respect to the other terms.

Equation (7) can be solved analytically if the kinetic term $\beta_K x^{3/2}\xi_0$ is replaced by $\beta_{K0}x\xi_0$ with β_{K0} being constant. Such an approximation is not expected to produce major differences with respect to the general case. In addition, the following model q-profile is assumed: $q(r)=q_0$ for $0<r<r_1-\delta$, with $\delta q_0=1-q_0>0$ and δ the typical lenght of the layer around the surface $q(r_1)=1$; $q(r)=1+\delta q_0(r-r_1)/\delta$ for $r_1-\delta<r$. In such a case the solution for $0<r<r_1-\delta$ is simply given by

$$\xi_0(x)=\frac{x^2}{(\beta_{K0}-8\delta q_0^2)}+Ax^{\nu} \qquad (8)$$

with $\nu=-1+(1+\beta_{K0}/\delta q_0^2)^{1/2}$ and A being a constant determined from the matching with the solution in the region $r_1-\delta<r$. On matching the solution in the inner region with that in the external region and taking, for the sake of simplicity, the limit $\delta\to 0$, the following threshold condition is obtained

$$\frac{\delta q_0^2}{\alpha_1^2 \Lambda_1} = \frac{1}{(\beta_{K0}/\delta q_0^2)-8} \left[\frac{1}{6} - \frac{2}{\nu\ (\nu+4)}\right] \tag{9}$$

with $\alpha_1=4p_0R_0r_1/r_0^2B_0^2$ for a parabolic pressure profile. The solution of Eq.(9) yields the following threshold β_p value, for $\delta q_0<<\beta_{K0}^{1/2}$ and $\delta q_0>0$:

$$\beta_p=\frac{45(\mu_1+\mu_2)}{64\pi} \frac{r_0^2}{\Lambda_1\ r_1^2} \left(\frac{2r_1}{R_0}\right)^{1/2} \tag{10}$$

with $\mu_1+\mu_2\approx 0.65$. In the limit $\delta q_0>>\beta_{K0}^{1/2}$ and $\delta q_0>0$, the following solution is obtained

$$\beta_p=\frac{15(\mu_1+\mu_2)}{16\pi} \frac{r_0^2}{\Lambda_1\ r_1^2} \left(\frac{2r_1}{R_0}\right)^{1/2} \tag{11}$$

Finally, for $\delta q_0<0$ the result of Ref.[5] is recovered, namely

$$\beta_p=\frac{45(\mu_1+\mu_2)}{64\pi} \frac{r_0^2}{\Lambda_1\ r_1^2} \left(\frac{2r_1}{R_0}\right)^{1/2} + 3\left(\frac{3}{2\Lambda_1}\right)^{1/2} \frac{R_0}{r_1} |\delta q_0| \tag{12}$$

In conclusion, we have shown that the effect of compressibility has a strong stabilizing influence on the internal kink mode. For finite shear values inside the $q=1$ surface the threshold β_p value given by Eq.(6) is about $\beta_p=0.3$ for $1-q_0=0.2$, $r_1/R_0=0.1$, $r_0^2/r_1^2=3$ and parabolic pressure profiles. For $1-q_0\rightarrow 0$ the mode can be stable also in the presence of a finite pressure gradient. The minimum β_p value for $1-q_0=0$, $r_1/R_0=0.1$, $r_0^2/r_1^2=3$ and $\Lambda_1=1$ turns out to be, from Eq(10), $\beta_p=0.2$.

References

1) ENEA fellow
[1] M.N. Bussac, R. Pellat, D. Edery and J.L. Soule, Phys. Rev. Lett. **35**, 1638 (1975)
[2] H. Lutjens, A. Bondeson and G. Vlad, Nucl. Fusion **32**, 1625 (1992)
[3] M.D. Kruskal and C.R. Oberman, Phys. Fluids **1**, 275 (1958)
[4] L. Chen, R.B. White and M.N. Rosenbluth Phys. Rev. Lett. **52**, 1122 (1984)
[5] R.J.Hastie and T. Hender Nucl. Fusion **28**, 585 (1988)

Two Novel Applications of Bootstrap Currents: Snakes and Jitter Stabilization

A. Thyagaraja and F.A. Haas*
AEA Technology, Fusion, Culham, Abingdon, Oxfordshire, OX14 3DB, UK.
(Euratom/UKAEA Fusion Association)

Abstract

Both neoclassical theory and certain turbulence theories of particle transport in tokamaks predict the existence of bootstrap (ie, pressure-driven) currents. Two new applications of this form of non-inductive current are considered in this work. The first is an explanation of the 'snake' phenomenon observed in JET based on steady-state nonlinear tearing theory. The second is an active method of dynamic stabilization of the $m = 1$ mode using the 'jitter' approach suggested by Thyagaraja *et al* in a recent paper.

1. Introduction: The bootstrap current is a striking prediction of neoclassical theory[1] which has received a measure of experimental support even though neoclassical transport is not observed in general. It was suggested independently by Yushmanov[2,3], Connor-Taylor[4] and Haas-Thyagaraja[5] that there might be a turbulence-enhanced, *anomalous* pressure-driven current associated with turbulent particle and energy losses and possibly anomalous resistivity. In a recent paper[6], we have reviewed various theories of particle and current transport in tokamaks and described their principal features and differences. Here, we consider two **contrasted** applications: ie, DC bootstrap, in helical geometry and use nonlinear tearing mode theory[7] to explain 'snakes' [8]; we suggest that an AC form of bootstrap, in poloidally symmetric geometry could be used to 'jitter stabilize' the $m = 1$ mode[9].

2. Snakes and bootstrap currents: We briefly summarise the salient features of our theory of the nonlinearly saturated $m = 1$ tearing mode (the details will be published in a forthcoming paper). Considering the nonlinearly saturated final states in reduced MHD following an $m = 1$ linear tearing instability in tokamaks with $q_0 < 1$, asymptotics[7] give a bifurcation relation, expressing the saturated island width w_{island} in terms of the shear parameter s. This relation involves the profile of the current density **inside** the (unsymmetrical) island. This is *different* from the $m > 1$ problem studied by Carrera *et al* [10]. In contradiction to their assumption that the pressure gradients within the island are flattened, the experimental observations of snakes show that this is *not* necessarily the case for $m = 1$. Using the non-dimensional forms established for the helical flux function $\Psi^*(Y, u, \lambda)$, and defining the parameter $\alpha \equiv (2 - s)/s, s \equiv r_i q'(r_i)$, the nonlinear 'inner' equations are solved to give

* Oxford Research Unit, The Open University, Boar's Hill, Oxford.

$2\alpha \int_0^{\frac{1}{2}} \left[J^*_{+,ohmic}(\Psi) - 1\right] d\Psi = 1 - 2\alpha \int_0^{\frac{1}{2}} J^*_{+,p}(\Psi) d\Psi$, where λ is proportional to the saturated island width. The expression for $J^*_{+,ohmic}$ was already obtained in Ref. 7. $J^*_{+,p}$ is calculated from neoclassical theory using the well-known expression for the bootstrap current: $j_{\|}^{BS} = -\kappa.(\frac{r}{R})^{1/2} \frac{c}{B_{pol}} \frac{dp}{dr}$, where κ depends on collisionality, ratios of density and temperature gradients etc. All phenomenological models of anomalous bootstrap currents lead to the same general form with $\kappa \simeq (\frac{R}{r})^{1/2}$. We treat all the cases in a unified way, setting $\Delta p \equiv p_{max} - p_{separatrix}$. For an arbitrary pressure profile, $F(\Psi)$ within the island, we get, $J^*_{+,p}(\Psi) = (\frac{\delta\beta^*_p}{\lambda}).\frac{dF}{d\Psi}$, where, $\delta\beta^*_p \equiv \kappa.\frac{\Delta p}{sB^2_{pol}(r_i)}.(\frac{r_i}{R})^{1/2}$. The bifurcation relation is a quadratic in λ for given Δp and shear:

$$\lambda = \lambda_0(1 - \frac{4\delta\beta^*_p}{s\lambda}), \tag{1}$$

where $\lambda_0 \equiv \frac{1}{2}\alpha^* \frac{d\log q(r_i)}{d\log \eta(r_i)}$ is the solution in the absence of pressure. The numerical constant $\alpha^* \equiv \left[\int_0^1 \frac{\pi dx}{2K(x)}\right]^{-1}$ with $1 < \alpha^* < \frac{3}{2}$. The island width is then given by, $w_{island} \equiv 2\lambda r_i$. This can also derived from Smolyakov's[11] Rutherford-type equation, $\frac{\partial w}{\partial t} = \mu_* D_R \left[\frac{1}{w} - \frac{1}{w_0} - \frac{8r_i\delta\beta^*_p}{s.w^2}\right]$. We use the notations, $w = 2\lambda r_i$ and $w_0 = 2\lambda_0 r_i$. When $\delta\beta^*_p$ is non zero, there are two real solutions, $\lambda_\pm$, for sufficiently small pressure within the island: $\lambda_\pm = \lambda_0.\left[\frac{1\pm\sqrt{(1-\frac{16\delta\beta^*_p}{s\lambda_0})}}{2}\right]$. If the island pressure is sufficiently high (ie when $\frac{4\delta\beta^*_p}{s\lambda_0} > 1$), there are no real solutions. As the pressure within the island rises, the two solutions approach each other and disappear when the critical value is exceeded. This result may indicate a 'β crash' of the saturated $m = 1$ island. The smaller of the two solutions with $\lambda = \frac{4\delta\beta^*_p}{s}$, leads to small, saturated islands even when s is *not* small! The model predicts **two** distinct types of islands: purely Ohmic 'hot islands' with T_e maxima within islands. With pressure-driven currents present, there could also be a 'cool' island scenario with merely a **pressure** maximum within the island; the temperature at the O-point can even be lower than at the separatrix and the resistivity can also be high.

In a recent paper, Gill *et.*[8] have documented observations of large, very localized pressure perturbations observed in JET due to the formation of a small region on the $q = 1$ surface which persists for a surprisingly long time, called the **snake**. The most common type are **pellet induced** snakes. More rarely, **spontaneous** snakes associated with increased resistivity changes and impurity accumulation prior to the onset of sawteeth are seen, as are more exotic **double** and **negative** snakes. We take a typical example of a pellet-induced snake. Thus, case **B** (Table 1, Ref. 8) is a pellet produced snake with a lifetime of nearly 2 seconds. From experiment we take: $\Delta p \simeq \delta n_e.T_e \simeq 2.0 \times 10^4$ ergs/cc. $r_s = r_i = 50$cm; $R = 300$cm; $B_z \simeq 3$ Tesla. The shear parameter s is not known in this case, but a reasonable estimate is, $s \simeq 10^{-1}$. We now estimate $\delta\beta^*_p \simeq \kappa.4 \times 10^{-3}$. Taking $\kappa \simeq 1$ we obtain, $\lambda \simeq \frac{4\delta\beta^*_p}{s} \simeq 0.16$. This leads to, $w_{island} \simeq 16$cm. This is in moderate agreement with experimental island

width of 20 cm. The case of spontaneous snakes involves impurity accumulation and increased resistivity. They are fairly rare and are not strictly steady-state phenomena. It seems that pressure-driven currents within the island offer the most plausible explanation for them as for the 'negative' snakes. Given the uncertainties in the theory and measurements, the estimates, $\delta\beta_p^* \simeq 5 \times 10^{-3}, w_{island} \simeq 20$cm for Case C, are in qualitative agreement with experiment. There are no detailed measurements available for the more exotic 'double' and the 'negative' snakes although the theory can also account for them. At present, both the model and the data are in too primitive a state to conclude *definitely* that the neoclassical bootstrap current is sufficient to explain snakes via our nonlinear saturation mechanism.

3. Application of AC Bootstrap to Dynamic Stabilisation: Active control of plasma instabilities, both of the dynamic and the feed-back variety can be expected to play an increasingly important engineering role in the reactor regime where severe constraints set by both gross/disruptive and fine-scale/transportive instabilities must be avoided for both economic and safety/operational grounds. We consider the possibilities of a type of active control of gross plasma instabilities suggested by the recent paper of Thyagaraja *et al.*[9] through the use of fluctuating pressure-driven currents. We present some estimates of the possible requirements. Using Ohm's law and taking $j_{\|}^{c.d}$ to be the 'noninductively' driven current source (of whatever origin), it follows that if $j_{\|}^{c.d.} = \frac{2}{\pi}(\frac{I^*}{2\pi r_s})(\frac{\Delta \cos \omega t}{\Delta^2+(r-r_s)^2})$, where Δ is the radial localization width of the driven current, I^* is the total maximum noninductive current and r_s is the resonance radius of the mode required to be jitter stabilized, the jitter amplitude of q is obtained as, $\frac{\delta q}{q} \simeq (\frac{c^2\eta_{\|}}{4\pi\Delta^2\omega})(\frac{I^*}{I_{plasma}(r_s)})$. For stabilization of the $m = 1$ mode, we require, $\frac{\delta q.V_{Alfven}}{R\omega} \geq 1$. This shows that low frequency, strong localization, large amplitude and high resistivity are 'good' for jitter stabilization. The localization width Δ is set by the method used to drive the noninductive current. The general formula shows that as the collisionality decreases, η decreases rather sharply with temperature (if assumed Spitzer, or neoclassical) and the requirements for penetration seem rather stringent. We get the following condition on $\frac{\delta p}{p}$: $(\frac{\delta p}{p})_{max} \geq (\frac{\omega R}{v_A}).(\frac{4\pi\Delta^2\omega}{c^2\eta}).(\frac{r_s}{2.L_p.(1-s).f^{BS}})$.where, $\Delta \ll L_p$, $f^{BS} \equiv j_{\|}^{BS}/j_{\|}^{Tot}$, $j_{\|}^{Tot} \simeq \frac{c}{4\pi}\frac{1}{r}\frac{\partial}{\partial r}(rB_\theta), q = \frac{rB_z}{RB_\theta}$, $s \equiv \frac{r_s q'(r_s)}{q(r_s)}$ and f^{BS} is the 'bootstrap' fraction. We first consider the COMPASS example and take $\omega \leq 3\times10^4\text{sec}^{-1}$ ($\simeq$ 5kHz), $v_A/R = 10^7\text{sec}^{-1}$, $\Delta = 2$cm, $r_s/L_p = 0.3$, $s = 0.1$, $f^{BS} = 0.5$, $n_e \simeq 2 \times 10^{13}/\text{cm}^3$, $T_e \simeq 1$keV. We find that $\frac{\delta p}{p} \simeq \epsilon \geq 2\%$ for stabilization to occur. This estimate is strictly neoclassical. In the case of JET, we take: $T_{e,i} \simeq 5$keV, $n \simeq 10^{14}\text{cm}^{-3}$, $B_z = 3$Tesla, $r_s/L_p = 0.3, f^p = 0.8$, $R = 300$cm, $Z_{eff} \simeq 2$, $\omega = 10^4\text{sec}^{-1}$, $\Delta = 3$cm. These parameters lead to (using neoclassical resistivity) $v_A/R \simeq 3 \times 10^6\text{sec}^{-1}$, $\eta \simeq 2 \times 10^{-18}$cgsu, $\frac{c^2\eta}{4\pi\Delta^2\omega} = 2 \times 10^{-3}$ and $\epsilon \geq 25\%$. This rather large perturbation can be considerably reduced if the 'anomaly' factor is 5, for example. For the turbulent bootstrap, in the Haas-Thyagaraja model $\eta = \eta_{\|}^{Neo} + \eta_\theta(\frac{B_{pol}}{B_{tor}})^2$, where η_θ could in general be very much larger than the neoclassical term. The frequency ω in the plasma frame may be achieved in various ways; for example by 'switching on and off' RF power or interrupting the beam suitably, etc. To estimate power requirements we suppose that the total

power input to the equilibrium plasma is P_{tot} and the associated energy confinement time is τ_E; taking a to be the minor radius and P_{jitter} to be the total power required to jitter the plasma pressure by the realtive amplitude, $\frac{\delta p}{p}$ at frequency ω and radial localization length Δ, we have, $\frac{P_{jitter}}{P_{tot}} \simeq (\omega\tau_E).(\frac{\delta p}{p}).(\frac{r_s\Delta}{a^2})$ and the condition,

$$\frac{P_{jitter}}{P_{tot}} \geq (\omega\tau_E).(\frac{r_s\Delta}{a^2}).(\frac{\omega R}{v_A}).(\frac{4\pi\Delta^2\omega}{c^2\eta}).(\frac{r_s}{2.L_p.(1-s).f^{BS}}) \quad (2)$$

For COMPASS-type numbers, taking $\tau_E \simeq 10$ ms, we find P_{jitter} to be between 5 to 10 % of the total power. In the case of JET the power fraction $\simeq$ 35%. Note that this power is really applied in 'bursts' in a localized region and does not add to the plasma β. The present scheme relies solely on heating the plasma rather producing $\delta j_{||}^{c.d}$ directly. Note that although the *effective* resistivity is increased, this does *not* mean that for a given total current the loop voltage or $E_{ext,||}$ is necessarily increased, since an increased bootstrap current can compensate the enhanced resistivity. In analogy with the well-known situation for the particle flux where the outward diffusive and the inward pinch can cancel, perturbative measurements are needed to verify the turbulent bootstrap.

4. Conclusions: Two different, new applications of bootstrap-like currents have been presented. Quite apart from the importance of describing snakes and active control using jitter techniques, the theory suggests experiments in both areas (DC and AC) which are likely to provide valuable insight into the nature of current diffusion and transport in tokamaks.

Acknowledgements: The authors thank Dr. J.W. Connor for useful suggestions. This work was (partially) funded jointly by the UK Dept. of Trade and Industry and Euratom.

[1]R.J. Bickerton, J.W. Connor and J.B. Taylor, Nature Phys. Sci. **229**, 110 (1971).
[2]P.N. Yushmanov, Sov. JETP Lett. **31**, 81 (1980).
[3]G.V. Pereverzev and P.N. Yushmanov, Sov. J. Plasma Phys. **6**, 543 (1980).
[4]J.W. Connor and J.B. Taylor, Comments Plasma Phys. Controlled Fusion **11**, 37 (1987).
[5]A. Thyagaraja and F.A. Haas, Europhys. Lett. **5**, 425 (1988).
[6]F. A. Haas and A. Thyagaraja, Plasma Physics and Controlled Fusion **35**, 1 (1993).
[7]A. Thyagaraja and F.A. Haas, Phys. Fluids B, **3**, 580 (1991).
[8]R.D. Gill, A.W. Edwards, D. Pasini and A. Weller, Nuclear Fusion **32**, 723 (1992).
[9]A. Thyagaraja, R.D. Hazeltine and A.Y. Aydemir, Phys. Fluids B, **4**, 2733 (1992).
[10]R. Carrera, R.D. Hazeltine and M. Kotschenreuther, Phys. Fluids **29**, 899 (1986).
[11]A. Smolyakov, Bulletin of American Physical Society, **37**, (9P21) 1594 (1992).

Magnetic equilibrium with fluid flow in a large m=2 island at RTP

B.Ph. van Milligen
(Asociación EURATOM-CIEMAT para Fusión, Avda. Complutense 22, Madrid, Spain)
N.J. Lopes Cardozo
(FOM-Institute "Rijnhuizen", PB 1207, 3430 BE Nieuwegein, The Netherlands)

Abstract

In recent work [1, 2] observations of a large m=2 island were presented that demonstrated the existence of a pressure gradient across the island. This fact disagrees with the usual assumption that the isobaric surfaces coincide with the flux surfaces. In [1, 2] a phenomenological model was proposed in which the observed gradients are explained from a short mean free path along the field lines due to the high collisionality in the outer regions of the plasma.

In this work we address the same problem from the equilibrium point of view. We describe the equilibrium in the presence of an island by means of a semi-analytical model. In the presence of pressure gradients along the flux surfaces the forces due to grad(p) and j x B do not cancel at all points in space. Due to the pressure gradient along the field lines, particle transport will take place from the inside (high-pressure) region of the island to the outside (low-pressure) region. Preliminary results indicate that the pressure gradient across the field lines, along with the j x B force, can drive a compensating cross-field fluid flow from the outside to the inside. This dissipative flow only occurs at sufficiently low temperatures (high collisionality), because with low collisionality transport along the field lines is dominant.

We present a computer simulation of the m=2 island, partly based on experimental data and partly on assumptions. The simulation demonstrates that fluid flow may be important in equilibrium calculations in islands in the outer regions of the plasma.

1. Introduction

The computation of a tokamak equilibrium taking acount of the existence of islands is a notoriously difficult problem, even when ideal MHD is assumed to be valid in most of the plasma volume. The situation becomes even more difficult when fluid flow must also be taken into account. Nevertheless, experimental observations (see section 2) lead us to believe that is exactly the situation we need to describe.

In this paper we make a first attempt at trying to understand the complex equilibrium with flow problem in magnetic islands. For that purpose, we rather arbitrarily define an "equilibrium" flux and afterwards check that the chosen flux functions indeed lead to a situation that can more or less be described as being in equilibrium. Of course, such a model cannot lay claim to a high degree of reality, but we believe the excercise is instructive. Then we observe how a deviation from equilibrium similar to the one we have observed in an experiment leads to fluid flows.

2. Experimental observations and interpretation

Previously, we have reported on the observation of a large m=2, n=1 island on RTP [1, 2]. The RTP tokamak has major radius $R_0 = 0.72$ m and the plasma minor radius is a = 0.165 m. The observations were made in an ohmically heated discharge with plasma current $I_p = 145$ kA, toroidal field $B_\phi = 2.1$ T, edge safety factor $q_a = 2.8$, central electron temperature $T_e(0) \approx 750$ eV and central electron density $n_e(0) \approx 5.5 \cdot 10^{19}$ m^{-3}. A large rotating m=2, n=1 mode occurred preceding a major disruption and lasted for about 12 ms., interrupted by a minor disruption 3 ms. before the major disruption. The analysis of the island, 2 ms. prior to the minor disruption, was made based on measurements of the poloidal field with a set of pick-up coils, a 20 channel heterodyne ECE radiometer and a 19 channel FIR interferometer. We observed both T_e- and n_e-gradients across the island. The T_e gradients could be understood by carefully analysing local transport across and along the field lines within the island, taking account of the mode geometry. The n_e gradients were more difficult to explain, although a possible cause for both types of gradients was found in mode rotation with respect to the plasma fluid. It was concluded that the island did not conform to the usual assumption that pressure is constant on a flux surface.

3. A simple mathematical model for an island equilibrium

Our model takes a simple analytical equilibrium upon which we superpose a disturbance that generates an island chain. We shall use the toroidal coordinate system (r, θ, ϕ) that relates to the common cylindrical coordinate system (R, Z, ϕ) by $R = R_0 + r\cos\theta$ and $Z = r\sin\theta$.

3.1 An analytic equilibrium

We assume an "equilibrium" as given by profile-consistency considerations [3]: a low-β plasma with circular and concentric flux surfaces. The current density is simply given as:

$$j(x) = j_0 \{1 + q_a x^2\}^{-2}, \tag{1}$$

where $x = r/a$ and a is the minor radius of the plasma. The central current density j_0 is given by $j_0 = I_p(1+q_a)/(\pi a^2)$, where I_p is the total plasma current and q_a the boundary safety factor. The poloidal field is given by: and the q-profile by

$$B_\theta(x) = \frac{\mu_0 j_0 a x}{2\{1 + q_a x^2\}}, \qquad (2) \qquad q(x) = q_a\left(\frac{1+q_a x^2}{1+q_a}\right) \tag{3}$$

Thus, taking $a = 0.165$ m (the RTP value) and $q_a = 2.8$, the $q=2$ surface is located at $r_{mn} = 0.129$ m. The plasma current I_p is calculated from q_a and $B_\phi = 2.1$T: $I_p = 141$ kA.

The total magnetic field can be written as

$$\mathbf{B} = -B_\phi \mathbf{e}_\phi - \frac{1}{R}\nabla\psi \times \mathbf{e}_\phi \tag{4}$$

where B_ϕ, the toroidal magnetic field and ψ is the usual poloidal flux. For simplicity, we take B_ϕ constant and likewise $R = R_0$, so that our model is effectively cylindrical. Anticipating the definition of a (m,n) magnetic island in Section 3.2, we introduce local coordinates (r, ζ, ξ):

$\zeta = m\theta - n\phi$ (coordinate across the field lines on an (m,n) rational surface) and

$$\xi = \frac{n r_{mn}}{R}\theta + \frac{mR}{r_{mn}}\phi \qquad \text{(coordinate along the field lines)}$$

These coordinates are chosen such that $\nabla\zeta \cdot \nabla\xi = 0$ on the rational surface. An alternative manner of writing the magnetic field is then:

$$\mathbf{B} = \nabla\psi_\zeta \times \nabla\zeta + \nabla\psi_\xi \times \nabla\xi, \tag{5}$$

where the fluxes ψ_ζ and ψ_ξ are, in terms of the quantities of Eq. (4):

$$\psi_\zeta = \frac{1}{g_{mn}}\left(\tfrac{1}{2}mB_\phi r^2 R/r_{mn} + n\psi r_{mn}/R\right) \tag{6a}$$

$$\psi_\xi = \frac{1}{g_{mn}}\left(\tfrac{1}{2}nB_\phi r^2 - m\psi\right) \tag{6b}$$

where $g_{mn} = m^2 R/r_{mn} + n^2 r_{mn}/R$. This way of writing the magnetic field has the advantage that $\nabla\psi_\xi$ vanishes on the rational surface, thus simplifying the description of the magnetic field in the vicinity of the rational surface.

From Eqs. (2) and (4) we calculate the main poloidal flux ψ:

$$\psi(x) = \frac{\mu_0 j_0 R_0 a^2}{4q_a}\ln(1+q_a x^2) \tag{7}$$

such that ψ_ξ can be written, using Eq. (6b):

$$\psi_\xi = \frac{a^2 B_\phi}{2g_{mn}}\left(nx^2 - \frac{m(1+q_a)}{q_a^2}\ln(1+q_a x^2)\right) \approx \frac{a^2 B_\phi}{g_{mn}}\frac{n^2}{m}\frac{q_a^2 x_{mn}^2 (x-x_{mn})^2}{1+q_a} + C \tag{8}$$

This flux function contains all the information we need to describe the magnetic field components *perpendicular* to the field line direction on the rational (m,n) surface. The approximation on the r.h.s. of Eq. (8) is to second order in $(x-x_{mn})$. The irrelevant constant C is chosen equal to zero.

3.2 The island

The island, located on the (m,n) rational surface referred to above, is generated by currents predominantly directed along the field lines on the rational surface. Therefore, the island can be described in terms of a single flux function $\tilde{\psi}_\xi$ that gives rise to a radial field perturbation. We arbitrarily define the island flux as

$$\tilde{\psi}_\xi = -\frac{N}{2}(1+\cos\zeta)\, e^{-(x-x_s)^2/\Delta^2} \tag{9a}$$

where x_s is the position of the island ($x_s \approx x_{mn}$), and N and Δ are factors determined by the island width w and the amplitude of the radial field disturbance on x_s. From the approximation of ψ_ξ, Eq. (8), we find

$$N \approx \frac{w^2 B_\phi}{4 g_{mn}} \frac{n^2}{m} \frac{q_a^2 x_{mn}^2}{1+q_a} e^{(w/(2a\Delta))^2} \qquad (9b) \qquad \tilde{B}_r(x_s) \approx -\frac{N g_{mn}}{2 R a x_s} \sin\zeta \qquad (9c)$$

Note that Eqs. (9b,c) are in exact agreement with White's formula for narrow islands [4], when $w/(2a) \to 0$. The actual position of the island x_s is chosen by demanding that the force $\mathbf{j}\times\mathbf{B}$ in the O-point of the island be very small. Note that $x_s < x_{mn}$ affects the interpretation of measurements of external field fluctuations due to the island, usually assumed to be generated at $x = x_{mn}$, and thus affects calculations of island widths. From Eq. (9) the perturbed field $\tilde{\mathbf{B}}$ and current density $\tilde{\mathbf{j}}$ may be derived by taking the appropriate derivatives (Eq. (5)).

3.3 Ideal MHD force balance

Ideal MHD equilibria must satisfy $\nabla p = \mathbf{j}\times\mathbf{B}$. Thus, since the total magnetic field can be written, in the presence of the island:

$$\mathbf{B} = \nabla\psi_\zeta \times \nabla\zeta + \nabla(\psi_\xi + \tilde{\psi}_\xi) \times \nabla\xi,$$

and with the plausible assumptions that $p = p(\zeta, r)$ and $\psi_\zeta = \psi_\zeta(r)$, it follows that $p = p(\psi_\xi + \tilde{\psi}_\xi) = p(\Psi_\xi)$.

One may ask to what degree Eqs. (1-3) combined with Eq. (9) actually do constitute an equilibrium. We choose $\tilde{B}_r^{max} = 7$ mT; w = 2.9 cm; $x_s = 0.65$. Eqs. (9b,c) then yield N and Δ and we compute the equilibrium using Eqs. (8) (the exact formula) and (9a). The flux Ψ_ξ is shown in Fig. 1. Because $x_s < x_{mn}$ the island is asymmetric (in accordance with observation, cf. eg. [5]). The radial component of the force $\mathbf{j}\times\mathbf{B}$ is much larger than its toroidal or poloidal components (except in a few internal points of the island), so we may compute $p(r,\theta,\phi)$ to good approximation by radially integrating this force inwards from the plasma boundary. The condition $p = p(\Psi)$ is satisfied to within 30% near the separatrix of the island, the deviation being much smaller (around 10%) in the island interior (Fig.2). The large deviation from the equilibrium condition near the separatrix is inevitable, because the island is embedded in a plasma with a considerable pressure gradient through the X-points.

3.4 Deviation from ideal MHD: plasma flow

As mentioned in the introduction, we proceed to calculate the flow in the island. We assume that some mechanism such as heat transport or mode rotation (cf. [1] and [2]) creates a pressure gradient across the island. More specifically, we impose the pressure profile as it is in the X-point region throughout the plasma. This must be regarded as an extreme case: in reality the mechanisms cited above will never quite be able to establish such a situation, although possibly they may come close.

In absence of ideal MHD equilibrium, the force balance equation must be modified. The steady state in a constant-density magnetofluid is described by (cf. eg. [6]):

$$\mathbf{j}\times\mathbf{B} - \nabla p = \rho\nu\nabla^2\mathbf{v} \qquad (10)$$

where ρ is the density, ν the kinematic viscosity and $\mathbf{v}$ the flow velocity. This equation allows computation of the "flow" $\mathbf{G} = \rho\mathbf{v}\nu$ under the assumption that ν, also, does not depend on space, given boundary conditions. We present preliminary results of this calculation. Fig. 3 displays the radial component of G in X- and O-point and Fig. 4 shows the flow field. It is observed that the flow is mainly radial and converges close to the inner island separatrix. Possibly the sink can be identified with transport along the field lines that twist around the O-point and connect the high-pressure to the low-pressure region.

4. Conclusions

The semi-analytical island model presented in the present work can lay only limited claim to reality. Nevertheless, it serves as a demonstration of the importance of flow in magnetic island regions. The flow arises when some mechanism creates a pressure gradient across the island. In earlier work candidates for such mechanisms were proposed (e.g. local transport within the island or mode rotation). In general, these mechanisms tend to be effective only at low local temperatures ($T_e < 500$ eV). This flow possibly exerts a significant influence on global radial transport, and it seems necessary to develop ways of estimating the size of this effect. The present work provides only a first attempt, and it is hoped that more realistic models can be constructed in the future.

References

[1] B.Ph. van Milligen, A.C.A.P. van Lammeren, N.J. Lopes Cardozo, F.C. Schüller, M. Verreck, Proc. 19th Eur. Conf. Innsbruck, 1992, Vol. 16C, Part I, EPS (1992) I-123
[2] B.Ph. van Milligen, A.C.A.P. van Lammeren, N.J. Lopes Cardozo, F.C. Schüller, M. Verreck, Submitted to Nucl. Fusion 1993
[3] F.C. Schüller, D.C. Schram, J. Konings, et al., in Contr. Fus. and Plasma Phys. (Proc. 18th Eur. Conf. Berlin, 1991), Vol. 15C, Part IV, European Physical Society (1991) IV-185
[4] R.B. White and D.A. Monticello, Phys. Fluids **20** (1977) 800 - 805
[5] J.A. Wesson, R.D. Gill, M. Hugon, et al., Nuclear Fusion **29** (1989) 641-666
[6] Y.Z. Agim and D. Montgomery, Plasma Physics and Controlled Fusion **33** (1991) 881 - 902

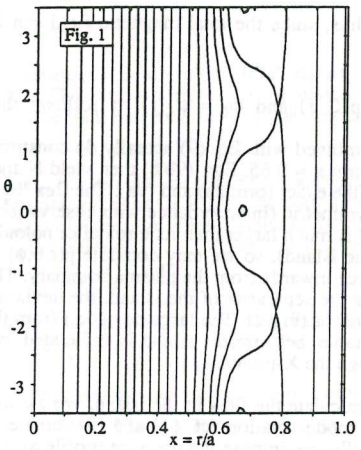

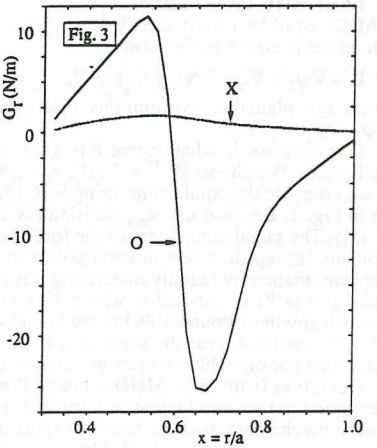

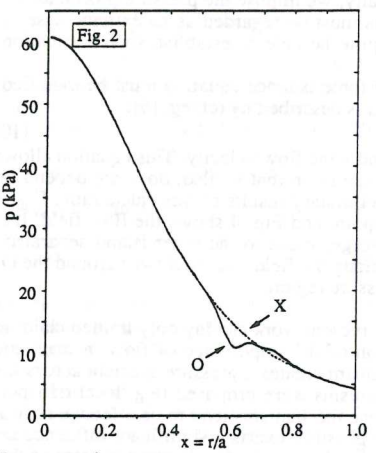

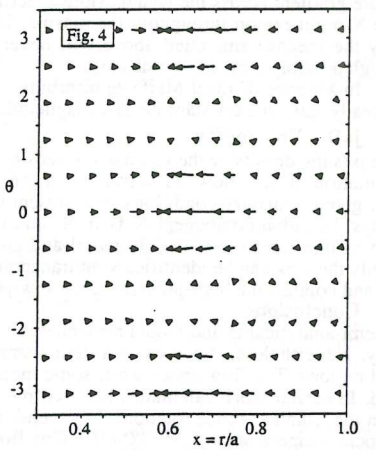

Figure captions

Fig. 1 Plot of Ψ_ξ-contours in the (x,θ) plane
Fig. 2 Pressure profile taken through the X- and O-points of the island
Fig. 3 Graphs of the "flow" G_r through the X- and the O-points
Fig. 4 Vector plot of G in the (x,θ) plane

PROPAGATING NONLINEAR MAGNETIC STRUCTURES

T.J. Schep*, F.Pegoraro** and B. Kuvshinov*

*FOM Instituut voor Plasmafysica Rijnhuizen, The Netherlands

**Dipartimento di Fisica Teorica, Università di Torino, Italy

I. Introduction

Coherent nonlinear magnetic structures, such as magnetic islands and current sheets, have been studied in the zero frequency limit. In this case the current density is constant on magnetic surfaces. In high temperature plasmas however, resistive modes are found to propagate with a finite velocity when diamagnetic and/or finite gyro-radius effects are accounted for. It is thus important to investigate the dynamics of such propagating nonlinear structures.

In this paper we discuss a physical model for such structures that include diamagnetic velocities and finite ion gyro-radius and electron mass effects.

Propagating magnetic structures are largely governed by the motion of the electron fluid. A number of features are rather independent of the ion response and are thus valid for arbitrary values of the ratio of the thermal ion gyro-radius to the characteristic scale-length of the structures.

These structure are characterised by a current density distribution that is not constant on magnetic surfaces and tend to develop large currents at magnetic separatrices. Electron mass effects arise from the electron inertia and from a finite gyro-radius contribution to the stress tensor. In the highly non-collisional regimes of interest finite electron mass effects limit the large current densities that arise at magnetic separatrices. Current density gradients, however, can still be large.

A fluid Hamiltonian can be derived from the electron equations, under mild restrictions on the ion response, and the equations can be cast in Hamiltonian form. It is shown that two infinite sets of conserved quantities (Casimirs) exist that reduce to the 2-D reduced MHD Casimirs in the limit of zero mass and small ion gyro-radii.

II. Description of the Model

We model a low-β tokamak configuration by a plane slab, periodic in (y, z) and inhomogeneous along the x-direction. The magnetic field is $\vec{B} = B_0(\vec{e}_z + \vec{e}_z \times \nabla\Psi)$. The flux $\Psi = \Psi_0(x) + \tilde{\Psi}(x, y, t)$ corresponds to the helical flux function in a torus. Here, $\Psi_0(x)$ represents the flux of the shear field and $\tilde{\Psi}$ the flux of a single helicity perturbation.

The main equations that govern the non-linear magnetic perturbations are the electron continuity equation and the momentum balance along magnetic field lines. In this parallel balance we take into account inertia and a finite gyro-radius contribution arising from the z-component of the stress tensor $\nabla\cdot\overleftrightarrow{\Pi}\,|_z = cm_eT/(eB_o)\vec{e}_z \times \nabla n \cdot \nabla\vec{v}_z$.

We consider structures that vary on a time scale that is fast compared to the resistive time scale and that propagate along y with constant velocity u. Then, the

momentum balance and continuity equation are:

$$\frac{1}{a}\frac{\partial}{\partial t}\ln n = [\ln n + \frac{u}{a}x - \Phi,\ \ln n] + \frac{1}{\beta_e}[\Psi_e,\ \tilde{J}], \tag{1}$$

$$\frac{1}{a}\frac{\partial \Psi_e}{\partial t} = [\ln n + \frac{u}{a}x - \Phi,\ \Psi_e] + d_e^2[\ln n,\ \tilde{J}], \tag{2}$$

where all quantities depend on $(t, x, \lambda = y - ut)$ and the brackets are defined by $[f,\ g] = \vec{e}_z \cdot \nabla f \times \nabla g$. In Eqs. (1) and (2), n is the electron density, $\Phi = e\phi/T$ is the normalized electric potential, $a = cT/(eB_o)$, $\beta_e = 4\pi n_o T/B_o^2$,

$$\tilde{J} = \nabla^2 \tilde{\Psi}, \qquad \Psi_e = \Psi + v_z/\Omega_e = \Psi - d_e^2 \nabla^2 \tilde{\Psi}, \tag{3}$$

are the perturbed current density and the generalized flux function (momentum), $d_e = c/\omega_{pe}$ being the electron inertial skin depth. The last term in Eq.(2) arises from the stress tensor. It is seen that the generalized flux Ψ_e is conserved if this term is negligible (zero electron temperature). In the limit of zero electron mass, Ψ_e and Ψ coincide and the last term in Eq.(2) vanishes. In this limit the magnetic flux Ψ is conserved. In the general case however, none of these fluxes is conserved.

III. General Properties of Stationary Solutions

In the stationary case $(\partial/\partial t = 0)$ Eqs.(1) and (2) can be written in the form

$$[\Phi - \frac{u}{a}x - \ln n \pm \frac{\rho_e}{\beta_e}\tilde{J},\ \Psi_e \pm \rho_e \ln n] = 0, \tag{4}$$

where ρ_e is the electron gyro-radius. Equation (4) can be integrated, and the functional relationship is determined by imposing that, far from the rational surface at $x = 0$, these expressions reproduce the linearized equations.

In case of a locally linear density profile, $\ln n_0(x)/n_0 = -x/l_n$, and a linear magnetic shear field related to $\Psi_0 = -x^2/2l_s$, these boundary conditions yield

$$(g_\pm)^2 = f_\pm, \tag{5}$$

where

$$g_\pm = -\frac{d_s}{a_e\hat{\beta}}(\tilde{J}l_s - a_e\hat{\beta}) \pm \frac{-l_n}{a_e}(\Phi - \ln\frac{n}{n_0(x)} - a_e\frac{x}{l_n}), \tag{6}$$

and

$$f_\pm = 2l_s(\Psi_s - \Psi + {d_e}^2\tilde{J}) + {d_s}^2 \pm 2d_s l_n(\frac{x}{l_n} - \ln\frac{n}{n_0(x)}). \tag{7}$$

where $u_* = a/l_n$, $a_e = u/u_* - 1$, $\hat{\beta} = \beta_e l_s^2/l_n^2$, Ψ_s is the reconnected flux and $d_s = d_e\hat{\beta}^{1/2}$. Note that $g_\pm$ and $f_\pm$ are combinations of quantities that are even and odd in x, such that they satisfy the mirror symmetry relation

$$g_+(x,\lambda) = g_-(-x,\lambda), \qquad f_+(x,\lambda) = f_-(-x,\lambda). \tag{8}$$

The even and odd parts of $g_\pm$ and $f_\pm$ become of the same order for $x = O(d_s)$.

The functional relationship (5) is valid outside regions where $f_\pm$ lines are confined to a finite part of the (x, λ)-plane. These regions are separated by lines that connect X-points given by $\nabla g_\pm = \nabla f_\pm = 0$. These points do not necessarily coincide with singular points of Ψ or Ψ_e. Inside islands a different relationship between $f_\pm$ and $g_\pm$ may hold, which is determined by matching conditions across separatrices.

The previous results do not depend on the specific form of the ion response and are valid for arbitrary values of the ratio of the thermal ion gyro-radius to the characteristic length of the perturbation. For a linear profile of the background density, the ion response to propagating modes is

$$\ln \frac{n}{n_0(x)} = -\tau\Phi + \frac{u_*}{u} a_i P\Phi, \tag{9}$$

where $\tau = T/T_i$, and $a_i = 1 + \tau u/u_*$. The shear field coupling to the parallel ion motion and ion temperature gradients have been neglected .

In fusion plasmas the inertial skin depth d_e is smaller than the ion gyro-radius ρ_i. In the MHD limit, where all scale-lengths are taken to be larger than ρ_i, we may neglect electron mass effects. Then the operator P in Eq.(9) is $P = 1 + {\rho_i}^2 \nabla^2$ and it can be shown that the mode equation is

$$\nabla^2 \tilde{\Psi} = -\frac{\hat{\beta}}{l_s} \frac{u}{u_*} a_i {\rho_i}^2 \frac{\nabla^2 (\Psi_s - \Psi)^{1/2}}{(\Psi_s - \Psi)^{1/2}}. \tag{10}$$

The large ρ_i limit applies either to small structures or to regions close to the current layers and the X-points. In this limit $\ln[n/n_0(x)] = -\tau\Phi$. Upon adding and subtracting ${g_\pm}^2 = f_\pm$ one obtains ($\sigma = sign\ x$)

$$(1+\tau)\Phi - a_e \frac{x}{l_n} = -\frac{a_e}{l_n}\sigma G, \qquad \tilde{J} = \nabla^2 \tilde{\Psi} = \frac{a_e a_i \hat{\beta}}{(1+\tau) l_s}\left[1 - \frac{|x|}{G}\right], \tag{11}$$

where G is positive and is given by

$$G = (2l_s)^{1/2}\left[\Psi_s - \Psi + \frac{{d_e}^2}{a_e}\left(\frac{u}{u_*} - \frac{l_s}{2\hat{\beta} a_e}\tilde{J}\right)\tilde{J}\right]^{1/2}. \tag{12}$$

Equations (11) and (12) show that in the limit of zero electron mass ($d_e \to 0$) the current density becomes singular along the separatrices $\Psi = \Psi_s$. The finite electron mass limits the current density through its contribution to the denominator G. Since the current density remains finite and since we require finite electric fields, it follows that G is proportional to x near $x = 0$.

IV. Position of X-points

The X-points of $f_\pm$ or, equivalently of $g_\pm$, are given by $\nabla g_\pm = 0$. Near the outermost X-point at (x_s, λ_s) we write, for a regular current distribution, $G = \alpha_o + \alpha(x - x_s) + ...$, where $\alpha_o (> 0)$ and α are related to the current density and its radial gradient at the X-point. Using Eqs.(6) and (11) the functions $g_\pm$ can be expressed in

terms of G and x. From $\nabla g_{\pm} = 0$ one finds that the position x_s of the X-point is $x_s = O(d_s)$ and that $\alpha_o = O(d_s)$ and $\alpha = O(1)$. In the limit $d_s \to 0$, the current density at the X-points remains finite and all X-points coincide.

V. Hamiltonian Formulation

The following energy integral can be obtained from the general Eqs. (1) and (2),

$$H = \int d^2x \{ \frac{1}{2}(\nabla\Psi)^2 + \frac{1}{2}d_e^2(\nabla\Psi)^2 + \frac{1}{2}\beta_e[(\ln n)^2 + 2\frac{u}{a}x\ln n - \Phi \ln \frac{n}{n_o(x)}]\}. \quad (13)$$

In its derivation it has been assumed that the ion density response $\ln[n/n_0(x)]$ is related to the electric potential through a linear, self-adjoint operator.

The total energy can be considered as a Hamiltonian that is a functional of $\ln n$ and Ψ_e . On the basis of Eq.(13), Poisson brackets $\{\mathcal{F}, \mathcal{G}\}$ can be defined and Eqs.(1) and (2) can be cast in Hamiltonian form. Functionals $\mathcal{C}$ that annihilate the Poisson brackets $\{\mathcal{C}, \mathcal{F}\}$ for arbitrary functionals $\mathcal{F}$, are the Casimirs of the problem. One finds two infinite sets of Casimirs

$$\mathcal{C}_{\pm} = \int d^2x \; \mathcal{F}(\Psi_e \pm \rho_e \ln n). \quad (14)$$

In the MHD limit, $u \to 0$, $m_e \to 0$ and $\ln n \propto \nabla^2\Phi$, these sets reduce to the well known Casimirs of 2-D MHD: $\mathcal{C}_1 = \int d^2x \; \mathcal{F}(\Psi)$ and $\mathcal{C}_2 = \int d^2x \; \omega \; \mathcal{G}(\Psi)$ where $\omega = \nabla^2\Phi$ is the vorticity.

VI. Conclusions

A set of equations has been derived that describe propagating non-linear magnetic structures. These structures tend to develop large currents at magnetic separatrices that are, however, limited by electron mass effects. This set of equations contains two infinite sets of conserved quantities that are functionals of $\Psi - d_e^2\tilde{J} \pm \rho_e \ln n$ and are valid for arbitrary values of the ion gyro-radius ρ_i. Near separatrices and X-points of $\Psi - d_e^2\tilde{J} \pm \rho_e \ln n$, the radial scalar-length becomes small and the large ρ_i-limit of the ion response applies. The position of the outermost X-points of $\Psi - d_e^2\tilde{J} \pm \rho_e \ln n$ is $x_s = O(d_s)$ and does not coincide, in general, with the position of the X-points of the magnetic flux Ψ.

References

[1] A. I. Smolyakov, Sov.J.Plasma Phys., **15** (1989) 667

[2] B. B. Kadomtsev, Nucl.Fus., **31** (1991) 1301

[3] T.J.Schep, F. Pegoraro and J.Rem, 19^{th} European Conference on Controlled Fusion and Plasma Physics, Innsbruck, paper 16 C, part II, 1425, (1992)

[4] T. J. Schep, F. Pegoraro, J. Rem, Proc. Workshop on Magnetic Turbulence and Transport, July 1992, Cargèse, France.

[5] P.J.Morrison, R.D. Hazeltine Phys. Fluids, **27** (1984) 886.

Differential mode rotation and the sawtooth instability in Tokamaks

R Fitzpatrick, C G Gimblett, and R J Hastie
AEA Technology, Fusion, Culham, Abingdon, Oxfordshire, OX14 3DB, UK
(Euratom/UKAEA Fusion Association)

Abstract
We present a model of the sawtooth trigger mechanism in a tokamak. Central to the model is the interaction between differentially rotating $q = 1$ and $q = 2$ surfaces. The electromagnetic torque due to the $m/n = 2/1$ toroidal sideband of a $1/1$ mode acts at the $2/1$ surface so as to bring about co-rotation of the two surfaces. As a result of this the perturbed magnetic field penetrates through the $q = 2$ surface from the plasma interior. This in turn further destabilises the system through toroidal coupling, precipitating the sawtooth crash phase.

1. Introduction. We propose a model of the sawtooth crash trigger that uses ideas similar to those employed in the interpretation of resonant magnetic perturbation experiments carried out on the COMPASS-C tokamak[1]. In these experiments, a static external coil created a perturbing $m/n = 2/1$ helical field which induced an electromagnetic locking torque at the (rotating) $q = 2$ surface. Initially, the rotation of the $q = 2$ surface shielded the plasma interior from the applied perturbation, but above a critical amplitude of the coil current the $q = 2$ surface was suddenly brought to rest, simultaneously permitting the field to reconnect through $q = 2$ to the plasma interior. In the case of the sawtooth, we imagine the driving helical perturbation to be due to the presence of a rotating $1/1$ displacement of the plasma inside the $q = 1$ surface, caused by the natural instability of the $1/1$ mode. Due to toroidicity, this perturbation has a $2/1$ sideband component that exerts an electromagnetic torque at $q = 2$. In general, the 'natural' rotation frequencies of the $q = 1$ and $q = 2$ surfaces are not the same, but above a critical amplitude of the $1/1$ perturbation the torque acts so as to bring about co-rotation. Reconnection can then proceed at $q = 2$, allowing field penetration through this surface into the previously shielded plasma exterior. As reconnection at $q = 2$ occurs, the $1/1$ driving mode is further destabilised due to toroidal coupling.
In this paper we give an outline of the basic features of the model. Full details will be provided in a future report.

2. Analysis and model equations. Our starting point is to assume the presence of a $1/1$ mode, and then calculate the profile of the associated $2/1$ toroidal sideband. In fact, we need only quote the result[2]

$$\left(r_2\Delta_{2/1} - r_2\Delta'_{2/1}\right)\,\Psi_{2/1}(r_2) = -\delta W_{12}\,\epsilon_1^2 B_0 \xi_0. \tag{1}$$

Here, ξ_0 is the $1/1$ top-hat displacement, r_1 and r_2 are the radii of the $q = 1$ and 2

surfaces, $\epsilon_1 = r_1/R_0$, R_0 is the major radius, B_0 the toroidal field, $\Delta_{2/1}$ the well-known stability index associated with the logarithmic discontinuity of the poloidal flux at the $q = 2$ layer, $\Delta'_{2/1}$ is the (toroidal) potential energy of the 2/1 mode[3], $\Psi_{2/1}(r_2)$ the value of the reconnected poloidal flux there, and δW_{12} is a toroidal coupling integral. Let $-\delta W_{12}\,\epsilon_1^2 B_0 \xi_0 \equiv D_{1/1}\exp(i\lambda_1)$ where $D_{1/1}$ represents the amplitude of the 1/1 driving term, and λ_1 gives the phase of ξ_0. Similarly, writing $\Psi_{2/1}(r_2) \equiv \Psi_{2/1}\exp(i\lambda_2)$, we find from (1) that

$$r_2\Delta_{2/1} \;=\; r_2\Delta'_{2/1} + (D_{1/1}/\Psi_{2/1})\exp i(\lambda_1 - \lambda_2). \tag{2}$$

3. Electromagnetic and viscous torques. Electromagnetic torques can only develop inside the resistive layers. The toroidal torque acting at the $q = 2$ surface $\propto \Psi_{2/1}^2 \mathrm{Im}\,(r_2\Delta_{2/1})$,[4,5] and is given by

$$T_{\phi \mathrm{EM}\,2} \;=\; \frac{2\pi^2 R_0}{\mu_0} \times D_{1/1}^2 \frac{\mathrm{Im}\,(r_2\Delta_{2/1})}{\left|r_2\Delta_{2/1} - r_2\Delta'_{2/1}\right|^2}, \tag{3}$$

using Eq.(2).

Neglecting plasma inertia in the outer regions, the change in the steady-state toroidal rotation profile $\Delta\Omega_\phi(r)$ induced by electromagnetic torques satisfies $d/dr(r\mu_\perp d\Delta\Omega_\phi(r)/dr) = 0$ where $\mu_\perp(r)$ is the (anomalous) perpendicular viscosity[4,5,6]. The rotation produces balancing viscous torques when $\Delta\Omega_\phi(r)$ suffers gradient discontinuities across the layers. Assuming that edge interactions are sufficiently strong to give $\Delta\Omega_\phi(a_0) = 0$ we can solve for $\Delta\Omega_\phi(r)$:

$$\Delta\Omega_\phi(r) = \begin{cases} -\dfrac{T_{\phi\,\mathrm{EM}\,2}}{4\pi^2 R_0^3}\displaystyle\int_{r_1}^{r_2} \frac{dr'}{r'\mu_\perp(r')} & 0 \le r \le r_1, \\ -\dfrac{T_{\phi\,\mathrm{EM}\,2}}{4\pi^2 R_0^3}\displaystyle\int_{r}^{r_2} \frac{dr'}{r'\mu_\perp(r')} & r_1 \le r \le r_2, \\ 0 & r_2 \le r \le a_0. \end{cases} \tag{4}$$

4. Layer physics. In a typical ohmically heated tokamak the layer dispersion relation at $q = 2$ takes the form $r_2\Delta_{2/1} = -i(\omega - \omega_2)\tau_2$, where ω is the rotation frequency of the driving 1/1 perturbation and ω_2 is the natural frequency of the 2/1 mode. This relationship describes 'visco-resistive' layer physics and an asymptotic layer analysis gives $\tau_2 \simeq 2.1\tau_H^{1/3}\tau_R^{5/6}\tau_V^{-1/6}$, where τ_H, τ_R and τ_V are local hydromagnetic, resistive and viscous timescales respectively. The driving 1/1 displacement of the core rotates at the natural frequency of the 1/1 mode, ω_1, Doppler shifted by the changes induced in toroidal plasma rotation due to the action of electromagnetic torques, so that $\omega = \omega_1 - \Delta\Omega_\phi(r_1)$.

5. Torque balance. Combining all these ingredients, torque balance at the rational flux-surfaces yields

$$\frac{1}{4}\frac{|\xi_0|^2}{\Lambda^2}\frac{\hat{\omega}}{\alpha^2+\hat{\omega}^2} = 1-\hat{\omega}, \text{ where } \hat{\omega} = \frac{\omega-\omega_2}{\omega_1-\omega_2}, \quad \alpha = \frac{(-r_2\Delta'_{2/1})}{|\omega_1-\omega_2|\tau_2}, \tag{5}$$

$$\Lambda^2 = \frac{1}{2}\left(\frac{R_0 s_1}{\delta W_{12}\epsilon_1}\right)^2 \times (\omega_1-\omega_2)^2\tau_2\frac{\tau_H^2(r_1)}{\tau_V(r_1)}\Big/\int_{r_1}^{r_2}\frac{\mu_\perp(r_1)}{r\mu_\perp(r)}dr\,, \tag{6}$$

and $s_1 = r_1(q'/q)_{r_1}$. The first of Eqs.(5) is similar to that obtained for the 'slip-frequency' of a linear induction motor, and displays bifurcated solutions for $\alpha^2 < 27$[7]. According to Eqs. (2) and (5) the reconnected magnetic flux driven at the $q=2$ surface satisfies

$$\Psi_{2/1} = \Psi^{\rm full}_{2/1}\alpha(\alpha^2+\hat{\omega}^2)^{-1/2}, \quad \text{where} \quad \Psi^{\rm full}_{2/1} = D_{1/1}(-r_2\Delta'_{2/1})^{-1} \tag{7}$$

is the fully-reconnected flux (i.e. that achieved when there is no frequency mismatch between the $q=1$ and $q=2$ surfaces).
In many tokamak plasmas we have $|\omega_1-\omega_2|\tau_2 \gg 1$[4,5] , implying $\alpha \ll 1$. In this limit Eqs. (5) and (7) yield

$$\begin{aligned} 2\omega &\simeq (\omega_1+\omega_2)+(\omega_1-\omega_2)\sqrt{1-|\xi_0|^2/\Lambda^2}, \\ \Psi_{2/1} &\simeq \Psi^{\rm full}_{2/1}(\alpha/2)(1+\sqrt{(1-|\xi_0|^2/\Lambda^2)})^{-1} \end{aligned} \tag{8}$$

for $|\xi_0| \le \Lambda$, and

$$\begin{aligned} \omega &\simeq \omega_2 + 4\alpha^2(\omega_1-\omega_2)\Lambda^2/|\xi_0|^2, \\ \Psi_{2/1} &\simeq \Psi^{\rm full}_{2/1}(1+16\alpha^2\Lambda^4/|\xi_0|^4)^{-1/2} \end{aligned} \tag{9}$$

for $|\xi_0| > \Lambda$. Thus, for $|\xi_0| \ll \Lambda$ the core displacement rotates close to the natural frequency of the 1/1 mode, and there is virtually no magnetic reconnection induced at $q=2$. As $|\xi_0|$ is slowly increased, there is a gradual change in the rotation frequency of the core displacement until, at $|\xi_0| = \Lambda$, it lies mid-way between the natural frequencies of the 1/1 and 2/1 modes. At this stage there is still very little reconnection at $q=2$. Any further increase in the amplitude of the core displacement leads to a discontinuous change in its rotation frequency to a value which is very close to the natural 2/1 frequency. This process is termed the mutual 'locking' of the 1/1 and 2/1 modes. After locking there is substantial tearing at the $q=2$ surface, and the driven reconnected flux there closely approximates to its fully-reconnected value.

6. Growth rate after mode locking occurs. As a general point we can expect an increase in the growth rate of the system as before locking the 2/1 harmonic 'sees' an effective ideal wall at r_2, after locking the effective wall is removed to $a_0(>r_2)$ and this

will have a destabilising effect.

7.Estimation of core displacement. A crude estimate of the critical core displacement required for co-rotation can be obtained from Eq. (1). We assume the $q = 2$ surface to be fully reconnected, and for uniform current density we may take $r_2\Delta'_{2/1} \sim -1$ and $\delta W_{12} \sim 2(r_1/r_2)^2$. Taking $r_1 \sim a_0/3 \sim r_2/2$ we find $\xi_0 \sim 12(R_0/a_0)^2(b_r^{2/1}/B_0)a_0$. For the COMPASS-C tokamak[1] ($R_0 = 0.56$ m, $a_0 = 0.2$ m, $B_0 = 1.1$ T) the critical field needed to lock $q = 2$ is observed to be $b_r^{2/1}(r_2) \sim 10^{-3}$ T. This field can be produced by a shift of the core of magnitude $\xi_0 \sim 1.7$ cm. In the DIII-D device ($R_0 = 1.67$ m, $a_0 = 0.64$ m, $B_0 = 1.3$ T) if we take $b_r^{2/1}(r_2) \sim 10^{-4}$ T, then the associated core displacement is $\xi_0 \sim 0.4$ cm. Finally, for JET ($R_0 = 3.0$ m, $a_0 = 1.1$ m, and $B_0 = 3.0$ T) and again taking $b_r^{2/1}(r_2) \sim 10^{-4}$ T gives $\xi_0 \sim 0.3$ cm.

8. Discussion. A number of experimental observations of sawtooth behaviour might be interpreted with the aid of the foregoing model, and these include :
(i) Experimental evidence that modification of bulk plasma momentum, for instance with the use of neutral beams, has a strong effect on the sawtooth period.
(ii) Evidence that the RMP experiments on COMPASS-C which lock the $q = 2$ surface lead to the removal of sawteeth.
(iii)The reconnection event at $q = 2$ may correspond to the appearance of the so-called 'gong' mode[8] at the time of the sawtooth crash. Further, measurements of centroidal displacement indicate two distinct growth phases. This could correspond to the $q = 2$ reconnection further destabilising the 1/1 driving perturbation.
(iv) As noted[5,6], there is a strong scaling of the locking phenomenon with device size and if this interpretation of the sawtooth trigger is largely correct it might help to explain the existence of 'precursorless' sawteeth in the larger tokamaks.

Acknowledgement. This work was funded jointly by the UK Department of Trade and Industry and Euratom.

[1] Hender T C *et. al.* Nucl. Fusion **32**, 2091 (1992).
[2] Bussac M N, Edery D, Pellat R, and Soulé J L, in *Plasma Physics and Controlled Nuclear Fusion Research 1976*, Proceedings of the 6th International Conference, Berchtesgaden (IAEA, Vienna, 1977), Vol. 1, p. 607.
[3] Connor J W, Cowley S C, Hastie R J, Hender T C, Hood A, and Martin T J, Phys. Fluids **31**, 577 (1988).
[4] Fitzpatrick R, and Hender T C, Phys. Fluids B **3**, 644 (1991).
[5] Fitzpatrick R, in *Theory of Fusion Plasmas*, Proceedings of the Joint Varenna-Lausanne International Workshop, Varenna 1992 (Società Italiana di Fisica, Bologna, 1992), p. 147.
[6] Fitzpatrick R, to appear in Nuclear Fusion.
[7] Gimblett C G, and Peckover R S, Proc. R. Soc. London A **368**, 75 (1979).
[8] Duperrex P A, Pochelon A, Edwards A, and Snipes J, Nucl. Fusion **32**, 1161 (1992).

BETA LIMITS FOR TOKAMAKS WITH A LARGE BOOTSTRAP FRACTION

A. Bondeson
Centre de Recherches en Physique des Plasmas, Association Euratom -Confédération Suisse,
Ecole Polytechnique Fédérale de Lausanne, Lausanne/Switzerland

I. INTRODUCTION. There is currently a strong interest in the possibility of operating a tokamak in steady state with the major part of the current coming from the bootstrap effect, supplemented by some "seed" current in the central region, e.g., from radio frequency current drive. There are several open questions concerning such bootstrapped tokamaks, e.g., the beta limits and the amount of current drive required. The bootstrap current tends to broaden the current profile, which typically has detrimental effects on the confinement time and beta limit [1]. A theoretical estimate for the beta limit of a bootstrapped tokamak limit was given in [2]. It was shown to scale as $\varepsilon^{1/2} g^2 c_{bs} (1+\kappa^2)$, where $g = \beta/I_N$ is the Troyon coefficient, $I_N = I[MA]/(a[m]B_0[T])$ the normalized plasma current, κ is the elongation and c_{bs} quantifies the efficiency of the bootstrap current generation. Although analytical estimates can be given for c_{bs}, and the behavior of g is quite well known, a realistic assessment of the bootstrapped tokamak requires quantitative knowledge of what values of g and c_{bs} can be obtained when the current and pressure profiles are related by the bootstrap mechanism. Here, we address this question by global numerical calculations and compute beta limits for bootstrapped tokamaks with differently shaped cross section. The main result is that this beta limit is highly sensitive to shaping and increases with elongation and triangularity.

II. PROFILE EFFECTS. In tokamaks operated at high current, the beta limit generally increases with the internal inductance; $g \leq 4l_i$ is reported from DIII-D [1]. This is characteristic of the "first stability" regime of high-n ballooning modes. The pressure profiles that are optimal for MHD stability are rather broad with peaking factors (PPF = $p_0/\langle p\rangle$) typically around 2. (Experimentally, the highest beta values tend to occur for more peaked pressure profiles, which may be in the second stability regime in the central region due to negative shear [3]). At high poloidal beta, the bootstrap mechanism broadens the current distribution, which is destabilizing for the n = 1 free boundary kink mode. On the other hand, for current profiles with low shear in the central region, the high-n ballooning modes can enter into the "second stability" region. This transition is favoured by D-shaping and high q. The possibility that also the external kink mode of toroidal mode number n = 1 could reach second stability was suggested in [4]. Figure 1 shows the results of an attempt to test this, using the ERATO stability code. The figure shows g-factors vs. internal inductance for the free boundary stability of strongly D-shaped equilibria with broad current profiles, $0.5 < l_i < 0.8$ and $1.8 < q_0 < 5$ and peaked pressure profiles, $3 \leq PPF \leq 4$. In this paper, we use the following definitions for beta, poloidal beta and internal inductance

$$\beta = \frac{2\mu_0\langle p\rangle}{\langle B^2\rangle} \quad , \qquad \beta_p = \frac{2\mu_0\langle p\rangle}{\langle B_p\rangle_s^2} \quad , \qquad l_i = \frac{\langle B_p^2\rangle}{\langle B_p\rangle_s^2} \quad , \qquad (1)$$

where $\langle\bullet\rangle$ means volume average and $\langle B_p\rangle_s = \mu_0 I_p / L$, with L the plasma circumference, denotes the line average on the surface. The moderate g-factors in Fig. 1 show that the free boundary n = 1 mode does not reach second stability for equilibria of this type, even for very

high q_0. Nevertheless, Fig. 1 shows some reminiscences of second stability, e.g., g increases with decreasing inductance when the pressure profile is peaked. Thus, for highly shaped equilibria with peaked pressure and broad current profiles, the l_i-dependence is opposite to that found in the standard regime of high inductance and broad pressure profiles. When the data points in Fig. 1 are plotted vs. the pressure peaking factor we find that for PPF > 3, the g-factors decrease strongly when the pressure is further peaked.

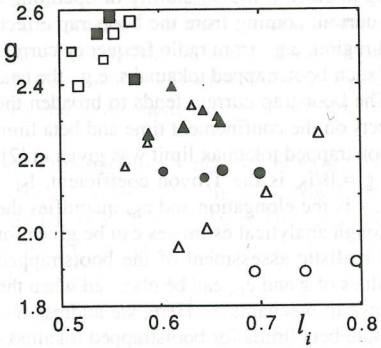

FIGURE 1. g-factors vs. l_i for peaked pressure profiles and A = 3, κ = 2.5, δ = 0.6.

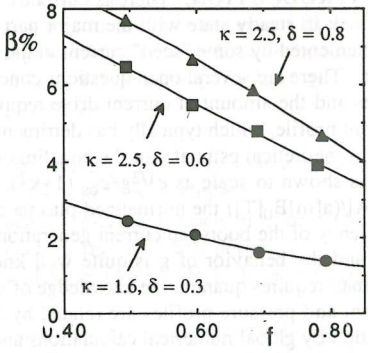

FIGURE 2. Optimized β vs. bootstrap fraction f for different cross sections.

III. NUMERICAL RESULTS. A beta-limit study for bootstrapped tokamaks has been carried out with a partial optimization of the profiles. Profiles are specified for the surface averaged toroidal current density $I^*(\psi) = \langle j_\phi/R \rangle$. Then, the pressure profile is chosen so that the parallel bootstrap current [computed from the formulas of Hirshman [5] with $T_e = T_i = T$, $Z = 1$, and $\eta = d(\log T)/d(\log n) = 1.5$] is a fixed fraction of the total parallel current for all ψ, except in the center where a cut-off has been applied to $dp/d\psi$. The resulting pressure peaking factor is generally between 2.5 and 3. The total bootstrap current is computed as

$$I_{bs} = \int_{\phi = \text{const}} \frac{\langle \mathbf{j}_{bs} \cdot \mathbf{B} \rangle}{\langle \mathbf{j} \cdot \mathbf{B} \rangle} \, j_\phi \, dS \qquad (2)$$

The current profile has been varied over a restricted set with $I^* = 0$ at the edge to find an optimum for the beta limit. With the pressure and current profiles related so that the bootstrap fraction is (almost) independent of ψ, the optimal current profiles are broad, in particular, for strongly shaped cross sections. It appears that the geometrical effects of shaped cross sections on the q-profile favour broader current profiles, and this is advantageous for the bootstrapped tokamak. The numerical results are shown in Fig. 2 as β_{max} vs. the bootstrap fraction $f = I_{bs}/I_p$. The curves represent three different cross sections, one JET-like with elongation $\kappa = 1.6$ and triangularity $\delta = 0.3$ and two DIII-D-like ($\kappa = 2.5$ and two triangularities $\delta = 0.6$ and 0.8) all at aspect ratio 3. The figure shows that D-shaping has a clearly favorable effect. The results indicate that operation with a high bootstrap fraction should be of interest in strongly shaped machines such as DIII-D and TCV, while this scenario gives very low beta limits in weakly shaped machines such as JET.

IV. THEORY. Analytical arguments [2] can be applied to the numerical results to understand the dependence on shaping. The equilibria can be characterized by two figures of merit which determine the beta limit of the bootstrapped tokamak. These are the Troyon coefficient $g = \beta[\%] / I_N$ and the bootstrap factor c_{bs}, defined by writing the bootstrap fraction as

$$f = \frac{I_{bs}}{I_p} = c_{bs}\, \varepsilon^{1/2}\, \beta_p \quad . \tag{3}$$

The definition (3) is motivated by the following considerations. To lowest order in inverse aspect ratio, the bootstrap current density is

$$j_{bs} \approx c\, \varepsilon(\psi)^{1/2}\, R_0\, (dp/d\psi) \quad , \tag{4a}$$

where $c = [2.44(T_e+T_i)n' + n(0.69T_e'-0.42T_i')]/p$. In the numerical examples, $T_e = T_i$ and $\eta = 1.5$, so that $c \approx 0.9$. Assuming a flat q-profile and parabolic pressure profile, the total bootstrap current can be integrated to give $I_{bs} = 3.2\pi\, c\, \varepsilon^{1/2}\, R_0 q \langle p \rangle / B_0$, which may be rewritten as

$$I_{bs,N} = \frac{I_{bs}[MA]}{a[m]B_0[T]} = 0.2c\, \varepsilon^{1/2}\, \frac{qI_N}{5\varepsilon}\, \frac{\beta[\%]}{I_N} \quad . \tag{4b}$$

Furthermore, the definitions (1) imply $\beta_p = (\beta[\%]/4I_N^2)\, (L/2\pi a)^2$, thus (4b) gives (3) with $c_{bs} = 0.8c\, (qI_N/5\varepsilon)\, (2\pi a/L)^2$. In the case of an elliptical cross section and q = constant, the geometrical factors in c_{bs} almost cancel because $qI_N/5\varepsilon = (1+\kappa^2)/2 \approx (L/2\pi a)^2$. Consequently, c_{bs} should be independent of ellipticity and approximately equal to 0.8c. Of course, in general, c_{bs} also depends on the pressure and current profiles. Taking the square of the Troyon law the beta limit can be expressed as $\beta[\%]\beta_p < (g_{max}^2/4)\, (L/2\pi a)^2$. In combination with (3), this gives the following beta limit for the bootstrapped tokamak

$$\beta[\%] < \varepsilon^{1/2}\, g_{max}^2\, (c_{bs}/4f)\, (L/2\pi a)^2. \tag{5}$$

It also follows that there is a limit to the bootstrap current set by MHD stability

$$I_{bs,N} < \varepsilon^{1/2}\, g_{max}\, (c_{bs}/4)\, (L/2\pi a)^2. \tag{6}$$

For weakly shaped cross sections, Eq. (6) gives rather low values of the bootstrap current. Examination of the numerical results in Fig. 2 shows that for each geometry and self-similar sequence of I*-profiles, g_{max} and c_{bs} are approximately constant for bootstrap fractions f between 50 % and 70 %. Thus, the 1/f scaling for the beta limit in (5) holds quite well and the results can be summarized by giving g_{max} and c_{bs}. These are quoted together with β at 70 % bootstrap fraction, l_i and $I_{bs,N}$ in Table I for equilibria of different cross sections, with profiles optimized as described in Sec. II. Table I underlines the favorable effect of shaping on the beta limit of bootstrapped tokamaks. Note that even modest variations of g affect β significantly because g is squared in (5). It appears that g is slightly reduced by ellipticity but increased by triangularity. For the bootstrapped current profiles with $\langle \mathbf{j}_{bs} \cdot \mathbf{B} \rangle \approx f \langle \mathbf{j} \cdot \mathbf{B} \rangle$, g reaches the highest values for rather low l_i. The optimal current profiles are flatter the more shaped the cross section is, as seen from the values of l_i in Table I. Furthermore, g decreases if the pressure profile becomes too peaked, say PPF > 3.

κ	δ	c_{bs}	g	β [%]	$I_{bs,N}$	l_i
1.6	0.3	0.82	2.23	1.6	0.50	0.72
2.0	0.5	0.82	2.63	3.2	0.84	0.64
2.5	0.6	0.83	2.68	4.7	1.24	0.56
2.5	0.8	0.80	3.06	6.2	1.39	0.56

TABLE I. Characteristics of beta-optimized equilibria with 70 % bootstrap current in different geometries at aspect ratio 3.

The bootstrap coefficient c_{bs} is insensitive to the equilibrium profiles, although broad profiles give somewhat higher values because of the $\varepsilon^{1/2}/B_p$ weighting in (4a). As seen from Table I, c_{bs} is also almost independent of the shape of the cross section and is close to the simple analytical estimate 0.8. (c_{bs} increases somewhat with the peaking of the density relative to the temperature, which has been held fixed in this study, although this dependence is weaker at low aspect ratio.) The profiles of pressure and parallel current $\langle j_{bs} \cdot B \rangle$ and $\langle j \cdot B \rangle$ for the case $\kappa = 2.5$, $\delta = 0.6$ (with 70 % bootstrap current and $\beta = 4.7$ %) are shown vs. $s = \psi^{1/2}$ in Fig. 3. The current profile is nonstandard and very broad. It is clear that this type of profile may be difficult to maintain and control in steady state.

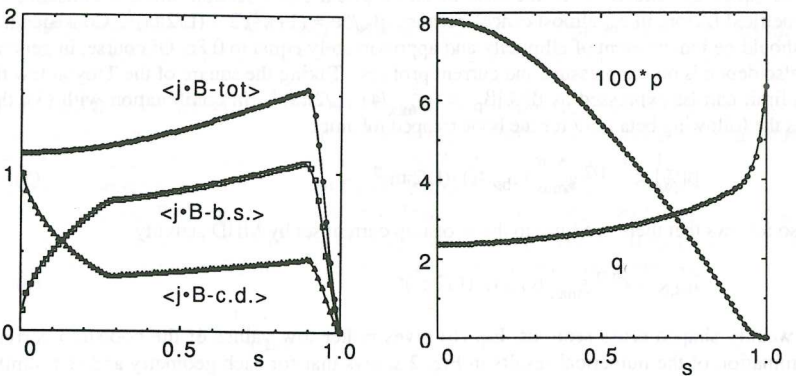

FIGURE 3. Profiles of parallel current $\langle j \cdot B \rangle$, pressure and q vs. $s = \psi^{1/2}$ for an equilibrium with 70 % bootstrap current, $\beta = 4.7$ %, $\kappa = 2.5$, $\delta = 0.6$ and $A = 3$ (see Table I).

REFERENCES

[1] T.S. Taylor, et al., Proc. 13th IAEA Conf., Wash., D.C., 1990, Vol. 1, p. 177.
[2] R.H. Weening and A. Bondeson, Comm. Plasma Phys. Contr. Fusion **15**, 77 (1992).
[3] E.A. Lazarus, et al, Phys. Fluids **B4**, 3644 (1992).
[4] J.J. Ramos, Phys. Fluids **B3**, 2247 (1991).
[5] S.P. Hirshman, Phys. Fluids **31**, 3150 (1988).

ON THE OPTIMIZATION OF A STEADY-STATE BOOTSTRAP-REACTOR.

A.R.Polevoy*, A.A.Martynov+, S.Yu.Medvedev+
(*) - RRC "Kurchatov Institute", Moscow, Russia
(+) - Keldysh Inst. of Applied Mathematics, Moscow, Russia

INTRODUCTION: According to [1] , a commercial fusion tokamak - reactor may be economically acceptable only for low recirculating power fraction $r_0 \equiv P_{CD}/P_\alpha < 0.2$. This restriction corresponds to high bootstrap fraction $\alpha_{BS} \equiv I_{BS}/I > 0.9$ to sustain the steady - state operation mode for high plasma densities $\langle n \rangle > 1.5\ 10^{20} m^{-3}$, fulfilled the divertor conditions. This paper presents the approximate expressions for the optimal set of reactor parameters for $r \ll 1$, $I_{BS}/I \approx 1$, based on the self - consistent plasma simulations by 1.5D ASTRA code [2]. The linear MHD stability analysis for ideal n = 1 kink and balooning modes has been carried out to determine the conditions of stabilization for bootstrap steady state tokamak reactor BSSTR configurations.

ASTRA TRANSPORT MODEL: To reveal the proper parametric dependencies, the reduced version of 1.5D ASTRA code [2] has been used. In these calculations we used the prescribed electron density profiles: $n_e = n_{e0}(1 - x^2)^{\alpha_n}$, with $x \equiv r/a$, $\langle n_e \rangle = 1.5 - 2\ 10^{20} m^{-3}$, $\alpha_n = 0$ and $\alpha_n = 0.5$ (ITER standard). All other parameters were calculated self-consistently: the heat transport with ion and electron heat fluxes $Q_\chi = \chi n \nabla T$, $\chi_e = \chi_i = \chi_0(1 + \alpha_\chi x^2)$, $\alpha_\chi = 0 - 2$, thermal alphas particle flux: $\Gamma_\alpha = D\nabla n_\alpha + V n_\alpha$, with $D = 1\ m^2/s$, $V = 2rD/a^2$, $n_d = n_t = (n_e - \Sigma\ Z\ n_z)/2$, plasma current transport with neoclassical conductivity by Hirshman .

PLASMA CURRENT: The bootstrap - current distribution was calculated by Hirshman formula [3] together with the bootstrap fraction, induced by fast alphas [4]. To provide the flat q distribution near the magnetic axis we use the deuterium NBI with a square footprint cross section of 1 m^2, neutral particle energy of E_b = 1.3-2 MeV, the input power P_{CD} = 75 - 95 MW and

tangential radius $R - a < R_b < R$ according to [5].

PARAMETRIC ANALYSIS OF A BOOTSTRAP - REACTOR: Using for β the parametrical dependence: $\beta \equiv g\ I/aB$, where $g \sim 10^{-2}$ is treated as a variable parameter, one obtains, according to [6], for fusion power and neutron flux density:

$$P_{fus} \sim \beta_{DT}^2 B^4 V = 40\ \alpha_F\ k\ R\ (g\ I\ B\ \alpha_{DT})^2, \qquad (1)$$

$$F_N = 0.8\ P_{fus}/S \approx 0.04\ P_{fus}/\ a\ R\ (k + 1),$$

with $\alpha_{DT} \equiv n_{DT}/n_e$ - the fuel fraction in the hot core, $\alpha_F \approx 1$ - the profile dependent parameter. All the variables are in practical units: I[MA], B[T], P[MW], a,R [m]. Using the same β dependence for the energy confinement time, one can obtain: $\tau_E \approx 11\ g\ k\ I\ B\ R\ a/P_{tot}$, with $P_{tot} \equiv P_\alpha + P_{CD} - P_{RAD} \equiv P_\alpha(1 + r)$, $P_\alpha = 0.2\ P_{fus}$, P_{CD} - the auxiliary heating power, P_{RAD} - radiated power. Then, substituting τ_E into the JET - DIII-D elm- free H- mode scaling law : $\tau_E = \tau_{H-EF} = 0.106\ I^{1.03}\ R^{1.48}/P_{tot}^{0.46}$ we can reveal the approximation for the plasma current:

$$I \approx 28\ a\ (k/(1+r)\alpha_F)^{0.5}/R\ H\ \alpha_{DT}, \qquad (2)$$

with $H \equiv \tau_E/\tau_{H-EF}$ - the H - mode enhancement factor.

The bootstrap fraction α_{BS} has rather complicated dependence on q, T, n profiles [7]. In a bootstrap - reactor with the proper seeding current the q profiles appeared to be similar, with $q_0/q_{95} \approx 0.5$, so according to [7], the bootstrap fraction can be described by known approximation [8] at least for peaked density profiles $\alpha_n = 0.5$: $\alpha_{BS} \approx 0.7\ \beta_p\ (a/R)^{0.5}\ \alpha_p$, with a poloidal beta $\beta_p \approx 25\ g\ k\ B\ a/I$ and α_p - the profile dependent factor $\alpha_p \approx 1$ for $\alpha_n = 0.5$, and $\alpha_p \approx 0.72$ ($\approx (a/R)^{0.35}$ see [8]) for flat density profiles. Thus

$$g\ B \approx 1.3\ \alpha_{BS}/(k\ (1+r)\ a\ R\ \alpha_F)^{0.5} H\ \alpha_p \alpha_{DT} \qquad (3)$$

Substituting (2), (3) into (1) one can obtain:

$$R \approx 10\ H^{-4/3}((1+k^{-1})F_n\alpha_F/2)^{-1/3}\alpha_{BS}^{2/3}(\alpha_p\alpha_{DT}(1+r))^{-2/3}. \qquad (4)$$

To minimize the magnetic field on the coil with any prescribed neutron shield thickness Δ : $B_c = B/(1 - (a + \Delta)/R)$, we obtain from (3) in contrast with [9], that the optimal minor radius for bootstrap reactor:

$$a \approx (R - \Delta)/3 . \qquad (R/a \approx 3) \qquad (5)$$

The magnetic field minimum is realized for β maximum corresponding to Troyon limit:

$$g = g_{Tr}. \qquad (6)$$

Taking into account the limits $\beta_p + li/2 < R/a$ and $B_{cmax} = 12 - 16$ T, we obtain the set or equations (2)- (8), which determines the operational limits for the steady - state bootstrap tokamak - reactor.

$$R/a > 2(\alpha_{BS}/0.85\alpha_p)^2 \qquad (7)$$

$$B_c < B_{c\ max}. \qquad (8)$$

MHD STABILITY: Linear analysis of the ideal MHD stability with a free boundary has confirmed the result [9], that low n ideal kinks can be stabilized by placing a conducting wall at 1.2 times the plasma minor radius ($a/a_w = 1.2$). This enables also to increase the Troyon limit to $g_{Tr} \sim 0.04$ and operate with reliable B_c values, $B_c < 12$ T. The distance to the conducting wall can be increased if one increases the edge shear by the counter-current-drive at plasma periphery [10].

BSSTR CONFIGURATIONS: Some BSSTR configurations with $\alpha_{BS} = 0.9$, $B_c < 12$ T, $\alpha_{DT} = 0.85$, H = 1 ($\tau_E \approx 1.9 - 2\ \tau_{L\text{-ITER-POWER}}$) were determined by solving the set of Eqs. (2) - (6), taking into account the restrictions (7), (8) (see TABLE 1), and verified by 1.5D transport simulations.

SUMMARY:

1. BSSTR optimization depends on the density profile and fuel dilution. It is possible to achieve the steady state bootstrap operation in configuration, suggested in [1] for H-mode ($\tau_E \approx 2\ \tau_{L\text{-ITER-POWER}}$ [6]), pure plasma ($n_{DT}/n_e \sim 0.8$-0.85) with peaked density profile ($n \sim (1 - x^2)^{0.5}$), placing the conducing wall at $a_w = 1.2$ a.
2. It is possible to achieve the BSSTR operational regime even for a flat density profile in high aspect R/a > 4 (high β_p) configuration.
3. For $n \sim (1 - x^2)^{0.5}$ the optimal aspect ratio for BSSTR is

R/a ≈ 3, for flat profile BSSTR aspect ratio is restricted by $\beta_p \varepsilon < 1$ (R/a > 4).

4. The value of plasma current I at the flat top is determined by plasma dilution α_{DT} because of scaling degradation: $\tau_E \sim P^{-1/2}$, $P \sim \beta_{DT}^2$ (Eq.2). It is difficult to provide burn control for $Q \gg 1$ ($r \ll 1$).

TABLE 1

F_n[MW/m^2]	k	R[m]	a[m]	I[MA]	B[T]	g %
2.9	1.61	7.75	2.8	14.5	6	4
1.7	1.61	10	2.9	12.8	7	3
2	1.8	9.6	2.8	13.4	6.9	3
1.6	*1.8*	*13.34*	*3.1*	*11.35*	*8.1*	*3*

Italic: Flat density profile $n_0 = const$

ACKNOWLEDGEMENTS

We express the sincerest gratitude to Dr. B.V.Robouch for his support of this investigation.

REFERENCES.

[1] P.-H. Rebut et.al. //Preprint JET-P(92)65, Abington, 1992

[2] G.V.Pereverzev,P.N.Yushmanov,A.Yu.Dnestrovskij,A.R.Polevoy, K.N.Tarasjan,L.E.Zakharov //Preprint IPP 5/42, Garching, 1991.

[3] S.P.Hirshman//Phys. Fluids,31 (1988), p. 3150.

[4] C.S.Chang//Proc. of 14th Int.Conf. on Plasma Physics and Contr. Fusion, Wurtzburg, 1992, IAEA-CN-56/E-3-8.

[5] V.M.Leonov,A.R.Polevoy //Preprint IAE-5013/8, Moscow, 1990.

[6] N.A.Uckan et.al. //ITER DOCUMENTATION SERIES, No 10, IAEA, VIENNA, 1990.

[7] V.D.Pustovitov//Fizika Plazmy (in Rus.) 18, N7, (1992), 819

[8] J.G.Cordey, C.D.Challis, P.M.Stubberfield// Plasma Phys. Control. Fusion 30 (1988) 1625.

[9] M.Kikuchi//Nucl. Fus., 30, (1990), 265.

[10] L.M.Degtyarev,S.Yu.Medvedev,A.G.Kirov,M.A.Stotland// Proc. of 14th EPS Conf. on Contr.Fusion and Plasma Phys., Madrid, 1987, v.11D, part III, p. 1133.

ALFVEN GAP MODES IN ELONGATED PLASMAS

L.Villard, J.Vaclavik, S.Brunner, H.Lütjens, and A.Bondeson

Centre de Recherches en Physique des Plasmas
Association Euratom - Confédération Suisse
Ecole Polytechnique Fédérale de Lausanne
21, av. des Bains – CH-1007 Lausanne/Switzerland

1. Introduction. In the context of the potential destabilization of Alfvén eigenmodes by fusion particles in tokamak reactors[1-3], it is crucial to develop a qualitative and quantitative theoretical prediction of the behaviour of these modes. Experiments are being planned at JET to excite gap modes using saddle coils. The aim of this paper is twofold. First we investigate the feasibility of gap modes excitation with saddle coils in typical JET type equilibria (single-null, up/down asymmetric configurations). Second we derive expressions for the wave-particle power transfer (in particular fast particles such as fusion alphas) that are ready to be used in global calculations of the damping/growth rates. Previous works on this type of instability[3] were theoretical analytical estimates of local growth rates.

2. Antenna excitation of gap modes. In order to compute ideal-MHD up/down asymmetric equilibria, modifications have been made on the CHEASE code[4]. In the actual version, plasmas with a separatrix cannot be computed and the computational boundary only approaches it. The equilibrium quantities are transferred to the global wave code LION[5]. The LION code solves the weak variational form of the wave equation with a linear finite hybrid element discretization. It computes the continuum absorption (in a non-perturbative way) and electron Landau damping due to parallel dynamics and to curvature drift in a perturbative way. The plasma is surrounded by a pure vacuum region enclosed by a perfectly conducting wall. In the vacuum region, the saddle coils are modelled by a thin current carrying sheet $D(\vec{x}) = 0$. The antenna current is written as

$$\vec{j}_a = \delta(D)\nabla D \times \nabla\alpha$$

$$\alpha(\theta,\varphi) = \sum_n \alpha_n(\theta) e^{i(n\varphi-\omega t)}, \qquad \alpha_n(\theta) = \alpha_{n0} \quad \theta_1 \le \theta \le \theta_2,$$

where θ_1 and θ_2 define the poloidal positions of the toroidal sections of the saddle coil and φ is the toroidal angle. The coefficients α_{n0} are obtained by making the toroidal Fourier decomposition of the actual saddle coil currents. The axisymmetry of the equilibrium allows us to compute the plasma response separately for each n. First the solution of the wave equation and the coupled power $P_n(\omega)$ are computed with $\alpha_{n0} = 1$ for each n and for various frequencies ω. To obtain the coupling impedance of a particular toroidal antenna (or antenna array), we evaluate

$$R(\omega) = \frac{2}{I_a^2}\left(\sum_n I_n^2 P_n(\omega)\right),$$

where I_n are the Fourier coefficients of the antenna current and I_a is the total antenna current amplitude. It is planned to have up to 8 saddle coils in the JET torus. Each of the coils extends almost $\pi/2$ in the toroidal direction. With different relative phasing of these antennas, different Fourier coefficients I_n are obtained. It is thus possible to select the dominant toroidal wavenumber n of the excited TAEs. An example of antenna coupling calculation is shown in Fig.1. The plasma parameters are $B_0 = 3.45T$, $R_0 = 3m$, $a = 1.05m$, $\kappa = 1.63$, $n_e = 5 \times 10^{19} m^{-3}(1 - 0.9s^2)^{0.5}$, $q_0 = 1.1$, $q_a = 3.34$, $I = 5.0MA$,

$\beta = 3.9\%$, $\beta_{pol} = 0.78$. Only the top saddle coils are activated. The dotted line in Fig.1 corresponds to the case of 2 top saddle coils at opposite toroidal locations with currents in phase opposition (+-), and the continuous line corresponds to the case of all 4 top saddle coils with currents in (+-+-) relative phasing. The 2 (+-) case excites mainly $n = 1$ modes but no $n = 2$ mode, wheras the 4 (+-+-) case excites mainly $n = 2$ modes but no $n = 1$ mode. It will therefore be possible to distinguish between TAEs having neighbouring frequencies but different n's (e.g. the $n = 1$ TAE at $f = 161.7kHz$ and $n = 2$ at $f = 164.5kHz$). The JET saddle coils excite both TAEs ($f = 80 - 250kHz$) and EAEs ($f = 250 - 450kHz$). Some of the eigenmodes couple rather poorly to the saddle coil antennas. For example, let us compare the modes labelled (a) and (b) on Fig.1. These are $n = 1$ modes. Fig.2. shows their respective eigenmode wavefield structures. The mode (a) has a rather large $m = 1$ component from the magnetic axis up to the $q = 1.5$ surface where it has strong gradients. The mode (b) has a more global structure and a comparatively larger amplitude near the edge. The mode (b) has the same phase from the magnetic axis to the outer (low lield side) edge wheras the mode (a) has a change of phase near the $q = 1.5$ surface. The two types of modes are also seen for $n = 2$ and were also seen in circular plasmas[5]. Which mode is the most easily destabilized by fast particles is a question that will need careful further studies. The "internal"-like mode (a) is probably more sensitive to the fast particles in the center, whereas the "external"-like mode (b), if destabilized, could be more effective in expelling fast particles from the center to the outside. The damping of these modes will probably be affected in a different way by the different parameters. The "internal" mode may be more ion-Landau damped for sufficiently high T_i plasmas, wheras the "external" mode may be more sensitive to electron-Landau damping for cases where $v_A \simeq v_{the}$ in the outer region.

3. Damping and growth rates. To evaluate the growth rates γ of the waves calculated by the LION code, it is necessary to establish a relation between the total time-averaged power $\bar{P}$ absorbed by hot species and the given EM fields $(\vec{E}, \tilde{\vec{B}})$: $\gamma = -\bar{P}/2W$, where W is the total energy of the wave. Working in the Alfvén frequency range, it is convenient to describe the evolution of the species using the drift kinetic equation (DKE). The equilibrium distribution functions of the guiding centers for electrons and ions are taken as local Maxwellians (functions of ψ = poloidal flux). The α-particles are described by a slowing-down distribution[6]:

$$F = N(\psi)\frac{C(\psi)}{v^3 + v_c^3(\psi)}H(v_0 - v),$$

where H is the Heaviside function and v_0 the birth velocity of the alphas.The fluctuating distribution function is then evaluated for given EM fields from the linearized DKE using a perturbation method. The parameter $b_p = B_p/|\vec{B}_0|$, where B_p is the poloidal component of the magnetostatic field, and the parameter $|\vec{v_d}|/\lambda_\perp\omega$, where $\vec{v_d}$ is the magnetic curvature drift, $\lambda_\perp$ the wavelength perpendicular to $\vec{B}_0$ and ω the frequency of the EM fields, are considered small. Integrating the resulting distribution function over the guiding center phase space, one can evaluate the total time-averaged power exchanged between the particles and the EM fields[7]. As the EM fields are provided by an ideal-MHD calculation, the component of $\vec{E}$ parallel to the magnetostatic field is zero and must therefore be obtained from a more general model. This can be done using the quasi-neutrality condition for electrons and ions. For the electrons and ions, we obtain:

$$\bar{P} = \sqrt{\pi}\epsilon_0 \int d^3x \frac{\omega_p^2 v_{th}}{4\Omega^2|k_\parallel|} \exp -z_0^2 \times \left(|a_{species}|^2 + \left|\vec{\beta}_\perp \cdot \vec{E} - i\omega \tilde{B}_\parallel\right|^2\right),$$

$$a_{electron} = \frac{1}{1-Z}\left(i\frac{\omega}{\Omega_i}\nabla\cdot\vec{E}_\perp + \vec{\beta}_\perp\cdot\vec{E}_\perp\right),$$

$$a_{ion} = \frac{T_e}{T_i}\frac{1}{1-Z}\left(i\frac{\omega}{\Omega_i}\nabla\cdot\vec{E}_\perp + \vec{\beta}_\perp\cdot\vec{E}_\perp\right) - i\omega\left(1+\frac{T_e}{T_i}\right)\tilde{B}_\parallel + \left[1+\frac{T_e}{T_i}+2\left(\frac{\omega}{k_\parallel v_{thi}}\right)^2\right]\vec{\beta}_\perp\cdot\vec{E}_\perp,$$

where ω_p is the plasma frequency, Ω the cyclotron frequency, $k_\parallel$ the parallel wave number, $z_0 = \omega/k_\parallel v_{th}$, $\vec{\beta}_\perp = \left(\nabla\times\vec{e}_{\parallel 0}\right)_\perp$, $\vec{e}_{\parallel 0}=\vec{B}_0/B_0$ and $Z = Z(\omega/|k_\parallel|v_{the})$ the dispersion function. For the α-particles we also consider the contributions due to the inhomogeneities of equilibrium:

$$\bar{P}^\alpha_{homo} = \pi^2\epsilon_0\int d^3x\frac{\omega_{p\alpha}^2 C}{|k_\parallel|\Omega_\alpha^2}\left\{\left[\frac{v_p^4}{|v_p|^3+v_c^3}+2v_p^2 I_0\right]\left|\vec{\beta}_\perp\cdot\vec{E}\right|^2 + 2\omega v_p^2 I_0\Im m\left(\tilde{B}_\parallel\vec{\beta}_\perp\cdot\vec{E}^*\right) + I_1\left|\vec{\beta}_\perp\cdot\vec{E} - i\omega\,\tilde{B}_\parallel\right|^2\right\},$$

$$\bar{P}^\alpha_{inhomo} = \frac{\pi^2\epsilon_0}{\omega}\Im m\int d^3x\nabla'\frac{\omega_{p\alpha}^2 C}{|k_\parallel|\Omega_\alpha^3}\left\{\left(v_p^4 I_0 + v_p^2\frac{I_1}{2}\right)\vec{\beta}_\perp\cdot\vec{E} + \left(v_p^2\frac{I_1}{2}+\frac{I_2}{4}\right)\left(\vec{\beta}_\perp\cdot\vec{E} - i\omega\,\tilde{B}_\parallel\right)\right\}(\vec{\beta}_\perp\cdot\nabla)E_b^*,$$

$$\text{where}\quad I_n = \int_{|v_p|}^{v_0} dv\frac{v\left(v^2-v_p^2\right)^n}{v^3+v_c^3}$$

and ∇' is equivalent to $|\nabla\psi|\partial/\partial\psi$ except that it operates only on density and temperature.

4. Conclusion. It was shown that saddle coils can be used to excite low n TAEs and EAEs in typical single-null JET plasmas. Toroidal mode number selection can be done by different phasings of the antennas. Some of the eigenmodes couple weakly but may be important to study. In the future, the expressions developed for global growth and damping rates will be used in the global calculation of gap modes.

Acknowledgements.
One of the authors (L.V.) wishes to thank Drs A.Fasoli, G.Huysmans, J.Jacquinot, J.B.Lister and W.Kerner for interesting discussions. This work was partly supported by the Swiss National Science Foundation.

References.

[1] K.L.Wong et al., Phys.Rev.Lett. **66** (1991) 1874.
[2] W.W.Heidbrink et al., Nucl.Fus. **31** (1991) 1635.
[3] G.Y.Fu, C.Z.Cheng, Phys.Fluids B4 (1992) 3722.
[4] H.Lütjens, A.Bondeson, A.Roy, Comput.Phys.Commun. **69** (1992) 287.
[5] L.Villard, G.Y.Fu, Nucl.Fus. **32** (1992) 1695.
[6] R.Koch, Phys.Lett. A **157**, (1991) 399.
[7] S.Brunner and J.Vaclavik, On Absorption of Low Frequency Electromagnetic Fields, LRP 471/93, CRPP, Lausanne (1993).

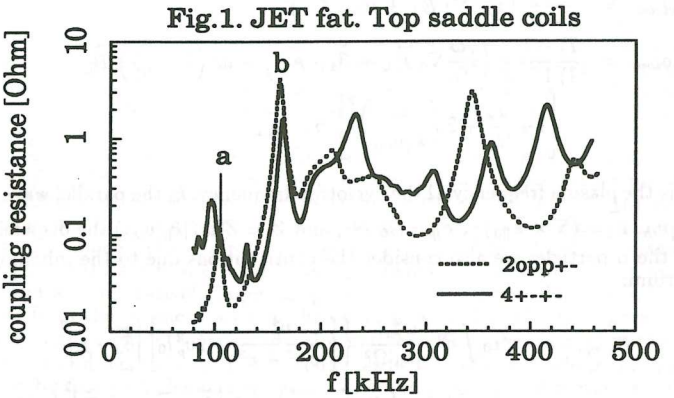

Fig.1. Coupling resistance of saddle coils . 2 antennas with opposite phasings (dotted line), 4 antennas with (+-+-) phasings (continuous line). Up-down asymmetric JET equilibrium with $R/a=2.77$, $\kappa=1.63$, $q_0=1.1$, $q_a=3.34$, $\beta=3.9\%$, $\beta_{pol}=0.78$, $B_0=3.45T$, $I_p=5.0MA$, $n_e=5.10^{19}(1-0.9s^2)^{1/2}\ m^{-3}$.

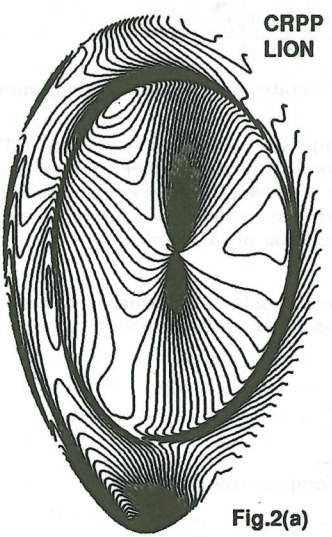

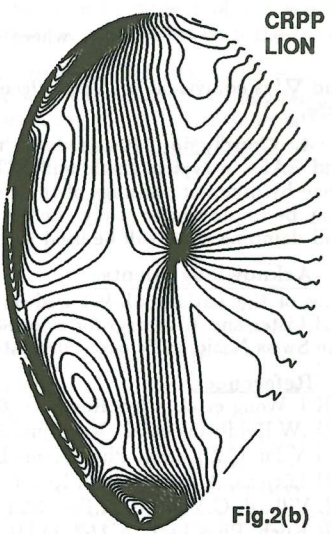

Fig.2. Level line plots of n=1 TAEs $Re(E_b)$ wavefields (radial displacement) for the cases (a) and (b) corresponding to Fig.1.

LINEAR AND NONLINEAR STABILITY OF TOROIDAL ALFVÉN EIGENMODES USING AN HYBRID CODE

G. Vlad, S. Briguglio, C. Kar*, F. Zonca and F. Romanelli

Associazione Euratom-ENEA sulla Fusione, C.R.E. Frascati,
C.P. 65 - 00044 - Frascati, Rome, Italy.

INTRODUCTION In the gaps of the continuum Alfvén spectrum discrete, global modes induced by toroidicity (the so called Toroidal Alfvén Eigenmodes or TAE) have been shown to exist.[1] These modes can be destabilized by the resonant interaction with the parallel motion of the energetic ions, as alpha particles produced in fusion reactions. The TAE stability is determined by the competition between such a driving mechanism and the coupling with the Alfvén continuum which provides a damping. The numerical study of the effect of high energy particles on MHD modes requires the solution of the fluid equations for the bulk plasma and of the kinetic equations for the energetic particles (from which the name of "hybrid codes"). In this paper we will present the hybrid code and we will present results regarding the MHD non-linear saturation. The non-linear interaction of two Fourier components of the mode with poloidal and toroidal mode numbers respectively (m, n) and $(m+1, n)$, which oscillate in time at a frequency $\omega_0 \sim O(\omega_A)$ (ω_A is the Alfvén frequency), leads to a perturbation of the poloidal flux function $\delta\psi$ with mode numbers $(m = 1, n = 0)$ slowly varying in time, which, in turn modifies the gap structure. When such a modification is sufficiently large, the global mode interacts with the continuum, leading to saturation.

FLUID MODEL The reduced, resistive magnetohydrodynamic (MHD) equations[2] expanded to the third order in the inverse aspect ratio $\epsilon = a/R$ and assuming a low-$\beta[O(\epsilon^2)]$ bulk plasma has been assumed.[3] This is in fact the lowest order to which the toroidal corrections enter the equations. A cylindrical coordinate system (R, ϕ, Z) has been used, and the subscript $\perp$ denotes components perpendicular to ϕ. The magnetic field can be written as $\vec{B} = R_o \vec{\nabla}\psi \times \vec{\nabla}\phi + \left(I_o + \tilde{I}\right) \vec{\nabla}\phi + O(\epsilon^3) B_\phi$, and the perpendicular component of the velocity $\vec{v}_\perp = (R^2/R_o)\, \vec{\nabla}U \times \vec{\nabla}\phi + O(\epsilon^3) v_A$, where ψ and U are stream functions, R_o is the major radius of the vacuum chamber, $I_o = R_o B_o$, B_o is the vacuum magnetic field at $R = R_o$ and $\tilde{I} \approx \epsilon^2 I_o$. Substituting the above expressions for $\vec{B}$ and $\vec{v}_\perp$ in the Faraday's law, using the resistive Ohm's law and taking only the poloidal component, the following equation for the evolution of the magnetic stream function is obtained:

$$\frac{\partial \psi}{\partial t} = \frac{R}{R_o} \left((\vec{\nabla}\psi \times \hat{\phi} \cdot \vec{\nabla}) U + \frac{B_o}{R} \frac{\partial U}{\partial \phi} - \eta J_\phi \right) + O(\epsilon^4) v_A B_\phi \,, \qquad (1)$$

where η is the resistivity. The toroidal current is given by $J_\phi = -\frac{R}{R_o} \Delta^* \psi$ where Δ^* is the Grad-Shafranov operator. Note that v_ϕ and $\tilde{I}$ enter only at the fourth order in ϵ. Upon applying the operator $\hat{\phi} \cdot \vec{\nabla} \times R^2 ...$ to the momentum equation, the following equation for the evolution of the velocity stream function is obtained:

*Permanent address: Saha Institute of Nuclear Physics, AF/1, Bidhanagar, Calcutta - 700064 India

$$\hat{\varrho}\left(\frac{D}{Dt} - \frac{2}{R_o}\frac{\partial U}{\partial Z}\right)\nabla_\perp^2 U + \vec{\nabla}\hat{\varrho}\cdot\left(\frac{D}{Dt} - \frac{2}{R_o}\frac{\partial U}{\partial Z}\right)\vec{\nabla}U =$$

$$= \vec{B}\cdot\vec{\nabla}\Delta^*\psi + \frac{1}{R_o}\vec{\nabla}\cdot\left(R^2\vec{\nabla}\cdot\overleftrightarrow{\Pi}_H\right)\times\vec{\nabla}\phi + O(\epsilon^4)\varrho\frac{v_A^2}{a^2} \tag{2}$$

where $\hat{\varrho} = \frac{R^2}{R_o^2}\varrho$, $\frac{D}{Dt} = \frac{\partial}{\partial t} + \vec{v}_\perp\cdot\vec{\nabla}$, $\nabla_\perp^2 \equiv \frac{1}{R}\frac{\partial}{\partial R}R\frac{\partial}{\partial R} + \frac{\partial^2}{\partial Z^2}$, the dependence on the density gradient has been retained explicitly and the pressure of the bulk plasma has been assumed to be zero. As a boundary condition we take a rigid conducting wall at the plasma edge.

The term which depends on the energetic particle pressure tensor $\overleftrightarrow{\Pi}_H$ in Eq. 2 is calculated by solving the gyrokinetic equations at each time step using the fields (the magnetic flux function ψ and the stream function U) obtained from the evolution of the reduced-MHD equations.

A previously existing code[4] which solves the $O(\epsilon^2)$ reduced-MHD equations has been modified in order to solve the $O(\epsilon^3)$ equations. The code is written using the toroidal coordinate system (r, θ, ϕ), with r being the radial coordinate ($r = 0$ corresponds to the geometrical centre of the vacuum chamber), θ and ϕ being respectively the poloidal and the toroidal angles. The code uses finite difference in the radial direction and Fourier expansion in the poloidal and toroidal directions. It uses a semi-implicit algorithm where all the linear terms that couple with the cylindrical part of the equilibrium (that is with poloidal and toroidal mode number $m = 0, n = 0$) are treated implicitly.

GYROKINETIC MODEL It is worthwhile to perform the numerical computation of the energetic particle contribution in the gyro-centre coordinate system. In this system, indeed, the characteristics of the Vlasov equation, which yields the time evolution of the energetic-particle distribution function, correspond to the gyro-averaged single particle equations of motion. The time evolution can then be followed without taking care of the details of the gyro-motion, i.e. using time steps much longer than the gyro-period.[5] The gyro-centre coordinates are obtained from the usual guiding-centre ones through an infinitesimal transformation, which makes the fundamental *1-form* of the system (from which the kinetic equations of motion are derived) free of gyro-phase dependence.[6] The optimal ordering for the energetic particle component is obtained by imposing the resonant condition between the mode frequency and the energetic particle transit frequency which yields $v_H \approx v_A$, where v_H is the hot particle thermal velocity. In addition, the magnetic drift frequency must be smaller than the ion transit frequency in order to avoid detuning of the wave-particle resonance. Therefore the hot ion Larmor radius is ordered as $\rho_H \approx \epsilon a$, which yields $\omega_{dH}/\omega \approx \epsilon$. On the basis of such an ordering the electrostatic potential is ordered as $e_H\varphi/T_H \approx 1$. The gyro-averaged equations are then obtained in the form

$$\begin{aligned}
\frac{d\vec{R}}{dt} &= \left(p - \frac{a_\parallel}{m_H}\right)\hat{b} + \frac{e_H}{m_H\Omega_H}\hat{b}\times\vec{\nabla}\left(\varphi - \frac{pa_\parallel}{e_H^2} + \right. \\
&\left. + \frac{a_\parallel^2}{2m_H e_H}\right) + \left(\frac{M}{m_H} + \frac{p}{\Omega_H}\left(p - \frac{a_\parallel}{m_H}\right)\right)\hat{b}\times\ln B\,, \\
\frac{dp}{dt} &= -\frac{e_H}{m_H}\left(\hat{b} + \frac{p}{\Omega_H}\hat{b}\times(\hat{b}\cdot\vec{\nabla})\hat{b}\right)\cdot\vec{\nabla}\left(\varphi - \frac{pa_\parallel}{e_H^2} + + \frac{a_\parallel^2}{2m_H e_H}\right) - \frac{M\Omega_H}{m_H}\hat{b}\cdot\vec{\nabla}\ln B.
\end{aligned} \tag{3}$$

Here $\vec{R}$ is the gyro-centre position, M is the exactly conserved magnetic momentum and p corresponds to the canonical parallel momentum; the fluctuating fields φ and $a_{\|}$ are calculated at the position of the gyro-centre and are related to the stream functions calculated by the fluid part of the code by $\varphi = -\frac{T_H a^2 v_A}{e_H R_o \rho_H v_H} U$ and $a_{\|} = \frac{e_H}{c}\frac{R_o}{R}\psi$. The hot-particle pressure tensor components can be written, in terms of gyro-centre coordinates as

$$\Pi_{H\,kj}(\vec{x}) = \frac{1}{m_H^2}\int d^6Z \left[\frac{M\Omega_H}{m_H}(\delta_{kj} - b_k b_j) + \left(p - \frac{a_{\|}}{m_H}\right)^2 b_k b_j\right] \times F_H(t,Z)\delta\left(\vec{x} - \vec{R}\right), \qquad (4)$$

where d^6Z includes the Jacobian of the transformation from canonical to gyro-centre coordinates. The phase-space distribution function F_H is determined, at each time step, by its weighted-particle representation, using the so-called δf algorithm.

NUMERICAL RESULTS The dynamics of the Alfvén continuum has been studied in detail to verify that the code describes correctly the physics contained in the fluid equations. Thus a preliminary, linear study in which the kinetic term is neglected has been performed.[7,8] In particular, it has been verified that the radial structure of the shear Alfvén continuum is well represented. Also it has been verified that the time dependence of the velocity stream function for the continuum oscillations, behaves asymptotically as $U_{m,n}(t) \approx e^{-i\omega_A t}/t + O(1/t^2)$.[9] The ϵ^3 terms will modify significantly the structure of the cylindrical Alfvén continuum. The toroidal coupling gives rise to "gaps" in the Alfvén continuum, resolving the degeneracy between the two cylindrical continua associated with the poloidal mode numbers m and $m+1$, at the specific radius $r = r_g$ where $k_{\|m,n} = -k_{\|m+1,n}$. It has been shown that, inside the gaps, the so-called toroidicity-induced (global) Alfvén eigenmode (TAE) can exist.[1] This is a marginally stable mode in the ideal limit, with a normalized real frequency given by $\omega/\omega_A = 1/3 \pm O(\epsilon)$, for $n = 1, m = 1,2$ (the Alfvén frequency is $\omega_A = v_A(r)/R$). The TAE is clearly observed by the numerical code, and the eigenfunctions have the expected radial profile. The effect of finite resistivity on the evolution of the TAE mode has been also studied analytically and numerically.[7,8] In the regime $\eta << \epsilon^3$, the damping γ scales linearly as a function of resistivity, $\gamma \sim (\eta/\epsilon^2)$. In the regime $\eta >> \epsilon^3$, the damping is a function only of resistivity and scales as $\gamma \sim \eta^{1/3}$.

The interaction of the TAE with the Alfvén continuum can occur at the edge of the plasma column if a density profile which decreases towards the edge is chosen. Analytical expressions for the damping rate of the TAE induced by the interaction with the Alfvén continuum are known only in the high-n limit.[10] In the low-n limit, the damping rate is expected to scale approximately as $\gamma \sim |L_n|^{-\alpha}$, with $\alpha \sim 1 \div 1.5$ and $|L_n|$ being the scale length of the density gradient where the interaction with the Alfvén continuum occurs. A similar scaling is obtained by the numerical code.[7,8]

NONLINEAR SATURATION In order to analyze the effects of nonlinearities, we take $\hat{\varrho} = \varrho_o$ in Eqs. 1 and 2, and we retain only the three components of each field ψ, U with mode numbers $(m,n) = (1,0),(1,1),(0,1)$. The nonlinear coupling (forcing scheme) is then $F_{1,0} \rightarrow$ forced by $F_{2,1} \times F^*_{1,1}$, $F_{1,1} \rightarrow$ forced by $F_{2,1} \times F^*_{1,0}$, $F_{2,1} \rightarrow$ forced by $F_{1,0} \times F_{1,1}$, where $F_{m,n}$ is the generic field. Typically the nonlinear effects are important when the $(1,0)$ component of the perturbations significantly modifies the equilibrium (i.e. the toroidal $O(\epsilon)$ corrections to the cylindrical equilibrium). Hence the nonlinear effects are expected to be important in the "gap region" (where $k_{\|1,1} + k_{\|2,1} = O(\epsilon)$), along with the effects of toroidicity (linear),[10] and when $U \approx v_A a \epsilon^{5/2}$ and $\delta\psi = \psi - \psi_{eq} \approx Ba\epsilon^{5/2}$. For sufficiently high perturbations, the TAE mode coalesces with the "nonlinear Alfvén continuum", and undergoes a nonlinear

continuum damping, in analogy to what happens in the linear case. The results of the numerical code has been compared with the predictions of a simple analytical model.[8] This model predicts the saturated amplitudes of the perturbed quantities to scale as $U_{1,1} \sim U_{2,1} \sim v_A a\epsilon^{5/2}$, $\delta\psi_{1,1} \sim \delta\psi_{2,1} \sim Ba\epsilon^{5/2}$, $U_{1,0} \sim v_A a\epsilon^3$, $\delta\psi_{1,0} \sim Ba\epsilon^3$. The term proportional to the pressure of the high energy particles in Eq. 2 has been modelled with an "ad hoc" growing term $\gamma_l U$ with γ_l being a numerical coefficient. In fig.1a we plot the time evolution of the total (kinetic plus magnetic) energy of the different Fourier components for a case with $\epsilon = 0.05, q_0 = 1.1, q_a = 1.9$. In fig.1b the numerical saturated amplitudes versus ϵ are shown, together with the predictions of the analytical model.[8] The numerical results show a scaling of $U_{2,1} \propto \epsilon^{2.5}$, $U_{1,1} \propto \epsilon^2$, $U_{1,0} \propto \epsilon^{2.5}$, close to the expected analytical predictions.

References

[1] CHENG, C. Z., LIU CHEN, CHANCE, M. S., Ann. Phys. (N.Y.) **161** (1985) 21

[2] STRAUSS, H. R., Phys. Fluids **20** (1977) 1354

[3] IZZO, R., MONTICELLO, D. A., PARK, W., et al., Phys. Fluids **26** (1983) 2240

[4] BONDESON, A., Nucl. Fusion **26** (1986) 929

[5] LEE, W. W., Journal of Comput. Phys. **72** (1987) 243

[6] CARY, J. and LITTLEJOHN, R., Ann. Phys. (N.Y.) **151** (1983) 1

[7] VLAD, G., BRIGUGLIO, S., KAR, C., ZONCA, Z. and ROMANELLI, F., Proceedings of IAEA TECHNICAL COMMITTEE MEETING, Montréal, Canada, 15-18 June 1992.

[8] VLAD, G., BRIGUGLIO, S., KAR, C., ZONCA, Z. and ROMANELLI, F., Theory of Fusion Plasmas, Varenna 1992 (Editrice Compositori, Bologna 1992), p. 361

[9] BARSTON, E. M., Ann. Phys. (N.Y.) **29** (1964) 282

[10] ZONCA, F., LIU CHEN, Phys. Rev. Lett. **68** (1992) 592 and ROSENBLUTH, M.N., BERK, H. L., VAN DAM, J. W. and LINDBERG, D. M., Phys. Rev. Lett. **68** (1992) 596

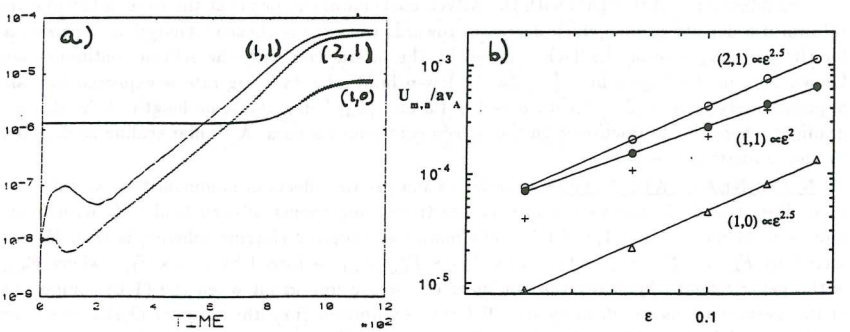

Fig.1 a) Time evolution of integrated total energies for different (m, n) Fourier components (the time is in Alfvén time unit, $\epsilon = 0.05$). b) Saturated amplitudes vs. ϵ. The crosses refer to the analytical values for the $(1, 1)$ mode.

THERMONUCLEAR INSTABILITY OF FMS MODES IN TOKAMAK

Gorelenkov N.N.,Polevoy A.R.

RSC "Kurchatov Institute"

INTRODUCTION: In recent deuterium experiments on tokamaks Ion Cyclotron Emission (ICE) with frequencies up to 500 MHz have been observed (see [1,2] and the references therein). The spectrum of the oscillations presented regular structure with oscillation amplitude peaked at deuteron cyclotron frequency 1 harmonics ($\omega = 1\omega_{BD}$). The signals of ICE were proportional to the neutron emission which indicates that the ICE could be driven by charged fusion products. Observed bursts of high-frequency ($1 \sim 1 - 10$) oscillations in JET, appeared with some delay after the sawtooth crash [1] and coincided with D_α signal on the plasma periphery, which could be explained by the finite time of heat wave generated at sawtooth crash and spread from the plasma center to the periphery. In ref.[2] observed ICE was associated with fusion proton driven Fast Magnetosonic (FMS) waves. In this paper we discuss the problem of FMS eigenmodes excitation by D-D fusion protons generated with superalfven velocity $V_{p0}=2.4\ 10^9$cm/s.

1. In order to calculate increments and thresholds of FMS instability we made use the neoclassical proton distribution function f_p which was the numerical solution of drift kinetic equation. The numerical code included the finite drift radial excursions of protons, radial unhomogenity and sawtooth evolution of proton source.

The typical time scale of the processes of interest is much greater than the bounce period $\tau_b = 10^{-6}$s. In this case the distribution function is known to be a function of integrals of motion [3-5]:

$$\mu = V_\perp^2/2B,\quad J=e_p\Psi(R,Z)/2\pi m_p c - V_\parallel R$$

were μ,J - adiabatic invariants, e_p,m_p- charge and mass of proton, Ψ - poloidal magnetic flux, B - magnetic field, R - major radius, $V_\parallel,V_\perp$ - parallel and perpendicular components of

proton velocity. Neoclassical kinetic equation from [3-5]:

$$\left\langle \frac{1}{v^2\tau_{pe}} \frac{\partial}{\partial v}(v^3+v_c^3) f_p \right\rangle + \left\langle \left[J - \frac{e_p \Psi}{2\pi m_p c} \right] \frac{1+v_c^3/v^3}{\tau_{pe}} \right\rangle \frac{\partial f_p}{\partial J} - \frac{\partial f_p}{\partial t} + \langle S \rangle = 0, \quad (1)$$

was solved numerically by integration over the characteristics with f_p- distribution function, $\tau_{pe}=0.01\ T^{3/2}[keV]/(n\ 10^{-20} m^{-3})$ - protons slowing down time on electrons, $V_c = 0.1\ V_{p0}\sqrt{T_e[keV]}$. The first term in (1) corresponds to the Coulomb friction. The second term in (1) corresponds to the change of integral J during the slowing down, S is the source of fusion protons.

To estimate the instability increments for JET experiments we used in our calculations plasma parameters similar to those, reported in [4]: R_0= 2.96m, a=1.2m, B_0=2.8T, T_{0e}= 10 keV, T_{0i}= 18keV, $T_{i,e} = T_{0i,e}(1-\Psi/\Psi_c)^2$, n_{0e}= 0.3 10^{14} cm^{-3}, $n_e = n_{0e}(1-\Psi/\Psi_c)^{0.1}$, elongation k = 1.8, Ψ_c- flux at the boundary. We simulate the sawtooth crush events by mixing of the plasma pressure all over the zone $0 < r < 1.4\ r_1$ with a safety factor $q(r_1 = 0.6a) = 1$ [4], and further heat wave propagation to plasma periphery. The calculated distribution function f_p in the point R = 3.9 m, Z = 0 for the sawtooth period τ_{ST} = 100 ms, and time of heat propagation 15 ms are shown in Fig. 1. The proton density in this point is $n_p \simeq 3.4\ 10^8 cm^{-3}$. Protons have substantially wide drift trajectories in radial direction comparable to the minor radius. Very complicate structure of f_p, resembling The Babylonian Tower, is caused by periodic proton source increasing due to heat wave propagation after the sawtooth crash and by different slowing down time for different flux surfaces. There is also a "loss cone" at the boundary between co passing and trapped particles with negative $V_\parallel$. This well pronounced f_p anisotropy with $\partial f_p/\partial v > 0$, and $\partial f_p/\partial v_\parallel \neq \partial f_p/\partial v$ might induce the instability of FMS eigenmodes.

2. Following to [6] the eigen mode spectrum and localization was determined in a hollow cylinder approximation for JET plasma parameters. FMS eigenmodes appeared to be

localized in a narrow zone near the plasma periphery $R_1 < R < R_2$ between reflection points R_1, R_2 with $k_\perp(R_1) = k_\perp(R_2) = 0$. Their spectrum fulfilled the quantization conditions:

$$\int_{R_1}^{R_2} \mathrm{Re}\, k_R(\omega, k_\parallel, R)\, dR = \pi\,(m + 1/2),\quad R\, k_\phi = l,$$

with l,m - toroidal and radial mode numbers, $\omega = \omega_{lm}$ the eigenfrequency. To estimate an order of magnitude of these mode increments, we calculated the proper values for Maxwellian bulk plasma and computed proton distribution function. According to our calculations the mode, has been obtained in experiment ($\approx$ 55 MHz) might be identified as FMS - eigenmode, exited by Cherenkov resonance thermonuclear protons. The localization of this mode appeared to be the same, as it was obtained in the experiment [1] $R_1 \approx 3.9$ m, $R_2 \approx 4.1$ m.

The increment of instability calculated numerically in WKB approximation [6] is of order $\gamma_p/\omega \approx n_p'(k_R\rho_L)^2 V_{p0}/(V_T n_i)$, where ρ_L - proton gyroradius, $V_T^2 = 2T_i/m_i$, n_p'- the density of protons produced by heat wave $n_p' \approx n_p/10$. For chosen parameters $\gamma_p/\gamma_e \leq 0.1$ with γ_e- the electron Landau damping. However for more precise calculations the real experimental measurements of plasma evolution and the more accurate method for increment simulations are required.

1. G.A.Cottrell,R.O.Dendy,Phys.Rev.Lett.60,33(1988)
2. P.Shild,G.A.Cottrell,R.O.Dendy,Nucl. Fusion Lett.29,834(1989)
3. Goloborodko V.Ya.,Kolesnichenko Ya.I.,Yavorskij V.A.//Nucl. Fusion.1983.V.23.P.399.
4. Nocentini A., Tessarotto M., Engelmann R.// Nucl.Fusion. 1975. V.15.P.359.
5. Gorelenkov N.N.,Putvinskij S.V.//Fizika plasmy 15 (1989) 145.
6. V.D.Yegorenkov, A.R.Polevoy,K.N.Stepanov, S.E.Sharapov //Proc. of 18th EPS Conf.on Contr.Nucl.Fus.and Plasma Phys., Berlin, V.IV, p.33, (1991)

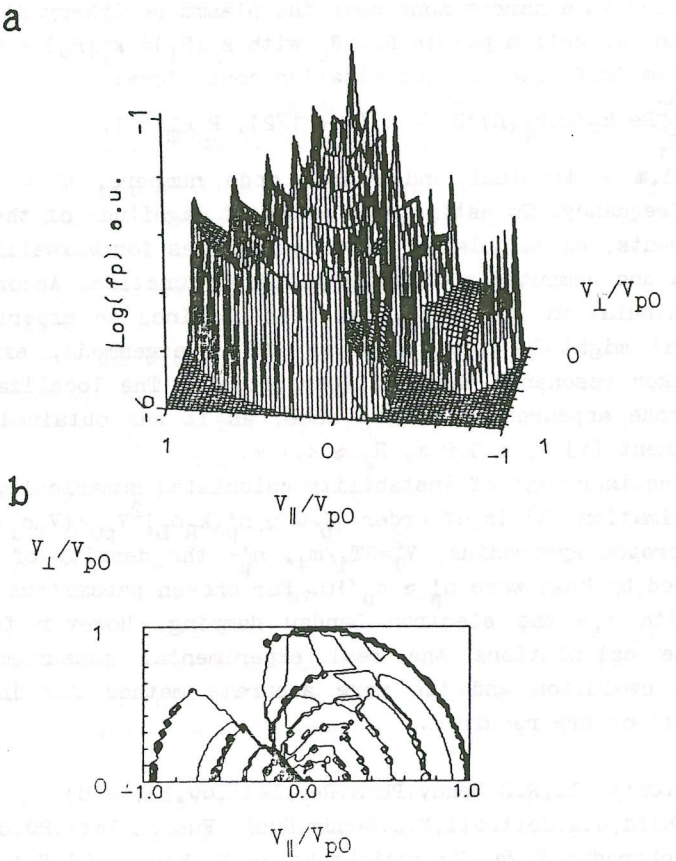

Fig.1 a) Proton distribution function f_p;
b) f_p contour map.

On the Kinetic Theory in a Strong Magnetic Field

Aldo Nocentini

Dipartimento di Scienze Matematiche dell'Università,
P.le Europa 1, 34127 Trieste (Italy)

Abstract: The collision integral for binary collisions between like particles whose dynamics is dominated by the presence of a magnetic field is calculated in the case of a spatially non-uniform plasma. Heat transport coefficients are derived.

The theory of collisional transport in tokamak plasmas ("neoclassical transport") is based on kinetic equations where the collision term takes into account binary coulomb collisions only. In current tokamak experiments the (electron) Larmor radius is of the order or even smaller (in particular, in the outer part of the plasma ring) than the Debye length. In this case, drifts become important during particle interactions involving electrons ("drift" collisions) and, therefore, the effect of the equilibrium magnetic field $\underline{B}$ on the (electron) collision process and, hence, on the $(e-e$ and $e-i)$ collision term is significant.

The first derivation of a collision term for binary coulomb collisions in the presence of a strong magnetic field, self consistently including the Debye shielding effect, is due to Rostoker (1960; see also Rostoker and Rosenbluth 1960). Rostoker's result applies to a spatially uniform, multispecies plasma, for any Larmor radius. The magnetic collision term obtained in this way is much more complicated than the coulomb collision term. For this reason, on the one hand it has not been used, on the other hand many papers have subsequently reconsidered the problem in various simplifying limits. Rostoker's result itself is severely limited by the assumption of spatial uniformity. In fact, an important aspect of "drift" collisions is that they generate diffusion in physical space, rather than in velocity space, and this aspect cannot be seen in a uniform plasma (see for example Nocentini, 1986).

In this paper the collision integral for $e-e$ collisions in the presence of a strong magnetic field is derived by using Dupree's method to solve the equation for the two-particle correlation function in a spatially non uniform plasma. The spatial non-uniformity is treated by developing the one-particle distribution function around the point where the collision integral is calculated. By "strong magnetic field" we mean that the electron dynamics can be described by drift equations.

A plasma embedded in a strong (Larmor radius much smaller than Debye length), uniform magnetic field, pointing in the z-direction, is considered. For electrons (only

e-e collisions are considered), the drift equations of motion are assumed. The coordinates of the Gibbs space are (the notation is standard):

$$\underline{r}_i \equiv \{x_i, y_i, z_i\}, \qquad u_i \equiv v_{zi}, \qquad \mu_i \equiv m\, v_{\perp i}^2 / 2\, B$$

and the equations of motion are:

$$\dot{\underline{r}}_{\perp i} = \frac{c}{B} \underline{E}^{(i)} \times \underline{e}_z, \qquad \dot{z}_i = u_i, \qquad \dot{u}_i = \frac{e}{m} E_z^{(i)}, \qquad \dot{\mu}_i = 0,$$

where

$$\underline{E}^{(i)} = \sum_{j \neq i} \underline{E}^{(ij)}, \qquad \underline{E}^{(ij)} = -\underline{\nabla}_i \Phi^{(ij)}, \qquad \Phi^{(ij)} = \frac{e}{|\underline{r}_i - \underline{r}_j|}.$$

The equation for the 1−particle distribution function $f(\underline{r}_1, u_1, \mu_1) = f(1)$ reads

$$\Big\{ \frac{\partial}{\partial t} + u_1 \frac{\partial}{\partial z_1} + \frac{c}{B} \underline{E} \times \underline{e}_z \cdot \underline{\nabla}_1 + \frac{e}{m} E_z \frac{\partial}{\partial u_1} \Big\} f(1) =$$

$$= -\frac{c}{B} \underline{\nabla}_1 \cdot \Big\{ \int_{-\infty}^{+\infty} d2\, g(1,2\,|\,t)\, \underline{E}^{(1,2)} \times \underline{e}_z \Big\} - \frac{e}{m} \frac{\partial}{\partial u_1} \Big\{ \int_{-\infty}^{+\infty} d2\, g(1,2\,|\,t)\, E_z^{(1,2)} \Big\}, \quad (1)$$

where $g(1,2\,|\,t)$ is the 2−particle correlation function and $\underline{E}$ the macroscopic electric field.

The equation for the 2−particle correlation function is closed by using the usual assumptions: negligibility of the 3−particle correlation function, pulverization (weak interaction limit) and negligibility of the effect of the macroscopic electric field on correlations. It reads

$$\Big\{ \frac{\partial}{\partial t} + u_1 \frac{\partial}{\partial z_1} + u_2 \frac{\partial}{\partial z_2} \Big\} g(1,2) +$$

$$+ \frac{c}{B} \Big\{ \int_{-\infty}^{+\infty} d3\, g(2,3)\, \underline{E}^{(1,3)} \times \underline{e}_z \Big\} \cdot \underline{\nabla}_1 f(1) + \frac{c}{B} \Big\{ \int_{-\infty}^{+\infty} d3\, g(1,3)\, \underline{E}^{(2,3)} \times \underline{e}_z \Big\} \cdot \underline{\nabla}_2 f(2) +$$

$$+ \frac{e}{m} \Big\{ \int_{-\infty}^{+\infty} d3\, g(2,3)\, E_z^{(1,3)} \Big\} \frac{\partial f(1)}{\partial u_1} + \frac{e}{m} \Big\{ \int_{-\infty}^{+\infty} d3\, g(1,3)\, E_z^{(2,3)} \Big\} \frac{\partial f(2)}{\partial u_2} =$$

$$= -\frac{c}{B} \underline{E}^{(1,2)} \times \underline{e}_z \cdot (\underline{\nabla}_1 - \underline{\nabla}_2) \big[f(1)\, f(2) \big] - \frac{e}{m} E_z^{(1,2)} \Big(\frac{\partial}{\partial u_1} - \frac{\partial}{\partial u_2} \Big) \big[f(1)\, f(2) \big]. \quad (2)$$

This equation is solved by using Bogoliubov's (adiabatic) hypothesis and by expansion in power series of the small parameter $|\underline{\nabla} f / f|$. No details of the derivation are reported here. The resulting collision term is obtained as a series of terms which depend on derivatives of the 1-particle distribution function in velocity and/or physical space. By keeping only the two leading terms, as far as velocity and space derivatives

are concerned, the kinetic equation reads

$$\frac{\partial f}{\partial t} + u\frac{\partial f}{\partial z} + \frac{c}{B}\underline{E}\times\underline{e}_z\cdot\underline{\nabla} f + \frac{e}{m}E_z\frac{\partial f}{\partial u} =$$

$$= \frac{4\pi e^4 ln\Lambda_{DR}}{m^2}\left\{\frac{\partial}{\partial u}\left[\bar{f}(\underline{r},u)\frac{\partial}{\partial u}f(\underline{r},u,\mu) - f(\underline{r},u,\mu)\frac{\partial}{\partial u}\bar{f}(\underline{r},u)\right] + \right.$$

$$\left. + \frac{1}{2\Omega^2}\underline{\nabla}_\perp\cdot\int_{-\infty}^{+\infty}\frac{du'}{|u-u'|}\left[\bar{f}(\underline{r},u')\,\underline{\nabla}_\perp f(\underline{r},u,\mu) - f(\underline{r},u,\mu)\,\underline{\nabla}_\perp\bar{f}(\underline{r},u')\right]\right\}, \qquad (3)$$

where $\Lambda_{DR} = \lambda_D/r_L$, and Ω, r_L and $\lambda_D = (T/4\pi e^2 N)^{1/2}$ denote respectively gyrofrequency, Larmor radius and Debye length of the species under consideration. The bar indicates integration over μ. The logarithm comes from imposing the Larmor radius as lower cut-off for the impact parameter, on the basis that collisions with smaller impact parameter are not drift collisions as considered here.

The first part of the collision term describes diffusion in (parallel) velocity space. It agrees with the zero-Larmor-radius limit of the collision term given by Rostoker (1960). The second part describes direct diffusion in space due to the displacement of the guiding center of particles during drift collisions. The corrections of these terms due to the spatial non-uniformity of the distribution function have been neglected because higher order in the expansion parameter. Nevertheless, they can be important in the cases where the lowest order terms vanish (as far as the first term is concerned, a case of this kind has been discussed by Psimopoulos and Li, 1992). The second part of the collision integral is itself smaller than the first one by two orders in the small parameter of the expansion. Nevertheless, the contributions of the two parts to the diffusion properties in physical space of the plasma are comparable in magnitude. This is due to the fact that the second part contributes to diffusion in physical space directly, while the first one causes diffusion in velocity space, and only indirectly in physical space.

The second part of the collision term is now considered in more detail. By taking the appropriate moments of eq.(3), the transport coefficients of various quantities, directly induced by drift collisions, can be determined. For example, the equation for the density of the kinetic energy related to the gyro-motion, $\mathcal{E}_\perp$, reads

$$\frac{\partial \mathcal{E}_\perp}{\partial t} + \frac{\partial}{\partial z}[\mathcal{E}_\perp V^{(2,\perp)} + NT_\perp V^{(1)}] + \underline{\nabla}\cdot\{\mathcal{E}_\perp\frac{c}{B}\underline{E}\times\underline{e}_z\} = \frac{2\pi e^4 ln\Lambda_{DR}}{m^2\Omega^2}\underline{\nabla}_\perp\cdot$$

$$\cdot\left\{\int_{-\infty}^{+\infty}\frac{du\,du'}{|u-u'|}\int_0^\infty d\mu\,\mu B\left[\bar{f}(\underline{r},u')\,\underline{\nabla}_\perp f(\underline{r},u,\mu) - f(\underline{r},u,\mu)\,\underline{\nabla}_\perp\bar{f}(\underline{r},u')\right]\right\},$$

where $V^{(1)}$ and $V^{(2,\perp)}$ are the macroscopic parallel "velocities" of particles and gyro-heat, respectively. For a local maxwellian with spatial-dependent (perpendicular) temperature (by imposing as lower limit of integration in $|u-u'|$ the critical value of the velocity difference, $u_{th}\sqrt{\lambda_L/\lambda_D}$ (where λ_L is the Landau distance of minimum approach) above which two particles moving along two magnetic field lines whose distance is λ_D overtake each other) its left hand side is the (perpendicular) divergence of

$$\frac{2\sqrt{2\pi}\, e^4 N^2 ln\Lambda\, ln\Lambda_{DR}}{m^2\Omega^2 u_{th}} \nabla_\perp T_\perp,$$

which corresponds to a perpendicular heat conductivity (for the gyro-kinetic energy)

$$\chi_\perp^{(\perp)} = \frac{3\, ln\Lambda_{DR}\, T_\perp\, N}{2\sqrt{2} m\, \tau_e \Omega^2} = \frac{ln\Lambda_{DR}}{4.4}\, \chi_\perp^{cl},$$

where $\chi_\perp^{cl} = 4.7\, N\, T_e/m_e\Omega_e^2\tau_e$ is the classical perpendicular heat conductivity of electrons ($ln\Lambda$ denotes the Landau logarithm). This effect was already discussed in a preceding paper (Nocentini 1986), but the heuristic calculation of its magnitude given there is not correct.

The parallel transport coefficient can be obtained by considering the stationary kinetic equation, where on the l. h. s. a local maxwellian with z-dependent density and temperature is used and on the r.h.s. the linearized collision operator for collisions between distribution functions near to local equilibrium is used. In the absence of a macroscopic electric field this equation reads

$$u\, f_M \Big\{ \frac{dN}{N\, dz} + \frac{du_{th}^2}{u_{th}^2\, dz} + \Big(\frac{\mu B}{T_\perp} - 1\Big) \frac{dT_\perp}{T_\perp\, dz} + \Big(\frac{u^2}{u_{th}^2} - \frac{3}{2}\Big) \frac{du_{th}^2}{u_{th}^2\, dz} \Big\} =$$

$$= \frac{4\pi e^4 ln\Lambda_{DR}}{m^2} \frac{N^2 B}{\pi u_{th}^2 T_\perp} \frac{2}{u_{th}^2} \Big(\frac{\mu B}{T_\perp} - 1\Big) V^{(2,\perp)} \frac{\partial}{\partial u} \Big\{ e^{-2u^2/u_{th}^2}\, e^{-\mu B/T_\perp} \Big\}.$$

By multiplying this equation by $(\mu B - T_\perp)u$ and integrating in velocity space we get

$$V^{(2,\perp)} = \frac{m^2 u_{th}^3}{4\sqrt{2\pi} e^4 ln\Lambda_{DR} N} \frac{u_{th}^2 N}{2T_\perp} \frac{dT_\perp}{dz}.$$

Hence, the parallel conductivity of the gyro-heat reads

$$\chi_\parallel^{(\perp)} = \frac{m^2 u_{th}^3}{4\sqrt{2\pi} e^4 ln\Lambda_{DR}} \frac{u_{th}^2}{2} = 0.3\, \frac{ln\Lambda}{ln\Lambda_{DR}}\, \chi_\parallel^{cl},$$

where $\chi_\parallel^{cl} = 3.2\, N\, T_e \tau_e / m_e$ is the classical value of the parallel electron heat conductivity.

References

Nocentini A 1986 *Proc XIII EPS Conference (Schliersee)* **1** 85
Psimopoulos M and Li D 1992 *Proc. R. Soc. Lond.* **437 A** 55
Rostoker N 1960 *Phys. Fluids* **3** 922
Rostoker N and Rosenbluth M N 1960 *Phys. Fluids* **3** 1

X-Point Effect on Neoclassical Kinetic Theory.

E. R. Solano and R. D. Hazeltine†,
Fusion Research Center, Institute for Fusion Studies†,
The University of Texas at Austin..

Traditionally, neoclassical transport calculations ignore poloidal variation of the poloidal magnetic field. Near an X-point of the confining field of a diverted plasma, the poloidal field is small, causing guiding centers to linger at that poloidal position. Indeed, the poloidal transit frequency approaches zero near the separatrix, so that ν* becomes locally large for any plasma temperature. The problem is solved in general first, and then a model poloidal flux function with an X-point is utilized to show that the plateau diffusion coefficient can change considerably (factort of 2). It is shown that ion rotation is unaffected by the X-point, when correctly interpreted.

The drift kinetic equation:

$$\xi v \nabla_{\|} f \; - \; v(1-\xi^2)\frac{\nabla_{\|}B}{B}\frac{\partial f}{\partial \xi} + \; e\frac{\xi v E_{\|}}{T} f_0 = \; C(f) \; - \; v_D^r . \nabla f_0 \qquad (1)$$

The first term in equation (1) represents streaming of the guiding center along field lines, the second term represents the mirror effect, the third represents the induced toroidal electric field (loop voltage), the fourth is the Coulomb collision operator and the last one represents the ∇B drift . Here v is the velocity of the guiding center, ξ is the pitch angle ($\xi = v_{\|}/v$), the subscript $\|$ indicates the component of the vector parallel to the magnetic field, v_D^r is the radial component of the first order drift velocity, $E_{\|}$ is the parallel component of the induced toroidal electric field (loop voltage), and f_0 is the zeroth order solution to the kinetic equation, a Maxwellian distribution function, with only radial variation.

Linearity of equation (1) allows recasting the problem as a set of equations of the form [1]:

$$v_{\|} . \nabla \, g_{ne} \; - C_l(g_{ne}) = \alpha_n \, f_{e0}$$

with different sources α_n, which would be functions of θ, v, ξ and f_0.

In the large aspect ratio approximation, the mirror force is ignored in first order, and $v_{\|}$ can be assumed to be independent of θ. In fact, that is a definition of the plateau regime: the transit frequency is much faster than collisions, which are much faster than the drift frequency. As an example, we consider

$$\xi v \nabla_{||} f \; - \; C(f) = - \; v_D^r . \nabla f_0 \qquad (2)$$

To further simplify the problem, we use a Krook collision operator, C(f)=ν f.

Given a poloidal flux function Ψ, the magnetic field can be written in symmetry coordinates as $\vec{B} = I\nabla\zeta + \nabla\zeta \times \nabla\Psi$. Here θ is the poloidal angle (geometric), ζ is the toroidal angle, $I = R B_t$. With such definitions, equation (2) can be rewritten as

$$\xi v \frac{\vec{B_p}.\nabla\theta}{B} \frac{\partial f}{\partial \theta} + \nu f = -\frac{mv^2}{2e}(1+\xi^2)\frac{I}{BR}\left[\frac{1}{n}\frac{\partial n}{\partial \Psi} + \left(\frac{v}{v_{th}^2} - \frac{3}{2}\right)\frac{1}{T}\frac{\partial T}{\partial \Psi} + \frac{e}{T}\frac{\partial \Phi}{\partial \Psi}\right] f_0 \frac{\vec{B_p}.\nabla\theta}{\vec{B}} \frac{\partial R}{\partial \theta}$$

Collecting all the terms in the rhs that are independent of θ in $\bar{S}$, we have:

$$\frac{\partial f}{\partial \theta} + \frac{\nu}{\xi v}\frac{B}{Bp.\nabla\theta} f = -\frac{\bar{S}}{\xi v} f_0 \frac{\partial R/b}{\partial \theta} \qquad (3)$$

And the solution of this equation is:

$$f(\theta) = -\frac{\bar{S}}{\xi v} f_0 \, e^{-p(\theta)} \int e^{p(\theta)} \frac{\partial R/b}{\partial \theta} d\theta$$

with $\quad p(\theta) = \frac{\nu}{\xi v}\int d\theta \frac{B}{B_p.\nabla\theta} = \frac{\nu}{\xi v} u(\theta) = \gamma \, u(\theta).$

A change of variable from θ to u(θ), and a Fourier decomposition of the integrand as a function of u, with $\alpha_l = 2\pi l/u(2\pi)$, allows computing the above integrals:

$$f(\theta(u)) = -\frac{\bar{S}}{\xi v}\frac{\partial f_0}{\partial \Psi} e^{-\gamma u} \int e^{\gamma u} \left(\frac{B_p.\nabla\theta}{B} \frac{\partial R/b}{\partial \theta}\right)_u du =$$

$$= -\frac{\bar{S}}{\xi v}\frac{\partial f_0}{\partial \Psi} e^{-\gamma u} \int e^{\gamma u} \sum_l (a_l \sin(\alpha_l u) + b_l \cos(\alpha_l u)) \, du =$$

$$= -\frac{\bar{S}}{\xi v}\frac{\partial f_0}{\partial \Psi} \sum_l \frac{[a_l(\gamma \sin(\alpha_l u) - \alpha_l \cos(\alpha_l u)) + b_l(\alpha_l \sin(\alpha_l u) + \gamma \cos(\alpha_l u))]}{\gamma^2 + \alpha_l^2}$$

In the plateau limit: $\lim_{\nu \to 0} \frac{1}{\xi v}\frac{\gamma}{\gamma^2+\alpha_l^2} \to \pi \, \delta(\xi v \alpha_l) = \frac{u(2\pi)}{2l} \delta(\xi)$. Only the part of the f even in ξ will be relevant to future calculations. It is:

$$f(u(\theta)) = \bar{S}\frac{\partial f_0}{\partial \Psi} \sum_l \frac{u(2\pi)}{2l} \delta(\xi) \; [\, a_l \sin(\alpha_l u) + b_l \cos(\alpha_l u) \,].$$

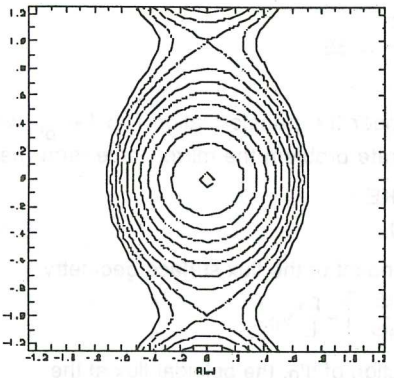

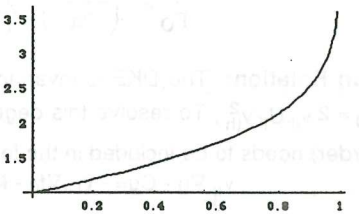

Example case:
Flux contours and q[Ψ] profile.

Fig. 1: Characterization of example flux function

From the knowledge of the complete distribution function f (based on similar calculations, with all sources), the transport coefficients can be calculated. For example, the particle diffusion coefficient is:

$$\Gamma_x = \frac{\pi\sqrt{\pi}}{2}\left(\frac{m}{eBR}\right| b\, v_{the}^2\Big)^2 \left(\frac{\partial \ln p_e}{\partial \Psi} + \frac{T_i}{ZT_e}\frac{\partial \ln p_i}{\partial \Psi}\right)\left(\oint \frac{d\theta}{B_p.\nabla\theta}\right)^{-1}$$

Or, more conveniently, we can compare it with the traditional circular plasma result, with $\frac{1}{B_p.\nabla\theta} = \frac{b}{B_{p0}}$ = constant:

$$\Gamma_O = -\frac{\sqrt{\pi}}{4}\frac{b}{R}\rho_{pol} B_{pol} \rho\, n_e\, v_{the}\left(\frac{\partial \ln p_e}{\partial \Psi} + \frac{Ti}{ZT_e}\frac{\partial \ln p_i}{\partial \Psi}\right)$$

$$\frac{\Gamma x}{\Gamma_O} = \left(\frac{u(2\pi)}{2\pi}\right)^2 \sum_l \frac{a_l^2+b_l^2}{l}$$

This result was previously obtained [2,3], although we arrived at it independently. Its importance appears not to have been appreciated in the particular case of a diverted plasma, which we discuss next.

Example: As a model of a poloidal flux function with a separatrix, we have

$$\Psi(r,\theta) = \Psi_0\left(\frac{r}{b}\right)^2\left[2 + \left(\frac{r}{b}\right)^2 \cos 2\theta\right] = \Psi_0\left(\left(\frac{x}{b}\right)^2 + \left(\frac{y}{b}\right)^2\right)\left(2 + \left(\frac{x}{b}\right)^2 - \left(\frac{y}{b}\right)^2\right)$$

Here, r is the polar radial coordinate, and it varies as a function of θ. A plot of the flux contours of Ψ and its q profile is shown in Fig. 1. In this case the Fourier series only has odd sine terms, and converges very quickly. For instance, at $\Psi/\Psi_0 = .9$, $a_1 = .4$, $a_2 = 0.$, $a_3 = .17$, we have:

$$\frac{\Gamma_X}{\Gamma_O} = \left(\frac{u(2\pi)}{2\pi}\right)^2 \sum_l \frac{a_l^2}{l} = .55$$

Ion Rotation: The DKE is invariant under the transformation $f \rightarrow f + f_d$, with $f_d = 2\, v_{||}.U_{||}/v_{th}^2$. To resolve this degenerate problem the mirror force term (next order) needs to be included in the ion DKE :

$$v_{||}.\nabla g - Cg = - v_D.\nabla f_0 - M(f_d)$$

In plateau regime, the solution is independent of the flux surface geometry:

$$U_{||} = \frac{T}{eB} I\left[\frac{1}{n}\frac{\partial n}{\partial \Psi} + 1.5\,\frac{\partial T}{\partial \Psi} + \frac{e}{T}\frac{\partial \Phi}{\partial \Psi}\right] \sim \frac{\rho_\theta}{L} v_{th}$$

So, the parallel rotation velocity is a function of Ψ_0, the poloidal flux at the LCFS. It is not a function of either the local or the flux surface averaged B_θ or of q. There is no infinity problem: simply, the more poloidal flux between the magnetic axis and the last closed flux surface, the slower the parallel rotation. Only in that sense is $U_{||}$"of order ρ_θ/L"

Adding the poloidal components of perpendicular and parallel rotation:

$$\vec{U}_{pol} = -\frac{1}{2}\frac{I}{B}\frac{\partial T/e}{\partial \Psi}\frac{\vec{B}_{pol}}{B}$$

The poloidal rotation speed is not a function of Ψ_0. Because $\vec{B}_{pol}/\Psi_0$ becomes small near the X-point, the poloidal rotation (using the usual cylindrical coordinate definition of poloidal) is a function of θ: it is slower near the X-point.

Comments: standard collisional transport theory [2,4] is already applicable to the X-point case. Trapping will be affected, so collisionless transport may be modified. The transition between plateau and collisional regime happens at lower ν in the presence of an X-point.

Acknowledgments: We would like to acknowledge valuable discussions with Prashant Valanju, and Allan Wootton. This work has been supported by USDOE under grants DE-FG05-88ER-53266 and DE-FG05-88ER-532088.

References:

[1] F. L. Hinton, R. D. Hazeltine, Rev. Mod. Phys. 48, 239 (1976).

[2] S. P. Hirshman, D. J. Sigmar, Nucl. Fus. 21,1079 (1981).

[3] H. K. Meier, S. P. Hirshman, D. J. Sigmar, Oak Ridge National Lab Report ORNL -TM -7584 (1980).

[4] R. D. Hazeltine, F. L. Hinton, Phys. Fluids 16, 1883 (1973).

Transport coefficients in magnetized plasmas.

D.Bennaceur and A.H. Khalfaoui
SERST/CDTA, laboratoire Interaction Laser-matière
2, Bd Franz Fanon, BP 1017 Alger-Gare, Algiers-16000, Algeria

This paper presents a theoretical analysis on transport coefficients of strongly coupled, fully ionized, classical and magnetized plasmas.

The plasma under consideration is a continuum of volume Ω containing N electrons, N/Z ions and an electron density $n=N/\Omega$ which exhibits 3N (high frequency branch) and 3N/Z (low frequency branch) characteristic frequencies $\omega_s(\vec{q})$ of longitudinal oscillations (s=e,i).

The high frequency branch corresponds to electron plasma oscillations and the low frequency branch are the ion sound waves.

The motion of electrons in strongly coupled plasmas is affected by the continuum oscillations (many-body interactions).

The plasma oscillations are quasi-particles or plasmons which obey Bose-Einstein statistics.

The electrons interacting with the plasma as a whole can emit and absorb the quasi-particles (plasmons and ion sound waves) with energy $\hbar\omega_s(\vec{q})$ and momentum $\hbar\vec{q}$ /1/, so the perturbed distribution function is relaxed in the process.

The oscillation frequencies are those of a classical plasma /2/.

The transport equation is written as:

$$\left.\frac{\partial f}{\partial t}\right|_{field} = - \left.\frac{\partial f}{\partial t}\right|_{coll} . \qquad (1)$$

The collision term for the e-e and e-i interaction is:

$$\left.\frac{\partial f}{\partial t}\right|_{coll} = \sum_{s=e,i} \left.\frac{\partial f}{\partial t}\right|_{es} = \frac{-f_1}{\tau_c} = - \frac{-\Phi \dfrac{\partial f_o}{\partial E}}{\tau_c} , \qquad (2)$$

where

$$\left.\frac{\partial f}{\partial t}\right|_{es} = \frac{-\Phi}{8\pi^2 m_s n_s k_B T} \int \frac{q^2 |U_s(q)|^2}{\omega_s(\vec{q})} N_q \, [f_o(\vec{k}')(1 - f_o(\vec{k}))]$$

$$\delta(E'-E+\hbar\omega_s) + f_o(\vec{k})[1 - f_o(\vec{k}')] \, \delta(E'-E-\hbar\omega_s) \, [1 - \frac{\Phi(\vec{k}')}{\Phi(\vec{k})}] d^3\vec{k}'$$

$$= \frac{-f_1}{\tau_{es}} \quad , s=e,i \; . \qquad (3)$$

$|U_s(q)|^2$ is the square of the Fourier transform of $U_s(r)$ which is a shielded Yukawa potential, N_q is the distribution of the plasmons, f_o is the Boltzmann distribution of the electrons, f_1 is the linear perturbation function of the electrons and Φ an arbitrary function proportional to the energy E of the electron: $\Phi = \vec{v}.C(E)$, (we assume spherical energy surfaces: $E = \hbar^2 k^2/2m$). The relaxation time τ_c for both interactions is taken to be $1/\tau_c = \sum_{s=e,i} 1/\tau_{es}$.

With the assumptions, $\hbar\omega_s \ll E$, $|\vec{k}'| = |\vec{k}|$ and isotropic scattering, $U_s(q)$ is bounded in the interval $(0,\hat{q}_s)$, $\hat{q}_s$ is the limit wave vector, and τ_c is evaluated analytically as:

$$\tau_c(E) = \frac{(5\sqrt{2}/3)\, m^{1/2} E^{3/2}}{8\pi\, n\, e^4 \, (R_e(\hat{\varepsilon}_e) + R_i(\hat{\varepsilon}_i))} \; , \qquad (4)$$

where $R_s(\hat{\varepsilon}_s) = Z_s(1 - 2/5\, \hat{\varepsilon}_s + 4 \sum_{\nu=1}^{\infty} \frac{B_{2\nu}\, \hat{\varepsilon}_s^{2\nu}}{(2\nu + 4)\,(2\nu)!} + \ldots.)$, s=e,i.

$B_{2\nu}$ are the Bernoulli numbers, $\hat{\varepsilon}_s = \hbar\omega_s(\hat{q}_s)/k_B T$, $Z_e=-1$ and $Z_i=Z$.

The LHS of equation (1) for a magnetized plasma can be written as:

$$\left.\frac{\partial f}{\partial t}\right|_{field} = \vec{v}.\frac{\partial f_o}{\partial E}\left\{\left[-\frac{E-\mu}{T} - \frac{\partial \mu}{\partial T}\right]\vec{\nabla}T - e\vec{\mathcal{E}}\right\} +$$

$$\frac{e}{m}\frac{(\vec{v}\wedge\vec{B})}{c}\cdot\frac{\partial f_1}{\partial \vec{v}} = -\frac{f-f_o}{\tau_c} = -\frac{f_1}{\tau_c} = -\frac{\Phi\,\frac{\partial f_o}{\partial E}}{\tau_c} \; . \qquad (5)$$

$\vec{\mathcal{E}}$ is the electrical field, μ the chemical potential, $\vec{\nabla}T$, the temperature gradient and $\vec{B}$ the magnetic field.

Expression of Φ /4/:

$$\Phi = \frac{\tau_c \vec{v}}{(1 + \tau_c^2 \omega_c^2)} . \left\{ \vec{A} + \tau_c (\vec{\omega}_c \wedge \vec{A}) + \tau_c^2 \vec{\omega}_c (\vec{\omega}_c . \vec{A}) \right\} , \qquad (6)$$

with $\vec{A} = [- \frac{E - \mu}{T} - \frac{\partial \mu}{\partial T}] . \vec{\nabla} T - e\vec{E}$ and $\vec{\omega}_c = \frac{e\vec{B}}{mc}$ is the electron gyrofrequency.

As a function of perpendicular and parallel components relative to the magnetic field, f_1 is given by /5/:

$$f_1 = - \tau_c \varphi \ (-e\vec{E} \ \partial f_o/\partial E + \vec{\nabla} T \ \partial f_o/\partial T) . \vec{v} + \tau_c^2 \varphi \ (-e\vec{E}_\perp \partial f_o/\partial E + \vec{\nabla} T_\perp \ \partial f_o/\partial T) . (\vec{v} \wedge \vec{\omega}_c) - \tau_c^3 \varphi \ (-e(\vec{E}_{\shortparallel} . \vec{\omega}_c) \partial f_o/\partial E + (\vec{\omega}_c . \vec{\nabla} T_{\shortparallel}) \partial f_o/\partial T)(\vec{\omega}_c . \vec{v}) , \qquad (7)$$

where $\varphi = 1/(1 + \tau_c^2 \omega_c^2)$.

In the direction parallel to $\vec{B}$, we have $\vec{\omega}_c \wedge \vec{A} = 0$ and $\Phi = \tau_c (\vec{v} . \vec{A})$. There are no effects of the magnetic field on the parallel components of the transport coefficients.

The transverse effects: $\vec{\omega}_c . \vec{A} = 0$, are such that:

$$f_1 = - \tau_c \varphi \ (-e\vec{E}_\perp \ \partial f_o/\partial E + \vec{\nabla} T_\perp \partial f_o/\partial T) . \vec{v} + \tau_c^2 \varphi \ (-e\vec{E}_\perp \ \partial f_o/\partial E + \vec{\nabla} T_\perp \ \partial f_o/\partial T) . (\vec{v} \wedge \vec{\omega}_c) . \qquad (8)$$

In the Boltzmann theory the electrical current and energy fluxes are given by:

$$\vec{J} = -e \int 2 \frac{d^3 p}{h^3} \vec{v} f_1 (\vec{v}) \qquad (9)$$

$$\vec{Q}_E = \int 2 \frac{d^3 p}{h^3} \ \frac{mv^2}{2} \vec{v} f_1 (\vec{v}) . \qquad (10)$$

The heat current $\vec{Q} = \vec{Q}_E + (\mu/T - \partial \mu/\partial T) \ \vec{J} . T/e$.

Using the result for f_1 into (9) and (10), we obtain:

$$\vec{E}_\perp = \vec{J}_\perp/\sigma_\perp + S_\perp \vec{\nabla}_\perp T + R_\perp \vec{B} \wedge \vec{J} + N_\perp \vec{B} \wedge \vec{\nabla} T \qquad (11)$$

$$\vec{Q}_\perp = TS_\perp \vec{J}_\perp - K_\perp \vec{\nabla}_\perp T + N_\perp T \vec{B} \wedge \vec{J} + L_\perp \vec{B} \wedge \vec{\nabla} T . \qquad (12)$$

Although, all the complete set of the transport coefficients can be deduced from the present model, only the electical and thermal conductivities are reported here, which are:

$$\sigma_\perp = e^2 K_{o1}[1 + \omega_c^2 (K_{o2}/K_{o1})^2] \qquad (13)$$

$$K_\perp = (K_{z1}/T)(1 + \omega_c^2 K_{12}^2/K_{z1}K_{o1}) - (e^2 K_{11}^2/\sigma_\perp)(1 + \omega_c^4 K_{o2}^2 K_{12}^2/K_{11}^2 K_{o1}^2) , \qquad (14)$$

where

$$K_{ij} = \int 2 \frac{d^3p}{h^3} \tau_c^j \varphi (v^2/3)(-\partial f_o/\partial E) E^i .$$

For weak magnetic fields: $\omega_c^2 \tau_c^2 \ll 1$, (13) and (14) become:

$$\sigma_\perp \simeq 8ne^2 A_\tau (k_B T)^{3/2}/(\pi^{1/2} m) \qquad (15)$$

$$K_\perp \simeq 32nA_\tau k_B (k_B T)^{5/2}/(\pi^{1/2} m) , \qquad (16)$$

where $A_\tau = (5\sqrt{2}/3)\, m^{1/2}/(8\pi ne^4[R_e(\hat{\varepsilon}_e)+R_i(\hat{\varepsilon}_i))]$.

And for strong magnetic fields: $\omega_c^2 \tau_c^2 \gg 1$, eqs. (13) and (14) are:

$$\sigma_\perp \simeq 3\pi^{1/2} ne^2 A_\tau (k_B T)^{3/2}/ 4m \qquad (17)$$

$$K_\perp \simeq 8nk_B (k_B T)^{-1/2}/(3\pi^{1/2} m\omega_c^2 A_\tau). \qquad (18)$$

For arbitrary magnetic fields, the coefficients K_{ij} are evaluated numerically.

/1/ D. PINES, Rev. Mod. Phys. 28, 184 (1956).

2/ Yu.L. KLIMONTOVICH and V.P. SILIN, Usp. Fiz. Nauk. 70, 247 (1960).

/3/ A.H. KHALFAOUI, IEEE Transactions on Plasma Science PS-12, n°3 (1984).

/4/ A. HAUG, Theoretical Solid State Physics, New York, Pergamon 2, (1972).

/5/ Y.T. LEE and R.M. MORE, Phys. Fluids 27, n°5 (1984).

PARTICLE AND HEAT TRANSPORT IN A PARTIALLY STOCHASTIC MAGNETIC FIELD

M.N. Bussac, CPHT, Ecole Polytechnique, 91128 Palaiseau (France)
L. Zuppiroli, IGA, EPFL 1015 Lausanne (Suisse)
R.B. White, PPPL, Princeton N.J. 08543 (USA)

Particle and heat transport in a low collisional plasma confined by a partially stochastic magnetic field are analysed. We show that the particle diffusion is ambipolar, but that the electronic heat diffusitivity χ_e is enhanced, such as near stochastic threshold $\chi_e = \chi_i \sim D\sqrt{m_i/m_e}$ (χ_i is the ionic thermal diffusivity and D the particle diffusion coefficient of both species).

We present an analysis of particle and heat transport in a low collisionnal plasma confined by a magnetic field partially stochastic. We assume that the plasma supports magnetic fluctuations of the level which is low enough to preserve undestroyed magnetic surfaces. The stochastic layers where the magnetic field lines wander around the islands as described in reference [1], are separated by K.A.M. Tori. Then near stochastic threshold the magnetic field geometry could be modelled as one dimensional and self similar with alternating laminar and stochastic layers (see Fig. 1). The width of a stochastic layer at the n^{th} scale is Δ_n where Δ_1 describes the largest scale and Δ_N corresponds to the smallest scale, that is the ion or electron Larmor radius.

In such configurations the particles experience magnetic field lines which are either stochastic or confined to magnetic surfaces. A particle can jump from one magnetic field line to another as a result of a collision and therefore explores the whole microstructure of the magnetic field.

In a previous paper, [2], we have considered the case where many collisions, with a frequency ν, were necessary for a particle of velocity $v \sim v_{th}$ (v_{th} is the thermal velocity) to explore a stochastic zone of width Δ_n namely $\Delta_n >> D_{st}\, v_{th}/\nu$, ($D_{st}$ is the diffusion coefficient of the magnetic field line).

In the present paper we instead consider the different situation where during the time between two collisions, a particle explores a whole stochastic region Δ_n, namely $\Delta_n^2 << D_{st}\, \nu_{th}/\nu$. The probability of particle presence within a stochastic domain becomes almost uniform after a filling time which is negligibly short with respect to ν^{-1}. The probability (per unit time) of a particle escape from a domain Δ_n scales as $\nu\, a_L/\Delta_n$. In the

laminar regions, the particle diffuses according to the neoclassical laws, provided that the layer thickness is larger than a few Larmor radii, a_L.

We begin by treating single species (ion or electron) transport and by ignoring the electric fields arising from the electron-ion interactions. The transport results from neoclassical diffusion in the laminar layers, and particle free streaming in the stochastic layers. The latter acts as a short-circuit for the diffusion. Moreover, the particle flux and the energy flux, are constant through the whole plasma sheet Δ_0, they are equal to the fluxes imposed at the sheet boundary. Therefore one expects for each species a density (or temperature) profile similar to that of figure 1, curve 1. Experimentally one relates the flux to an apparent gradient on the whole plasma sheet Δ_0. If α is the fraction of stochastic layers at a given scale, the total thickness of the laminar layers is $\Delta_o (1-\alpha)^N$. Therefore the apparent gradient is related to the real local gradient n' or T' by $n'_{ap} = n' (1-\alpha)^N$, $T'_{ap} = T' (1-\alpha)^N$. The apparent diffusion coefficient can be now written written as $D_{ap} = D_{neo} / (1-\alpha)^N$, where D_{neo} is the neoclassical diffusion coefficient and N is determined by the coarse-graining $(1-\alpha)^N \sim a_L/\Delta_0$, then $D_{ap} \sim D_{neo}\ \Delta_0/a_L \vee a_L \Delta_0/2$.

To simulate this phenomenon, we use a Chirikov-Taylor model, with a stochastic parameter $\varepsilon = 0.98$. In Fig. 2 is shown the ratio of the numerically measured collisional diffusion D to the classical value $D_{cl} = \nu\ a^2_L/2$, for a probability 1/100 of a collision each time step. The result clearly confirm the $1/a_L$ dependence of D/D_{cl} for small a_L.

When ions and electrons are taken into account, one can show that the effect of short circuit in the stochastic layers is correct only for the heat diffusivity problem. Indeed the ions average the microstructure on an ion Larmor radius scale, which is larger than the electron Larmor radius scale at the origin of the microstructure. Therefore, in the stochastic layers of width Δ_n , satisfying $a_e < \Delta_n < a_i$, (where $a_{e,i}$ are the electron or ion coarse graining scale, i.e. Larmor radii or banana width), a constant electron density in the layers $\Delta_n$is not compatible with an ion density gradient $n'_i = dn_i / dx$. For constant electron density the resulting electric potential Φ due to the ion density gradient would reach a value $\frac{e\Phi}{T} \sim \left(\frac{\Delta_1}{\lambda_D}\right)^2 \left(\frac{n'\Delta_1}{n}\right) >> 1$ violating plasma stability, (λ_D is the Debye length). Thus the electron distribution will rearrange itself in such a way as to maintain an electron density gradient in these stochastic layers. This is possible if the electrons are in Boltzmann equilibrium in an electrostatic potential Φ, $n_e \sim \exp(e\Phi/T_e)$. Moreover, the equilibrium distribution function f_e has to satisfy the Vlasov equation.

Expanding $f_e = f_e^0(E, \vec{r}) + \left(\frac{a_e}{\Delta_0}\right) f^1(\vec{v}, \vec{r})$, where $E = 1/2\ mv^2 - e\Phi$ is the particle energy, we obtain $v_{//}(\vec{B}.\nabla) f^0(E, \vec{r}) = 0$ which yields $f_e \sim \exp\left(-\frac{v^2}{2v_{th,e}^2} + \frac{e\Phi(r)}{T_e}\right)$, and $\vec{B} . \vec{\nabla} T_e = 0$. Therefore the electron temperature should be constant in the stochastic layers, as shown in Fig. 1, curve 2, but not in the laminar layers where $T = T(x)$, $\vec{B} . \vec{\nabla} x = 0$. But the plasma configuration supports an electronic density gradient everywhere. The electric neutrality condition determines the radial electric field, $n_e = n_i \sim \exp(e\Phi/T_e)$ and $(e\Phi'/T_e) = n'_e/n_e$.

Note that the particle motion along a field line in the stochastic layers is a random walk with a bias due to the electric $\phi'_0(x)$.

Therefore the ion density and temperature profile are determined by the neoclassical transport in the laminar layers, and by free-streaming mixing in the stochastic layers of width $\Delta_n > a_i$, where $n'_i = T'_i = 0$. The electronic density adjusts to the ion density profile through the radial electric field $\Phi' \sim (n'_i/n)(T_e/e)$ [Fig. 1, curve 3].

Then in a partially stochastic magnetic field, the ratio between ion heat diffusivity χ_i and particle diffusion D is equal to its neoclassical value $D \sim D_{neo}\ \Delta_0/a_i$, $\chi_i = \chi_{i\ neo}\ \Delta_0/a_i$ $\chi_i\chi_i/D \sim \sqrt{m_i/m_e}$, whereas the electronic heat diffusivity is enhanced $\chi_e \sim \chi_{e\ neo}(\Delta_0/a_e) \sim \chi_i$. If the turbulent scale Δ_1 is of the order of the ion coarse graining a_i [4] the ionic heat diffusivity and the particle transport are neoclassical, while the electronic heat diffusivity is $\chi_e \sim \sqrt{m_i/m_e}\ \chi_{i\ neo}$.

In conclusion, in a low collisional plasma ($\nu_e << v_{th,e}/R$) confined by a partially stochastic magnetic field near stochastic threshold, one expects the electronic and ionic heat diffusivities to be of the same order, and larger than the particle diffusion coefficient. In the ohmic regime one gets : $\chi_e \sim \chi_i \sim D\sqrt{m_i/m_e}$.

[1] M. Hugon et al., proceedings of the 7th International Conference on Plasma Physics (Kiev 1987).

[2] M.N. Bussac and L. Zuppiroli in Theory of Fusion Plasmas p. 187, J. Vaclavick, F. Troyon et E. Sindoni (Eds) SIF Bologna 1990.

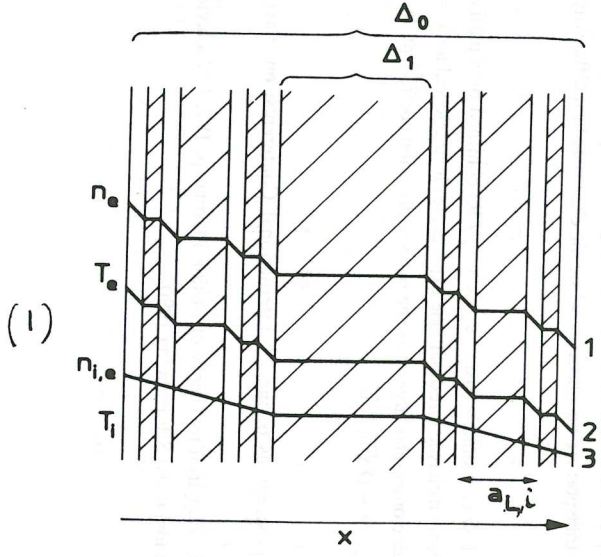

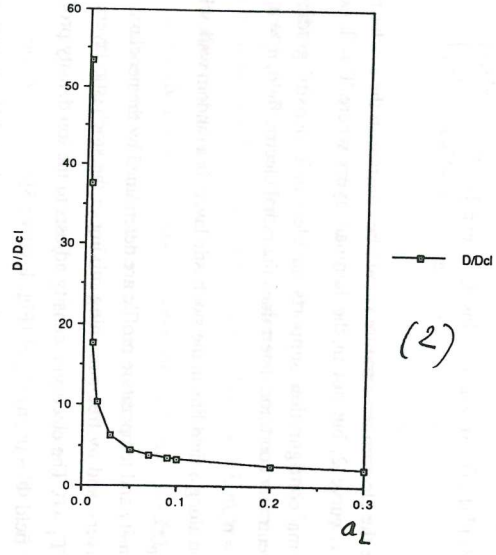

Fig. 1 : Schematic representation of the magnetic topology. The stochastic layers are dashed. Curve 1 represents the electron density profile when electron-ion interactions are ignored. When ion and electrons are both taken into account the electronic temperature profile follows curve 2 while the densities and the ionic temperature follow curve 3

Fig. 2 : Ratio of the numerical diffusion to the classical value $D_{cl} = \nu\, a_L^2/2$ for $\nu = 0.01$ and $\varepsilon = 0.98$.

Compatibility of Drift Wave Models for Tokamak Transport with Experimental Results

J. Weiland and H. Nordman

Institute for Electromagnetic Field Theory and
EURATOM/NFR Association
Chalmers University of Technology,
S-41296 Göteborg, Sweden

The dominance of toroidal effects, as seen in gyrokinetic simulations, is discussed in relation to the compatibility of drift wave models for transport with experiments.

Although several experimental observations seem to be in agreement with predictions from drift wave models regarding transport, several questions seem to remain although solutions have been suggested.[1,2] A recent very useful tool in the transport work is toroidal gyrokinetic simulations. The most striking feature seen in these is the dominance of toroidal effects.[3,4] In particular it was found[4] that the commonly observed growth of χ_i with radius in experiments is due to toroidal effects in the gyrokinetic simulations. The systematic inclusion of toroidal effects in drift wave models causes problems because the magnetic drift frequency is comparable to the mode frequency and this in general requires a kinetic description linearly as well as nonlinearly.[5] It is not until the last year, with the toroidal gyrokinetic simulations, that it has been possible to treat the nonlinear kinetic problem in toroidal geometry. These simulations have now verified the result of our fully toroidal fluid model that the radial growth of χ_i is caused by toroidal effects. This has not been seen in previous kinetic models which all linearize in velocity space and it was recently pointed out that nonlinear effects in velocity space may effectively deactivate kinetic resonances,[5] thus making a fully toroidal fluid description[6,7] the most relevant one, next to the gyrokinetic simulations.

The strong influence of toroidal curvature on ion temperature gradient driven modes has been observed by several authors. In particular a regime where the density gradient scales out and only the temperature and magnetic field gradients determine stability[8-13] has been found to persist over most of the plasma region.[10] An essentially symmetric fluid version of the collisionless trapped electron mode with the same strong dependence on toroidal effects was found in Ref.6.

The radial growth of χ_i in our model is, as mentioned above, due to toroidal effects. These enter linearly by a reduction of the growthrate for large L_n/L_B and nonlinearly through pinch fluxes. An important ingredient in the model is the estimate of the saturation-level as a balance between the linear growth and the main nonlinearity. This leads to the saturation level[14,15]

$$\frac{e\phi}{T_e} = \frac{\gamma}{k_x \rho_s k_y c_s} \tag{1}$$

where k_x and k_y are to be regarded as inverse correlation lengths and γ is the main growthrate. The use of (1) in quasilinear diffusion coefficients[6,7,15] leads to

$$\chi \sim \frac{\gamma^3/k_x^2}{\omega_r^2 + \gamma^2} \tag{2}$$

where ω_r is the typical real eigenfrequency. This type of diffusion coefficient which includes a non-Markovian reduction of the transport when $\omega_r > \gamma$ was recently rederived[16] by using a memory-function in a transition probability approach. In this derivation also the nonlinear corrrection to ω_r was obtained. Since, due to toroidal effects, ω_r/γ increases with L_n/L_B also the non-Markovian effects contribute to a realistic radial profile of χ_i.

In a recent reduction[17] of the general expression for χ_i in the limit $L_n/L_B \gg 1$ a fairly simple expression was obtained

$$\chi_i = C \frac{1 - \frac{20(1-f_t)}{9\tau}\varepsilon_{Ti} - \frac{2}{3} f_t \Delta_i}{\left(\tilde{\omega}_r + \frac{5}{3\tau}\right)^2 + \tilde{\gamma}^2} \tilde{\gamma}^3 \qquad (3a)$$

where

$$C = \frac{2}{k_x \rho_s} \frac{\rho_s}{L_B} \frac{cT_e}{eB} \qquad (3b)$$

$$\Delta_i = 2\varepsilon_{Ti} \tilde{\omega}_r^{-2} \frac{1 + (5/3 - \tilde{\omega}_r)^{-1} \varepsilon_{Te}^{-1}}{(\tilde{\omega}_r - 5/3)^2} \qquad (3c)$$

and $\varepsilon_{Tj} = \frac{L_{Tj}}{L_B}$, $\tilde{\omega} = \omega/\omega_{De}$

Here the strong pinch flux in the inner region is clearly displayed (we note that $\varepsilon_{Tj} \to \infty$ towards the axis). It was also found that (3) may give $\chi_i \sim (\eta_i - \eta_{ith})^{1/2}$ as seen also in Ref.18. The pinch fluxes in our model may also lead to net pinch fluxes when the scale lengths L_n, L_{Ti} and L_{Te} become sufficiently different. The consistency of these effects with experiments has recently been demostrated[19] by the reproduction of the electron energy pinch in DIII-D[20] in our code.

References

1. P. C. Liewer, Nuclear Fusion 25, 543 (1985).
2. J. Y. Kim, W. Horton and B. Coppi, Bull. Amer. Phys. Soc. 37, 1432 (1992), Paper 3S8.
3. S. E. Parker, R. A. Santoro and W. W. Lee, Bull. Amer. Phys. Soc. 37, 1555 (1992), Paper 8E6.
4. M. J. Lebrun, T. Tajima, M. G. Gray, G. Furnish and W. Horton, Phys. Fluids B5, 752 (1993).

5. J. Weiland, Phys. Fluids B4, 1388 (1992).
6. J. Weiland, A. Jarmén and H. Nordman, Nuclear Fusion 29, 1810 (1989).
7. H. Nordman, J. Weiland and A. Jarmén, Nuclear Fusion 30, 983 (1990).
8. A. Jarmén, P. Andersson and J. Weiland, Nuclear Fusion 27, 941 (1987).
9. R. R. Dominguez and R. E. Waltz, Phys. Fluids 31,3147 (1988).
10. A. Rogister, G. Hasselberg, F. Waelbroeck and J. Weiland, Nuclear Fusion 28, 1053 (1988).
11. F. Romanelli, Phys. Fluids B1, 1018 (1989).
12. H. Biglari, P. H. Diamond and M. N. Rosenbluth, Phys. Fluids B1, 109 (1989).
13. P. K. Shukla, Phys. Fluids B2, 848 (1990).
14. W. Horton, B. G. Hong and W. M. Tang, Phys. Fluids 31, 2971 (1988).
15. J. Weiland and H. Nordman in "Theory of Fusion Plasmas", Proc. Varenna-Lausanne Int. Workshop Chexbres, Switzerland 1988.
16. A. G. Zagorodny, J. Weiland and H. Wilhelmsson, Preprint CTH-IEFT/PP-1993-07, Chalmers University of Technology, Göteborg Sweden 1993.
17. A. Heikkilä and J. Weiland, Phys. Fluids B5, July 1993.
18. S. Hamaguchi and W. Horton, Phys. Fluids B2, 1833 (1990).
19. J. Weiland and H. Nordman, Phys. Fluids B5, May 1993 (in press).
20. T. C. Luce, C. C. Petty and J. C. M. deHaas, Phys. Rev. Lett. 68, 52 (1992).

TWO-SCALE DESCRIPTION OF A TURBULENT TOKAMAK PLASMA

E. K. Maschke
Ass. EURATOM-CEA sur la Fusion, D.R.F.C.
Centre de Cadarache, Saint-Paul-lez-Durance, CEDEX (France)

Abstract

We consider plasma states, which are relatively far from a static axisymmetric equilibrium state due to applied sources.

I. INTRODUCTION

In recent analysis of tokamak confinement [1] it was found that the behaviour of local confinement (for fixed beta and collisionality) shows Bohm-like scaling, whereas most theories predict gyro-Bohm scaling. The authors conclude that this indicates the presence of long-wavelength fluctuations that scale like the machine size.

There is increasing experimental evidence that large-scale perturbations of the magnetic and electric fields are permanently present in tokamaks [2,3]. Such a situation should be considered as rather natural since the radial profiles of the physical quantities (temperature, current density etc.) are maintained by external sources (heating, current drive) whose radial distribution can often not be controlled experimentally.

Transport theory for tokamaks often proceeds by first determining growth rates from equations linearized about a given axisymmetric equilibrium, and then by calculating nonlinear saturation levels and the corresponding transport under the implicit assumption that the turbulent state is still sufficiently close to the original axisymmetric equilibrium state.

The observed presence of large-scale stationary perturbations (e.g. steady magnetic islands) leads us to consider an approach in which finite perturbations of the electromagnetic field can be taken into account. Such an approach is possible if the turbulent state of the plasma is characterized by two well-separated spatial scale lengths. Thus, we shall consider situations where the plasma shows on the one hand large-scale phenomena having low poloidal mode numbers and relatively large radial extension, and on the other hand small-scale (electric and magnetic) turbulence with poloidal and radial wave lengths of the order of the ion Larmor radius.

II. EQUATIONS FOR LARGE-SCALE PHENOMENA

In the present paper we assume that the large-scale phenomena can be described by one-fluid MHD equations. We also assume that the turbulent state is quasi-stationary (e.g. quasi-periodic). Averaging the magnetic field over time and over the toroidal angle ϕ, we obtain a time-independent axisymmetric reference field $\mathbf{B}_0$, which allows us to define an appropriate flux coordinate system r,θ,ϕ, where r labels the magnetic surfaces of $\mathbf{B}_0$. We then use a general representation of toroidal MHD in terms of scalar potentials [4]. The magnetic field and the fluid velocity are written in the following (exact) form:

$$\mathbf{B} = (\Delta U)\nabla\phi - \nabla(\partial U/\partial\phi) - \nabla\psi\times\nabla\phi\ , \qquad \mathbf{V} = V_{\parallel}\,\mathbf{B}_0/B_0 + \mathbf{V}_{\perp}$$

with $\quad \mathbf{V}_{\perp}\times\mathbf{B}_0 = \nabla\Phi_V - \nabla a \times \nabla\phi + (\Delta u)\nabla\phi - \nabla(\partial u/\partial\phi)$

Here Φ_V is essentially the electric potential, a is related to the compressibility, the quantity u is usually negligible.

As shown in ref. 4 , the MHD equations can be replaced by a completely equivalent set of evolution equations for the scalar potentials introduced above. For small inverse aspect ratio $\varepsilon << 1$, reduced MHD equations of various complexity can be used. The simplest system, which has the same ideal MHD stability limits as the full MHD equations [6], has the following form (assuming constant density for sake of simplicity).

$$\Delta_p{}^{+}\Phi_V = w \qquad \text{with } \Delta_p{}^{+} = (I^2/R^2)\nabla.(R^2/I^2)\nabla_p \text{ and } I = RB_{0,\phi}$$

$$\frac{\partial w}{\partial t} = \frac{I^2\,R_a}{rR^4}\{\frac{R^4}{I^3}w\ ,\Phi_V\} - \beta\frac{I^2\,R_a}{rR^4}\{\frac{R^2}{I}\ ,p\}$$

$$+\frac{I^3}{R^4}[\frac{\partial}{\partial\zeta}(\frac{j_\zeta}{I}) + \frac{R_a}{rI}\{\psi,\frac{j_\zeta}{R^2}\}] + \mu_\perp\Delta_p w + S_{mom}$$

$$\frac{\partial\psi}{\partial t} = \frac{R_a}{rI}\{\psi,\Phi_V\} + \frac{\partial\Phi_V}{\partial\zeta} + \eta\,\Delta_p{}^{*}\psi + E_o \ , \text{ with } \Delta_p{}^{*} = R^2\nabla.R^{-2}\nabla_p$$

$$\frac{\partial p}{\partial t} = \frac{R_a}{rI}\{p,\Phi_V\} - \nabla.\mathbf{q}_H + S_H\ , \qquad \mathbf{q} = -\kappa_\perp\nabla_\perp p\ -\kappa_{\parallel}\nabla_{\parallel} p$$

The evolution equations contain local transport coefficients, as for instance the effective heat conductivity, which have to be determined taking into account the small-scale turbulence. The latter depends strongly on the large-scale fields which we shall simplify as follows.

Let us assume the externally applied heat sources are such that some low-m magnetic islands exist in the plasma due to tearing instability. For instance, let the $m/n = 2/1$ mode be linearly unstable and saturated to a finite amplitude. This mode is localised about a magnetic surface of the reference field $\mathbf{B}_0$ where the safety factor is $q_0(r_{m,n}) = m/n$. The toroidicity leads to "satelite" islands on magnetic surfaces where $q_0 = 3$ and $q_0 = 1$ The perturbed flux function ψ can be represented as a Fourier series

$$\psi(r,\theta,\phi) = \Sigma_{\mu,\nu}\, \psi_{\mu,\nu}\,(r)\, \exp(i\mu\theta + \nu\phi)$$

Now two different situations may arise.

(i) If the above perturbed field has everywhere well-defined magnetic surfaces (for sufficiently weak perturbation), we approximate ψ near a surface where $q_0 = m/n$, by $\psi_1 = \psi_0(r) + \psi_{m,n}(r) \exp i(m\theta + n\phi)$. This field, the helicity of which varies as one moves from the neighbourhood of one of the considered rational surface to another, may the be used to calculate global confinement properties (see, e.g., ref. 5) . In addition, one may calculate particle trajectories and micro-instabilities locally in the field ψ_1 , assuming a Maxwellian particle distribution function depending on space through ψ_1. This problem ressembles that of a stellarator possessing good magnetic surfaces. The lack of symmetry of the field ψ_1 may lead to stochasticity of the particle trajectories and thus to enhanced transport.

(ii) If the above perturbed field has regions where the field lines have stochastic behaviour (e.g. near the separatrix of a magnetic island), strong modifications of the local heat and particle transport occur and will react on the large-scale perturbations. A problem of self-consistency arises, which requires numerical calculations. Also, the problem of micro-turbulence must be formulated to take into account the new structure of the magnetic field.

III. SMALL-SCALE PHENOMENA

The various transport coefficients occurring in the above macroscopic equations depend strongly on the small-scale turbulence, the theory of which is still incomplete. Here we discuss only some general aspects which will guide future numerical studies.

Among the transport coefficients, the resistivity in the presence of magnetic turbulence has recently been studied [7], and it was

found that for tokamak conditions it may change by a factor of 2 or 3 compared to neo-classical values. Such a change will probably not give rise to strong modifications of the macroscopic behavior, so that it should be sufficient to use the neo-classical resistivity in the MHD equations ($\eta \approx \eta_{nc}$).

The viscosity tensor has been extremely simplified in the above MHD equations. The effects of viscosity on the velocity fields may be significant, but the general structure of the magnetic field is probably not strongly modified by more realistic descriptions of the viscosity.

The heat transport coefficients are strongly modified in regions where the magnetic field is stochastic. For the case of time-independent magnetic perturbations, the magnetic diffusion regime of Rechester and Rosenbluth leads to $\kappa_{eff} >> \kappa_{\perp}$ (see ref. 8). The corresponding enhanced thermal transport will be essential for the macroscopic behaviour.

CONCLUSION

In our approach, we consider that the state of the plasma is determined by the external sources, which may drive the system relatively far from a static axisymmetric equilibrium. Assuming that the resulting turbulent state is characterized by two well separated wave-length scales, we have sketched a theoretical procedure which uses this feature systematically. A more detailed account and numerical applications will be given elsewhere.

References

[1] Perkins, F.W., et al. , Phys.Fluids B **5** (1993) 477, and references quoted in that paper.

[2] Drawin, H.W. and M.A.Dubois, Nucl. Fusion 32 (1992) 1615.

[3] Nave, M.F.F., et al., Nucl. Fusion 32 (1992) , 825.

[4] Maschke, E.K. and J. Morros Tosas, Plasma Phys. Contr. Fusion 31 (1989) 563 and 549.

[5] Hegna, C.C. and J.D.Callen, Phys.Fluids B4 (1992), 4072.

[6] Maschke, E.K. and J. Morros Tosas, to be published.

[7] Colas, L. and G.Giruzzi, Nucl. Fusion 33 (1993), 156.

[8] Isichenko, M.B., Plasma Phys. Contr. Fusion 33 (1991) 795.

PLASMA TRANSPORT IN TOKAMAKS

E. Minardi

Istituto di Fisica del Plasma, Associazione EUR-ENEA-CNR,
Via Bassini 15, Milano, Italy.

1- Introduction

To any macroscopic magnetic or electrostatic plasma equilibrium (a static solution of the Vlasov equation) characterized by a known inhomogeneous distribution of the current density or of the charge density (with given boundary and geometrical conditions) one can associate a functional of these quantities with the properties of entropy, as are conventionally defined in the classical thermodynamics of the macroscopic systems /1/. The existence of this functional provides the basis for the thermodynamics of the Vlasov equilibria, in general non-maxwellian and non-uniform. A significant insight into the physical meaning of the functional and of its variations is gained from its relationship to the variation of the action and to the Hamilton principle in the lagrangian description of the motion of the underlying system of particles /1/.

When the system can be considered as isolated, as is the system constituted by the plasma and a perfectly conducting current-carrying shell enclosing it, the most probable state should correspond to the maximum of the entropy. In contrast, the magnetic configuration of an open system, as is the case of a tokamak subject to ohmic and auxiliary heating, cannot be described by the maximum of entropy. Nevertheless, we can investigate the constraints imposed on a stationary magnetic configuration introducing the condition that the time derivative of the magnetic entropy (called entropy production in the present context) vanishes. Although this condition can be violated in practice, it could constitute a useful reference in making comparisons with the experiments.

2- Isoentropic states and magnetic stochasticity

The entropy production is given, in the case of the tokamak, by the following relation (Minardi and Lampis, 1990)

$$\frac{dS}{dt} = \frac{1}{\tau}\int\left(\frac{\vec{E}}{\mu^2}\,\Delta\vec{j} + \vec{E}\vec{j} + p_A\right)dV \qquad (1)$$

where τ is a (negative) generalised temperature, $\vec{E}$ is the axial inductive electric field, p_A is the auxiliary power density, $\vec{j}(r)$ is the axial current density and μ is a free parameter, related to the arbitrariness of the gauge (see /1/) which will be determined later, according to a specific equilibrium. We shall call "isoentropic" a state of the tokamak where magnetic entropy is not produced in the confinement zone. A family of isoentropic states, labelled by μ, is given in cylindrical geometry, by the solutions of the equation

$$\Delta j + \mu^2 j = -\mu^2\,\frac{p_A}{E} \qquad (s\lambda \le r \le s) \qquad (2)$$

with the boundary conditions $j(s) = j_s$ and $j(\lambda s)=\hat{j}$. Here $r=s\lambda$ and $r=s$ are the boundaries of the confinement zone defined by the following conditions on the safety factor $q(r)$:

$$\hat{q} \equiv q(\lambda s) = \frac{\lambda s B}{R B_\theta(\lambda s)} = 1, \quad q_s \equiv q(s) = \frac{sB}{RB_\theta(s)} \sim 2 \tag{3}$$

In the following we shall neglect Ej with respect to p_A, assuming intense auxiliary heating. Also we shall take a one-fluid approximation of the power balance and consider that the $j(r)$ profile is ohmically relaxed with $j(r) \propto ET^{3/2}(r)/A(Z)$ where $A(Z)$ is related to the Spitzer resistivity (Z uniform). Assuming provisionally that p_A is uniform, the comparison between the power balance $d(rq_e)dr = p_A r$ and the isoentropic condition (2) gives

$$n\chi_e = -\frac{q_e}{T'} = \frac{Er\Delta j}{2\mu^2 T'} = F\hat{T}^m\left(\frac{T(r)}{\hat{T}}\right)^{1/2}, \quad \mu^2 \equiv \frac{3E^2}{2F\hat{T}A(Z)} \tag{4}$$

where $\hat{T}$ is uniform (e.g. $\hat{T}=T(0)$) and m is arbitrary (only m=3/2 will be considered).

Let us compare χ_e with the form of χ_e following from marginally stochastic /2/ or fully stochastic /3/ magnetic fluctuations

$$\chi_e \approx v_e \frac{w^3 k}{qR}, \qquad \chi_e \approx qRv_e \Sigma b^2 \tag{5}$$

where v_e is the thermal velocity, w is the islands width, k the wave number of the island structure and the summation is performed over resonant modes. The two forms scale equivalently in the limit kw~1 of strong magnetic island pumping /2/.

Under conditions of marginal stochasticity we can presume that the magnetic fluctuations in different parts across a partially ergodic region are partially connected, irrespective of plasma gradients. That is, the magnetic fluctuations, particularly under the conditions of self-organization considered by Kadomtsev /2/, do not depend exclusively on local plasma conditions, but are subject, through space interconnection, to the global physical conditions in the whole partially ergodic region. Thus it seems reasonable to assume that the island width is sensitive in leading approximation more to the average values of the plasma parameters across this region, than to their local values. For instance, let us suppose that the magnetic stochasticity diffuses into the region q>1 from the mixing surface q=1, considered to be the source of permanent seeding of the braiding magnetic field. If the coefficient of the anomalous magnetic diffusion is sufficiently large with respect to the thermal diffusivity, the gradient of the fluctuation amplitude may be lower than the thermal gradient (uniform magnetic braiding).

The electrons, in contrast to the lines of force, are pointlike localizable entities (classically) whose thermal velocity can only depend on the local temperature. In this picture the space dependence of χ_e should mainly occur through $v_e \sim T(r)^{1/2}$ rather than through the magnetic fluctuations b^2. Now this behaviour is just the same as that of the expression (4) of the diffusivity (considering n as uniform). Thus the assumption above should be considered as an idealization which corresponds to the isoentropic state.

3- Inhomogeneous Power Deposition

In the case of p_A uniform, the expression

$$n\chi_e = -\frac{q_e}{T'} = \frac{1}{2}F\hat{T}T^{1/2}\left(1 + \frac{rT'}{2T} + \frac{rT''}{T'}\right) \qquad (6)$$

is equivalent to (4) (with m=3/2). We retain this form also in the case of inhomogeneous p_A. In accordance with the assumption above on χ_e, eq. (6) can be split into two separate conditions

$$\chi_e(r) = \frac{1}{n_o}F\hat{T}T^{1/2}(r) \quad , \quad n = \frac{n_o}{2}\left(1 + \frac{rT'}{2T} + \frac{rT''}{T'}\right) \qquad (7)$$

Since Δj is still related to q_e by (4), the expression (1) gives

$$\frac{dS}{dt} = \frac{1}{\tau}\int (p_A(r) - \bar{p}(r))dV \qquad (8)$$

where $\bar{p} = \left(2\int^{r} p_A r\, dr\right) / r^2$. The time dependence of the entropy is then a consequence of the inhomogeneity of the power deposition. The density profile now depends on the temperature profile through (7). When only terms linear in T' are retained, this expression is somewhat related to that analysed by Becker in Asdex /4/. Clearly an additional (convective) term is needed in the equation of the particle transport in order to be consistent with (7).

4- Profile Resiliency

We consider a simple case of inhomogeneous power deposition where $p_A(r)$ is concentrated in a region $0 \leq r \leq c$ with c lower than the mixing radius λs. Inserting q_e given by (4) in the power balance equation and integrating, one obtains

$$j(r) = j_s - \hat{j}\frac{\gamma}{2}\left(\ln\frac{r}{s}\right)^2 + \ln\left(\frac{r}{s}\right)\frac{\hat{j}}{\ln\lambda}\left[1 - \frac{j_s}{\hat{j}} + \frac{\gamma}{2}(\ln\lambda)^2\right] \qquad (9)$$

where $\hat{j} = j(s\lambda) = cB / 2\pi R$, $j(s) = j_s$ and γ is related to μ^2 and p_A as follows

$$\gamma = \frac{2\mu^2}{E\hat{j}}\int_0^c p_A r dr \qquad (10)$$

We can now proceed to the integration of the equation for the poloidal field $d(rB_\theta)/dr = 4\pi rj/c$ with the two boundary conditions (3). Since only one integration constant is available we obtain a relation between the parameters of the discharge. This relation, denoted by $L(\lambda, q_s, j_s / \hat{j}, \gamma) = 0$, does not depend on μ and on p_A. When the value or the form of $p_A(r)$ changes, the variation can be taken up by a change of μ^2 with γ fixed, according to the relation (10). Thus the current density profile, characterized by $\gamma, \lambda, q_s, j_s / \hat{j}$ and by L=0, remains invariant when p_A varies. The condition L=0 is the mathematical expression of the profile resiliency. Note however that this condition does not exist when one of the two conditions (3) is relaxed, e.g. when q>1, as could be the case in the absence of sawteeth.

The profiles of the current density are typically triangular (or trapezoidal, depending on the value of λ) or slightly concave in the interior of the confinement region. They do not differ essentially from those predicted in the homogeneous case /1/. The density profiles are concave and tend to be flat.

5- Scaling of the Confinement Time and Isoentropic Condition

The same mathematical structure as above persists when the second term of eq.(2), which corresponds to the ohmic heating Ej, is retained. We combine the isoentropic condition $L=L(\lambda, q_s, j_s/\hat{j}, \mu s, p_A/E\hat{j}) = 0$ with the Kadomtsev scaling of χ_e for high power magnetic island pumping (kw~1). For $2<P_A/P_\Omega<10$ (P_A and P_Ω are the auxiliary and ohmic power respectively, in the region $r\leq s$) the isoentropic condition implies a dependence $P_A^{-0.50}$ of the confinement time τ. Assuming uniform braiding we have

$$\left(\frac{w}{a}\right)^2 \propto \frac{qa}{R}\frac{\bar{n}\bar{T}}{\overline{B_\theta^2}}\left(\frac{m_e}{m_i}\right)^{1/2} \quad \text{with} \quad \overline{B_\theta^2}(s) = \frac{2}{s^2}\int_0^s B_\theta^2(r)rdr = \ell_i B_\theta^2(s) = \frac{4\ell_i I^2(s)}{c^2 s^2} \qquad (11)$$

This leads to the following scaling of the confinement time

$$\tau \propto P_A^{-0.50}\ \bar{n}^{0.125}\ I^{0.875}\ \ell_i^{0.432}\ R^{1.50}\ m_i^{0.22}\ a^{-0.312}\ B^{-0.125}\ Z^{0.06} \qquad (2 < P_A/P_\Omega < 10) \qquad (12)$$

The dependence with respect to P_A, n, I, compares very well with that of ITER89-P /5/ which is $\tau \propto P_A^{-0.50}\ n^{0.1}\ I^{0.85}$. In the case $P_A/P_\Omega>10$ one obtains $\tau \propto P_A^{-0.60}\ n^{0.20}\ I^{0.80}$ which is less precise with respect to ITER89-P than the scaling (12).

We conclude by observing that, once the scaling of χ_e is known, a scaling of the confinement time follows on purely dimensional grounds without solving explicitly the power balance equation, apparently without the need of isoentropic ideas. But it can be seen immediately that this procedure assumes implicitly the invariance of the profile (and implies also constraints on the boundary conditions) under the change of the quantities occurring in the scaling law. Now it is precisely in the frame of an additional constraint as above that the scaling law acquires its validity and it is just the constraint that needs to be explained. It is at this point that the isoentropic condition plays its role, so that, in the context of this condition, the scaling law acquires the status of a "state law".

References

/1/ E. Minardi (1992) J. Plasma Phys. 48, 281, 309.
/2/ V.B. Kadomtsev (1991) Nucl. Fusion 31, 130.
/3/ A.B. Rechester and M.N. Rosenbluth (1978) Phys. Rev. Lett. 40, 38.
/4/ G. Becker (1987) Nucl. Fusion 27, 11.
/5/ Y.N. Yushmanov et al. (1990) Nucl. Fusion 30, 1999.

THE RADIAL CORRELATION LENGTH OF ELECTROSTATIC TURBULENCE

F. Romanelli, F. Zonca,

Associazione EURATOM-ENEA sulla Fusione
C.R.E. Frascati, C.P. 65,00044, Frascati, Roma, Italy

The most important discrepancy between mixing-length estimates of the anomalous thermal conductivity and experimental values is in the radial dependence. This can be traced back to the estimate given for the radial correlation length L_r of the turbulence, which is assumed to scale as the ion Larmor radius and therefore monotonically decreases toward the edge. In this paper the radial correlation length of electrostatic turbulence is estimated both for moderate to high magnetic shear values ($s=rq'/q$, with q the safety factor), which characterize the outer part of a discharge, as well as for low s values, typical of the region around the magnetic axis.

In a two dimensional system the electrostatic potential Φ can be expressed as a superposition of different poloidal harmonics, $\Phi=\Sigma_p\Phi_p(x)\exp[i((m_o+p)\theta+n\zeta-\omega t)]$ where n is the toroidal mode number, $\zeta(\theta)$ the toroidal (poloidal) angle, ω the mode frequency and $x=r-r_o$ the radial variable, with r_o being a reference radius and m_o being defined by $q(r_o)= m_o/n$. Within the context of the ballooning mode representation[1] it is assumed that neighboring poloidal harmonics Φ_p have similar shape, simply shifted by an amount $1/nq'$ which corresponds to the distance between neighboring rational surfaces. The global mode structure is given by a superposition of harmonics with similar shape and modulated by a slowly varying envelope function A(x), defined by $\Phi_p(x)=A(x)\Phi_o(x-p/nq')$. The radial extent of A(x) determines the effective range of toroidicity-induced coupling between different harmonics. An eikonal representation is usually employed for A(x) $[A(x)=\exp(i\int dx'nq'\theta_k(x'))]$. The solution of the global eigenmode problem is thus accomplished in two steps. At the lowest order, the determination of the eigenmode structure along the magnetic field lines of the usual ballooning formalism corresponds to deriving an expression for the shape function Φ_o. At the next order the envelope A(x) and the global eigenvalue are obtained. This fact allows us to construct the global structure as a superposition of local solutions.

It is convenient to illustrate such a procedure by considering the quasineutrality equation in the fluid approximation. Defining the Fourier transform of the function Φ_o as $\Phi_o(x)=\int d\theta\ \phi_o(\theta)\exp(-in\theta q'x)$, the following differential equation is obtained

$$\frac{\omega_{ti}^2\partial^2\phi_o}{\omega^2\ \partial\theta^2}+\left[\frac{1/\tau}{1-\frac{\omega^*T_i}{\omega}}+(k_\theta\rho_i)^2(1+s^2(\theta-\theta_k)^2)-\frac{\omega_D}{\omega}(\cos\theta+s(\theta-\theta_k)\sin\theta)\right]\phi_o=0 \qquad (1)$$

with $\omega_D=-2ck_\theta T_i/(eBR)$, $\omega^*_{Ti}=-ck_\theta T_i/(eBL_T)$, $L_T^{-1}=-d\ \ln\ T_i/dr$, $\tau=T_e/T_i$, $\omega_{ti}=v_{ti}/qR$, B being the equilibrium magnetic field, R the major radius, $v_{ti}=(T_i/m_i)^{1/2}$ the thermal velocity and $\rho_i=v_{ti}/\Omega_i$ the ion Larmor radius. The usual low-β equilibrium with circular magnetic surfaces is employed here.

With the boundary condition of exponentially vanishing solution for $|\theta| \to \infty$, Eq.(1) determines a one dimensional eigenvalue problem, leading to a local dispersion relation of the form

$$F(\omega, x, \theta_k)\, A(x) = 0 \quad . \tag{2}$$

The derivation of Eq.(2) is the final result which may be obtained from the usual ballooning mode formalism at the lowest order. At next order we need to solve the pseudo-differential problem obtained from Eq.(2) with the substitution $\theta_k = -i(1/nq')\partial/\partial x$. With the explicit form of $F(\omega, x, \theta_k)$ it is possible to find an approximate solution for $A(x)$ by using the standard WKBJ theory [2]. Far from the turning points it is possible to employ the eikonal representation for the envelope function. The turning points $\theta_k = \theta_T$ are defined by the condition[2] $(\partial F/\partial \theta_k)=0$. The radial position x_T of the turning point is obtained by substituting the value found for θ_T into the local dispersion relation, Eq.(2). Close to the turning points the pseudodifferential equation can be solved analytically by expanding the function F around θ_k and x_T. After solving around the turning points, connection formulae are obtained to match the eikonal solutions of Eq.(2). A global solution can be constructed following standard WKBJ theory. Imposing the boundary condition $|A| \to 0$ as $|x| \to \infty$, such a procedure yields the following global dispersion relation[2]

$$\int_0^{\theta_T} d\theta_k\; nq'\, x(\theta_k) = \pi\, [\, l + \beta] \tag{3}$$

with $x(\theta_k)$ being determined from Eq.(2), l being an integer and β a numerical constant which depends on the topology of the phase space trajectories. To be specific, $\beta = 1/2$ for the case of closed trajectories and $\beta = 0$ for the case of open trajectories.

We now apply the above formalism to the solution of Eqs.(1)-(3) for $s \geq 1$ and $s<1$ respectively. The poloidal wavelength will be ordered in both cases as $k_\theta \rho_i \approx \varepsilon_T^{1/4}$, with $\varepsilon_T = L_T/R$. It is convenient to begin the discussion from the moderate shear limit[3]. In this case the eigenfunction has a moderate ballooning structure which can be determined within the strong coupling approximation. The associated ordering corresponds to balancing parallel ion compressibility, curvature, inertia and adiabatic electron response on the connection length scale $\theta \approx 1$, yielding

$$F = \frac{\omega_D}{2\omega}\left[\frac{2\omega^2}{\tau\omega_{*Ti}\omega_D}\left(1+\frac{\omega}{\omega_{*Ti}}\right) + i\frac{s}{q} + 2\cos\theta_k\right] = 0 \tag{4}$$

Equation(4), which is valid up to $O(\varepsilon_T^{1/2})$, can be solved by making a Taylor expansion around $r=r_o$ and keeping the linear terms in $r-r_o$. Such an approximation is valid if the term $\partial F/\partial r$ does not vanish in the region of interest and the eigenfunction is sufficiently localized around $r=r_o$. The turning points are located at $\theta_k = 0, \pi$. From Eq.(3), the resulting dispersion relation for the l=0 eigenvalue is

$$\frac{2\omega^2}{\tau\omega_{*Tio}\omega_{Do}}\left(1+\frac{\omega}{\omega_{*Tio}}\right) + i\frac{s(r_o)}{q(r_o)} = 0 \tag{5}$$

The eigenvalue is given by $\omega \approx (-i\tau\omega_{*Tio}\omega_{Do}s(r_o)/2q(r_o))^{1/2}$, where the subscript o means that each quantity has been evaluated at $r=r_o$. The radial correlation length L_r can be estimated as the distance between the turning points,yielding $L_r = 2\,\mathrm{Re}(x_T)$ with

$$\mathrm{Re}(x_T) \approx 2^{1/2}\left(\frac{q}{s}\right)^{1/2}(\tau\varepsilon_T)^{1/2}\frac{d\ln[q(r)T_i'/r]/dr}{\{d\ln[s\,q\,T_eT'_i/r^2]/dr\}^2} \propto a_p\,\varepsilon_T^{1/2}\left(\frac{q}{s}\right)^{1/2} \qquad (6)$$

with a_p being the minor radius. The resulting L_r is much larger than the ρ_i and scales as the macroscopic dimention of the device. Note also that the shear dependence is algebraic $x_T \approx s^{-1/2}$.

In the low shear limit ($s \ll 1$), the eigenfunction becomes broad and the strong coupling approximation can no longer be applied. In this case, two branches exist, a toroidal and slablike branch[4]. The eigenfunctions belonging to the toroidal branch exhibit a fast variation, along the equilibrium field, over the connection length scale with a superimposed slow variation over a secular scale. The other branch, which exists also in slab geometry, is characterized by a variation along the equilibrium magnetic field dominated by the secular scale, with superimposed small oscillations on the connection length scale. The optimal ordering for the toroidal eigenmodes, as given in Ref.[4], is obtained by balancing parallel compressibility and adiabatic electron response on the scale $\theta \approx 1$, yielding $\omega \approx (\tau\omega_{*pi}\omega_{ti}^2)^{1/3}$. For the case of the slablike branch the ordering is obtained by balancing inertia, parallel compressibility, and adiabatic electron response on the secular scale rather than on the connection length scale, yielding $\omega \approx (\tau\omega_{*pi}k_\theta\rho_i\omega_{ti})^{1/2}$. In order to determine the radial mode width, the explicit form of the local dispersion function must be found. This, however, is not straigthforward as in the moderate shear limit, because a regular perturbation theory fails to give any θ_k dependence of the dispersion relation at all the orders in s. The reason is that the toroidal coupling tends to vanish faster than any power in s, since each poloidal harmonic tends to become localized with respect to the distance between mode rational surfaces. Thus it is convenient to solve Eq.(1) using a variational method. To this aim a quadratic functional can be obtained by multiplying Eq.(1) by ϕ_o and integrating between $+\infty$ and $-\infty$. Appropriate trial functions can be obtained from approximate solutions of Eq.(1) using asymptotic techniques. Starting from the toroidal branch and considering, for the sake of simplicity, only the case of modes propagating in the ion diamagnetic direction, the following local dispersion relation is obtained

$$F = -\frac{\omega^3}{2\tau\omega_{*Ti}\omega_{ti}^2} - \frac{1}{8} - \frac{3}{8}e^{1/2\varepsilon}\cos\theta_k = 0 \qquad (7)$$

with $\varepsilon = -s\omega\omega_D/\omega_{ti}^2$ evaluated at $r=r_o$. The eigenvalue is given by $\omega \approx (-\tau\omega_{*Tio}\omega_{tio}^2/4)^{1/3}e^{2i\pi/3}$. The radial variation of the function F is associated to the first term of the r.h.s.. If no point exists at which $\partial F/\partial r = 0$, it is possible to expand around a generic point $r=r_o$, keeping only the linear term. The mode is localized between the turning points at $r_o \pm x_T$ with $x_T \approx 3L_1/8e^{1/2\varepsilon}$ and $1/L_1 = -(\partial/\partial r)[\omega^3/(2\tau\omega_{*Ti}\omega_{ti}^2)]$. The most important difference with respect to the moderate shear case, is the appearance of the exponential factor. Such a term is a measure of the toroidal coupling strength between different harmonics. As a result, the radial eigenmode width (and therefore the radial correlation length

$L_r \approx 2Re(x_T)$) decreases exponentially as exp(-c/(qs)), with $c \propto \varepsilon_T^{1/3}(k_\theta \rho_i)^{-4/3}(q\tau)^{-1/3}$ being of order unity for $k_\theta \rho_i \approx (\varepsilon_T/q\tau)^{1/4}$. Such a fast dependence cannot be recovered by a regular perturbation expansion, because the dependence on the parameter ε is not analytic for $\varepsilon=0$. For the slablike branch the following dispersion relation is obtained which generalizes that of Ref.[4]

$$F = 1 + i\frac{\omega^2}{\tau\omega_{*Ti}\omega_{ti}k_\theta\rho_i s(1+2q^2)^{1/2}} + \left(\frac{\varepsilon^3}{512\, s\, \sigma^4} - \frac{\varepsilon}{4\sigma^2}\right) e^{-1/8\sigma} \cos\theta_k = 0 \qquad (8)$$

with $2\sigma = -i(\omega/\omega_{ti})k_\theta\rho_i s(1+2q^2)^{1/2}$. Note that the function F has a minimum located at $r=r_0$. Upon expanding around r_0 and defining the length L_0 by $1/L_0^2 = d^2/dr^2[-i\omega^2/\tau\omega_{*Ti}\omega_{ti}k_\theta\rho_i s(1+2q^2)^{1/2})]$, the eigenvalue tuns out to be $\omega \approx e^{i\pi/4}[\tau\omega_{*Ti}\omega_{ti}k_\theta\rho_i s(1+2q^2)^{1/2})]^{1/2}$, and the mode is localized between $r_0 \pm x_T$ with $x_T = (2\varepsilon)^{1/4}(L_0/nq'\sigma)^{1/2}|(1-\varepsilon^2/128\sigma^2 s)^{1/4} e^{-1/32\sigma}$. Again the radial correlation length $L_r \approx 2Re(x_T)$ decreases exponentially as $s \to 0$.

If the radial correlation length becomes smaller than the distance between mode rational surfaces there is no longer any coupling between different poloidal harmonics. Such a transition occurs at $nq'x_T \approx 1$. Since the radial dependence of x_T comes mainly from the exponential factor, the latter condition can be written as

$$rq' = \alpha \frac{\varepsilon_T^{1/3}}{(k_\theta\rho_i)^{4/3}(q\tau)^{1/3}} \qquad (9)$$

with α being a numerical factor of order unity and $k_\theta \rho_i \approx (\varepsilon_T/q\tau)^{1/4}$.

In conclusion, the shear dependence of the radial correlation length L_r is very different in the case s=O(1) and s<<1. For moderate shear values the radial correlation length is comparable with the equilibrium scale length and has an inverse algebraic dependence on s, $L_r \approx (q/s)^{1/2}$. For low shear values the radial correlation length decreases as exp(-c/(qs)), with c being of order unity. On applying a mixing length estimate the above results predict a strong reduction of transport for s<1 and, in particular, close to the magnetic axis. This is in agreement with several experimental findings which seem to indicate very low level of transport near the plasma center [5] or when sawtooth activity is stabilized using RF current drive [6].

References

[1]J.W. Connor, R.J. Hastie, and J.B. Taylor, Proc. Roy. Soc. London Ser. A 365, 1 (1979)

[2]F. Zonca Ph.D. Thesis, Princeton University (January,1993); F.Zonca and Liu Chen International Sherwood Fusion Theory Conference Santa Fe, N.M., (April, 1992)

[3] F. Romanelli, Phys. Fluids B 1, 1018 (1989)

[4] Liu Chen, S. Briguglio and F. Romanelli, Phys. Fluids B 3, 611 (1991)

[5] D. Pasini, R. Giannella, L. Lauro-Taroni, G.Magyar, M. Mattioli Proc. 1992 International Conference in Plasma Physics Vol.I, p.283

[6] G.V. Pereverzev, F.X. Soldner, R. Bartiromo, F. Leuterer, V.V. Parail Nucl.Fusion 32, 1023 (1992)

GENERALIZED ESCAPE–PROBABILITY METHOD IN THE THEORY OF NONLOCAL TRANSPORT BY ELECTROMAGNETIC WAVES. APPLICATION TO GLOBAL HEAT TRANSPORT IN A TOKAMAK

A.B.Kukushkin
RRC "Kurchatov Institute", 123182 Moscow Russia

1.**Introduction**. Heat transport by electromagnetic (EM) waves, both transverse (i.e. photons) and longitudinal waves (i.e. plasmons), in the wide range of parameters (which includes, in particular, magnetically confined thermonuclear plasmas) is characterized by its nonlocal (non–diffusion) nature which manifests itself in nonlocal correlation of plasma temperatures and, correspondingly, non–diffusion law of heat propagation. Mathematically, the non–diffusion behaviour is expressed by the fact that the original equation for heat transfer which is, in general, an integral equation in space variables, cannot always be reduced to a differential diffusion–type equation in those variables. Such a reduction leads to an infinite diffusion coefficient in case of unbounded media or medium–size–dependent diffusion coefficient in case of bounded media, so that the very concept of diffusion coefficient appears to be meaningless.

The phenomenon of nonlocal, non–diffusion transport has been revealed and thoroughly investigated in the theory of radiative transfer in resonance atomic lines (RTRAL) in the late forties and early fifties in the pioneer works by Biberman, Holstein and Sobolev (BHS). Further advances of their analytic approaches are known in literature as "escape probability method". (see, e.g., [1]).

Extension of the BHS-approach to emission/absorption by plasma electrons gives universal formulae for total power losses by a bounded media due to emission of electromagnetic (both transverse and longitudinal) waves in the regimes of nonlocal (non–diffusion) heat transport, which, in particular, generalize Trubnikov's formula for synchrotron losses to the case of arbitrary emission/absorption process and inhomogeneous non–stationary plasma. The results suggest a qualitative model for the global heat transport in a tokamak.

2.**Generalized escape–probability method and universal formula for total energy losses**. Let us consider the transfer of EM energy which is described by equation

$$\left(\frac{1}{v_g}\frac{\partial}{\partial t}+\vec{n}_g\frac{\partial}{\partial \vec{r}}\right)\left(\frac{J(\phi,\vec{r},t)}{(N_r)^2}\right)=-\kappa\left(\frac{J(\phi,\vec{r},t)}{(N_r)^2}\right)+\frac{Q}{(N_r)^2}, \qquad (1)$$

for the intensity $J(\phi,\vec{r},t)$, where $\phi\equiv\{\omega,\vec{n},\zeta\}$, ω, $\vec{k}$ and ζ are EM frequency, wave vector and polarization, respectively, $\vec{n}\equiv\vec{k}/k$. Here $\kappa(\phi,\vec{r},t)$ is absorption coefficient, $Q(\phi,\vec{r},t)$

is the source function, N_r is ray refractive index, v_g and $\vec{n}_g$ are the group velocity a .d its direction. In a medium with dispersion the substitution of the dependence $k = k(\omega, \vec{n}, \zeta)$ from the dispersion relation is implied.

In case of radiative transfer by emission/absorption of EM waves by plasma electrons, the quantities Q and κ contain averaging over electron velocity distribution (EVD). Therefore the source function Q may implicitly depend on the intensity J via corresponding distortions of the EVD, caused by radiative transfer. If these distortions are small then Q doesn't depend on J, and eq.(1) appears to be a closed equation for energy carriers. The multiple reflection at the medium boundary (e.g., tokamak wall) prevents from straightforward use of the analytic solution of eq.(1) in the form of the integral over ray path.

Another example of the reduction of transport problem to a closed equation is the Biberman–Holstein equation for accumulators of energy, namely excited atoms, in the theory of the RTRAL for complete redistribution in photon frequencies (see, e.g., [2]).

In both above–mentioned cases the energy transport appears to be characterized by the following general features.

(*) The dominant contribution to energy loss stems from those long–free–path energy carriers (photons or plasmons) whose long flights are of medium's size L_0 in length ,or greater, $L_0/(1-R)$, for the case of reflection at boundaries, R is reflection coefficient (for the RTRAL, these are the photons in line wings).

(**) Each of the variables of the total phase space $\{\Gamma\} \equiv \{\phi, \vec{r}\}$ manifests one of two limiting forms of its evolution ("redistribution") along the trajectory of energy carrier from its birth to its death (by convertion into medium's heat); either no redistribution ("independent" variables) in which case for each value of thisvariable the energy transport takes place independently (e.g., ω, for absorption/emission by free electrons with fixed velocity distribution, and $\vec{r}$, for the RTRAL) or complete redistribution in which case for each of those variables the transport equation may be properly averaged.

The whole set of first-type variables we shall denote as Γ_{ind} and the second-type, Γ_{crd}.

The properties (*) and (**) enable us to obtain finally the following general result for total power losses:

$$\frac{dE}{dt} = \int d\Gamma_{ind}\ (1 + \nu_{que}/\nu_{esc})^{-1} \int d\Gamma_{crd}\ Q(\Gamma)\ , \qquad (2)$$

Here, ν_{que} is the rate of such an absorption of EM energy by the medium, which converts transported EM energy into medium's heat (temperature), (this is the quenching of atom excitation by, e.g., medium particle's impact for the RTRAL, and the absorption of the photon(plasmon) by plasma electrons for the radiative transfer in continuous spectrum), and ν_{esc} is the rate of free escape of EM energy out of the medium. Both quantities ν_{que} and ν_{esc} are averaged over Γ_{crd}.

For the RTRAL, we have $\Gamma_{ind}=\vec{r}$ and $\nu_{esc} =< T(\vec{r}) > /t_{rad}$, where $< T(\vec{r}) >$ is Holstein function averaged over the angles of photon escape, t_{rad} is radiative lifetime of excited atom, and we thus arrive at the well-known result of the RTRAL theory. Therefore formula (2) may be interpreted as a generalization of escape–probability methods to the case of

heat transport via emission/absorption of (transverse and longitudinal) EM waves by fr.. electrons with fixed velocity distribution.

Note that formula (2) covers both limiting regimes of energy loss, volumetric ($\nu_{que} \ll \nu_{esc}$) and surface loss ($\nu_{que} \gg \nu_{esc}$). In the latter case, the intensity of escaped EM field is close to the equilibrium Planck distribution with some effective, space–averaged temperature, the heat transport inside the medium being characterized in corresponding domain of phase space by diffusion–type regime of radiative thermoconduction. Nevertheless,the total losses in eq.(2) are determined dominantly by those part of the total phase space Γ in which the process of energy transport has essentially nonlocal character, namely the non–diffusion regime of free escape. The latter statement just constitutes the essence of a "generalized escape–probability"(GEP) method which enables us to obtain eq.(2) within the framework of principles (*) and (**).

3. Heat transport by plasma waves. Contrary to the RTRAL theory, nonlocal character of the transport by plasma longitudinal waves and its possible role have been realized much later starting from the paper by Rosenbluth and Liu [3]. For the transport by transverse waves (i.e. electron cyclotron radiation) in inhomogeneous plasma, the concept of non-diffusion transport has been fruitfully exploited by Tamor [4].

The straightforward analogy between heat transport by plasma waves and the RTRAL was traced in [5] where the non-diffusion law of heat propagation by Bernstein modes was also obtained (approximately $t \propto r$ contrary to the standard diffusion law $t \propto r^2$).

The existing analytic descriptions have the character of the fit of numerical results and pertain to (a) specific mechanism of emission, namely cyclotron radiation, and (b) specific profiles of temperature and density: homogeneous, the well-known Trubnikov's formula [6], or tokamak-like, formula [7]. The required analytic description may be obtained from our general result (2) for a specific case of tokamak geometry under following, usually satisfied conditions, namely not too large aspect ratio, non–circular (in particular, elongated) cross–section and multiple reflection at plasma boundaries (e.g., for transverse waves the latter is assured by highly reflecting tokamak walls, $(1 - R) \lesssim 0.1$). Neglecting the mixing of different modes in reflections at the boundaries, we have $\Gamma_{ind} = \{\omega, \zeta\}$ and eq.(2) reduces to the form:

$$\frac{dE}{dt} = \sum_{\zeta} \int d\omega \, \frac{\int dV \int d\Omega_n \; Q(\phi, \vec{r})}{1 + \tau_{eff}} \, , \tau_{eff} = \frac{\int dV \;\; \int d\Omega_n \; \kappa(\phi, \vec{r})}{\int d\Omega_n \;\; \int (\vec{n}, d\vec{S}_s) \; (1 - R(\phi, S_s))} , \qquad (3)$$

where $\tau_{ef}(\omega, \zeta) = \nu_{que}/\nu_{esc}$ is the effective (dimensionless) optical length which describes the trapping of plasmons/photons. Here V and S_s are plasma volume and surface, respectively, and $R(\phi, S_s)$ describes the dependence of reflection coefficient on wave parameters (first of all, frequency). The comparison of formula (3) with the results of numerical calculations [4,6] and formulae [6,7] shows good agreement in the regions of applicability of these results. The GEP method allows also to obtain a universal analytic description for spatial profile of wave energy balance and for arbitrary degree of mixing of different waves at plasma boundaries, for both stationary and non–stationary cases.

4. **On the global heat transport in a tokamak.** The application of the GE concept to global heat transport in a tokamak, within the general framework of non-diffusion transport by longitudinal waves [3,5], suggests a qualitative model which exploits the fact of the strong coupling of essentially nonlocal and local characteristics of a plasma in eq. (3) for total power losses, namely, the coupling of space-averaged emission/absorption coefficients and the coefficient for the reflection of plasma waves at plasma boundary. In this model, (i) the global energy transport is conducted by the long-free-path quanta of longitudinal EM waves (plasmons) which are responsible for such a strong coupling due to their multiple reflection (either from plasma boundary or from gradients of density and temperature inside plasma volume) and appear to be the main carriers of energy whereas plasma energy is invariably accumulated mainly in plasma particles, and (ii) nonlocal formation of temperature profile is guided by local behaviour of reflection coefficient R. Here, the quantity (1-R) takes into account the transforming of longitudinal waves into, e.g., (freely escaping) photons. Such a model suggests the possibility of an effective control of plasma global (nonlocal) parameters via a proper control of the reflection of plasma waves in, presumably, edge plasma. From this viewpoint, the L-H transition may appear to be stimulated by a sharp change of the reflection coefficient due to, e.g., increased gradient of poloidal rotation of tokamak plasma or increased stability of magnetic surfaces which are responsible for the reflection of most significant energy carriers.

Analytic and numerical analysis of heat transport by longitudinal waves across magnetic field shows that the non-local thermoconductivity by plasmons in a tokamak plasmas strongly depends on the character of wave dispersion and may be properly evaluated only within the framework of a combined description for non-diffusive heat transport by plasma waves and kinetics of plasma non-thermal electrons.

REFERENCES

1. Rybicki G.B. In: Methods in Radiative Transfer (Kalkofen W., Ed.) Cambridge Univ. press, Cambridge, U.K. (1984).

2. V.A.Abramov, V.I.Kogan and V.S. Lisitsa, In: Reviews of Plasma Physics, Eds. Leontovich M.A. and Kadomtsev B.B., Consultants Bureau, New-York, Vol.12, 151 (1987).

3. M.N.Rosenbluth and C.S.Liu, Phys. Fluids **19**, 815 (1976).

4. S.Tamor, Fusion Technology **3**, 293 (1983); Nucl.Instr. and Meth.Phys.Res., **A271**, 37 (1988).

5. A.B.Kukushkin, V.S.Lisitsa and Yu.A.Savel'ev, JETP Lett., **46**, 448 (1987); Proc. Int. Conf. Plasma Phys., New Delhi, India, **3**, 897 (1989).

6. B.A.Trubnikov, In: Reviews of Plasma Physics, Ed. M.A.Leontovich, Consultants Bureau, New-York, Vol.7, 345 (1979).

7. S.Atzeni, B.Coppi and G.Rubinacci, Report PTP-81/7, MIT (1981).

8. M.Bornatici, R.Cano, O. De Barbieri and F.Engelmann, Nucl.Fusion, **23**, 1153 (1983).

GUIDING CENTER DIFFUSION INDUCED BY STOCHASTIC ∇B AND CURVATURE DRIFTS

J. E. Vitela and M. Coronado
Instituto de Ciencias Nucleares
National University of Mexico
04510 Mexico, D.F.

I. Introduction.

Turbulent processes ocurring in the plasma seems to be the origin of the anomalous transport observed in tokamaks. The transport induced by stochastic fluctuation has been studied by consideration of the diffusion of guiding centers due to the stochastic electric drift or the motion of the centers along fluctuating magnetic lines.[1] However the diffusion induced by the stochastic ∇B and curvature drifts has not received special attention because it is believed that these diffusive processes are too weak in comparison with other processes. The treatment of stochastic ∇B and curvature drifts requires the development of a formalism to treat fluctuation with both time and space dependence. In a recent paper[2] a mathematical approach to deal with these type of fluctuations has been presented, and here we apply these results to a model for the magnetic field turbulence and evaluate the diffusion of guiding centers due to these drifts.

II. Mathematical Approach.

To apply the results from Ref. [2] we assume a uniform magnetic field B_0 in the Z-direction with stationary and homogeneous stochastic fluctuations, $\vec{b}(\vec{x},t)$ that are in addition Gaussian with cylindrical symmetry.[2,3] The guiding center equations we consider are

$$\frac{dx}{dt} = V_{\parallel}\frac{b_x}{B_0} - \frac{V_{\perp}^2}{\omega_g}\frac{\partial}{\partial y}(b_z/B_0) - \frac{V_{\parallel}^2}{\omega_g}\frac{\partial}{\partial z}(b_y/B_0) \tag{1a}$$

$$\frac{dy}{dt} = V_{\parallel}\frac{b_y}{B_0} + \frac{V_{\perp}^2}{\omega_g}\frac{\partial}{\partial x}(b_z/B_0) + \frac{V_{\parallel}^2}{\omega_g}\frac{\partial}{\partial z}(b_x/B_0) \tag{1b}$$

$$\uparrow \qquad\qquad \uparrow$$

$$\nabla \text{ B-drift} \qquad \text{curvature drift}$$

$$\frac{dz}{dt} = V_{\parallel} \qquad \text{(constant)} \tag{1c}$$

where $\omega_g = 2qB_0/mc$, and the parallel and perpendicular velocity, $V_{\parallel}$, $V_{\perp}$, are taken

constant. In this case the 9 correlation functions

$$\beta_{ij}(\vec{\xi},\tau) \equiv < b_i(\vec{x},t)b_j(\vec{x}',t') > \tag{2}$$

with $\vec{\xi} \equiv \vec{x}' - \vec{x}$ and $\tau \equiv t' - t$ reduce to only four functions β_0, β_1, β_2 and β_3, since

$$\beta_{ij} = \begin{pmatrix} \beta_0\xi_x^2 + \beta_1 & \beta_0\xi_x\xi_y & \beta_0\xi_x\xi_z + \beta_3\xi_x \\ \beta_0\xi_y\xi_x & \beta_0\xi_y^2 + \beta_1 & \beta_0\xi_y\xi_z + \beta_3\xi_y \\ \beta_0\xi_z\xi_x + \beta_3\xi_x & \beta_0\xi_z\xi_y + \beta_3\xi_y & \beta_0\xi_z^2 + 2\beta_3\xi_z + \beta_1 + \beta_2 \end{pmatrix}, \tag{3}$$

being β_0, β_1 and β_2 even functions in ξ^2, ξ_z and τ, while β_3 is even in ξ^2 and τ but odd in ξ_z.

The diffusion coefficients perpendicular to the average magnetic line is compose of the following terms,

1) Diffusion resulting from the motion of the guiding center along the field lines, i.e. $V_\parallel \vec{b}/B_0$:

$$D_\perp^{(1)} = \int_0^t d\tau \frac{V_\parallel^2}{B_0^2} \beta_1(\vec{\xi} = \vec{\xi}_0, \tau) \tag{4}$$

2) The diffusion appearing from the ∇B-drift:

$$D_\perp^{(2)} = -\int_0^t d\tau \frac{2V_\perp^4 l_\perp^2}{\omega_g^2 B_0^2} \left[\frac{\partial(\beta_1 + \beta_2}{\partial u} + V_\parallel^2 \tau^2 \frac{\partial \beta_0}{\partial u} + 2V_\parallel \tau \frac{\partial \beta_3}{\partial u} \right]_{\vec{\xi}=\vec{\xi}_0} \tag{5}$$

3) The diffusion resulting from the curvature drift:

$$D_\perp^{(3)} = -\int_0^t d\tau \frac{V_\parallel^4 l_\parallel^2}{B_0^2 \omega_g^2} \left(\frac{\partial^2 \beta_1}{\partial v^2} \right)_{\vec{\xi}=\vec{\xi}_0} \tag{6}$$

4) The diffusion due to the correlation between the ∇B and curvature drifts:

$$D_\perp^{(4)} = -\int_0^t d\tau \frac{2V_\perp^2 V_\parallel^2}{B_0^2 \omega_g^2} \left[\beta_0 + V_\parallel l_\parallel \tau \frac{\partial \beta_0}{\partial v} + l_\parallel \frac{\partial \beta_3}{\partial v} \right]_{\vec{\xi}=\vec{\xi}_0} \tag{7}$$

where $\vec{\xi} = (\xi_x, \xi_y, \xi_z)$, $\vec{\xi}_0 = (0, 0, V_\parallel \tau)$, $u = (\xi_x^2 + \xi_y^2)/l_\perp^2$ and $v = \xi_z / l_\parallel$. Here $l_\perp$ and $l_\parallel$ are the perpendicular and the parallel correlation length of the magnetic fluctuations. The correlation time is designed by τ_c.

III. A model for the correlations.

The condition that the magnetic fluctuations are divergence free reduces the number of independent β_j functions from four to only two. By choosing β_1 and β_2

as the independent functions and giving an analytical form for them we can evaluate the diffusion coefficients $D_{\perp}^{(j)}$. In this paper we consider the particular case

$$\beta_1 = A\ exp(-s^2)\ ,\quad \beta_2 = B\ exp(-s^2) \tag{8}$$

where $s^2 = (\xi_x^2 + \xi_y^2)/l_{\perp}^2 + \xi_z^2/l_{\parallel}^2 + \tau^2/\tau_c^2$. We also write $\beta_3 = \xi_z\tilde{\beta}_3$, where $\tilde{\beta}_3$ is now an even function in ξ_z.

The two coupled partial differential equations for β_0 and $\tilde{\beta}_3$ resulting from $\nabla\cdot\vec{b}=0$ can be solved to yield

$$\begin{aligned}
\beta_0 &= \left(\frac{A}{l_{\perp}^2}\right) e^{-\tau^2/\tau_c^2}\left\{G(2,\omega) + (\epsilon-1)G(\frac{5}{2},\omega) - 2(\epsilon-1)v^2\left[G(\frac{7}{2},\omega) - G(3,\omega)\right]\right\} \\
\tilde{\beta}_3 &= \left(\frac{A}{l_{\perp}^2}\right)(\epsilon-1)e^{-\tau^2/\tau_c^2}G(\frac{5}{2},\omega)\ ,
\end{aligned} \tag{9}$$

where $G(n,\omega) = \gamma(n,\omega)/\omega^n$, with $\gamma(n,\omega)$ the incomplete gamma function, and $\omega \equiv (\xi_x^2 + \xi_y^2)/l_{\perp}^2 + \xi_z^2/l_{\parallel}^2$ The correlation functions, β_j, are determined in terms of A, $R = B/A$, $\epsilon = \eta^2(R+1)$, where $\eta = l_{\perp}/l_{\parallel}$, and the correlation time and lengths. The additional conditions imposed on β_j, by the fact that β_{xx}, β_{yy} and β_{zz} have a maximum at $\vec{\xi}=0$, imply $\eta < 1$ and $R+1 > 0$.

IV. Diffusion coefficients.

The diffusion coefficients can be written in terms of effective correlations functions as

$$\begin{aligned}
D_{\perp}^{(1)} &= \frac{AV_{\parallel}^2}{B_0^2}\int_0^t f_1(\tau)d\tau\ , \qquad D_{\perp}^{(2)} = \frac{4AV_{\perp}^4 l_{\parallel}^2}{\omega_g^2 B_0^2 l_{\perp}^4}\int_0^t f_2(\tau)d\tau \\
D_{\perp}^{(3)} &= \frac{2AV_{\parallel}^4}{\omega_g^2 B_0^2 l_{\parallel}^2}\int_0^t f_3(\tau)d\tau\ , \qquad D_{\perp}^{(4)} = \frac{2AV_{\perp}^2 V_{\parallel}^2}{\omega_g^2 B_0^2 l_{\perp}^2}\int_0^t f_4(\tau)d\tau
\end{aligned} \tag{10}$$

where

$$\begin{aligned}
f_1(\tau) &= exp[-(t_c^2 + t_L^2)] \\
f_2(\tau) &= 5[(\epsilon - \frac{4}{5})G(2,t_L^2) - (\epsilon-1)G(\frac{5}{2},t_L^2)]exp(-t_c^2) \\
f_3(\tau) &= (1-2t_L^2)exp[-(t_c^2+t_L^2)] \\
f_4(\tau) &= 3G(2,t_L^2) - \frac{2}{3}exp(-t_L^2) + (\epsilon-1)[3G(2,t_L^2) - 4G(\frac{5}{2},t_L^2)]exp(-t_c^2)
\end{aligned} \tag{11}$$

with $t_c = \tau/\tau_c$ and $t_L = \tau/\tau_L$. The effective correlation functions $f_j(\tau)$ depend only on ϵ, τ_c and τ_L, where $\tau_L \equiv l_\parallel/V_\parallel$. All diffusion coefficients depend on A, which is proportional to the strength of the magnetic fluctuations. As may be expected the diffusion due to ∇B and curvature drifts depend on the correlation lengths and they show an explicit B_0^{-4} dependence, however a further dependence on B_0 can be hidden in the correlation time and lengths as well as in A. The diffusion due to ∇B-drift, $D_\perp^{(2)}$, gets larger as $l_\perp$ reduces and the diffusion produced by the curvature drift, $D_\perp^{(3)}$, increases as $l_\parallel$ gets shorter. These diffusion coefficients have a very sensitive dependence on the guiding center energy. Further, assuming ions and electrons have the same energy, the ∇B and curvature diffusion coefficients show a dependence on the mass of the particles only through the dependence on the parallel velocity $V_\parallel$ of the effective correlation coefficients. On the other hand as follows from Eq. (11), the perpendicular diffusion of particles caused by their motion along field lines, i.e. $D_\perp^{(1)}$, is much larger for electrons than for ions.

A numerical evaluation of the diffusion coefficients can be made by considering $\tau_c \sim 3 \times 10^{-5} sec$, $l_\perp \sim 1cm$, $b_\perp/B_0 \sim 10^{-4}$, $T_e, T_i \sim 25eV$ and $B_0 \sim 5KG$. We assume $l_\parallel \sim 100 l_\perp$ and in order to satisfy the additional conditions on the proposed correlation functions we take the lowest value allowed for $b_\parallel$, this is $b_\parallel/B_0 \sim 6 \times 10^{-3}$. Using these parameters and choosing $V_\parallel \sim V_\perp \sim V_{thermal}$ we find for times, $t \gg \tau_c, \tau_L$ that the diffusion coefficients in Eq. (10) for electrons are: $D_\perp^{(1)} \sim 4 \times 10^2 cm^2/s$, $D_\perp^{(2)}/D_\perp^{(1)} \sim 5$, $D_\perp^{(3)}/D_\perp^{(1)} \sim 10^{-10}$ and $D_\perp^{(4)}/D_\perp^{(1)} \sim 10^{-7}$; similarly for ions we get: $D_\perp^{(1)} \sim 5cm^2/s$, $D_\perp^{(2)}/D_\perp^{(1)} \sim 3 \times 10^4$, $D_\perp^{(3)}/D_\perp^{(1)} \sim 2 \times 10^{-4}$ and $D_\perp^{(4)}/D_\perp^{(1)} \sim -1$. We can then conclude that in the case $l_\parallel \gg l_\perp$ together with $\delta B_\parallel \gg \delta B_\perp$ (not in tokamaks) the stochastic ∇B-drift may play a leading role in the diffusion induced by stochastic magnetic fields.

References

1.- P.C. Liewer; Nuclear Fusion 25 (1985) 543.

2.- M. Coronado, J. Vitela E. and A.Z. Akcasu; Phys. Fluids B, 27 (1992) 3935.

3.- G.K. Batchelor; Proc. R. Soc. London 186 A (1946) 480.

A DYNAMICAL MODEL FOR THE IGNITOR EXPERIMENT

A.Airoldi [▪] and G.Cenacchi [*]

[▪] Istituto di Fisica del Plasma, CNR, Milano (Italy)
[*] Centro Ricerche Energia, ENEA, Bologna (Italy)

Introduction - The goal of Ignitor is to investigate the conditions under which fusion performance can be achieved in a D-T tokamak experiment characterized by high magnetic field and plasma current. The reference data of the machine involve a plasma current reaching up to 11MA and a toroidal field up to 13T /1/. Plasma confinement and performance may be limited by magnetohydrodynamic activity along the rampup phase; it is therefore important to carefully program the current rise. This paper presents dynamical simulations of the plasma rampup and flattop phase, carried out using an enhanced version of the free-boundary equilibrium-transport code JETTO /2/. The plasma discharge is followed along the current rise from 3 to 11MA, with a toroidal field growing from 7 to 13 tesla. Different plasma growth scenarios have been analysed to optimize the global plasma performance, taking into account MHD stability constraints. The effects of the current ramp rate and geometry are discussed. The importance of the density rise, as far as both the average value and the profile are concerned, is also pointed out, confirming the conclusions drawn from previous simulations relevant to the flattop phase /3,4/.

Simulations - The evolution of current, density and temperature profiles in Ignitor has been analysed using an advanced equilibrium-transport code where a splitting technique is applied /5/. In the equilibrium package the MHD equilibrium problem is solved as a free-boundary problem consistent with the currents in the poloidal field coils. The flux-surface formulation of the Grad-Shafranov equation is adopted, using a radial coordinate ρ , chosen to label the magnetic surfaces, which depends upon the toroidal magnetic flux Φ linked to them: $\rho = \sqrt{\Phi/\pi B_{to}}$, where B_{to} is a reference constant representative of the toroidal magnetic field. In order to estimate the currents producing a desired magnetic configuration, calculations have been carried out with another equilibrium solver for some "key" plasma configurations, taking into account the constraints of the design /6/. The coil currents required by other equilibria are computed by linear interpolation between the "key" values. For attaining the desired plasma geometry during the ramp different sets of coil currents are required depending upon the rate of current rise, which affects the current density profile. The plasma current step for equilibrium computations has been assumed to be 0.5MA and the toroidal magnetic field is the one associated with the plasma current according to the design. Plasmas started from small major radius have been considered.

The equilibrium flux-coordinate is also used in the transport package, where flux-surface-averaged transport equations for temperature, electron and ion densities, and current density are evolved in time. The anomalous thermal diffusivity follows the Coppi-Mazzucato-Gruber ohmic model with an additional term based on the ubiquitous modes /7/, entering when additional power is involved. A fraction of this term is also added to the Chang and Hinton expression for the ion thermal

diffusivity. Neoclassical resistivity is used. Sawteeth are not considered. The primary ion species consists of a (50%-50%) mixture of deuterium and tritium ions. Their depletion resulting from fusion reactions is assumed to be negligible until ignition. Two impurity species are explicitely treated. The α particle production is considered just as an auxiliary heating source for electrons and ions. During the ramp the particle average density is raised at a constant rate controlled by a given parameter. An inward particle diffusion is also introduced. A volume averaged electron density of $10^{20} m^{-3}$ and an average temperature of 700 eV are set for the initial 3 MA configuration.

Results- Two main scenarios have been analysed for the growth of current and magnetic field. They are shown in Figs 1 and 2, where the small markers indicate the time when equilibrium evaluation is updated and the big markers indicate the time when external currents are supplied according to the design constraints. The theoretically accessible region in the (l_i , q_ψ) space /8/, empirically checked in existing tokamaks as JET, ASDEX, JT60, has been taken into account as a constraint for achieving satisfactory performance.

For both scenarios the influence of the density growing has been studied by trying many variations on the inward flux (controlled by the parameter α_{inw}). Table I includes the main data of four reference shots.

Table I

Shot	1	2	3	4
dI/dt (MA/s)	2.0	2.0	2.5	2.5
t_{bft} (s)	4.0	4.0	3.2	3.2
α_{inw}	2.0	2.2	2.0	2.2
$<n_e>$ at t=0. ($10^{14} cm^{-3}$)	1.0	1.0	1.0	1.0
$<n_e>$ at t_{bft} ($10^{14} cm^{-3}$)	5.1	5.8	6.7	6.7
q(0) at t_{bft}	1.1	1.1	1.3	1.3
$q(\psi_b)$ at t_{bft}	3.2	3.1	3.1	3.1
$<T_e>$ at t_{bft} (keV)	2.4	2.4	2.0	2.1
$T_e(0)$ at t_{bft} (keV)	6.7	5.9	5.5	5.1
$t_{ign} - t_{bft}$ (s)	2.1	2.3	2.3	2.6
$t_{q(0)<1} - t_{bft}$ (s)	0.4	0.6	0.5	0.7
P_Ω at t_{bft} (MW)	15.6	16.5	18.6	18.6
P_α at t_{bft} (MW)	2.1	1.8	1.4	1.3

The quantities in the Table are self-explanatory; t_{bft} indicates the time of the beginning of flattop and t_{ign} the ignition time. The trajectories in the (l_i , q_ψ) plane for shots 1 and 3, whose difference is the dI/dt rate, are very similar and within the stability region. On the other hand, by enhancing the inward flux, the (l_i , q_ψ) trajectory shifts towards the instability region, as shown in Figs 3 and 4. Moreover the ignition time increases with density peaking. These results confirm that the density evolution noticeably influences the plasma performance. Partial particle

penetration produces an inverted density profile during the density rise (see Figs 5,6), as observed in JET. The energy confinement time during the ramp phase has been found to increase with the inward flux. We recall that in Ohmically heated plasmas the energy confinement time grows steadily during the current ramp, when the plasma density is also increased and drops slowly during the current flattop, as the fusion heating becomes significant. The examined shots, chosen between many simulations with different density conditions, point out that the flattop phase can be reached with a magnetic field line parameter $q(\psi)$ kept above one over all the plasma cross-section. These favourable conditions should be exploited by trying to achieve ignition shortly after rampup, before sawtooth oscillations develop. The delay in the growth of the $q < 1$ region increases with the inward flux and the current rise rate assumed (see Table I). The q profile evolution during the ramp phase for shots 1 and 3 is shown in Figs 7 and 8. Also the plasma geometry has an influence on the global performance: if the coil currents are adjusted so as to guarantee the nominal plasma cross-section, ignition can be attained within a shorter time and with a lower average temperature than in the case of smaller dimensions.

The results show that a careful control of current ramp rate, plasma dimensions and density allows to reach the flattop with l_i inside the stability region and the safety factor above one over all the plasma cross-section.

References

1 - B.Coppi, M.Nassi et al., MIT Report PTP 92/8 (1993)
2 - G.Cenacchi, A.Taroni, JET-IR(88)03, (1988)
3 - A.Airoldi, G.Cenacchi, *Fusion Tech.* **19**,78(1991)
4 - A.Airoldi, G.Cenacchi, *Plasma Phys. Contr. Fus.* **33**,91(1991)
5 - G.Cenacchi, A.Taroni, *Proc. 8th Eur. Conf. Comp. Phys.*,Eibsee,Germany,1986
6 - G.Cenacchi et al., ENEA Report RTI/INN(92) 16, C.R.E. Bologna (1992)
7 - B.Coppi et al., *14th IAEA Fus.Conf.*, Wurzburg,1992,Paper CN-56/D-3-1(C)
8 - C.Z. Cheng et al., *Plasma Phys. Contr. Fus.* **29**,351(1987)

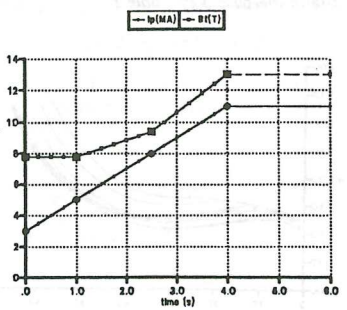

Fig.1- Growth scenario of I_p and B_t in the case of $dI/dt = 2MA/s$

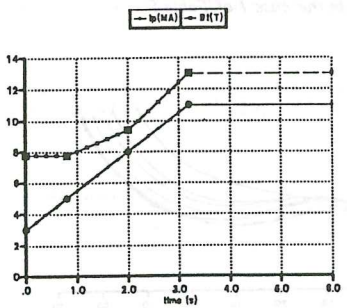

Fig.2- Growth scenario of I_p and B_t in the case of $dI/dt = 2.5MA/s$

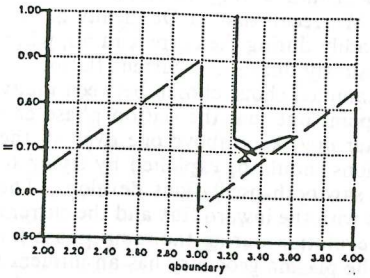

Fig.3- Trajectory in the plane (l_i , q_ψ) in the case 3 of Table I

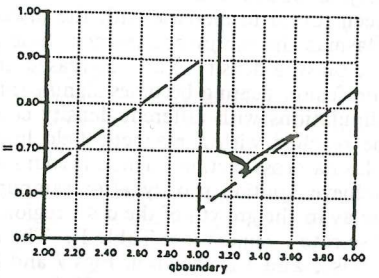

Fig.4- Trajectory in the plane (l_i , q_ψ) in the case 4 of Table I

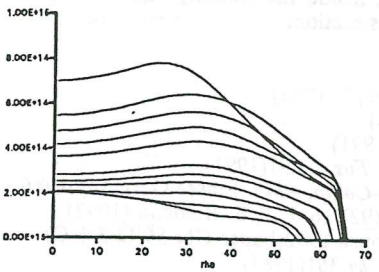

Fig.5- Time evolution of the electron density profile in the case 1 of Table I

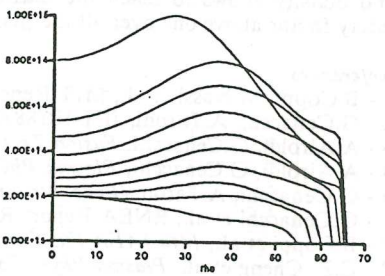

Fig.6- Time evolution of the electron density profile in the case 3 of Table I

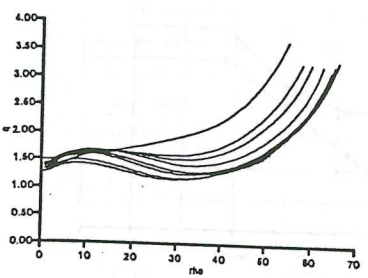

Fig.7- Time evolution of the q profile in the ramp phase for case 1 of Table I

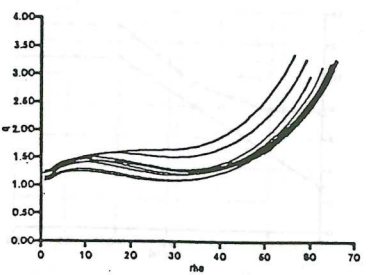

Fig.8- Time evolution of the q profile in the ramp phase for case 3 of Table I

Thermal Energy and Bootstrap Current in Fusion Reactor Plasmas

G. Becker
Max-Planck-Institut für Plasmaphysik,
Euratom-IPP Association, Garching
Federal Republic of Germany

ABSTRACT. For DT fusion reactors with prescribed alpha particle heating power P_α, plasma volume V and burn temperature $< T_i > \approx 10\ keV$ specific relations for the thermal energy content, bootstrap current, central plasma pressure and other quantities are derived. It is shown that imposing P_α and V makes these relations independent of the magnitudes of the density and temperature, i.e. they only depend on P_α, V and shape factors or profile parameters. For model density and temperature profiles analytic expressions for these shape factors and for the factor C_{bs} in the bootstrap current formula $I_{bs} \approx C_{bs}(a/R)^{\frac{1}{2}}\beta_p I_p$ are given.

In the design of next-step devices and fusion reactors, the fusion power is a fixed quantity. Prescription of the alpha particle heating power and plasma volume results in specific relations which can be helpful for interpreting computer simulations and for the design of fusion reactors.

Transport simulations of ITER |1,2| with volume-averaged density $< n > \approx 10^{20}\ m^{-3}$ and temperatures $< T_e > \approx < T_i > \approx 10\ keV$ have shown that the simplifying assumptions

$$n_e(r) = n_i(r) = n(r) = n_0 g_n(r) \tag{1}$$

$$T_e(r) = T_i(r) = T(r) = T_0 g_T(r) \tag{2}$$

are good approximations in the case of low impurity levels |3|. Furthermore, the deuteron and triton densities may be set equal ($n_d = n_t = n/2$). In the region where the fusion power is produced, the ion temperature was found to vary between 10 and 20 keV. In this temperature range, the DT fusion rate coefficient can be represented by

$$< \sigma v >_{DT} = C_f T^2 \tag{3}$$

with $C_f = 1.08 \times 10^{-24}\ m^3 s^{-1}(keV)^{-2}$. Assuming that the energy of the alpha particles is totally deposited in the plasma, we obtain for the alpha particle heating power

$$P_\alpha = \tfrac{1}{4} C_f E_\alpha 2\pi R \int_0^a n^2 T^2 2\pi r dr \tag{4}$$

Here, $E_\alpha = 3.5\ MeV$ is the alpha particle energy and R and a denote the major and minor plasma radii, respectively. Substitution of Eqs. *(1)* and *(2)* in Eq. *(4)* yields

$$P_\alpha = \tfrac{1}{4} C_f E_\alpha V (n_0 T_0)^2 f_1 \tag{5}$$

with the plasma volume $V = 2\pi^2 R a^2$ and the shape factor

$$f_1 = \tfrac{2}{a^2} \int_0^a (g_n g_T)^2 r dr \tag{6}$$

From Eq. *(5)* it follows that

$$n_0 T_0 = 2\left(\frac{P_\alpha}{C_f E_\alpha V f_1}\right)^{\frac{1}{2}} \tag{7}$$

so that the central plasma pressure $p_0 = 2 n_0 T_0$ reads

$$p_0(MJm^{-3}) = 0.82 f_1^{-\frac{1}{2}} \left[\frac{P_\alpha(MW)}{V(m^3)}\right]^{\frac{1}{2}} \tag{8}$$

It depends on the α particle heating power, the plasma volume and the shapes of the density and temperature profiles, but is independent of n_0 and T_0.

The thermal energy content is given by

$$W_{th} = 6\pi R \int_0^a nT 2\pi r dr = 3Vn_0T_0f_2 \tag{9}$$

where

$$f_2 = \frac{2}{a^2}\int_0^a g_n g_T r dr \tag{10}$$

is another shape factor. Elimination of n_0T_0 by means of Eq. *(7)* results in

$$W_{th} = 6\frac{f_2}{f_1^{\frac{1}{2}}} V^{\frac{1}{2}} \left(\frac{P_\alpha}{C_f E_\alpha}\right)^{\frac{1}{2}} \tag{11}$$

and, in readily applicable form,

$$W_{th}(MJ) = 1.23\frac{f_2}{f_1^{\frac{1}{2}}}[V(m^3)P_\alpha(MW)]^{\frac{1}{2}} \tag{12}$$

For the model density and temperature profiles

$$g_n = \left(1 - \frac{r^2}{a^2}\right)^{\alpha_n} \tag{13}$$

$$g_T = \left(1 - \frac{r^2}{a^2}\right)^{\alpha_T} \tag{14}$$

the integrals in Eqs. *(6)* and *(10)* are determined analytically, yielding the shape factors

$$f_1 = \frac{1}{2(\alpha_n+\alpha_T)+1} \tag{15}$$

$$f_2 = \frac{1}{\alpha_n+\alpha_T+1} \tag{16}$$

The factor required in Eq. *(12)* thus reads

$$\frac{f_2}{f_1^{\frac{1}{2}}} = \frac{[2(\alpha_n+\alpha_T)+1]^{\frac{1}{2}}}{\alpha_n+\alpha_T+1} \tag{17}$$

It is a rather weak function of α_n and α_T, whereas both f_2 and $f_1^{\frac{1}{2}}$ sensitively depend on these parameters. Rectangular profile shapes $g_n = g_T = 1$, i.e. $\alpha_n = \alpha_T = 0$, correspond to $f_2/f_1^{\frac{1}{2}} = 1$. For more realistic profiles represented by $\alpha_n = 0.5$ and $\alpha_T = 1$ (like those assumed for ITER |1|) one obtains $f_2/f_1^{\frac{1}{2}} = 0.8$.

According to Eq. *(12)*, the thermal energy is proportional to the square root of the α particle heating power. When P_α and V are prescribed, W_{th} no longer depends on n_0 and T_0 but rather is determined by the shapes of the density and temperature profiles. Consequently, in transport simulations with P_α and V imposed only the radial dependences of the electron and ion heat diffusivities $\chi_e(r)/\chi_{eo}$ and $\chi_i(r)/\chi_{io}$ are important for the thermal energy content during the ignited state, but not χ_{eo} and χ_{io}. They determine, however, whether ignited operation is possible. For the approximate evaluation of W_{th} by Eq. (12), it is sufficient to know the readily accessible quantities P_α, V, α_n and α_T.

With the help of Eq. *(12)*, the volume averaged density consistent with a prescribed burn temperature $< T > \approx 10\ keV$ can be calculated. Replacing W_{th} by the usual expression

$$W_{th} = 3 < n >< T > V \tag{18}$$

results in

$$< n > (m^{-3}) = 2.56 \times 10^{21} \frac{f_2}{f_1^{\frac{1}{2}}} \left[\frac{P_\alpha(MW)}{V(m^3)}\right]^{\frac{1}{2}} \frac{1}{<T>(keV)} \tag{19}$$

Another quantity entering the reactor design is the allowable divertor heat load P_{div}, which is equal to the sum of the heat conduction P_{cond} and heat convection P_{conv} at the separatrix. If it is necessary to restrict P_{div} to a fraction γ of the alpha particle heating,

$$P_{div} = \gamma P_\alpha \tag{20}$$

this can be achieved by significant bremsstrahlung and impurity line radiation within the separatrix. A typical figure for ITER is $\gamma \approx 0.5$. With the global energy confinement time defined as

$$\tau_E = \frac{W_{th}}{P_{cond}+P_{conv}} \tag{21}$$

one thus obtains

$$\tau_E(s) = 1.23 \frac{1}{\gamma} \frac{f_2}{f_1^{\frac{1}{2}}} \left[\frac{V(m^3)}{P_\alpha(MW)}\right]^{\frac{1}{2}} \tag{22}$$

This requirement for the energy confinement has to be met by the reactor plasma when the divertor heat load is prescribed.

With P_α and V imposed, specific relations for the non-inductive current drive by the bootstrap effect result. As the reactor plasma is collisionless (electron collisionality factor $\nu_{*e} \approx 10^{-2}$), the neoclassical bootstrap current valid for the banana regime is applied |4,5|. With the approximations of Eqs. *(1)* and *(2)* the bootstrap current density reads:

$$j_{bs}(MAm^{-2}) \approx 1.60 \times 10^{-22} \epsilon^{-\frac{1}{2}} \frac{q}{B_t(T)} \left[-2K_{13} T \frac{\partial n}{\partial r} + (1.67K_{13} - K_{23}) n \frac{\partial T}{\partial r}\right] \tag{23}$$

with T in keV, n in m^{-3} and r in m. Here, ϵ is the inverse aspect ratio r/R, B_t is the toroidal magnetic field in T and K_{13} and K_{23} are dimensionless transport coefficients in the banana regime |4|. Setting $K_{13} \approx K_{13}^{(0)} = 2.30$ and $K_{23} \approx K_{23}^{(0)} = 4.19$, which is a good approximation for the low ν_{*e} values, leads to

$$j_{bs}(MAm^{-2}) \approx 1.60 \times 10^{-22} \epsilon^{-\frac{1}{2}} \frac{q}{B_t(T)} \left(-4.60 T \frac{\partial n}{\partial r} - 0.35 n \frac{\partial T}{\partial r}\right) \tag{24}$$

It is evident that the main contribution is caused by the density gradient. The ratio of the $\partial n/\partial r$ and $\partial T/\partial r$ terms is somewhat reduced by the experimental fact that density profiles are broader than temperature profiles. Very flat density profiles like those in H mode plasmas of open divertor tokamaks are unfavourable since the gradient is shifted to the periphery resulting in high edge currents.
Substitution of Eqs. *(1)* and *(2)* in Eq. *(24)* yields

$$j_{bs}(MAm^{-2}) \approx 1.60 \times 10^{-22} \epsilon^{-\frac{1}{2}} \frac{q}{B_t(T)} n_0 T_0 \left(-4.60 g_T \frac{\partial g_n}{\partial r} - 0.35 g_n \frac{\partial g_T}{\partial r}\right) \tag{25}$$

Eliminating the factor $n_0 T_0$ by means of Eq. (9) and applying the model profiles of Eqs. *(13)* and *(14)* results in a formula for the bootstrap current which does not underly a burn temperature restriction

$$I_{bs} \approx C_{bs} \left(\frac{a}{R}\right)^{\frac{1}{2}} \beta_p I_p \tag{26}$$

with

$$C_{bs} \approx 0.5(\alpha_n + \alpha_T + 1)(4.60\alpha_n + 0.35\alpha_T) \int_0^1 \left(\frac{r}{a}\right)^{\frac{3}{2}} \left(1 - \frac{r^2}{a^2}\right)^{\alpha_n + \alpha_T - 1} h d\left(\frac{r}{a}\right) \quad (27)$$

Here, β_p is the poloidal beta value, I_p is the plasma current and h is given by $h = q/q_a$ with q_a being the cylindrical q value at $r = a$. For $\alpha_n = 0.5, \alpha_T = 1$ and $h = (r/a)^{3/2}$ a factor $C_{bs} \approx 0.44$ is obtained.

Specific expressions for the α particle heating and DT fusion rate can also be given. The cumulative alpha particle heating power (integrated over a cylinder of radius r) reads

$$P_\alpha(r) = \tfrac{1}{4} C_f E_\alpha 2\pi R \int_0^r n^2 T^2 2\pi r' dr' \quad (28)$$

with $P_\alpha(a) = P_\alpha$ (see Eq. *(4)*). Substituting Eqs. *(1)*, *(2)* and *(5)* in Eq. *(28)* yields

$$\frac{P_\alpha(r)}{P_\alpha} = \frac{1}{f_1} \frac{2}{a^2} \int_0^r (g_n g_T)^2 r' dr' \quad (29)$$

For the model density and temperature profiles it thus follows that

$$\frac{P_\alpha(r)}{P_\alpha} = 1 - \left(1 - \frac{r^2}{a^2}\right)^{\frac{1}{f_1}} \quad (30)$$

The density of the DT fusion rate is given by

$$S_\alpha(r) = \tfrac{1}{4} C_f n^2 T^2 \quad (31)$$

so that one obtains correspondingly

$$S_\alpha(r) = \frac{1}{f_1} \frac{P_\alpha}{E_\alpha V} (g_n g_T)^2 = S_\alpha(0)(g_n g_T)^2 \quad (32)$$

with

$$S_\alpha(0)(m^{-3} s^{-1}) = 1.77 \times 10^{18} \frac{1}{f_1} \frac{P_\alpha(MW)}{V(m^3)} \quad (33)$$

With the model density and temperature profiles, Eq. *(32)* yields

$$\frac{S_\alpha(r)}{S_\alpha(0)} = \left(1 - \frac{r^2}{a^2}\right)^{2(\alpha_n + \alpha_T)} \quad (34)$$

Prescription of the alpha particle heating power and plasma volume makes the thermal energy, bootstrap current, central plasma pressure and fusion rate independent of the magnitudes of the density and temperature, i.e. they are functions of P_α, V and profile shapes only. The formulas given in Eqs. *(8)*, *(12)*, *(19)* and *(33)* have the advantage that they merely require a knowledge of P_α, V, f_1 and f_2. They also hold in flux surface coordinates if f_1 and f_2 are expressed in such coordinates. Applying the bootstrap current formula presented in Eqs. *(26)* and *(27)* is also easy if α_n, α_T and h are known. The calculated values of W_{th} and p_0 are found to deviate by a few per cent from the predictions of transport simulations. This difference results from the approximations in Eqs. *(1)* and *(2)*, especially from setting $n_{io} T_{io} = n_0 T_0$ in Eq. *(5)*.

References

|1| Tomabechi, K., Gilleland, J.R., Sokolov, Yu.A., Toschi, R. and the ITER Team, Nucl. Fusion 31 (1991) 1135.
|2| Uckan, N.A., et al., "ITER Design Information Document, Physics", ITER-TN-PH-0-5 (1990).
|3| Becker, G., to be published in Nucl. Fusion.
|4| Hinton, F.L., Hazeltine, R.D., Rev. Mod. Phys. 48 (1976) 239.
|5| Becker, G., Nucl. Fusion 29 (1989) 1291.

MODELLING OF A HEAT PINCH UNDER OFF-AXIS HEATING IN TOKAMAKS

Yu.N.Dnestrovskij, S.E.Lysenko
Russian Research Center "Kurchatov Institute", Moscow, Russia

1. INTRODUCTION. Recently in some experiments with ECRH [1,2] and ICRH [3] off-axis heating the structure of the electron thermal flux Γ_e have been determined. The results of these experiments are not in the coincidence with each other.

Usually the electron flux is written as:

$$\Gamma_e=-n\chi_e\cdot\partial T_e/\partial r \qquad (1)$$

But the existence of the profile consistency effect leads to an idea that the flux can contain the second convective term

$$\Gamma_e=-n\chi_e\cdot\partial T_e/\partial r+nvT_e \qquad (2)$$

referred as the heat pinch. It is possible to distinct between (1) and (2) in experiments, using a well localized source of off-axis additional heating, for example, ECRH. The experimental results could be described by the effective heat diffusivity

$$\chi_e^{eff}=-\Gamma_e/(n\cdot\partial T_e/\partial r). \qquad (3)$$

If the heat pinch in the flux (2) overcomes within some region $r_1<r<r_2$, then

$$\chi_e^{eff}(r) < 0, \quad r_1<r<r_2. \qquad (4)$$

The condition (4) is sufficient for the existence of the heat pinch, but it is not necessary. The heat pinch could be detected also, when elsewhere $\chi_e^{eff}>0$, using the detailed analysis of non-stationary discharges with off-axis heating.

It was shown on T-10 [1] that under off-axis ECRH the χ_e^{eff} value reduced by several fold. But the problem of the heat pinch existence was unresolved. The negative χ_e^{eff} values have been observed on DIII-D [2] under off-axis ECRH (P_{EC}=1.25MW) at the low density $\bar{n}=2.2\times10^{19}m^{-3}$. The structure of the flux (2) was confirmed. On JET [3] the strong on-axis and off-axis ICRH has been conducted with the power P_{IC}=10MW. The experimental results were similar to obtained ones in [1]: with off-axis heating the flat $T_e(r)$ profiles were maintained during a long time and the heat pinch was absent.

In the present paper we try to resolve the contradiction between [2] and [1,3] by means of the canonical profiles model, including the heat pinch and the forgetting effect, which destroys the pinch.

2. MODEL. The canonical profiles model with forgetting [4] was modified for the correct description of $T_{e,i}(r)$ profiles. The usual energy balance equations for the electrons and ions and the equation for the poloidal field were solved. The plasma density n was assumed to be known from the experiments. The thermal fluxes have a form:

$$\Gamma_k=\Gamma_k^{neo}+\Gamma_k^{an}+\Gamma_k^{PC} \quad (k=i,e) \qquad (5)$$

where Γ_k^{neo} are the neoclassical fluxes,

$$\Gamma_k^{an} = -\kappa_k^{an} \frac{\partial T_k}{\partial r}, \qquad \Gamma_k^{PC} = -n\chi_k^{PC} \frac{rT_k}{a^2} z_{Tk} F_k(z_{pk}), \tag{6}$$

$$z_{Tk} = \frac{a^2}{r} \frac{\partial}{\partial r} \ln \frac{T_k}{T_{kc}}, \quad z_{pk} = \frac{a^2}{r} \frac{\partial}{\partial r} \ln \frac{p_k}{p_{kc}}, \quad F_k(z_{pk}) = \exp\left(-\frac{z_{pk}^2}{2z_{0k}^2}\right). \tag{7}$$

Here F_k is the forgetting factor [4], $z_{0k}=z_{0k}(r)$ is the influence zone width of the canonical profiles. The χ_k^{an} and χ_k^{PC} values are calculated in [4], T_{kc} and p_{kc} denote the canonical profiles of the temperature and pressure

$$T_{kc}(r)/T_{kc}(0) = (1+r^2/a_j^2)^{-\gamma_k}, \qquad p_{kc}(r)/p_{kc}(0) = (1+r^2/a_j^2)^{-\delta_k} \tag{8}$$

The comparison with experiments showed that $\gamma_k \sim 1$, $\delta_k \sim 3/2$. The real $T_{e,i}$ and $p_{e,i}$ profiles during the on-axis heating are more peaked than the canonical ones, therefore $z_{Tk}<0$ and $z_{pk}<0$. Under off-axis heating these profiles are more flat than the canonical ones, therefore $z_{Tk}>0$ and $z_{pk}>0$. So we have to introduce two functions z_{0k}^+ and z_{0k}^-, which describe the influence zone width:

$$z_{0k}(r) = \begin{cases} z_{0k}^+(r)>0, & \text{if } z_{pk}>0, \text{ (off-axis heating)} \\ z_{0k}^-(r)>0, & \text{if } z_{pk}<0 \text{ (on-axis heating)} \end{cases} \tag{9}$$

The functions $z_{0k}^+(r)$ and $z_{0k}^-(r)$ should be found from comparison with experiments. Eq. (6) for the flux Γ_k^{PC} can be rewritten as

$$\Gamma_k^{PC}(z_{Tk}) = -n\chi_k^{PC} \frac{rT_k}{2} z_{Tk} \exp[-(z_{Tk}+z_n)^2/(2z_{0k}^2)], \tag{10}$$

where

$$z_n = (a^2/r) \frac{\partial}{\partial r} \ln(n/n_c), \qquad n_c(r)/n(0) = (1+r^2/a_j^2)^{-\nu}, \qquad \nu = \delta_k - \gamma_k. \tag{11}$$

The curve $\Gamma_k^{PC}(z_{Tk})$ at $z_n=0$ is qualitatively presented in Fig.1. If $z_{0k}^+ < z_{0k}^-$, the threshold value $(\Gamma_k^{PC})_{max}$ for off-axis heating in several folds smaller than one for on-axis heating. It means that the plasma under off-axis heating "easy forgets" the canonical profile. After start of the strong off-axis heating the deviation z_{pk} would be greater than z_{0k}^+ and the heat pinch will be destroyed.

The Eq. (10) for the flux and Fig.1 yield that two stationary solutions may exist, corresponding to the peaked and flat T_e profiles. They are marked in Fig.1 as (1) and (2). Realization of these solutions depends on the process history. After the pulse impact on plasma (ramp-up or ramp-down the power, pellet injection and so on) the bifurcation from one solution to another is possible.

Let us consider the scenario of the step-wise power ramping with the step value δP and its duration δt. The model shows that the critical values δP_{cr} and the derivative dP_{cr}/dt exist. Only if the conditions

$$\delta P < \delta P_{cr}, \quad \delta P/\delta t < dP_{cr}/dt \tag{12}$$

are satisfied simultaneously, the temperature tends to more peaked profiles (solution 1 in Fig.1) and the heat pinch is maintained. In other cases the solution 2 would be realized.

It is possible to propose the alternative scenario for the heat pinch

maintaining. At first we use the mixed on- and off-axis heating, when the main part of the power is deposited far from the center and only 15-20% of power deposited near the center. After reaching the steady state the on-axis power is disconnected. The plasma becomes slightly colder, but the temperature profile should be peaked (the solution 1 in Fig.1 is valid). Such experiment is crucial to verify a validity of the proposed version of the canonical profiles model.

3. MODELLING OF EXPERIMENTS WITH OFF-AXIS AND MIXED HEATING. The model contains internal parameters and functions. For the off-axis heating the most important is the function $z^+_{Oe}(r)$ in the region between the plasma center and the power deposition zone. We shall assume that $z^+_{Oe}(r)$ has a slight radial dependence, so the parameter to be determined is $z^+_{Oe}(0)$. The modelling of the experiments [1-3] have shown that $z^+_{Oe}(0) \equiv z_0 \approx 1.5$ and slightly depends on the plasma parameters. At on-axis heating $z^-_{Oe}(0) \sim 5\text{-}6$ [4].

The results of modelling the off-axis ECRH on DIII-D [2] are presented in Figures 2 and 3 for different z_0 values. For all cases in the region $0.3<r/a<0.45$ the pinch is not destroyed and $\chi_e^{eff}<0$.

Fig.4 shows the evolution of the experimental [3] and calculated electron temperature profiles with P_{IC}= 10MW, I=3MA, B=2.8T, the equivalent minor radius $a^* = \sqrt{ab} = 1.37$m. We suppose that P^e_{IC}=7MW, P^i_{IC}=3MW, but variation of the relation P^e_{IC}/P^i_{IC} only slightly affects the calculations results. The Δt denotes a time from start of heating. We see that during a long time the flat T_e profile is maintained. The heating power profile is shown also. Fig.5 presents χ_e^{eff} profiles at Δt=0.5s and 1s. Note, that behavior of T_e profile under ICRH on JET is determined by strong applied power. When inequalities (12) are not satisfied, the solution 2 from Fig.1 is realized and the heat pinch is destroyed. As a result the flat even the hollow T_e profile is exists. For detection the heat pinch on JET one needs to use other heating scenario.

The most favorable conditions for the heat pinch detection on T-10 are attained under ECRH of the dense plasma. The results of calculations are shown in Fig.6 for $\bar{n}=5.8\times10^{19}$m^{-3}. For mixed heating with P=1MW(off)+0.15MW (on) the T_e profile becomes more peaked than the canonical one (curve 3) and the thermal flux elsewhere directed outward. After disconnecting of the on-axis power the electrons in the center slightly cool down (curve 1), the solution 1 from Fig.1 is realized and the heat pinch is occurred. After start of off-axis heating with the same power P_{EC}=1MW (curve 2) the pinch is destroyed because the solution 2 from Fig.1 is realized.

REFERENCES

1. V.V.Alikaev, et al, in Plasma Phys. and Control. Nucl. Fusion Research (Proc. 11th Int. Conf. Kyoto, 1986) Vol.1, IAEA, Vienna (1985) 111.
2. T.C.Luce, C.C.Petty, J.C.M.de Haas, Preprint GA-A20541, 1991.
3. B.Balet, et al, in Contr. Fusion and Plasma Phys. (Proc. 19th Europ. Conf., 1992, Innsbruck), Pt.1, p.59.
4. Yu.N.Dnestrovskij, et al, in Control Fusion Plasma Phys. (Proc 18th Europ. Conf. 1991, Berlin) Pt.1, p.413.

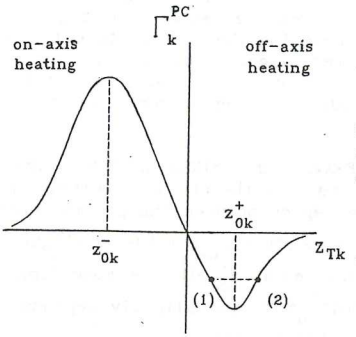

Fig.1

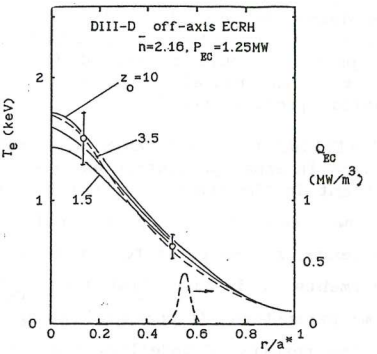

FIG.2

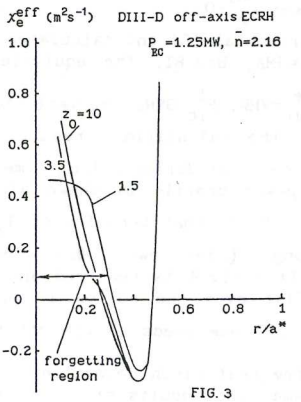

FIG. 3

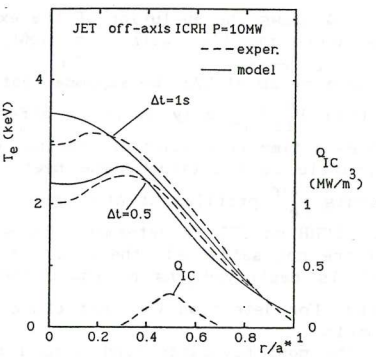

FIG.4

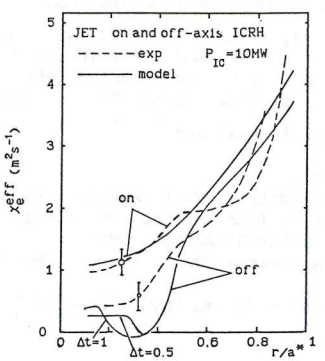

FIG. 5

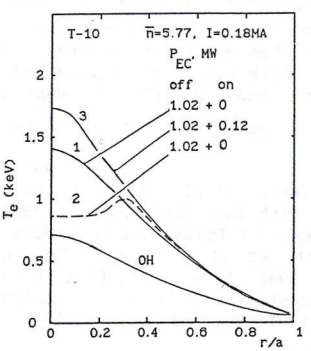

FIG.6

Drift Wave Turbulence in the Transcollisional Regime

B. Scott, Max-Planck-Institut für Plasmaphysik, Garching, Germany

A fluid model for electrons is derived, which extends the usual two-fluid collisional treatment to regimes of arbitrary collisionality, and matches the zero-Larmor radius collisionless model at zero collisionality. The scheme is calibrated by computation of drift-wave evolution in a shearless slab and comparison to identical computations using drift-kinetic electrons. The fluid model is then extended to sheared magnetic fields. Linear waves, known to be damped at large and zero collisionality are found to be damped for arbitrary collisionality. Turbulence in the two-dimensional slab, known to be self-sustaining at large collisionality, is found to retain this property for arbitrary collisionality, although somewhat weakened. The physics of the interaction between parallel and perpendicular (drift) electron dynamics is found to be of the same character, whether collisional or Landau effects provide the dissipation.

I. Introduction

It is a well known problem with collisional fluid treatments of tokamak edge turbulence that the electron mean free path is longer than the connection length of the field lines, which formally invalidates the theory. Moreover, for the parametric regime usually encountered, the collision frequency for electrons, ν_e, is commensurate with frequencies near the upper range of those measured. Interpreting these measurements as indicative of drift-wave dynamics, with the known dispersion relation, one faces a situation in which the longer and shorter wavelengths are in different collisionality regimes: the former are deeply collisional, but the latter are at least "transcollisional": $\omega \sim \nu_e$ for wave frequency ω. This regime becomes still more important when it is realised that the usual situation during the transition from L- to H-mode operation is also included.

In a search for a reasonable model to treat this regime it would be unwise to take a collision-free approach, as is often done. Models are available at both extremes of the collisionality: the collisional two-fluid equations (Braginskii 1965, Hassam 1980) and the zero Larmor radius collisionless model of Hammett and Perkins (1990). The former is an asymptotic expansion in inverse collisionality; the latter is obtained by matching the results to the known properties of the plasma dispersion ("Z") function. This paper extends the matching process to arbitrary collisionality through computation of drift-wave dynamics using drift-kinetic electrons and cold ions, and requiring that an appropriate fluid model for the electrons re-produce the drift-kinetic results. Once this is done, turbulence simulations are carried out with the transcollisional fluid model, in order to see whether the recently discovered nonlinear instability of drift-wave turbulence (Scott 1990, 1992) carries over into that regime. The overall result is that it does, but over a more restricted range of temperature gradient values. Contrary to the expectations of this author, the decrease in parallel thermal conductivity experienced at lower collisionality leads to weaker, not stronger, turbulence.

II. The Transcollisional Model and its Calibration

Since the focus is on electron dynamics, the ions are taken as a cold fluid which provides inertia (Scott 1992). The model produced herein can be incorporated into gyrofluid treatments to relax their restriction to adiabatic electrons (Dorland and Hammett 1993), at a later time. Due to the expense of kinetic computation, the calibration of the fluid model is performed for linear drift waves in a shearless slab: the parallel gradient, $k_\parallel$, is taken as constant, and parallel ion motion is neglected (re-incorporation of this in the sheared case is straightforward). The directions are x, down the gradient, y, electron drift, and z, the magnetic field at a resonant surface. "Shearless slab" is equivalent to evaluation of the sheared slab at a reference distance from the resonant surface, so that $k_\parallel$ is constant. In the linear, drift-kinetic model for electrons, the governing equations are

$$\frac{\partial}{\partial t}\nabla_\perp^2\phi = -v_T\nabla_\parallel \int d^3w\, w_\parallel (f - f_0\phi), \tag{1}$$

$$\frac{\partial f}{\partial t} = -(c_s/L_n)\omega_T\frac{\partial\phi}{\partial y} - w_\parallel v_T\nabla_\parallel(f - f_0\phi) + \frac{\nu_e}{w^3}\frac{\partial}{\partial z}(1-\zeta^2)\frac{\partial f}{\partial z}, \tag{2}$$

where $\omega_T = 1 + \eta_e(w^2 - \frac{3}{2})$, $\eta_e = L_n/L_T$, $\nu_e = 2\pi n\lambda e^4/m_e^2 v_T^3$, w is the electron velocity in the ion frame, $\zeta = w_\parallel/w$ is the pitch angle cosine, and ϕ is normalised to T/e, x and y to $\rho_s = c(M_iT)^{1/2}/eB$, and w to $v_T = (2T/m_e)^{1/2}$. In these units the background Maxwellian is $f_0 = \pi^{-3/2}e^{-w^2}$. In the shearless slab, Eqs. (1,2) are re-expressed in wavenumber space with one Fourier component (in which $\partial/\partial y \to ik$, $\nabla_\perp^2 \to -k^2$, and $\nabla_\parallel \to ik_\parallel$, with k and $k_\parallel$ constant), and solved *ab initio*: at $t = 0$ ϕ is set to 10^{-8} and f to $f_0\phi$, with the ζ-dependence to be excited by ω_T.

Since the collision model in Eqs. (1,2) is the Lorenz one, the fluid equations in the collisional regime are taken from Hassam (1980) and not Braginskii (1965). In the collisionless limit they are assumed to approach those given by Hammett and Perkins (1990). For this reason parallel viscosity is neglected (it is negligible along with electron inertia in the collisional regime), and one is left with the following system, which is to be valid for arbitrary collisionality:

$$\frac{\partial}{\partial t}\nabla_\perp^2\phi = V_e\nabla_\parallel(\mu_e u_\parallel - v_\parallel), \tag{3}$$

$$\frac{\partial n}{\partial t} = -\frac{c_s}{L_n}\frac{\partial\phi}{\partial y} - V_e\nabla_\parallel v_\parallel, \tag{4}$$

$$\frac{n_f}{2}\frac{\partial T}{\partial t} = -\frac{n_f}{2}\eta_e\frac{c_s}{L_n}\frac{\partial\phi}{\partial y} - V_e\nabla_\parallel\left[v_\parallel + \alpha\left(v_\parallel - \mu_e u_\parallel\right)\right] + \kappa_\parallel\nabla_\parallel^2 T, \tag{5}$$

$$\frac{\partial}{\partial t}v_\parallel = -V_e\nabla_\parallel\left[n + (1+\alpha)T - \phi\right] - \frac{\sqrt{\pi}}{4}\nu_e(v_\parallel - \mu_e u_\parallel), \tag{6}$$

$$\frac{\partial}{\partial t}u_\parallel = -\mu_e V_e\nabla_\parallel(\alpha T + \phi) + \frac{\sqrt{\pi}}{4}\nu_e(v_\parallel - \mu_e u_\parallel), \tag{7}$$

where $V_e = (T/m_e)^{1/2}$ and $\mu_e = (m_e/M_i)^{1/2}$ (note the difference between V_e and v_T above), n_f is the number of degrees of freedom, $\kappa_\parallel$ is the thermal conductivity, and

α is the thermal force coefficient. These last three quantities are those whose changes track the transition between collisionality extremes: In the collisional limit $\alpha = 3/2$, $\kappa_\parallel = 16\sqrt{\pi}(V_e^2/\nu_e)$, and $n_f = 3$ (Hassam 1980); in the collisionless limit $\alpha = 0$, $\kappa_\parallel = \sqrt{2/\pi}(V_e/|k_\parallel|)$, and $n_f = 1$ (Hammett and Perkins 1990). No change to the momentum transfer was assumed, since the collisional slowdown process does not depend on the mean free path. It remains only to provide the transition. To this end, Eqs. (3–7) were solved in the same way in the same situation as Eqs. (1,2) above, taking care to run at like parameters, *e. g.*, $k_\parallel v_T(L_n/c_s) = 4$ means $k_\parallel V_e(L_n/c_s) = 2\sqrt{2}$. The details of the way one effects the transition from $k_\parallel V_e \gg \nu_e$ to $k_\parallel V_e \ll \nu_e$ are somewhat arbitrary; it was chosen to do it via a roll-over of the form $(1 + ax^2)^{-1/2}$, with the constant a adjusted to get the best matching. This was settled at

$$\alpha = \frac{3/2}{\sqrt{1+3x^2}}, \qquad \kappa_\parallel = \sqrt{\frac{2}{\pi}}\left|\frac{V_e}{k_\parallel}\right| \frac{8\sqrt{2}x}{\sqrt{1+128x^2}}, \qquad n_f = 1 + \frac{2}{\sqrt{1+x^2}}, \tag{8}$$

where $x = |k_\parallel V_e/\nu_e|$. Final refinement of this procedure is still in progress.

III. Turbulence in the Sheared Slab

Making the foregoing transcollisional fluid model nonlinear in this electrostatic treatment is straightforward: simply replace each $(\partial/\partial t)$ by the ExB advective derivative: $(d/dt) = (\partial/\partial t) + \hat{\mathbf{z}} \cdot (\nabla\phi \times \nabla)$. In the sheared slab the parallel gradient becomes $\nabla_\parallel = x(\partial/\partial y)$, the $\nabla_\perp^2$ operator becomes $(\partial/\partial x)^2 + (\partial/\partial y)^2$, and in nonlinear cases there are several Fourier components, coupled variously through the ExB advection. In the linear regime stability was tested by multiplying the density gradient term by $(1+i\gamma_d)$, and allowing the external drive $\gamma_d \to 0$. It was observed in every case that the growth rate vanishes before γ_d reaches zero, proving that the linear waves are damped for all parameters.

Turbulence runs were initialised with adiabatic electrons in a broad-band, random-phase initial state for ϕ, with $n = \phi$ and $T = v = u = 0$. The initial amplitude was $2.0\rho_s/L_n$. The computational domain was $x \in [-20, 20]$ and $y \in [0, 2\pi/k_0]$, where $k_0 = 0.05$. The grid in x used 129 points, unequidistantly spaced, and 85 harmonics of k_0 were carried (see Scott 1992 for further details).

In the case of collisional drift wave turbulence, the turbulence is "self-sustaining": although all linear waves are damped, fluctuations at two separate scales, k_0^{-1} and Δ_D, are able to act coherently, greatly increasing the efficiency with which the free energy available in the density and temperature gradients is tapped (Scott 1990, 1992). Here, Δ_D is the hydrodynamic layer width–the distance from the resonant surface at which ${k_\parallel}^2 V_e^2/\nu_e \approx \omega_*$, where ω_* is the diamagnetic frequency of the wave whose k_y is k_0; more precisely defined, $\Delta_D = 0.51(\nu_e/\omega_*)(m_e/M_i)(L_s/L_n)^2$, and it takes values of 1–3ρ_s in tokamak edge regions. The self-sustainment may be alternatively termed a "nonlinear instability". It was open to the criticism that the large change expected in the dynamics of parallel dissipation caused by a lowering of the collisionality might invalidate it. Specifically, collisional thermal conduction is a purely dissipative process, while resonance with parallel motion through the inertia is reactive. It was then asserted (Scott 1992) that while this is so, it merely results in the replacement of ν_e by ω_* in Δ_D: there is still a hydrodynamic layer for the

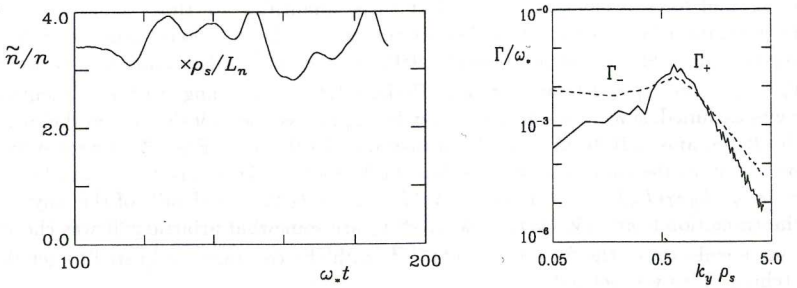

Fig. 1. Results for the collisionless case, with $\eta_e = 0.2$. (left) Density fluctuation amplitude, in terms of ρ_s/L_n. (right) Spectra of free energy source (Γ_+) and sink (Γ_-) rates, showing the net surplus at $k_y\Delta_D \sim 1$ and deficit at longer and shorter wavelengths.

same reason and with the same physics as before; it should just have a new definition, $\Delta_D \to (m_e/M_i)(L_s/L_n)^2$. To test this, a particular run was taken in the pure Hammett and Perkins (1990) collisionless system: Eqs. (3–7) with $\nu_e = 0$ and $\alpha = 0$, $n_f = 1$, and $\kappa_\parallel = \sqrt{2/\pi}(V_e/|k_\parallel|)$. A realistic mass ratio was used, $\mu_e = 1/42$, and L_s/L_n was 10. The time dependence of the fluctuation amplitude in saturation and the spectra of the source and sink rates of the energetics are shown in Fig. 1. These figures and other features of the mode structure are very much like those of collisional drift wave turbulence (see Scott, 1992, for the most detail), confirming the assertion that the parallel electron dynamics has the same role, irrespective of the collisionality regime. Although further investigation of the transcollisional system, Eqs. (3–7), is at this moment still in progress, it is reasonable to expect that the physical interactions responsible for the mode structure in saturation act in the same way in all collisionality regimes, and that the only differences will be in the quantitative amplitude and transport scaling.

References

Braginskii, S. I. (1965) in *Reviews of Plasma Physics*, M. A. Leontovich, ed. (Consultants Bureau, New York), Vol. 1, p. 205.

Dorland, B., and G. Hammett (1993) *Phys. Fluids B* 5, 812.

Hammett, G., and F. Perkins (1990) *Phys. Rev. Lett.* 64, 3019.

Hassam, A. B. (1980) *Phys. Fluids* 23, 38.

Scott, B. (1990) *Phys. Rev. Lett.* 65, 3289.

Scott, B. (1992) *Phys. Fluids B* 4, 2468.

Toroidal Gyrokinetic Simulation of Tokamak Turbulence and Transport

S. E. Parker, W.W. Lee, H.E. Mynick, G. Rewoldt, R.A. Santoro, and W.M. Tang
Princeton Plasma Physics Laboratory, Princeton University, Princeton, New Jersey, USA 08543

Recent developments in both nonlinear δf methods for gyrokinetic simulation[1], and massively parallel supercomputing now make it possible to simulate a sizable fraction of a tokamak plasma using realistic physical parameters. As a first step in utilizing these advances, a three dimensional electrostatic toroidal gyrokinetic simulation has been developed. Here, the code is used to investigate the nonlinear evolution of the ion temperature gradient (ITG) driven instability and the associated turbulence and transport. The ITG mode has long been considered a plausible candidate to explain the anomalous ion heat transport above neoclassical values in tokamak plasmas[2]. In these simulations, the ions are fully gyrokinetic, including trapped particles. The electrons are treated as adiabatic which permits a moderate size timestep (simulations with kinetic electrons are feasible, but the timestep would need to be smaller by the factor v_{te}/v_{ti}). The simulation is efficiently running on massively parallel supercomputers (currently the CM-200 and CM-5) which allow simulations of relatively large systems (e.g., $a \gtrsim 100\rho_i$ minor radius, $\Delta x \approx \rho_i$). Large scale runs have been made with one to *eight million particles* usually with one to two particles per grid cell, and with a cpu time of 2-3 microseconds per particle per timestep on a full 64K processor CM200. Fine grid resolution is needed in the toroidal direction because the mode structure is helical (elongated along the magnetic field lines i.e., $k_{\|} \ll k_{\perp}$), resulting in a smaller number of particles per grid cell relative to slab simulations.

The parameters for the simulation are as follows: 1 million particles, a 128x128x64 grid in (x, y, ψ), with a perpendicular grid cell size $\Delta x = \Delta y = \rho_s$, and a time step of $\Delta t c_s/L_T = 0.45$, $\epsilon_T \equiv L_T(r_0)/R_0 = 0.075$, $1/L_n(r_0) = 0$, $T_i = T_e$, $a = 64\rho_s$, and $R_0 = 892\rho_s$, $q_0 = 1.25$, $\Delta q = 3$, $l = 20\rho_s$, $r_0 = \frac{1}{2}a$ (r_0 and l are defined below), $q(r_0) = 2$, $\hat{s} \equiv \dfrac{r}{q}\dfrac{dq}{dr} = 0.75$ at r_0. The local parameters at $r = r_0$ are similar to the TFTR perturbed supershot experiment[3], except for the aspect ratio. Another connection to the TFTR plasma is the nonlinear fluctuation spectra taken from the simulation as shown in Figs. 1(a) and (b),

[1] S.E. Parker and W.W. Lee, Phys. Fluids B 5 77 (1993).
[2] W.M. Tang and G. Rewoldt, to appear Phys. Fluids B 1993
[3] M.C. Zarnstorff, et al., Proc. of the 13th Int. Conf. on Plasma Phys. and Contr. Nucl. Fus. Res., Washington D.C., 1990, Vol. 1, p. 39.

which resemble the recent beam emission spectroscopy (BES) fluctuation measurements [4].

Let us elaborate. In the initial phase of the run, we observe a clean linear growth of the most unstable toroidal harmonic and the associated 2D eigenmode in (r, θ) with a ballooning type mode structure [see Fig. 2 (a) and (b)]. Linear comparisons with detailed eigenmode calculations of Rewoldt and Tang[2] show agreement to within 15% in terms of real frequency, growth rate and mode structure. In the steady-state, both long and short perpendicular wavelengths are enhanced with the spectrum peaking around $k_r\rho_s \sim 0$ and $k_\theta\rho_s \sim 0.1-0.2$, and the ballooning structure reduced, but still prevalent [see Fig. 2 (d) and (e)]. Broad scale (i.e., many modes are present) turbulence with a fluctuation level of $e|\phi_k|/T \lesssim 1\%$ is observed. Fig. 2 (c) and (f) show the excited poloidal and toroidal harmonics (m, n) at the $q(r = \frac{1}{2}a)$ flux surface, for the linear and nonlinear phases. The size of the circle indicates the amplitude of the modes. A downward shift in the dominant (m, n) from the linearly most unstable mode is observed. The dominant eigenmode grows linearly and saturates at a level of $e|\phi(r = r_0, \theta = 0, n = 4)|/T_e = 0.03$, which is in the range of the mixing length level $1/(k_\perp L_T) = 0.06$, using $k_\perp \approx k_\theta$. At saturation, $\chi_i = 1.6\rho_s^2 c_s/L_T$ taken at $r = r_0$, then drops to a steady-state value of $\chi_i = 0.2\rho_s^2 c_s/L_T$; for comparison $\gamma/k_\perp^2 = 0.5\rho_s^2 c_s/L_T$.

Figures 1(a) and (b) are the k_θ and k_r spectra taken at the turbulent steady-state of a run with $a = 64\rho_s$. These measurements were made over the half annular region of $\theta \in [-\pi/2, +\pi/2]$, $r \in [\frac{1}{4}a, \frac{3}{4}a]$ and $\psi \in [-\pi, \pi]$. The region has approximately a $32\rho_s$ $(= a/2)$ radial width and a $100\rho_s$ $(= \pi a/2)$ poloidal length. Figures 1(a) and (b) give $S(k_\theta) \equiv \sum_{n,k_r} |\phi(k_r, k_\theta, n)|^2$ and $S(k_r) \equiv \sum_{n,k_\theta} |\phi(k_r, k_\theta, n)|^2$, respectively. These measurements show similar features as the recent BES experimental measurements in that the k_r spectrum peaks at zero and k_θ spectrum peaks in the range of $k_\theta\rho_s \sim$ 0.1-0.2. These properties of the spectrum have so far been found to be fairly insensitive to the choice of simulation parameters. One notable difference between the numerical result and the experimental measurement is that the width in the k_r spectrum is broader in the simulation. One possible explanation is that the small minor radius of the simulation causes more localization of the modes radially, hence artificially broadening the k_r spectrum. This will be tested in the future by increasing the size of the simulation.

Lastly, let us briefly describe our simulation model. Starting with the electrostatic gyrokinetic equations with a nonuniform equilibrium B-field[5], we write $f(\mathbf{z}, t) = f_0(\mathbf{z}) + \delta f(\mathbf{z}, t)$, where $\mathbf{z} = (\mathbf{R}, v_\parallel, \mu)$; and expand $\dot{\mathbf{z}}$ into its equilibrium and perturbed parts: $\dot{\mathbf{z}} = \dot{\mathbf{z}}^0 + \dot{\mathbf{z}}^1$. $f_0(\mathbf{z})$ is a Maxwellian. The equation for the perturbed ion distribution function δf is then[1] $\partial_t \delta f + \dot{\mathbf{z}} \cdot \partial_{\mathbf{z}} \delta f = -\dot{\mathbf{z}}^1 \cdot \partial_{\mathbf{z}} f_0$. The particles follow their full nonlinear trajectories, δf is represented by $B\delta f(\mathbf{z}, t) = \sum_i w_i \delta(\mathbf{z} - \mathbf{z}_i)$, and particle weight w_i is then evolved using[1] $\dot{w}_i = -(1 - w_i)\left[\dot{\mathbf{z}}^1 \cdot \partial_{\mathbf{z}} f_0/f_0\right]_{\mathbf{z}=\mathbf{z}_i,t}$. As usual, finite size particles are used in the configuration space. The electrons are are assumed adiabatic ($\delta n_e = n_0 e\phi/T_e$). A square cross-section is used which is suitable for spectral solution of the field equation. The coordinates (x, y, ψ) in terms of the usual toroidal coordinates (r, θ, ψ) are: ($x = r\cos\theta, y = r\sin\theta, \psi$). We assume $(k_\parallel/k_\perp)(B_\theta/B_\psi) \ll 1$, and neglect the variation in ρ_i

[4] R Fonck, et al., Plasma Phys. and Contr. Fus. **32** 1993 (1992)

[5] T.S. Hahm, Phys. Fluids **31** 2670 (1988).

and ρ_s in the field equation obtaining the familiar gyrokinetic "Poisson" equation[6]. For the radial boundary condition we set the perturbed ion density to zero for $r \geq (a - 4\rho_s)$ within the square cross-section. The magnetic field is fixed and specified using $B_\psi = B_0 R_0/R$, $B_\theta = rB_\psi/R_0 q(r)$, and $q(r) = q_0 + \Delta q(r/a)^2$. Initial equilibrium density and temperature profiles are used such that $L_n^{-1} \equiv |\nabla n|/n$ and $L_T^{-1} \equiv |\nabla T|/T$ have a radial variation proportional to $\mathrm{sech}^2[(r - r_0)/l]$, where r_0 and l as well as the peak normalized gradients $L_n^{-1}(r_0)$ and $L_T^{-1}(r_0)$ are all specified parameters. For the results presented, the particles are loaded homogeneously and the variation in the profile appears only in the right hand side of Eq. (4).

We have demonstrated the feasibility of using large scale nonlinear gyrokinetic simulations to study the nonlinear evolution of kinetic microinstabilities. Current whole tokamak simulations are limited to minor radii of 100-200ρ_s. In the future, teraflop scale massively parallel supercomputers will allow simulations with a minor radius in the range of 500ρ_s, which is typical of the size of present day tokamaks. Future work will include adding a more detailed kinetic electron model (including the trapped fraction), electromagnetic perturbations, and collisional effects.

Work supported by the U.S. DOE Contract No. DE-AC02-76-CHO-3073. Computing resources where provided by the Advanced Computer Laboratory, Los Alamos National Laboratory.

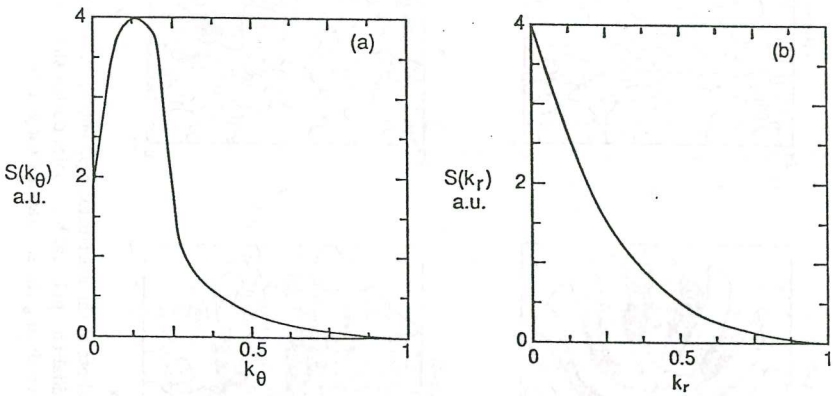

Figure 1: Wavelength fluctuation spectrum for k_θ and k_r. (a) Fluctuation energy vs. k_θ, and (b) fluctuation energy vs. k_r. k_r and k_θ are in units of ρ_s^{-1}, and S is in arbitrary units.

[6]W.W. Lee, J. Comput. Phys. 72, 243 (1987).

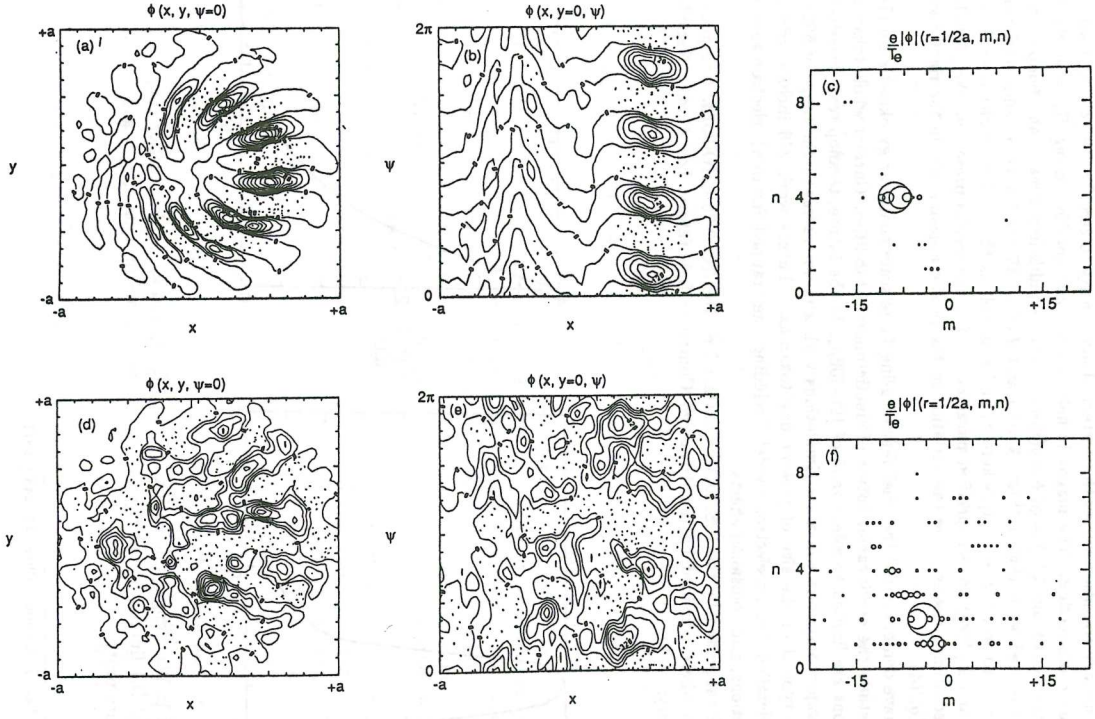

Figure 2: Snapshots of the electrostatic potential. (a) Poloidal and (b) toroidal cross-sections during the linear phase, (c) excited toroidal and poloidal harmonics during the linear phase at the $r = \frac{1}{2}a$, $q = 2$ surface; (d)-(f) are the same diagnostics, taken during the saturated steady-state.

Self-Regulated Shear Flow Turbulence in Confined Plasmas

B. A. Carreras, L. A. Charlton, and K. Sidikman
Oak Ridge National Laboratory, Oak Ridge, TN 37830-8070

P. H. Diamond
University of California at San Diego, La Jolla, CA 92093-0319

L. Garcia
Universidad Carlos III, Madrid, Spain

I. Introduction

Simple considerations of momentum balance in a cylindrical plasma indicate that the radial profile of poloidal flow evolves according to

$$\left(\frac{\partial}{\partial t}+\mu\right)\langle V_\theta(r)\rangle=-\frac{1}{r^2}\frac{\partial}{\partial r}\left(r^2\langle\tilde{V}_r\tilde{V}_\theta\rangle-\frac{1}{n_0 m_i\mu_0}r^2\langle\tilde{B}_r\tilde{B}_\theta\rangle\right). \qquad (1)$$

Here $\langle\tilde{V}_r\tilde{V}_\theta\rangle$ and $\langle\tilde{B}_r\tilde{B}_\theta\rangle$ are the Reynolds stress and magnetic Reynolds stress, respectively; μ represents a generic collisional damping; n_0 is the ion density; and m_i is the ion mass. The angular brackets, $\langle\ \rangle$, indicate average over toroidal and poloidal angles at a fixed radial position. It is apparent that flow evolution requires

(a) a net imbalance between fluid stresses (related to vorticity transport) and magnetic stresses (related to magnetic-flutter-induced electron particle transport) associated with a local (i.e., not averaged over fluctuation correlation length) ambipolarity breakdown;

(b) a radially inhomogeneous fluctuation spectrum (i.e., local symmetry breaking); and

(c) a local radial wave propagation mechanism active in the fluctuation dynamics.

Furthermore, it is clear from Eq. (1) that fluid and magnetic stresses only act (up to end-point contributions and ionization effects) to locally redistribute poloidal momentum and cannot generate it. Thus, flow profile modification should be thought of as a mechanism for local amplification of flow shear or flow curvature.

The need for a radially inhomogeneous fluctuation spectrum has been shown analytically and numerically. For the long-wave-length drift wave turbulence model,[1] where a radial inhomogeneity can result from self-binding effects near low-q resonances and edge effects, the calculated Reynolds stress is nonzero only in these spatial regions. In tokamaks, the radial inhomogeneity of the turbulence is particularly important at the plasma edge. Tokamak edge plasmas in OH or L-mode are characterized by large fluctuation levels[2] and strong radial symmetry breaking (i.e., boundaries, or just the observation that $\Delta r/L_n \le 1$, where Δr is the radial correlation length and L_n is the gradient scale). Thus, it is clear that edge flows will be regulated by fluctuations. Indeed, the only real question is the mechanism for radial propagation. The possibilities include

(a) diamagnetically induced radial wave propagation in the ambient fluctuations, and

(b) seed shears (V_θ') and dilatations (V_θ''), which in turn induce radial propagation.[3]

Here, we consider only the second mechanism.

II. Poloidal Shear Flow Amplification.

Let us consider the parallel ion flow gradient driven (PIFGD) instability, in the limits of flat density and $V_{\|0} << c_s$. In this instability model, poloidal shear (V_θ') amplification may occur if $x \rightarrow -x$ symmetry of the fluctuation spectrum is broken and a seed shear is ambient. A reduced set of equations has been derived in reference 4 to study this instability in slab geometry. The equations for the fluctuating quantities are

$$\left(\frac{\partial}{\partial t}+V_\theta(x)\frac{\partial}{\partial y}\right)\left(\tilde{n}-\rho_s^2\nabla_\perp^2\tilde{n}\right)+V_{*_n}\frac{\partial\tilde{n}}{\partial y}+L_nD_0\left[\vec{\nabla}_\perp\left(\frac{\partial\tilde{n}}{\partial y}\right)\times\hat{z}\right]\cdot\vec{\nabla}_\perp\tilde{n}-D_0\frac{\partial^2\tilde{n}_i}{\partial y^2}$$
$$+\rho_sc_s\left[\vec{\nabla}_\perp\tilde{n}\times\hat{z}\right]\cdot\vec{\nabla}_\perp\left(\rho_s^2\nabla_\perp^2\tilde{n}\right)+\rho_sc_s\frac{\partial\tilde{n}}{\partial y}\frac{\partial}{\partial x}\left(\rho_s^2\frac{\partial^2\langle n\rangle}{\partial x^2}\right)-c_s\nabla_\|\tilde{V}_\|=0\,, \qquad (2)$$

$$\frac{\partial\tilde{V}_\|}{\partial t}+V_\theta(x)\frac{\partial\tilde{V}_\|}{\partial y}-\rho_sc_s\vec{\nabla}\tilde{n}\times\vec{z}\cdot\vec{\nabla}\tilde{V}_\|=-c_s\nabla_\|\tilde{n}-V_{*V}\frac{\partial\tilde{n}}{\partial y}\,, \qquad (3)$$

and the average poloidal flow evolution is given by

$$\frac{\partial\langle V_\theta\rangle}{\partial t}=\rho_s^2c_s^2\frac{\partial}{\partial x}\left\langle\frac{\partial\tilde{n}}{\partial x}\frac{\partial\tilde{n}}{\partial y}\right\rangle-\mu\langle V_\theta\rangle. \qquad (4)$$

Here, $V_{*V}=\rho_s(dV_{\|0}/dr)$ is the diamagnetic drift velocity for the parallel velocity. These equations are derived with the approximation of quasiadiabatic electrons, $\tilde{\Phi}$ = [1-(D_0 / V_{*_n}) $\partial\tilde{n}/\partial y$], where $V_{*_n}=c_s\,\rho_s/\,L_n$ is the diamagnetic drift velocity, $\rho_s = c_s/\Omega_i$, $D_0=1.71V_{*_n}^2\eta_e/\chi_\|\overline{k_\|^2}$, $\eta_e = L_n/L_T$, and $\overline{k_\|^2}$ is the average parallel wave number. In this derivation, $\eta_e >> k_\perp^2\rho_s^2$ has been assumed. The instability source is the gradient of the parallel velocity.

The PIFGD instability is a negative compressibility instability. In the flat density limit $(V_{*_n}=0)$ with no external poloidal flow $(V_\theta=0)$, and for low-k modes, the instability is purely growing with the linear growth rate $\gamma=k_y\rho_s|V_{\|0}'|/2$. The parallel flow gradient shifts the instability away from the resonant surface by a distance $\delta_\|=\rho_sL_sV_{\|0}'/2c_s$, and the eigenfunction is radially localized by coupling to sound waves. The radial width of the eigenfunction is $W^2=\gamma\rho_sL_s/k_yc_s$. In this limit, the PIFGD instability does not propagate radially, and thus does not contribute to the Reynolds stress. The addition of a shear poloidal flow, $V_\theta(x)=V_0'u$, with $u=x-\delta_\|$, reduces the growth rate to $\gamma=k_y\rho_s|V_{\|0}'|\left[1-\left(L_sV_{\theta0}'/c_s\right)^2\right]^{1/2}/2$ and modifies the eigenfunction, $\tilde{n}=\bar{n}\exp\left[-(u-i\delta_\perp)^2/2W^2\right]\exp(\gamma t+ik_yy)$. The imaginary part of the eigenfunction shift, $\delta_\perp=-\gamma L_s^2V_{\theta0}'/k_yc_s^2$, induces radial propagation of the instability. Hence, the presence of the poloidal shear flow induces the symmetry-breaking effect needed for this instability to generate a nonzero Reynolds stress. The straightforward result is that the inclusion of a small, constant seed shear flow yields

$$\frac{\partial \langle V_\theta' \rangle|_{u=0}}{\partial t} + \mu \langle V_\theta' \rangle|_{u=0} = 2 \langle V_\theta' \rangle|_{u=0} \sum_k \frac{k_y^2 \rho_s^2 |\tilde{n}_k|^2 \Omega_i^2}{\gamma_k} \quad (5)$$

and

$$\frac{\partial \langle V_\theta'' \rangle|_{u=0}}{\partial t} + \mu \langle V_\theta'' \rangle|_{u=0} = 0. \quad (6)$$

Thus, the seed shear is amplified, while no curvature generation occurs. It is interesting to note that in this case, the seed shear itself induced the radial propagation necessary for a nonzero Reynolds stress. Furthermore, Eq. (6) naturally defines a critical $\tilde{n}/n$ necessary for the onset of amplification, $|\tilde{n}_k|^2 \approx \mu \gamma_k / 2 k_y^2 \rho_s^2 \Omega_i^2$. For density fluctuation levels above the threshold but low enough that they are in the linear regime, the gradient of the poloidal flow increases faster than exponential

$$\frac{\partial \ln\left(\langle V_\theta' \rangle|_{u=0}\right)}{\partial t} = 2 \sum_k \frac{k_y^2 \rho_s^2 |\tilde{n}_k|^2_{t=0} e^{2\gamma_k t} \Omega_i^2}{\gamma_k} - \mu. \quad (7)$$

In this regime, when a single mode dominates the spectrum, the poloidal flow shear has a radial dependence like the second derivative of a Gaussian (see Eq. 4).

To test these results, nonlinear calculations in the single helicity limit have been performed using the KITE code.[5] Typical tokamak plasma edge parameters have been used, with $c_s = 3.76 \times 10^6$ cm/sec, $\rho_s = 1.98 \times 10^{-2}$ cm, $L_s = 156$ cm, and an effective collisionality $\mu = 295$ sec^{-1}. In this test of the analytical theory, the value of the gradient of the parallel flow has been taken artificially large, $V'_{0\|} = 2.65 \times 10^6$ sec^{-1}, for the purpose of having a large growth for the instability. These calculations have been performed for the 8/3 helicity, using 45 components with poloidal mode numbers ranging from $m = -176$ to $m = 176$.

The perturbations have been initialized to a very low level: $\tilde{n}/n_0 \approx 10^{-8}$. In this way, their evolution has a relatively long period of exponential growth. When the density fluctuations reach a critical level, $\langle V_\theta' \rangle$ grows sharply (Fig. 1). If we define the normalized shearing rate as $\Omega_s' \equiv k_y \langle V_\theta' \rangle|_{x=0} W / \gamma_k$, there is a sudden quenching of the fluctuations when $\Omega_s' > 10$. Three different values for the poloidal seed flow have been considered: $V_0' = 2.65 \times 10^{-5}$ sec^{-1}, $V_0' = 2.65$ sec^{-1}, and $V_0' = 331.25$ sec^{-1}. The nonlinear evolution is very similar for these three initial conditions and follows the pattern just described. The threshold in the fluctuation level for flow amplification is approximately the same for these three values of the seed flow. This result has been illustrated in Fig. 2, where we plotted the increment of the poloidal shear flow, $\langle V_\theta' \rangle - V_0'$, versus the density fluctuation level. In the three calculations, the poloidal flow amplification begins at about $|\tilde{n}/n_0| \approx 8.1 \times 10^{-4}$, in good agreement with the analytical prediction, $|\tilde{n}/n_0| \approx 6.1 \times 10^{-4}$. The poloidal flow gradient steepens at about $r \approx 0.89\ a$, the radial position of the peak of the instability. The $\langle V_\theta' \rangle$ radial profile is close to the second derivative of a Gaussian.

During the exponential growth regime of the fluctuations, $\langle V_\theta' \rangle$ grows faster than exponentially, as is shown in Fig. 3. In this figure we have plotted $\langle V_\theta' \rangle$ and $\ln(\langle V_\theta' \rangle / V_0')$, both in logarithmic scales. It is clear that $\ln(\langle V_\theta' \rangle / V_0')$ is well described by an exponential dependence in time, and the detailed time evolution of $\langle V_\theta' \rangle$ is well described by Eq. (7).

ACKNOWLEDGMENT

* Research sponsored by the Office of Fusion Energy, U.S. Department of Energy, under contract DE-AC05-84OR21400 with Martin Marietta Energy Systems, Inc.

REFERENCES

1. B. A. Carreras et al., Phys. Fluid B 4 (1992).
2. A. J. Wootton et al., Phys. Fluids B 2, 2379 (1990).
3. J. F. Drake et al., Phys. Fluids B 4, 488 (1992).
4. A. S. Ware et al., Phys. Fluids B 4, 102 (1991).
5. L. Garcia et al., J. Comput. Phys. 65, 253 (1986).

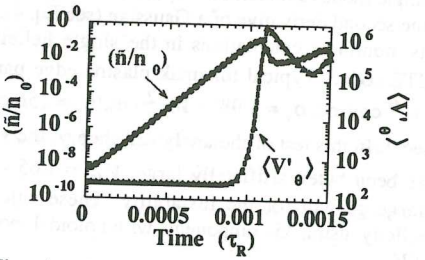

Fig. 1. Time evolution of the density fluctuations and average shear poloidal flow.

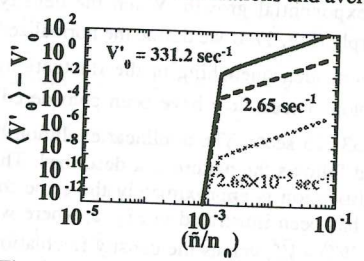

Fig. 2. There is a threshold on the fluctuation level to cause flow profile modification.

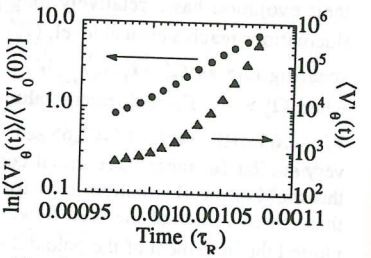

Fig. 3. The average poloidal flow increases faster than exponential.

STEADY STATE EQUATIONS FOR A TOKAMAK PLASMA WITH STRONG ELECTRIC FIELD AND LARGE FLOW

C. S. Chang* and H. Strauss
Courant Institute of Mathematical Sciences
New York University, U.S.A.

Studies of plasmas with the properties of strong radial electric field and large rotation has recently been quite active. In order to put such studies on more solid footings, it is important to understand and establish the fundamental physical processes of plasmas at large mass rotation, which can be quite different from the usual understandings we have for small rotation cases.

In the present report, for simplicity and physical clarity, we use the circular flux surface geometry of Shafranov.[1] The minor radius of a flux surface is denoted by r and its center is given by the major radius $R_0(r)$. The poloidal angle relative to the center of the flux surface is denoted by θ, and the angular dependence of the major radius on a flux surface is denoted by $R(r,\theta)/R_0(r) \equiv h(r,\theta)$, where $h = 1 + \epsilon\cos\theta$, $\epsilon = r/R_0$. Then the toroidal magnetic field strength B_ζ satisfies $B_\zeta = B_{\zeta 0}/h \cong B$ on a magnetic surface, where $B_{\zeta 0}$ is B_ζ at the center of the flux surface and $B = \sqrt{B_\zeta^2 + B_\theta^2}$.

The angular dependence of the poloidal magnetic field strenth B_θ is described by a parameter Λ, $B_\theta = B_{\theta 0}(r)(1 + \epsilon\Lambda\cos\theta)$, where $B_{\theta 0}$ is the θ averaged value of B_θ. Poloidal flux ψ, then, exhibits the property

$$\nabla\psi = \hat{r}\, RB_\theta = \hat{r}\, R_0 B_{\theta 0}[1 + \epsilon(1+\Lambda)\cos\theta] = \hat{r}\,[1 + \epsilon(1+\Lambda)\cos\theta]\frac{\partial\psi}{\partial r} \qquad (1)$$

and the quantity $\epsilon(1+\Lambda) = -R_0'$ represents shift of flux surfaces.

A physical quantity Y on a flux surface is separated into the θ averaged part $\overline{Y}$ and the θ dependent part $\tilde{Y}$. For a linear analysis, it is necessary to assume that $\tilde{Y} = \mathcal{O}(\epsilon\overline{Y})$ and ϵ is small.

The basic set of equations we consider in the present work, in addition to the usual Maxwell's equations, are the steady state continuity and force balance equations:

$$\nabla \cdot n\vec{V} = 0, \qquad (2)$$

$$\nabla p + m_i n\vec{V}\cdot\nabla\vec{V} + \nabla\cdot\mathbf{\Pi} - \vec{j}\times\vec{B} = \vec{F}^{Anom}. \qquad (3)$$

where $m_e(m_i)$ is the electron (ion) mass, n is the electron or ion density with $n = n_e = n_i$, the electron inertia has been neglected, $\mathbf{\Pi}$ is the plasma stress tensor corresponding to the anisotropic part of the pressure tensor, and $\vec{F}^{Anom}$ represents any possible anomalous force on the plasma including those from turbulence, beam injection, orbit loss, and other edge effects. We assume that F^{Anom} is not strong enough to influence the force balance equation to the lowest order, but it is strong enough to influence an averaged force balance relationship. In the present work we assume, for simplicity, that the ions are adiabatic and the electrons are isothermal.

The plasma mass flow can be devided into perpendicular and parallel parts relative to the equilibrium magnetic field $\vec{B}$: $\vec{V} = \vec{V}_\perp + \vec{V}_\parallel$. Here, the perpendicular mass

flow is taken to the $E \times B$ drift: $\vec{V}_\perp = (c/B)\hat{b} \times \nabla\phi$, where $\hat{b} = \vec{B}/B$. We can consider that the electrostatic potential ϕ is approximately constant on a flux surface, $\phi = \phi(\psi)$, if we assume that the potential difference $\Delta_r\phi$ in the radial direction across the large $V_\perp$ layer is larger than the potential variation in the poloidal direction, $\Delta_r\phi \gg r\nabla_\theta\phi$. This condition can usually be justified in an H-mode layer since the plasma exhibits the relation $\Delta_r\phi \gg kT/e$ while $r\nabla_\theta\phi \lesssim \epsilon kT/e$. By writing $\nabla\overline{\phi}$ in the form, $\nabla\overline{\phi} = \gamma\nabla\psi$, the perpendicular flow can be expressed as

$$\vec{V}_\perp = V_\perp \hat{e}_\perp, \quad V_\perp = c\gamma\nabla\psi/B = \overline{V}_\perp[1 + \epsilon(2+\Lambda)\cos\theta] \tag{4}$$

where $\hat{e}_\perp$ is the unit vector in the direction $\hat{b} \times \nabla\psi$, and Eq. (1) has been used.

The parellel flow information can be obtained from the continuity equation (2) $\nabla \cdot n\vec{V}_\perp + \nabla \cdot (n\vec{B}V_\parallel/B) = 0$. Using the property $\nabla \cdot \vec{B} = 0$ and Eq. (4), we obtain$n\hat{b} \cdot \nabla\tilde{V}_\parallel = -\overline{V}_\perp(B/B_\theta)\,\hat{b} \cdot (n\nabla h + \nabla nh) - nV_\parallel\hat{b} \cdot \nabla(nh)$, which becomes, in the linear limit,

$$\tilde{V}_\parallel = -(\overline{V}_\perp/b_\theta)(\tilde{n}/\overline{n} + 2\epsilon\cos\theta) - \overline{V}_\parallel(\tilde{n}/\overline{n} + \epsilon\cos\theta) = -(\overline{V}_\theta/b_\theta)[\tilde{n}/\overline{n} + \epsilon(\gamma+1)\cos\theta], \tag{5}$$

where $b_\theta = \overline{B}_\theta/\overline{B}$ and γ is the ratio between the perpendicular flow and the poloidal flow speeds, $\gamma = \overline{V}_\perp/\overline{V}_\theta = \overline{V}_\perp/(\overline{V}_\theta + b_\theta\overline{V}_\parallel)$. A general expression for the poloidal rotation speed V_θ is then written as

$$V_\theta = (B_\zeta/B)V_\perp + b_\theta\overline{V}_\parallel + b_\theta\tilde{V}_\parallel = \overline{V}_\theta[1 - \frac{\tilde{n}}{\overline{n}} + \epsilon\{\gamma(\Lambda+1) - 1\}\cos\theta].$$

We use the plasma viscosity tensor $\mathbf{\Pi}$ of by Chew-Goldberger-Low.
From Ref. [2], we have:

$$\Pi_\parallel = -2\Pi_\perp = \frac{2}{3}(P_\parallel - P_\perp) = m_i n_i v_i^2 \hat{V}_\theta(\mu_1\tilde{X} - \mu_2 r\hat{\theta} \cdot \nabla\tilde{X}),$$

$$\vec{B} \cdot \nabla \cdot \mathbf{\Pi} = \frac{2}{3}\vec{B} \cdot \nabla(P_\parallel - P_\perp) - (P_\parallel - P_\perp)\frac{\vec{B} \cdot \nabla B}{B},$$

where $\tilde{X}$ is the velocity strain

$$\tilde{X} = r\hat{\theta} \cdot \nabla[(\tilde{n}/\overline{n}) + (2\gamma+1)\tilde{h}]. \tag{6}$$

The heat flow driven part of viscosity is not considered here. It is because of the assumption that the convective energy flow due to large mass motion dominates over the thermal flow.

For μ_1 and μ_2, we use the analytic form of Ref. [2]:

$$\mu_1 \simeq \frac{2}{3}\frac{\hat{\nu}_c}{1 + \hat{\nu}_c^2 + \hat{V}_\theta^2} + \frac{2\sqrt{\pi}}{3}\frac{\hat{\nu}_c^2}{\hat{\nu}_c^2 + \epsilon^3}e^{-\hat{V}_\theta^2}(1 - 2\hat{V}_\theta^2 + 2\hat{V}_\theta^4)e^{-2\hat{\nu}_c}, \tag{7}$$

$$\mu_2 \simeq \frac{2}{3}\frac{\hat{V}_\theta}{1 + \hat{\nu}_c^2 + \hat{V}_\theta^2}\left[\frac{\hat{\nu}_c}{1 + \hat{\nu}_c} + \frac{3}{2}\frac{(1.2 - \hat{V}_\theta^2)^2\{(1.8 - \hat{V}_\theta^2)^2 + 50\}}{200 + \hat{V}_\theta^8}e^{-\hat{\nu}_c}\right]. \tag{8}$$

The viscosity coefficient μ_2 has usually been neglected in the limit of small poloidal flow speed. However, we find that μ_2 is not negligible compared to μ_1 for finite

poloidal rotation speeds. As a matter of fact, μ_2 becomes more significant as the poloidal flow speed gets larger.

From the so called "vorticity equation," which is obtained by taking cross-product of Eq. (3) by $\vec{B}/B^2$, it can be shown that the magnetic shift parameter Λ satisfies the relation

$$1+\Lambda = \frac{1}{1-\gamma\alpha^2}\left[\frac{8\pi(<\overline{p}>-\overline{p})}{B_{\theta 0}^2}+\frac{\ell_i}{2}+\gamma\alpha^2\right], \tag{9}$$

where $\ell_i = <B_{\theta 0}^2>/2B_{\theta 0}^2$ is the internal inductance and $\alpha \equiv \overline{V}_\theta/b_\theta V_A$ is the poloidal speed normalized to the poloidal component of the parallel Alfven speed V_A.

Notice that the value of Λ grows as $\gamma\alpha^2$ approaches unity in Eq. (9) and it exhibits the Alfven resonance behavior at $\gamma\alpha^2 = 1$. It is obvious that for $\gamma\alpha^2 \sim 1$, a nonlinear analysis may be required, including the Kelvin-Helmholtz type of instabilities.[3]. It can be seen that the shift amount at a reasonable value of $\overline{V}_\theta \sim 1/4$ (corresponding to $\alpha \sim 0.1$) can be twice as large as that by the β and ℓ_i alone in a typical H-mode layer.

Poloidal plasma density variation due to poloidal flow can be calculated from the parallel component of the plasma force balance equation (3):

$$\nabla_\parallel P + m_i n(\vec{V}\cdot\nabla\vec{V})_\parallel + (\nabla\cdot\vec{\Pi})_\parallel = F_\parallel^{Anom}. \tag{10}$$

The following solutions for the sin and cos θ components of the density variations are obtained

$$\hat{n}_s = n_s/\overline{n} = \epsilon\frac{\alpha b_\theta\hat{\mu}_1[(2\gamma+1)\beta_* - \alpha^2]}{[\beta_* - \alpha\{\alpha - b_\theta\hat{\mu}_2\}]^2 + \{\alpha b_\theta\hat{\mu}_1\}^2}, \tag{11}$$

$$\hat{n}_c = n_c/\overline{n} = \epsilon\frac{\alpha[\beta_* - \alpha\{\alpha - b_\theta\hat{\mu}_2\}]\{2\gamma\alpha - (2\gamma+1)b_\theta\hat{\mu}_2\} - (2\gamma+1)(\alpha b_\theta\hat{\mu}_1)^2}{[\beta_* - \alpha\{\alpha - b_\theta\hat{\mu}_2\}]^2 + \{\alpha b_\theta\hat{\mu}_1\}^2} \tag{12}$$

where the dimensionless parameters are defined as

$$\beta_* \equiv \frac{T_e + \frac{5}{3}T_i}{m_i V_A^2} = \frac{1}{2}\beta_e + \frac{5}{6}\beta_i, \quad \hat{n} \equiv \frac{\tilde{n}}{\overline{n}}, \quad \alpha \equiv \frac{\overline{V}_\theta}{b_\theta V_A}, \quad \hat{\mu}_{1,2} \equiv \frac{v_i}{V_A}\mu_{1,2}.$$

Notice that the up-down density variation $\hat{n}_s$ is driven by the viscous drag of the poloidal flow motion. On the other hand, the in-out density asymmetry $\hat{n}_c$ is driven by the interaction of the rotating plasma with ∇B. Notice also that there is a resonance structure at "poloidal Mach number=1,"denoted by $\alpha \sim \sqrt{\beta_*}$, or by $\overline{V}_\theta^2 \sim b_\theta(T_e + 5T_i/3)/m_i$. Since the normalized density variation is only allowed up to unity, a renormalization of the density variation near the resonance is necessary for a smooth transition across the resonance layer.

From the flux surface averaged parallel force balance equation,

$$\left\langle \vec{B}\cdot\nabla P\right\rangle + \left\langle \vec{B}\cdot m_i n\vec{V}\cdot\nabla\vec{V}\right\rangle + \left\langle \vec{B}\cdot\nabla\cdot\vec{\Pi}\right\rangle = \left\langle \vec{B}\cdot F_\parallel^{Anom}\right\rangle, \tag{13}$$

we obtain

$$\frac{1}{2}\alpha b_\theta\epsilon\left[\alpha\hat{n}_s\{(1+\Lambda)(1-\gamma)+1\} + \frac{3}{2}\{\hat{\mu}_1[(2\gamma+1)\epsilon + n_c] - \hat{\mu}_2\hat{n}_s\}\right]$$
$$= \frac{r}{m_i\overline{n}B_0V_A^2}\left\langle BF_\parallel^{Anom}\right\rangle. \tag{14}$$

This equation gives the balance between the flux surface averaged parallel plasma resistance force at the flow speed α and the parallel external force $F_{\|}^{Anom}$. For any combination of anomalous forces (including those by turbulence and orbit loss effect), the parallel component will have to satisfy this equation for a steady state plasma flow.

If we multiply the poloidal force balance equation by B_0^2/B^2 and integrate over θ, the ambipolarity relation $\int d\theta j_r/B = 0$ anihilates the unspecified radial current term, yielding

$$\epsilon \left[\beta_* \hat{n}_s - 0.5\alpha^2 b_\theta^2 \{1 + \gamma(\Lambda + 1)\}\hat{n}_s + 2\alpha\hat{\mu}_1\{(2\gamma + 1)\epsilon + \hat{n}_c\} - 2\alpha\hat{\mu}_2\hat{n}_s\right]$$
$$= \frac{r}{m_i \overline{n} V_A^2} \frac{1}{2\pi} \int_0^{2\pi} d\theta h^2 F_\theta^{Anom}. \qquad (15)$$

The first term in the left hand side is from the pressure force ∇P, the second is from the convection force, and the third is from the viscous force. It can be easily seen that the convective force is smaller than the pressure force by $\sim \overline{V}_\theta^2/v_i^2$.

Both of the force balance equations should be satisfied simultaneously for a steady state equilibrium in a tokamak. Preliminary studies of the present force balance equations show that, in the presence of an anomalous force, a few different equilibrium solutions are possible at large poloidal rotation speeds. The actual solution for the equilibrium poloidal rotation speed is also function of the toroidal flow speed. It was able to be concluded that the large negative poloidal rotation equilibrium can be easierly obtained with a net neutral beam momentum input in the negative toroidal direction than with the momentum input in the positive toroidal direction. Since the orbit loss alone would yield an anomalous momentum input mainly in the parallel direction, and the parallel plasma force is much weaker than the poloidal plasma force it likely that the orbit loss force alone can not be responsible for the H-mode equilibrium.

This work was supported by the U.S. Department of Energy.

References

[1] V. D. Shafranov, in *Reviews of Plasma Physics*, edited by M. A. Leontovich (Consutants Bureau, New York, 1966), Vol. 2, p. 103.

[2] C. S. Chang, Submitted to Phys. Fluids B.

[3] H. Strauss, Phys. Fluids B **5**, (1993).

[4] K. C. Shaing, R. D. Hazeltine, and H. Sanuki, Phys. Fluids B **4**, 404 (1992).

---

*Also at Korea Advanced Institute of Science and Technology.

Theory of L-mode, L/H Transition and H-mode

S.-I.Itoh*, K.Itoh**, A.Fukuyama+,Y.Miura++, M.Yagi++ and M.Azumi++

* Research Institute for Applied Mechanics, Kyushu University 87, Kasuga 816, Japan

** National Institute for Fusion Science, Nagoya 464-01, Japan

\+ Faculty of Engineering, Okayama University, Okayama 700, Japan

++ Japan Atomic Energy Research Institute, Ibaraki 311-01, Japan

Introduction Anomalous transport of the plasma across the magnetic field in confinement devices has been a key issue since the early stage of fusion research. The L-mode confinement is the generic feature.[1,2] Recently a new theory of self-sustained turbulence has been developed to determine the transport coefficients.[3-5] Nonlinear interactions of the microscopic pressure-driven instability are renormalized in a form of diffusion effect on the mode, and the renormalized transport coefficients are obtained by using the mean field approximation. The eigenmode equation, which contains the nonlinearly developed transport coefficients, is solved to obtain the marginal stability condition, (i.e., the renormalized force balance eq.). The mode is found to be destabilized by electron dissipations, i.e., the resistivity η and the current diffusivity λ(owing to electron viscosity μ_e) and stabilized by ion viscosity μ and the thermal conductivity χ. The balance simultaneously determines the fluctuation amplitude and χ itself provided that the Prandtl numbers (μ/χ, μ_e/χ) are constant.

In H-mode plasmas the facts are recognized that the radial electric field $E_r(r)$ likely takes a large negative or positive value near edge and that it reduces the transport from that of L-mode.[6-8] Based on the L-mode transport formula, we obtain the L/H transition condition. Furthermore, we newly extend our L-mode theory to the H-mode one, incorporating the inhomogeneity of E_r. The reduction of χ is obtained.

Basic Equations We consider a circular tokamak with toroidal coordinates (r,θ,ζ). The reduced set of equations, is employed to consider nonlinear ballooning mode. The classical viscosity, conductivity, current-diffusivity and thermal conductivity are retained and the electron inertia term in Ohm's law is kept. The E× B nonlinearity is renormalized by use of one point renormalization, where the isotropic turbulence is assumed. Employing the mean field approximation, where the transport coefficient(μ_k, λ_k, χ_k) of the test mode are considered to be independent of the wave number, we use a simple set of diffusion coefficients(μ, λ, χ).

The basic equations consist of the equation of motion, $n_i m_i\{d(\nabla_\perp^2\phi)/dt-\mu\nabla_\perp^4\phi\}=B^2\nabla_{/\!/} J+B\nabla p\times\nabla(2r\cos\theta/R)\cdot\zeta$, generalized Ohm's law, $E+v\times B=J/\sigma-\nabla_\perp^2\lambda J$, and the energy balance equation $dp/dt=\chi\nabla_\perp^2 p$. Notations: m_i is the ion mass, n_i is the ion density, ϕ is the static potential, B is the main magnetic field, p is the plasma pressure, J is the current and σ is the classical conductivity. The detailed derivation was reported in Ref.[5]. The derivative d/dt is $\partial/\partial t + [\phi,]/B$ where [,] denotes the Poisson bracket. The doppler shift of frequency is offset for the homogeneous E×B rotation. Only the contribution of E_r' to d/dt is retained.

The ballooning transformation[9] is employed as $p(r,\theta,\zeta) = \sum_n \exp(-in\theta+in\zeta)\int p(\eta)\exp\{in\theta-inq\eta\}d\eta$, (q is the safety factor), since we are interested in microscopic modes. Eliminating $\tilde{\Phi}$ and $\tilde{J}$ from basic equation, we have the eigenmode equation for p

$$\frac{d}{d\eta}\frac{F}{\hat{\tau}+\Xi F+\Lambda F^2}\frac{d}{d\eta}\left(\hat{\tau}+\omega_{E1}\frac{d}{d\eta}+KF\right)p + \alpha[\kappa+\cos\eta+(s\eta-\alpha\sin\eta)\sin\eta]p$$

$$-\left(\hat{\tau}+\omega_{E1}\frac{d}{d\eta}+MF\right)F\left(\hat{\tau}+\omega_{E1}\frac{d}{d\eta}+KF\right)p = 0. \qquad (1)$$

We use the normalizations $r/a\to\hat{r}$, $t/\tau_{Ap}\to\hat{t}$, $\chi\tau_{Ap}/a^2\to\hat{\chi}$, $\mu\tau_{Ap}/a^2\to\hat{\mu}$, $\tau_{Ap}/\mu_0\sigma a^2\to\iota/\hat{\sigma}$, $\lambda\tau_{Ap}/\mu_0 a^4\to\hat{\lambda}$, $\tau_{Ap}\equiv a\sqrt{\mu_0 m_i n_i}/B_p$, $\tau\tau_{Ap}\to\hat{\tau}$, and notation $\Xi=n^2q^2/\hat{\sigma}$, $\Lambda=\hat{\lambda}n^4q^4$, $K=\hat{\chi}n^2q^2$, $M=\hat{\mu}n^2q^2$, τ is the growth rate, $s=r(dq/dr)/q$, $F=1+(s\eta-\alpha\sin\eta)^2$, $\kappa\equiv-(r/R)(1-1/q^2)$ (average well), $B_p=Br/qR$, $\alpha=q^2\beta'/\varepsilon$, $\varepsilon=r/R$, a and R for the major and minor radii, $\beta=2\mu_0 p/B^2$, and $\beta'\equiv d\beta/d\hat{r}$. The parameter ω_{E1} denotes the effect of the radial electric field shear,

$$\omega_{E1} = \tau_{Ap}(dE_r/d\hat{r})(srB)^{-1}. \qquad (2)$$

If we neglect ω_{E1}, Eq.(1) reduces to the transport-driven ballooning mode equation for the L-mode plasma[4,5]. The marginal stability condition (Eq.(1) with $\gamma=0$) corresponds to the new force balance equation in the presence of anomalous transport.

L-mode The stability limit of α for the least stable mode in the absence of $E_r(\omega_{E1}=0)$ is obtained as $\alpha^{3/2} = f(s)\sqrt{\mu}\chi^{3/2}\lambda^{-1}$. The Prandtl numbers($\mu/\chi$, μ_e/χ) are less affected by the fluctuation amplitude and they are assumed to be constant to obtain

$$\chi_L = \frac{q^2}{f(s)}\left(\frac{R}{r}\frac{\partial\beta}{\partial r}\right)^{3/2} \delta^2 \frac{v_A}{R} \qquad (3)$$

where δ is the skin depth. The characteristics of χ_L have been reported[5], the expected heat flux q_r vs ∇T for fixed ∇n is shown in Fig.1. At the location denoted by *, $|T/\nabla T| = |n/\nabla n|$.

L/H Transition Based on the obtained χ_L(Eq.(3)), we examine the L/H transition condition. The condition is roughly estimated by $d_0\lambda_0 \simeq 1$[7,10], where $d_0 = \sqrt{\varepsilon}D_e/F\nu_i\rho_p^2$ and $\lambda_0 = -\rho_p(T_e/T_i)(n'/n + \alpha_0 T_e'/T_e)$. Taking $D_e \simeq \chi_L$, we obtain the critical condition ($T_e = T_i$) as

$$\left(\frac{2\sqrt{2}}{F}\frac{m_e}{\sqrt{m_i}\,e^2}\right)\frac{\alpha_0}{f(s)}\frac{q^2}{\varepsilon B^2}\frac{|dT/dr|^{5/2}}{\rho_p\nu_i T} = 1 \qquad (4)$$

for $\nabla n = 0$. The critical temperature gradient for the onset of the H-mode is obtained. Sawtooth triggered L/H transition can be explained. The threshold power is also derived.

H-mode From the solution of unified equation(1), the transport coefficients for the H-mode plasma are obtained. The radial derivative E_r' is estimated as E_r/Δ, where we use $\Delta \sim \sqrt{\rho_p^2 + \mu/\nu_i}$. By means of similar process we obtain χ_H as

$$\chi = \chi_L\left[1 + \frac{\beta}{2}\left(\frac{r}{\rho_p s}\right)^2 \frac{\alpha}{(1+\chi/\nu_i\rho_p^2)}X^2\right]^{-1} \qquad (5)$$

in a convoluted form($X \equiv \rho P_p E_r/T$). The χ_H is strongly reduced from χ_L for large value of X_L.(Fig.2) Further theory is in progress.

References

[1] R.J.Goldston: Plasma Phys. Control. Fusion **26** (1984) 87.

[2] P.Liewer: Nucl. Fusion **25** (1985) 543

[3] K.Itoh, S.-I.Itoh, A.Fukuyama:Phys.Rev.Lett. **69** (1992) 1050

[4] K.Itoh, S.-I.Itoh, A.Fukuyama, M.Yagi, M.Azumi: in Proc. 14th Int. Conf. on Plas. Phys. Contr. Nucl. Fusion Res., Wurzburg, 1992, IAEA-CN-56/H-2-2; K.Itoh, et al.: Plas. Phys. Contr. Fusion **35** (1993) in press.

[5] K.Itoh, S.-I.Itoh, A.Fukuyama, M.Yagi, M.Azumi: 'Self-sustained Turbulence and L-mode Confinement in Toroidal Plasmas' NIFS-219(NIFS, 1993) Plas. Phys. Contr. Fusion.

[6] F.Wagner, G.Becker, K.Behringer, et al.: Phys. Rev. Lett. **49** (1982) 1408; ASDEX Team: Nuclear Fusion **29** (1989) 1959

[7] S.-I.Itoh and K.Itoh: Phys. Rev. Lett. **60** (1988) 2276
S.-I.Itoh and K.Itoh: Nucl. Fusion **29** (1989) 1031

[8] J.Groebner, et al.: Phys. Rev. Lett. **64** (1990) 3015; K.Ida, et al.: Phys. Rev. Lett. **65** (1990) 1364; K.H.Burrel, et al.: Plasma Phys. Cont. Fusion **34** (1992) 1859

[9] Connor, J.W., et al.: Proc. R. Soc. London, **A365** (1979) 1.

[10]S.-I.Itoh and K.Itoh: J. Phys. Soc. Jpn. **59** (1990) 3815

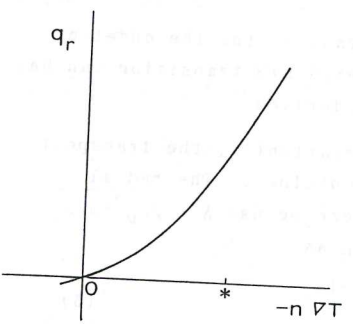

Fig. 1

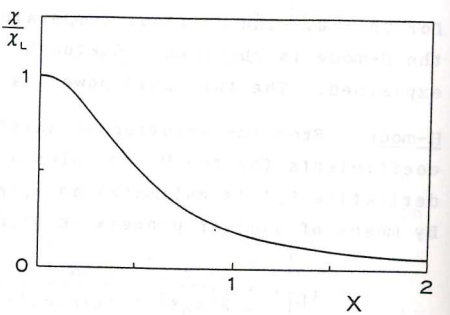

Fig. 2

THE MODEL OF THE SELF-OSCILLATING L-H TRANSITIONS IN TOKAMAK

A.Yu. Dnestrovskij, V.V. Parail
Russian research Center "Kurchatov Institute", Moscow, Russia

INTRODUCTION.

Numerous experiments on L-H transitions performed at several facilities allowed to observe the regime accompanied by periodic splashes of D_α intensity line and also edge temperature/density and of the turbulence level in plasma [1,2], the so-called ELMs. These phenomena are observed during the transition from L to H regime as well as during the quasi-stationary H-mode [2]. According to experimental studies, ELMs effect positively the discharge while reaching the stationary H-mode [1,2] and favoring the impurities withdrawal from plasma [2]. The present paper describes the model of ELMs as self-oscillating L-H transitions on the basis of the model of L-H transitions described in [3,4]. The results of numerical simulation and the dependence of self-oscillation characteristics on plasma parameters in particular are given. Comparison of the results obtained with experimental dependencies [1,2] is presented.

DESCRIPTION OF THE MODEL.

Let us start with the model of L-H transition described in [3,4]. This model describes self-consistently the fluctuations evolution at the plasma periphery and the setting of radial electric field at the non-ambipolar plasma flow across the magnetic field together with energy and particle balance by the following set of equations:

$$\frac{dW}{dt} = \gamma_1 W - \gamma_2 |\Delta\varphi| \frac{W - W_T}{W + W_0} - \gamma_3 W^2 \qquad (1)$$

$$e\nabla\varphi \sim T_e \left(\frac{\nabla n}{n} - \frac{\nabla T_e}{2T_e} \right) \qquad (2)$$

$$\frac{\partial n}{\partial t} = div_\perp (D\nabla n) + S \qquad (3)$$

$$\frac{3}{2} \frac{\partial n T_e}{\partial t} = div_\perp (\kappa n \nabla T_e) + P \qquad (4)$$

$$D = C_0 W + C_1, \quad \kappa = D \qquad (5)$$

The first and the third terms in the right hand side (1) describe the drive and nonlinear saturation of fluctuation's density energy W; the second term describes the process of fluctuation's suppression due to sheared poloidal plasma rotation emerging in sheared radial electric field (ϕ - field potential), γ_{1-3} are the

numerical coefficients. Equation (2) is an ambipolarity condition written for the simplest case when the electron flow, determined by anomalous transport on electromagnetic fluctuations [5], is much larger than the ion flux. This approach is valid near plasma edge where intrinsic ambipolarity of particle transport on electromagnetic fluctuations can be violated because the fluctuations momentum is lost on the wall [5], i.e. equation (2) describes the plasma periphery region which is of the order of several Larmor ion radii in the vicinity of the wall. Such a simplification seems to be reasonable since as it was shown in [4] the bifurcation of plasma parameters is the result of plasma turbulence level bifurcation in our model, not of the radial electric field. Equations (3), (4) where S, P are the sources of heat and particles, describe the electron temperature and plasma densities evolution. The source of particles is prescribed to be allocated at the periphery zone. The source of electrons heating (e.g., by EC waves) is preset by the Gauss function. And, finally, equation (5) describes the relationship between the level of fluctuations in plasma and the diffusion D and thermal conductivity κ coefficients; C_1 describes the neoclassical transport which is not connected with fluctuations.

CALCULATIONS RESULTS.

The calculations for the T-10 tokamak configuration are done. As an example, Fig. 1 shows time display of W and energy confinement time τ_E during self-oscillations excitation. The nature of these oscillations could be qualitatively understood from the following. Let us suppose that the plasma is in the L-mode and the potential ϕ (from (2)) is too low for the stabilization of the fluctuations so the transport coefficients D and κ are large enough. The rise of input power P results in T_e increase and then in $e\nabla\phi$ increase (see (2)). Fluctuations begin to be suppressed in the strong electric field that gives the confinement improvement at the end. Thus the discharge passes to H-mode during the short time determined by the decrement of fluctuation's suppression and the transport barrier is set at the edge plasma. The density profile is steepened as a result (that is shown on Fig.2) and then the absolute value of $e\nabla\phi$ begins to decrease (see (2)). If the value of potential at the stationary stage is large enough to suppress the turbulence (1) then discharge remains in the H-mode. In the opposite case the discharge passes back to the L-mode and the oscillations are realized.

The density and temperature profiles at the L and H stage during oscillations are shown on the Fig. 2. It is seen from Figs.1 and 2 that the oscillations between L and H regimes are the oscillations of the density profile and turbulence level at the plasma edge with practically constant edge temperature which can be seen in many experiments with ELM [1,2]. In our model this is explained by the fact that the particle source is located at the plasma edge and as a result of H-mode formation, i.e. decrease of

transport on the periphery, the plasma density is first to change.

Now let us examine in more detail what guides the availability and duration of the oscillations obtained. The calculations show that such oscillations exist only within a certain range of the plasma parameters. Beyond this range plasma tends to either stable L-mode, or to H-mode. The region where such oscillations exist on the plane of total particle **S** and heat **P** sources is shown in Fig. 3. The obtained dependence on heating power (at low power plasma tends to stable L-regime and at a rather high power - to stable H-regime) qualitatively satisfies, for instance, experiments at DIII-D [2] for the same type of ELMs which could be observed at the plasma heating power close to threshold values for the L-H-transition. Also, from Fig.3 it is seen that as the particle source is reduced, the plasma shifts from ELM zone to the stable H-mode and on the contrary, the increase of the source causes peripheral plasma cooling with subsequent potential reduction and transfer into the ELM regime [6] and then to the L-mode. The dependence of the time of L-mode duration during the oscilation normalized to the period of oscillation, t/T, on the input power is shown on Fig.4. The decrease of this value while the power grows also agrees with the experiment [2].

CONCLUSIONS.

1. It is shown that the proposed model describes self-oscillating L-H transitions which could be interpreted as ELMs, i.e. it allows to describe both stable L and H regimes as well as H-regimes with ELM without any additional instabilities.

2. The obtained dependencies of ELM characteristics on plasma parameters (injected power, neutral atoms flow) qualitatively correctly describe the experiment.

ACKNOWLEDGEMENTS

Concluding, the authors express their sincerest gratitude to Dr. I.A. Voitsekhovich for many valuable discussions.

References

[1] H.Matsumoto, R.J.Goldston,et al. Nucl. Fus. 31,(1991),93.
[2] Luxon J.L., Bramson G. et al. Plasma Physics & Contr. Fus. 32 (1990), 869-887.
[3] Voitsekhovich I.A., Kislov V.V. et al., in Proc. of 19th Eur. Conf. on Contr. Fus. and Pl. Ph., Innsbruck, I-207, 1992.
[4] A.Yu. Dnestrovskij, V.V. Parail, I.A. Voitsekhovich, in Proc. on 14th Int. Conf. on Pl. Ph. and Contr. Nucl. Fus. Res., Wurzburg, 1992, IAEA-CN-56/D-4-22.
[5] Waltz R.E., Phys.Fluids 25(1982), 7, 1269.
[6] D.Stork, D.J.Campbell et al., in Proc. of 18th Eur. Conf. on Contr. Fus. and Pl. Ph., Berlin, I-357, 1991.

Figure captions

Fig.1. Time evolution of fluctuation level W, a.u. (a), energy confinement time τ_E, ms, during oscillations.

Fig.2. Plasma density n, $10^{19}m^{-3}$ (a), and electron temperature T_e, keV, (b) profiles during oscillations.

Fig.3. Regions of L-mode, ELMs and ELM free H-mode on the plane of the total particle **S** and heat **P** sources.

Fig.4. Dependence of the time of duration L-mode during the oscilation normalized to the period of oscillation, t/T, on the total heat power **P**.

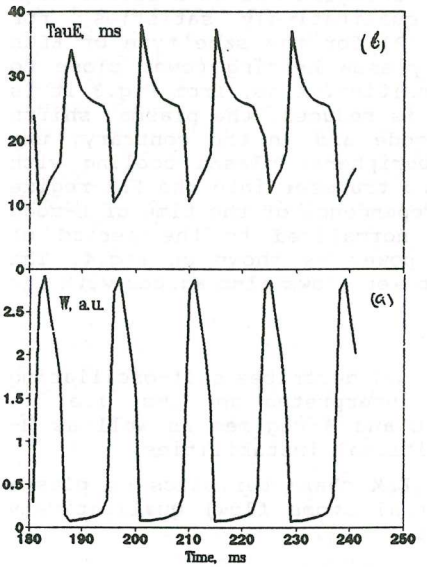

Fig. 1

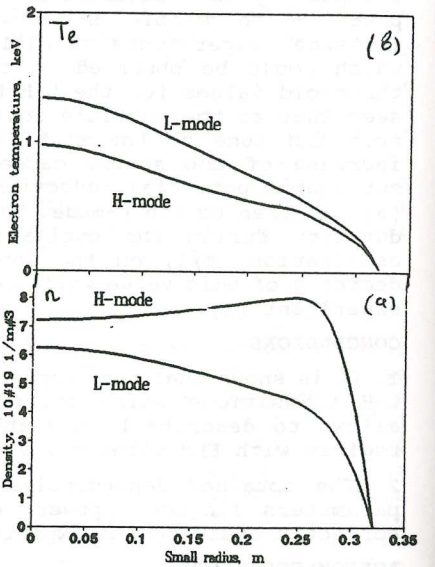

Fig. 2

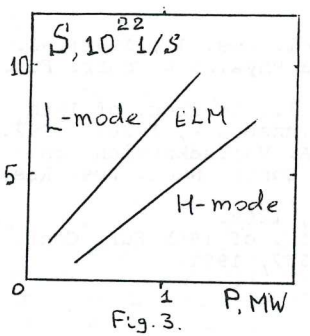

Fig. 3.

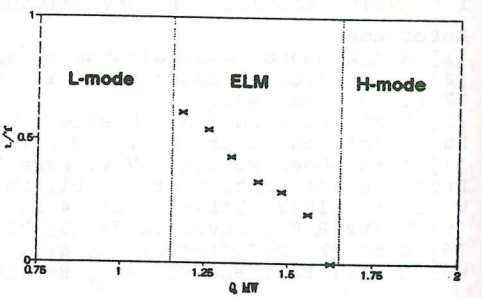

Fig. 4

NEOCLASSICAL TRANSPORT, POLOIDAL ROTATION AND RADIAL ELECTRIC FIELD AT THE L-H TRANSITION.

E.Minardi, G,Gervasini, E.Lazzaro
Istituto di Fisica del Plasma, Associazione EURATOM- ENEA-CNR, Via Bassini 15, 20133 Milano, Italy

I.Introduction

The transition to a high confinement regime in tokamaks operating with a magnetic divertor configuration is accompanied by the strong steepening of the edge temperature profile and the onset of a large positive poloidal mass rotation associated with a negative radial electric field.The latter phenomena are signatures of a neoclassical transport mechanism.We address the question of establishing whether neoclassical transport is indeed sufficient to establish high edge gradients and drive poloidal rotation under strong auxiliary heating .The heat transport equation is solved numerically in a narrow edge layer interfaced to the plasma body through heat flux continuity, but allowing for heat conductivity discontinuity. The results compared with recent experimental measurements support the assumption that a highly sheared neoclassical poloidal velocity profile can suppress the anomalous part of the heat transport, and that the neoclassical residual transport, characterizes the plasma behaviour at the edge during H modes.

II. Assumptions on the Heat Transport in a Heated Edge Layer.

We consider a single fluid description of a tokamak plasma in the large aspect ratio approximation $a/R<<1$, with a given, stationary, density profile and particle fluxes and temperature evolving according to the momentum and heat transport equations derived from the appropriate moments of the gyrokinetic distribution function [1] .

We assume that in a layer of width $\Delta<<a$ just inside the separatrix, on which T=0 exactly, the thermal conductivity of the plasma, subject to a strong auxiliary power input, is dominated by the neoclassical behaviour of the ions in presence of one impurity species, in a multicollisional regime depending on the time evolution of the temperature profile.It is a central characteristic of the *neoclassical theory* the fact that the dT/dr driven cross field fluxes are related to the parallel flows through the viscous forces.As a consequence in the plateau and Pfirsch-Schlueter regimes just near the separatrix, a positive poloidal ion and impurity velocity can be generated together with a negative radial electric field when sufficient temperature or density gradients develop.

We assume that the anomalous effects are suppressed by the onset of sufficiently high poloidal velocity shear [3]. The thickness of the edge layer should be essentially determined by the region of high neoclassical poloidal velocity appearing just inside the separatrix.In an idealized situation the thermal conductivity of the plasma can be discontinuous across the boundary s of an edge layer $s\leqslant r\leqslant s+\Delta$ and can take large anomalous values at $r\leqslant s$; at s continuity is required for the heat flux, the temperature and its derivative.The power balance equation,in cylindrical geometry for the one-fluid plasma model with temperature T and (uniform) plasma density n in the layer $s\leqslant r\leqslant s+\Delta$ can be written as :

$$\tfrac{3}{2} n \frac{\partial T}{\partial t} + \frac{1}{r}\frac{\partial}{\partial r}[rQ(r)] = \eta P_A \qquad (1)$$

where Q is the radial heat flux per unit surface and P_A is the net power input term (including Ohmic and auxiliary heating, radiation losses) averaged in the region $r\leqslant s$ and η represents the fraction $(0\leqslant\eta\leqslant 1)$ of power deposited in the edge layer.

In the layer $s<r<s+\Delta$ the heat flux is expressed in the general form $Q(r)=-n_i\chi_+(dT/dr)+C/r$, where χ_+ is the ion thermal conductivity, n_i the ion density and C is a constant determined by the continuity conditions at r=s. On the inner side r<s we consider a radial heat flux of the form $q_r = -n\chi_- dT/dr$, where χ_- is the anomalous heat diffusivity of the plasma in the internal region (mainly due to electrons).

Assigning the value of T at $a=s+\Delta$ and prescribing the initial profile T(r,0), eq.(1) determines completely the evolution of T(r,t). According to this picture the only divergent contribution to the heat flux in the layer is due to the ions while the divergence-free part can account for part of the heat flux (mainly anomalous) impinging upon the layer from the core of the plasma.

Thus the resulting temperature profile is entirely produced by the viscous and frictional neoclassical effects of the ions in presence of one (dominant) impurity species of atomic number Z_I.

III. Neoclassical Heat Transport.

The banana-plateau heat flux normal to the magnetic surface ψ=const. consists of a diffusive and a convective term expressed in terms of the surface averaged parallel viscous stress forces[1]:

$$q^{\psi} = \underline{q}\cdot\nabla\psi = \frac{cRB_T T}{eZ\langle B^2\rangle}\left[\left\langle \underline{B}\cdot\nabla\cdot\underline{\underline{\Theta}}\right\rangle - \frac{5}{2}\left\langle \underline{B}\cdot\nabla\cdot\underline{\underline{\Pi}}\right\rangle\right] \qquad (2)$$

where we retain only the parallel part of the stress tensors $\underline{\underline{\Pi}}$ and $\underline{\underline{\Theta}}$. The ion parallel viscous forces are related to the poloidal flows as follows:

$$\begin{bmatrix}\left\langle \underline{B}\cdot\nabla\cdot\underline{\underline{\Pi}}_{//}\right\rangle \\ \left\langle \underline{B}\cdot\nabla\cdot\underline{\underline{\Theta}}_{//}\right\rangle\end{bmatrix} = \nu_{ii} n_i m_i \begin{bmatrix}\mu_1 & \mu_2 \\ \mu_2 & \mu_3\end{bmatrix}\begin{bmatrix}0 & K_1 \\ 0 & -\frac{\mu_1}{\mu_2}K_1\end{bmatrix}\begin{bmatrix}V_{0\psi} \\ V_{1\psi}\end{bmatrix} \qquad (3)$$

where μ_i and K_1 are the (dimensionless) viscosity coefficients [1] and ν_{ii} the ion-ion collision frequency :

$$\nu_{ii} = \frac{4}{3\sqrt{\pi}}\frac{4\pi n_i Z^4 e^4 \ln\Lambda}{m_i^2 v_{th_i}^3} \quad ; \quad v_{th_i} = \left(\frac{2T}{m_i}\right)^{1/2} \qquad (4)$$

$V_{0\psi}$ and $V_{1\psi}$ are the neoclassical poloidal diamagnetic and EXB mass and heat flow in the notation of Kim et al.[1]:

$$V_{0\psi} = -\frac{cB_\phi}{ZeB_\theta}\left[\frac{\partial T}{\partial r} - ZeE_r\right] \quad ; \quad V_{1\psi} = \frac{cB_\phi}{ZeB_\theta}\frac{\partial T}{\partial r} \qquad (5)$$

where B_ϕ and B_θ are the toroidal and poloidal components of the magnetic field and E_r is the radial ambipolar electric field.

We use the viscosity coefficients valid in all collisionality regimes with the rational combination by Kim et al.[1] of the asymptotic coefficients.

In absence of an external momentum source or sink, relation (3) implies the parallel *momentum balance* of the ions $\langle \underline{B}.\mathrm{div}.\underline{\Pi}_{//}\rangle=0$ .Consequently in our approximation the banana-plateau radial heat flux (2) *is purely diffusive* :

$$q^{r}_{BP} = -\frac{n_i \rho_i^2 \nu_{ii}}{2}\left(\frac{Rq}{a}\right)^2 \frac{B^2}{\langle B^2\rangle}\left[\mu_1\mu_3 - \mu_2^2\right]\frac{K_1}{\mu_2}\frac{\partial T}{\partial r}$$

Here ρ_i is the ion Larmor radius and q the safety factor. The total heat flux comprises the classical and Pfirsch-Schlueter regime contributions.

IV .Poloidal Rotation and radial Electric Field .

The poloidal rotation of the impurity is a consequence of the relationship between the ion diamagnetic flows $V_{0\psi}$ and $V_{1\psi}$ and the nonvanishing parallel flow of the impurity produced by the parallel friction force of the ions .In a situation in which the parallel ion flow vanishes ,the electric field is given by $E_r=(1-K_1)(dT/dr)/Z$.

We have considered the case of the L-H transition on DIII-D[2].Fig.1a shows the time evolution of the temperature profile T(r,t) with $\eta=0$ and $\chi_{\perp}\sim 2\ m^2/s$ simulating a case in which the power is deposited in the plasma body and diffuses to the edge across the surface s=0.58m .Starting from an initially flat profile T(r,0)=10 eV, a sharp temperature gradient is formed and reaches a steady state in about 5ms, while the inboard temperature T(s) reaches a value of 300 eV , very close to the experimental data. In Fig. 2 the profiles of $E_r(r,t)$ associated with Fig. 1 are displayed.The field grows more and more negative in the plateau region reaching the experimental values of about 30-40 kV/m . Fig.3 shows the evolution of the net ion poloidal velocity profile, which in the banana region is slightly negative , as expected, but grows positive and reaches a peak value of ~25 km/s in the plateau zone exhibiting a shear length shorter than the layer width .This is in good qualitative agreement with the experimental results and with the theoretical assumptions. The residual neoclassical heat transport appears to be quantitatively sufficient to sustain the temperature pedestal and the high poloidal velocity shear, which,in turn, is the mechanism of suppression of transport anomalies.Fig. 4 shows the rotation velocity profile for the impurities.

All these results support the initial conjecture that the observed L-H transition phenomena can be explained in terms of standard neoclassical physics.

References

[1]Y, Kim, Ph. Diamond,R.J.Groebner,Phys.Fluids B **3** ,2050 (1991)
[2[K.Burrell,T.N.Carlstrom, E.J.Doyle et al. Plasma Physics Contr. Fus.**34**,1859(1992)
[3] H. Biglari, P.H. Diamond ,P.W.Terry , Phys.Fluids B **2**, 1 (1990)

Figure Captions

Fig.1- Edge temperature pedestal formation in DIII-D with B_ϕ of 1.2 T, q_ψ of 2.7, R=1.69 m, a=0.6m ,total input power of 5 MW, density at r=s $n_i=1.0\ 10^{19} m^{-3}$, $m_i=2$ a.m.u., $Z_I=6$, $\chi_{\perp}\sim 4\ m^2/s$, $\alpha=n_I Z_I^2/n_i Z_i^2=1$ with a single null separatrix configuration.
Fig.2 -Profile of the radial electric field for the case of Fig.1
Fig.3 -Profile of the poloidal ion velocity for the case of Fig.1
Fig.4 -Profile of the poloidal Carbon velocity for data of Fig.1

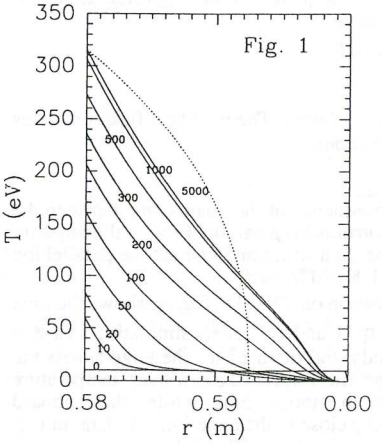
Fig. 1
T (eV)
r (m)
0
50
100
150
200
250
300
350
0.58
0.59
0.60
5000
1000
500
300
200
100
50
20
10
0

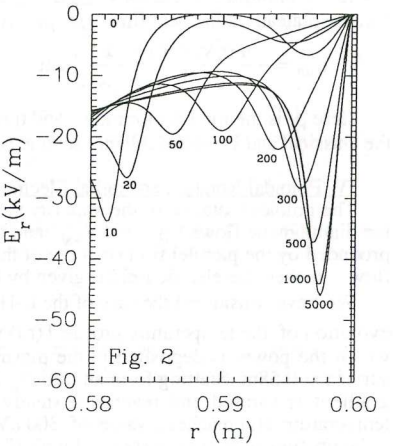
Fig. 2
E_r(kV/m)
r (m)
0
−10
−20
−30
−40
−50
−60
0.58
0.59
0.60
0
10
20
50
100
200
300
500
1000
5000

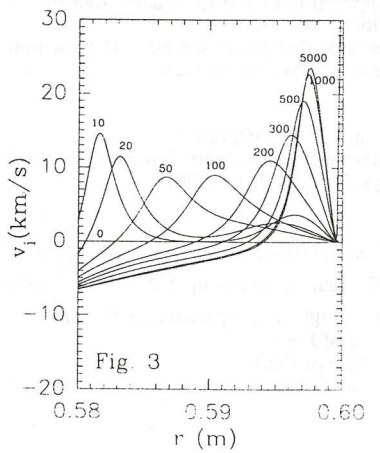
Fig. 3
v_i(km/s)
r (m)
30
20
10
0
−10
−20
0.58
0.59
0.60
10
20
50
100
200
300
500
1000
5000
0

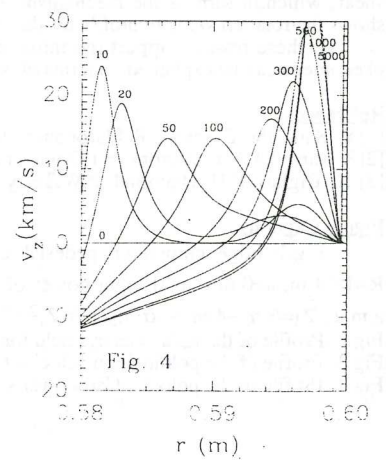
Fig. 4
v_z(km/s)
r (m)
30
20
10
0
0.58
0.59
0.60
10
20
50
100
200
300
500
1000
5000
0

THE EFFECT OF COLLISIONS ON DIRECT ION ORBIT LOSS IN THE PRESENCE A RADIAL ELECTRIC FIELD IN A TOKAMAK

T.K. Kurki-Suonio, M.J. Alava, S.K. Sipilä, and J.A. Heikkinen

Department of Technical Physics
Helsinki University of Technology
Rakentajanaukio 2C, 02150 Espoo, FINLAND

In this paper we investigate the effect of both collisions and a constant radial electric field on the dynamics of a hot ion population near the plasma edge using a guiding center following code ASCOT [1].

The model for L-H transition by Shaing and Crume [2] has so far best agreed with experimental observations. In this model, the L-H transition is triggered by Direct Ion Orbit Loss (DIOL) near the plasma edge. In the velocity space, the ions contributing to DIOL lie in the DIOL loss cone which is defined by the trapped-untrapped boundary and a $v_{\parallel,min}$ -line, see Fig. 1. A radial electric field has a profound effect on the topology of the ion trajectories and affects the loss cone boundaries [3,4]. When addressing the effect of collisions on the particle orbits, usually only the pitch angle scattering has been considered. This has been justified by the fact that a change in particle energy due to collisions does not affect the depth of the magnetic well. However, as indicated in Fig. 1, only those ions in the trapping region whose banana orbits are bulged outward and wide enough to cross the plasma edge will contribute to DIOL – i.e. ions with $|v_\parallel| > |v_{\parallel,min}|$. In reality, only ions reaching the divertor, limiter, or the chamber wall actually contribute to DIOL. However, for simplicity, we will here consider an ion crossing the plasma edge as lost. The pitch angle scattering, moving an ion along a circular trajectory in the $(v_\parallel, v_\perp)$-space, can make the ion to cross either the trapping boundary or the $v_{\parallel,min}$ -boundary. The energy operator, consisting of slowing down and diffusion, moves the ion only in the radial direction. Therefore, although the energy operator does not affect trapping of the particles, it does move particles across the $v_{\parallel,min}$ -boundary and thus affects the DIOL loss cone.

The effect of collisions on a test particle scattering from a background plasma can be modeled by using binomially distributed Monte Carlo scattering operators derived from the Fokker-Planck equation[5]. The change in the particle pitch, $\xi \equiv v_\parallel/v$, during an orbit integration time step Δt is obtained from the Lorentz scattering operator,

$$\Delta\xi = -\nu_\xi \xi \Delta t + \delta_1 [(1-\xi^2)\nu_\xi \Delta t]^{1/2},$$

where δ_1 is the evenly distributed random sign of the stochastic part of the operator, and ν_ξ is the pitch collision frequency. The change in the particle energy during time step Δt can be given in a similar form:

$$\Delta\epsilon = -\sum_j 2\nu_{\epsilon,j}\left[\epsilon - \frac{3}{2}k_B T_j\right]\Delta t + \delta_2\sqrt{\sum_j 4k_B T_j \epsilon \nu_{\epsilon,j}\Delta t},$$

where δ_2 is the evenly distributed random sign, subscript j denotes different plasma species, and $\nu_{\epsilon,j}$ is the energy scattering frequency. For 1 keV deuterons scattering off 100 eV electron background, one can show by expanding the Rosenbluth potentials that define the scattering frequencies:

$$\nu_{\epsilon,e} \approx \frac{E}{k_B T} \nu_{\xi,e}.$$

Therefore slowing down and diffusion dominate pitch angle scattering for high energy ions scattering from background electrons. The value for the energy collision frequency at these temperatures is $\nu_{\epsilon,e} \approx 120\ s^{-1}$, when the plasma density is $10^{19}\ m^{-3}$. At the same parameters, but for background deuterons, the energy and pitch scattering frequencies are comparable: $\nu_{\epsilon,i} \approx 150\ s^{-1}$ and $\nu_{\xi,i} \approx 290\ s^{-1}$. Thus, at the parameter range relevant for DIOL, the high energy ions scatter from both background electron and background ion population.

Because of collisions, it is necessary to follow the ions within the DIOL loss cone to determine the probability for them to scatter out of the loss cone before they escape from the plasma. Similarly, some ions originally outside the loss cone can scatter into it and thus contribute to DIOL. Using ASCOT [1] we have assessed the effect of collisions on high energy deuterons in a pure deuterium plasma. We follow a group of deuterons launched in the equatorial plane one centimeter from the plasma edge in a D-shaped magnetic configuration of $B_T = 3.45$ T, I = 4.8 MA, and $\kappa = 1.68$. The major radius is taken to be R = 3 m and the plasma minor radius $a_p = 1.2$ m. The plasma temperature at this location is about 180 eV, the density is about $7.7\times10^{18}\ m^{-3}$, and the ion collisionality $\nu_{i,*} \approx 0.16$. Test particle runs without collisions gave the minimum energy $E_{min} = 387$ eV for the DIOL loss cone, and the trapped-untrapped boundary at the pitch value of $\xi = -0.7461$. The minimum parallel velocity is thus $v_{\parallel,min} = 1.4\times10^5$ m/s.

Turning on the collisions, we follow an ensemble of 500 deuterons. The particle energy is chosen from particle density considerations: the energies are chosen to be above the minimum value for the loss cone, but less than $E_{min} + 4k_BT$, where T is the plasma temperature. At the upper limit, the density has dropped almost two orders of magnitude from the value at E_{min} and thus it is unlikely that particles with even higher energies would significantly contribute to DIOL. The pitch of the test particles is chosen so that the particles lie within or near the direct ion orbit loss cone. The collisions are from a Maxwellian background plasma with equal ion and electron temperatures. The ions are followed for 4 ms, which corresponds to a few bounce times but is short enough compared to the collision time so that the ions leaving the plasma do so via DIOL.

For ions well inside the DIOL loss cone, we have studied the escape fraction for three different energies: E=390 eV and 570 eV with $\xi = -0.72$, and 1.2 keV with $\xi = -0.60$. At the high energy of 1.2 keV, 99% of the ions escaped, as one might expect. However, at the lower energies, less than 40% of the ions left the plasma via DIOL.

Launching ions right inside the trapping boundary, even at E=1.2 keV only 87% of the ions escaped. At E = 570 eV and 390 eV the fractions were 49% and 31%, respectively. Increasing the pitch so that the ions start with $\xi = 1.1 \cdot \xi_{cr}$, 72% of the

1.2 keV ions still escaped. For lower energies, the difference to the trapping boundary case is even smaller: 46% of the 570 eV ions and 28% of the 390 eV ions escaped from the plasma. Therefore, in the presence of collisions the loss cone boundaries are no longer well defined.

The $v_{\|,min}$-boundary is of particular interest because any difference between the number of DIOL ions at this boundary and at the trapping boundary must be due to the energy part of the scattering operator. Launching 1.2 keV ions right inside the $v_{\|,min}$-boundary, only 76% escaped; for E = 570 eV and 390 eV the fractions were 48% and 38%, respectively. Therefore, while at lower energies the statistics are similar to the trapping boundary case, for higher energies the fraction of DIOL ions is lower than at the trapping boundary. This difference can be accounted for by the fact that for a fast ion slowing down is strong enough to pull the ion out of the loss cone.

When a radial electric field is present, the effect of the energy changing part of the scattering operator becomes even more important. Because of the electric field, the trapping boundary is now a hyperbola centered around $v_{\|,c} < 0$ [4] in this magnetic geometry. However, since for DIOL only high energy ions are relevant, the boundaries for the trapped ion region can be roughly approximated by the asymptotes to the hyperbola. The velocity cone thus defined is similar in shape to the fieldless case, but it is shifted by $v_{\|,c} = \frac{1}{2}\frac{1+\epsilon}{1-\epsilon}\frac{E_r}{B_p}$ with respect to the origin. Therefore, in the presence of a radial electric field, even changes in particle energy can trap/untrap ions.

Repeating the ASCOT collisionless test particle calculations for a constant radial electric field of 10 kV/m, the slope of the asymptote of the trapping boundary was found, in agreement with the theory, to be the same as the slope of the boundary of the fieldless case. However, since the trapping cone is shifted by $v_{\|,c}$ with respect to the origin, the critical pitch now depends on the energy. Also the value for $v_{\|,min}$ was found to increase from the fieldless value but, in accordance with theory, by less than $v_{\|,c}$. With the constant electric field of 10 kV/m, $v_{\|,min}$ lies at -1.2×10^5 m/s. This corresponds to a shift in the minimum energy to E_{min} = 438 eV. Thus for a radial electric field of 10 kV/m, the shifts in the DIOL loss cone boundaries are insignificant. However, for a larger electric field value the effect of collisions could be qualitatively different from the fieldless case. We shall investigate such a case in a future paper.

In this paper we have assessed the importance of collisions and a radial electric field on the direct ion orbit loss of a hot ion population in a tokamak. In the absence of a significant radial electric field, test particle runs show that because of collisions the boundaries of the loss cone become diffuse. Furthermore, for very high energy particles, the slowing down part of the scattering operator plays a significant role in pulling particles out of the DIOL loss cone. The role of the energy collision operator becomes even more important in the presence of a radial electric field, when the trapping boundary no longer corresponds to a constant pitch.

It should be noted that our approach allows one to assess the effect of collisions on DIOL dynamics for a test particle ensemble only because the model doesn't account for any changes in the background plasma. If DIOL were entirely due to the Maxwellian tail ions, as suggested in Shaing's model for a DIOL based L-H transition[2], the loss

cone dynamics would probably be dominated by the very sharp velocity gradient formed in the distribution function as the hot ions escape from the plasma. This kind of an effect would require more elaborate test particle calculations than what we have done here. However, experiments on JFT-2[6] have indicated that L-H transition can take place even at $\nu_{i,*} \gg 1$. This, together with the observation of a high energy particle population close to the edge[7] indicates that the radial current could be due to DIOL of a hot ion component in the plasma[8]. The dynamics of these particles can be studied using simple test particle calculations like ours.

In the future, we shall study not only what fraction of ions escape via DIOL but also the time scale in which they do so. This will allow us to estimate the radial current due to DIOL. Furthermore, we wish to investigate how the DIOL probability depends on the distance from the plasma edge. Future development of the project involves test particle studies in the presence of a nonuniform radial electric field, steep ion temperature gradient, and impurities in the background plasma.

[1] J.A. Heikkinen, S.K. Sipilä, and T.J.H. Pättikangas, accepted for publication in Comput. Phys. Comm.
[2] K.C. Shaing, and E.C. Crume, Phys. Rev. Lett. **63** (1989) 2369
[3] H.L. Berk, and A.A. Galeev, Phys. Fluids **10** (1967) 441
[4] Y.B. Kim, private communication.
[5] A.H. Boozer, and G. Kuo-Petravic, Phys. Fluids **24** (1981) 851
[6] K. Ida et al., Phys. Rev. Lett. **65** (1990) 1364
[7] Y. Miura et al., Phys. Rev. Lett. **69** (1992) 2216
[8] K.C. Shaing, and P.J. Christenson, Phys. Fluids **B 5** (1993) 666

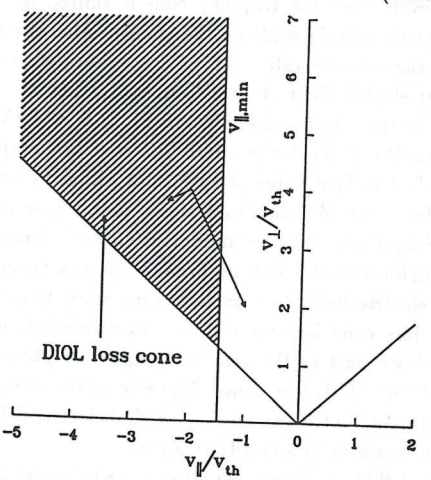

Figure 1. The DIOL loss cone in $(v_\parallel, v_\perp)$-space. The effect of pitch angle and energy part of scattering are indicated by a short and a long arrow, respectively.

Simulation of vapor shield evolution at carbonized target plates

P. Spathis and L. Lengyel

Max-Planck-Institut für Plasmaphysik - Euratom Association
D-85748 Garching bei München, Germany

A time-dependent quasi-1-D MHD model has been developed for simulating the time evolution of vapor clouds at carbonized target plates bombarded by plasma particles. In this approximation, the limited extent of the target plate in the lateral direction is not taken into account and only thermal plasma electrons are considered as energy carriers. The electrons are assumed to be confined to magnetic flux lines whose angle of incidence measured with respect to the target plate is assumed to be given. The Maxwellian energy distribution of the incident electrons is approximated by five discrete energy groups. The energy deposition in the shielding cloud and at the target plate are determined by stopping length calculations taking electrostatic shielding into account. The internal redistribution of the deposited energy by thermal conduction and radiative transport is also calculated. Finite rate equations are used for detemining the ionization dynamics of the neutral carbon particles released. In the model, collisional ionization and radiative recombination are taken into account in defining the populations of the different ionization levels. The deceleration and stopping of the vapor motion in the direction perpendicular to the magnetic field lines resulting from ionization and interaction with the magnetic field is calculated in a self-consistent manner.

It will be noted that this process is inherently time-dependent. The surface is initially exposed to incident plasma particles without any shielding present. In the case of carbon or carbonized surfaces, the erosion begins when the surface temperature reaches the sublimation temperature, i.e. the order of 4000 K. The velocity distribution of the particles leaving the wall is half-sided Maxwellian, and it takes a certain distance (Knudsen layer thickness) until it becomes fully Maxwellian, making some of the particles return to and recondense on the wall. The relation between the vapor pressure and temperature, taking partial recondensation into account, is given by a saturated vapor pressure relation of the form $p_s = p_s(T_s) = A\exp(-B/T_s)$, where A und B are constants. Outside the Knudsen layer, the vapor state can be described, with a sufficent degree of accuracy, by an equation of state such as the van der Waals equation or the ideal gas state equation. The expansion velocity of the eroded particles is of the order of 10^4 m/s and their typical ionization time is of the order of $\approx 1\,\mu s$. After ionization, the expansion in the direction normal to the magnetic field is stopped and, depending upon the relative magnitudes of the erosion rate and the ionization time, a relatively high-density vapor cloud may form at the wall surface, which can now only expand along the magnetic field lines. (Anomalous processes such as the onset of flute instability, turbulent mixing, etc. are at present not taken into account.) The dilution of the vapor during this second (field-aligned) expansion phase is much slower than during the neutral gas expansion phase. The energy carriers of different energies penetrate the cloud to different depths, only the energetic ones reaching the solid surface. A fraction of the incident energy carriers is intercepted by the cloud. A fraction of the energy received is lost by radiation, thus reducing the energy flux affecting the wall. The time evolution of the vapor cloud with its radiating and

shielding properties decisively depends on the heat deposition profile and the expansion and ionization dynamics of the vapor.

On the basis of the existing ablation codes developed for hydrogen and impurity pellets (IPP Rpt. 5/50, Dec. 1992) a 1-D time-dependent code has been developed that simulates the evolution of vapor layers at carbon (or carbonized) surfaces subjected to incident, magnetically confined plasma particles. In the code the following effects are taken into account:

collisional energy transfer to the wall and vapor cloud by plasma particles;

finite rate ionization and recombination processes;

interaction of the ionized particles with the magnetic field, i.e. deceleration of the cross-field expansion and the magnetic funneling of the ionized substance;

conductive and radiative energy transport within the cloud and radiant energy loss to the environment (in diffusive radiation transport approximation).

In the following, results of a typical scenario calculation are given. The geometry considered is given in Fig. 1. A plane carbonized wall normal to the y axis and extending to infinity is subject to bombardement by incident plasma particles confined to magnetic field lines. The angle of incidence of the magnetic field with respect to the wall, α, is given: $\alpha = 10\ degr$. The field and plasma parameters chosen are as follows: $B = 3$ tesla, $T_e = 7\ keV$, and $n_e = 10^{20}\ m^{-3}$.

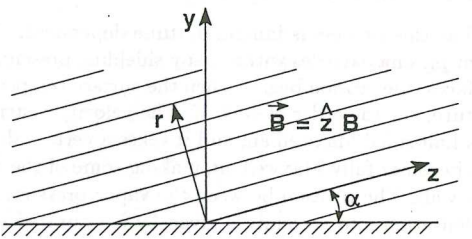

Fig. 1: Simplified plate geometry (see text for details)

Figure 2 shows the temporal variation of the vapor layer expansion velocity in the direction normal to the wall. As can be seen, following a short initial acceleration period, ionization sets in and the cross-field expansion is stopped. The residual expansion is due to expansion along the magnetic field lines.

Figure 3 shows the temperature distribution in the direction normal to the wall $2\mu s$ after the start of the plasma-wall contact. The corresponding distribution of the radiant energy density, $U(J/m^3)$, and the corresponding black-body radiant energy density, U_{bb}, are shown in Fig. 4 for the same time instant.

Figure 5 shows the distribution of the radiant energy flux over the layer. The inward-directed negative flux represents an effective energy transport to the cold core, while the outward directed positive flux represents energy loss and contributes to radiative cooling of the layer thus reducing the heat load affecting the solid surface.

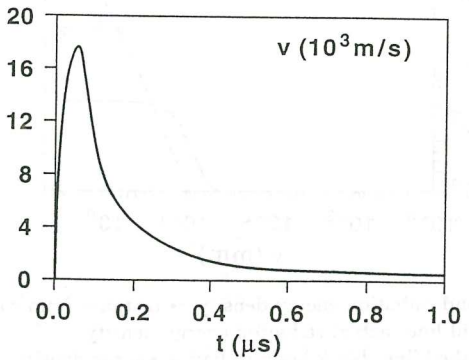

Fig. 2: Cloud expansion velocity *vs* time

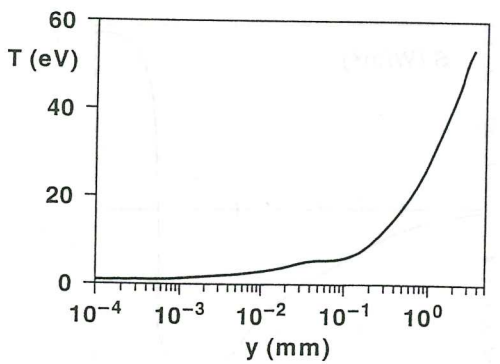

Fig. 3: Cloud temperature *vs* distance from wall ($t = 2\mu$s)

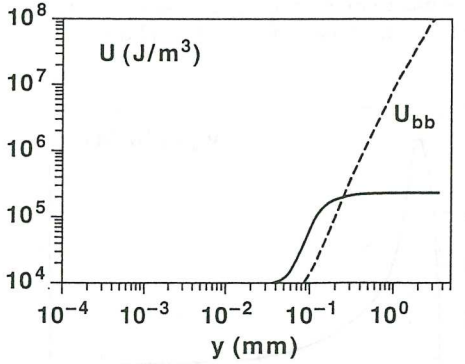

Fig. 4: Cloud radiation energy density *vs* distance from wall ($t = 2\mu$s)
Solid line: actual radiation energy density
Dashed line: black body radiation energy density
corresponding to local temperature

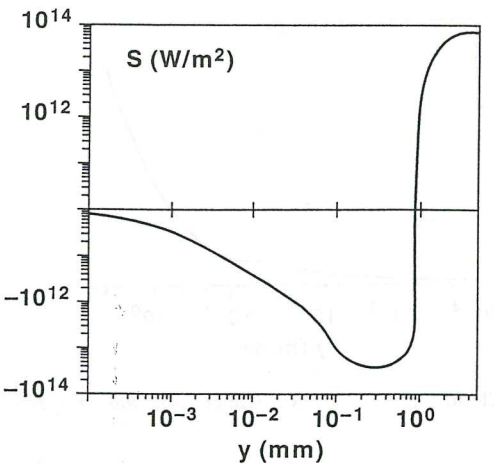

Fig. 5: Radiation energy flux *vs* distance from wall ($t = 2\mu$s)

A time-dependent, self-consistent, slab-symmetric ablation model with allowance for transverse expansion and magnetic confinement effects

L. Lengyel and P. Spathis

Max-Planck-Institut für Plasmaphysik - Euratom Association
D-85748 Garching bei München, Germany

A time-dependent, slab-symmetric ablation model has been developed. The ablation of a pellet surrounded by a magnetically confined plasma is calculated in a self-consistent manner. The erosion rate of the pellet surface is defined by the balance of the incident energy flux carried by plasma particles and the efflux of energy from the pellet surface with the ablated particles of given sublimation energy and initial enthalpy. In the present approximation, only plasma electrons are considered as energy carriers and their energy distribution is assumed to be Maxwellian and is simulated by five discrete energy groups. The energy deposition in the shielding cloud is determined by stopping length calculations applied along the magnetic field lines with allowance for electrostatic shielding effects. The condition of vanishing net incremental current (additive to the toroidal current in tokamaks) is assumed for every flux tube cross-section. The stopping length calculations are supplemented by thermal diffusion calculations, thus redistributing the energy deposited in the discrete energy group approximation. The neutral cloud is allowed to expand also in the direction perpendicular to the magnetic field. The deceleration and full stopping of the cross-field motion is calculated by means of an MHD model (iteratively with the axial expansion dynamics), thus determining the transient variation of the lateral cloud dimension and the corresponding modifications of the field-aligned density and temperature distributions used in the stopping length calculations. Finite rate equations are used for determining the time history of the ionization state of the ablated substance. In the case of hydrogen pellets, collisional and radiative ionization and recombination processes are taken into account. The variation of the ablation rate along the pellet path (i.e. that of its value averaged over the residence time of a pellet of given injection velocity in a flux tube defined by the local ionization radius of the ablatant) is presented for an ASDEX-UP discharge with pellet injection and compared with the measured parameter distributions.

The ablation model presented here is described in detail in [1]. It comprises two parts, each aimed at solving part of the whole problem: (a) determination of the energy flux transported by plasma particles to the pellet surface along the magnetic field lines, (b) determination of the shielding characteristics of the particle cloud evolving around the pellet. For this purpose two time-dependent 1.5-D variable-mass Lagrangian codes were coupled, thus in fact replacing a rather complex 2-D code that would otherwise be necessary for solving the problem. Both codes are based on the full set of conservation equations with mass-source terms present and are of the single-temperature single-velocity type. Each code has its principal direction: the direction of the magnetic field and the one perpendicular to it. The essential effects of the complementary direction are taken reciprocally from the other code, by means of iterative feedback coupling. In both codes, the calculations are performed with finite rate atomic processes: collisional and radiative ionization and recombination processes are taken into account.

The first code, being the actual ablation code, takes care of the processes associated with the direction of the magnetic field lines: (a) penetration of plasma particles into the shielding cloud, collisional energy transfer to the cloud particles, particle and energy flux depletion calculations; (b) field-aligned electrostatic field calculations based on the zero net current condition in the direction parallel to B (not counting, of course, the discharge currents in the background plasma); (c) gasdynamic expansion of the ablatant along the magnetic field lines in a quasi-one-dimensional channel flow approximation (the effect of the complementary dimension manifested in the evolution of the transverse channel dimension is taken from the second code); (d) variation of the ionization state of the species in time and space (along the magnetic field lines). In this series of calculations, the Maxwellian energy distribution of the incident plasma particles was represented by 5 discrete energy groups.

The second code is a self-consistent MHD code based on the usual set of continuity equations and Maxwell's equations. The code calculates, for given background plasma parameters, magnetic field strength, and ablation rate, (a) the expansion and ionization processes in the transverse direction; (b) the magnitude of the induced $\vec{v} \times \vec{B}$-emf, the resulting azimuthal current density $\vec{j}$, and the associated deceleration force $\vec{j} \times \vec{B}$; (c) the time variation of the cloud radius, the stopping time of the transverse expansion, and the confinement radius; (d) the degree of diamagnetism (reduction of the magnetic flux in the cloud). Since each Lagrangian cell used in these calculations is allowed to expand also in the axial direction (the expansion rates are calculated from the pressure values known on both sides of the cloud-plasma interface), the effect of the complementary dimension is thus also taken into account. Energy is supplied to the cloud by means of flux-limited thermal conduction along the magnetic field lines and by anomalous conduction in the transverse direction from the side of the ambient plasma. The transverse energy flux is in general negligible compared with the field-aligned value, but is sufficient for initiating the ionization at the cloud-plasma interface. Noteworthy is that the ablation rate used in this second code is an input quantity obtained from the first (ablation) code.

Results of calculations

The parameters of the ASDEX-UP pellet shot analyzed are as follows: a = 50 cm, T_{e0} = 0.9 keV, $n_{e0} = 5.4 \times 10^{19}\ m^{-3}$, and B = 2 tesla. The measured spatial variations of T_e and n_e were used in the present calculations. The size of the pellet injected (equivalent radius of a spherical pellet) was $r_{pel} = 1.04$ mm, the injection velocity $v_{pel} = 880$ m/s. For the present calculations, the ablation rate and the associated pellet size reduction were determined sequentially at a discrete number of radial positions along the pellet path. At each position, first a cloud radius was assumed and the time-dependent ablation rate corresponding to this cloud radius and the local plasma parameters $T_e(r)$, $n_e(r)$ was calculated using the ablation code. Next, the ablation rate functions thus obtained was transferred to the transverse expansion program. The time history of the transverse expansion was now calculated. The major results of these calculations are the confinement radius (i.e. cloud radius) R_{cld} and the magnetic shielding factor B/B_0. which allow the ablation rate to be recalculated by using the ablation code. The procedure is iterated till it converges.

Figures 1 and 2 show the measured electron temperature and density profiles prior to

and after pellet injection (shot # 2708), respectively. Figure 3 shows the calculated radial variations of the radius of the shielding cloud, R_{cld}, and the magnetic shielding factor, B/B_0. At the periphery of the plasma, the plasma temperature is low and the ionization time of the ablated particles is relatively long. A relatively large cloud radius (in agreement with the diffuse cloud structure experimentally observed at the plasma periphery) results. As the pellet penetrates further inward, the ionization time becomes shorter and a continuously decreasing cloud radius results. Accordingly, the cloud density is rather low at the plasma periphery, yielding poor shielding, and notably higher at magnetic flux surfaces located closer to the plasma centre, resulting in more efficient shielding there. The local ablation rate is defined by the combination of the magnitudes of the pellet surface exposed to the energy carriers, the energy flux available, and the shielding efficiency of the cloud.

Figure 4 shows the variation of the calculated ablation rate along the pellet path. The values displayed correspond to local ablation rates averaged over the first 10 μs of the residence time of the pellet at each radial position. Noteworthy is the good correspondence between the resulting pellet penetration depth and the locations of the temperature minimum and density maximum on the post pellet curves.

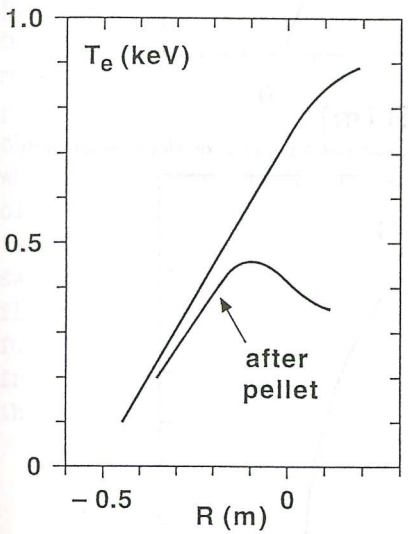

Fig 1 Electron temperature profile before and following pellet injection. (ASDEX-UP shot #2708)

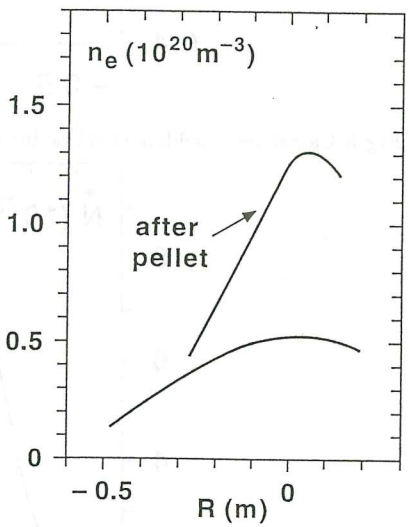

Fig 2 Electron density profile before and following pellet injection. (ASDEX-UP shot #2708)

ACKNOWLEDGMENT: The authors would like to thank the ASDEX-UP group for providing the measurement data cited in this paper.

[1] LENGYEL, L.L and SPATHIS, P.N., A time-dependent, slab symmetric ablation model with allowance for transverse expansion and magnetic confinement effects. IPP Rept. 5/50, Dec. 1992.

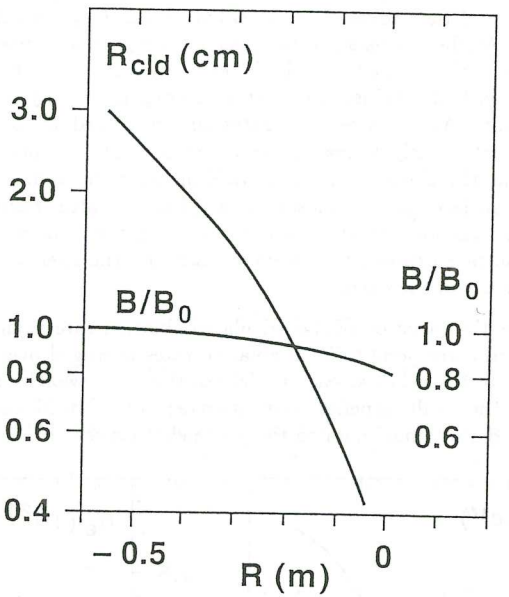

Fig 3 Calculated shielding cloud radius and magnetic shield factor along pellet path.

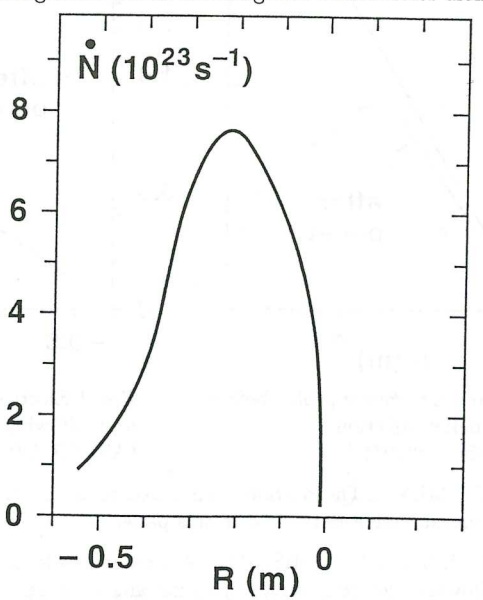

Fig 4 Calculated ablation rate along pellet path.

PLASMA PROPAGATION ALONG MAGNETIC FIELD LINES AFTER THE PELLET INJECTION

V.Rozhansky, I.Veselova

St.Petersburg Technical University
195251 Polytechnicheskaya 29 St.Petersburg Russia

After the evaporation and ionization of the pellet material the injected plasma propagates along magnetic field $\vec{B}$ and also drifts across B in the self-consistent electric fields [1]. At later stages when the density becomes almost uniform at the flux surfaces the radial anomalous transport of deposited particles takes place. In the present work only one aspect of this problem is considered - the 1-D ionized pellet ablatant propagation along a magnetic field. Numerical simulation is based on the model described in [1], [2]. According to this model the plasma source is deposited at t=0 and Z=0 (Z axis is parallel to the magnetic field B). The plasma source is characterized by the ablation rate $\dot{N}$ and its transverse size l_i which corresponds to the perpendicular dimension of the neutral cloud around a pellet. These parameters ($\dot{N}$ and l_i) should be taken from an experiment. After $t=\tau$ the plasma source is switched off according to the pellet shift from the considered flux surface so τ corresponds to the particle deposition time for the given flux surface. For $t > \tau$ the injected plasma freely propagates along magnetic field while it is heated by the electrons from the ambient plasma. The basic equations are

$$\frac{\partial n}{\partial t} + \frac{\partial}{\partial Z} nu = 0, \tag{1}$$

$$nm_i\left(\frac{\partial u}{\partial t} + u\frac{\partial u}{\partial Z}\right) = -\frac{\partial (nT_e)}{\partial Z}, \tag{2}$$

$$3/2n\left(\frac{\partial T_e}{\partial t} + u\frac{\partial T_e}{\partial Z}\right) + n\,T_e\frac{\partial u}{\partial Z} = -\frac{\partial q_{e\parallel}}{\partial Z}. \tag{3}$$

The boundary conditions were taken

$$n(Z \to \infty) = n_0, \quad T_e(Z \to \infty) = T_e^{(0)}, \quad u\,(Z \to \infty) = 0. \tag{4}$$

$$u\,\Big|_{Z=0} = C_s(0) = \sqrt{T_e^{(0)}/m_e}$$

$$n\Big|_{Z=0} = \frac{\dot{N}}{8C_s(0)l_i^2} \qquad \text{for } t \leqslant \tau \qquad (5)$$

$$T_e\Big|_{Z=0} = T_e^{(0)},$$

where $C_s(0)$ - the local sonic velocity. For $t>\tau$ the boundary conditions at $Z = 0$ are transformed:

$$u\Big|_{Z=0} = 0, \quad \frac{\partial n}{\partial Z}\Big|_{Z=0} = 0, \quad \frac{\partial T_e}{\partial Z}\Big|_{Z=0} = 0. \qquad (6)$$

The particle deposition time τ for was taken $\tau = 2.5$ μs, which roughly corresponds to the time of the pellet shift l_i/v_p (v_p is the pellet velocity). For the medium electron temperatures $T_e \leqslant 1$ keV the right side of the Eq.(3) is modelled by non-local heat conductivity [3]. For the high temperature plasma the right side could be obtained in the form similar to the one of hydrodynamic heat transport equation of Braginskii [4].

1. Medium temperature plasma.

Simulations were performed for the hydrogen pellet and following ambient plasma parameters $n_o = 3\cdot10^{19}m^{-3}$, $T_e^{(o)} = 500$ eV, $l_i = 0.25$ cm. The character of expansion is rather sensitive to the ablation rate value. Calculations were performed for the low, medium and high ablation rates $\dot{N}=10^{23}s^{-1}$, $\dot{N}=2.5\cdot10^{23}s^{-1}$, $\dot{N}=5\cdot10^{23}s^{-1}$ correspondingly. At fig.1 the density and temperature profiles are presented for $t=\tau=2.5$ μs and $\dot{N}=5\cdot10^{23}s$. The obtained profiles are in good agreement with the analytical self-similar solution for the isothermal plasma with $T_e = T_e^{(0)}$ (dotted lines)

$$n = \frac{\dot{N}}{8C_s(o)l_i^2}\exp(-Z/C_s(o)t) \qquad (7)$$

$$u = C_s(o)[1+Z/C_s(o)t]$$

At times much larger than τ when the electron temperature is close to the ambient one, plasma profile could be described by isothermal self-similar solution when $T_e=T_e^{(0)}$, $n=n(Z/t)$, $u=u(Z/t)$

$$n=A/t,\ u=Z/t, \quad \text{for } |Z| < Wt,$$
$$n=n_o,\ u=0, \quad \text{for } |Z| > Wt, \qquad (8)$$

where W is the shock velocity

$$W = C_s^{(o)} \cdot \sqrt{2\ln \frac{A}{n_o T}}, \qquad C_s^{(o)} = \sqrt{T_e / m_i} \cdot \tag{9}$$

where W is the shock velocity. The constant A corresponds to the particle deposition during $t = \tau$

$$A = \dot{N}\tau / (8\pi l_i^2 W) \tag{10}$$

At fig.2 the comparison between the self-similar solution and results of simulation are presented for $\dot{N}=5\cdot10^{23}s^{-1}$(a) and $\dot{N}=10^{23}s^{-1}$(b) at t=50 μs. It can be seen that for the small ablation rate the relatively fast heating is observed, the shock is formed in front of the cloud and obtained profile practically coincides with the analytical solution given by Eqs.(8)-(10). The velocity of the front is presented at fig.(3) for $\dot{N}=5\cdot10^{23}s^{-1}$(1) and $\dot{N}=10^{23}s^{-1}$(2). For all cases the supersonic expansion is observed so the Mach number calculated with respect to the ambient temperature is equal to 1.5 - 2.0. Density variation in time at a distance one meter from a pellet is shown at fig.4. Such type of signal was observed on TFTR in experiment [5] and on stelarator Heliotron E [6].

2. High temperature plasma.

The following set of ambient parameters were taken: $T_e^{(o)}$=5 keV, $n_o = 10^{20}\ m^{-3}$, $\dot{N} = 10^{25}s^{-1}$, l_i= 0.5 cm. The ablatant heating in this case is a much slower process, the expanding plasma temperature for a long time remains fairly low compared to the ambient one. The expanding velocity is subsonic calculated with respect to the ambient temperature. The case for $t<\tau$ qualitatively agrees with the calculations performed in [7] based on the model [8].

REFERENCES

1. Rozhansky,V., Veselova,I., Sov.J.Plasma Phys.17 (1991) 817.
2. Rozhansky, V., Veselova, I., in Controlled Fusion and Plasma Physics (Proc.18th Eur.Conf. Berlin. 1991). Vol.15A, Part I, European Physical Society (1991) 341.
3. Luciani,J.F. et al. Phys.Rev.Lett. 51 (1983) 1663.
4. Braginskii,S.I. in Reviews of Plasma Physics, edited by M.A. Leontovich (Consultant Bureau, New York, 1964), Vol.1, 183.
5. Mansfield, D.K. et al. Phys.Rev.Lett. 66 (1991) 3140.
6. Sudo, S. et al. Workshop on Pellet Injectors, ENEA, Frascati (1992).
7. Spathis, P. IPP Report 5/38, Jan.1992.
8. Lengyel, L.L., Zavala, G.G., Kardaun, O.J.W.F., Nucl.Fusion 31 (1991) 1107.

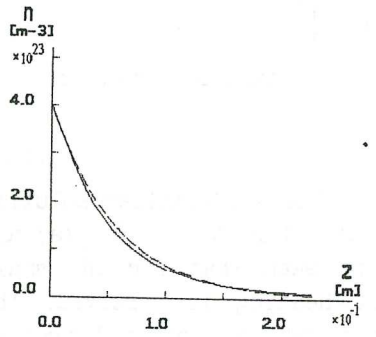

Fig.1a

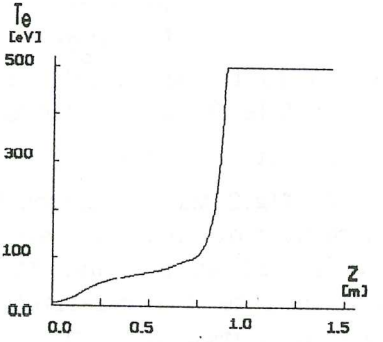

Fig.1b

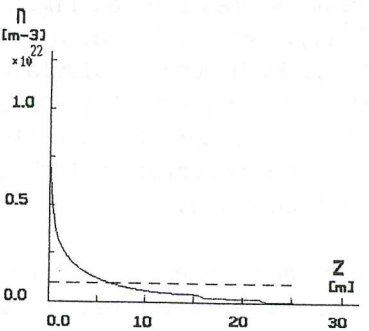

Fig.2a

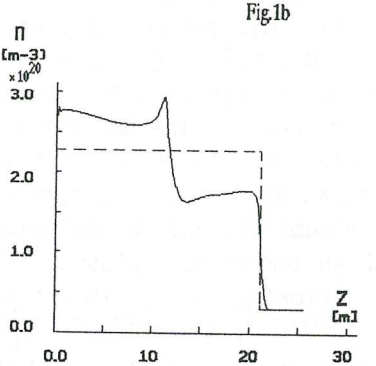

Fig.2b

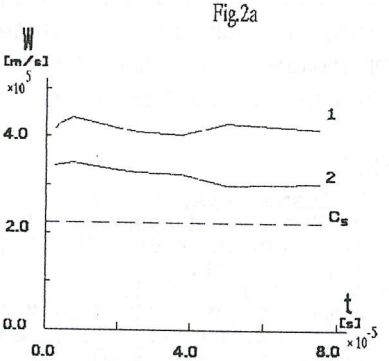

Fig.3

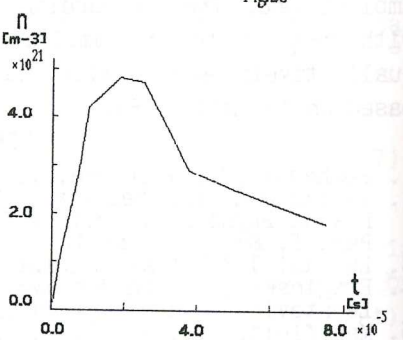

Fig.4

Solution to boundary problem for inhomogeneous kinetic equation describing particle sources

Zhykharsky A.V.
Scientific-technical Centre "Kinetika", P.O. Box 36, 630078, Novosibirsk, Russia

In the present work the stationary one-dimensional boundary kinetic problem taking account of the existence of particle sources in the plasma area in question has been formulated and analytically solved. This problem has been solved in the general form since the distribution of particle sources was specified as an arbitrary function of the coordinates and velocities.

1. Solution to boundary problem for the case of the point particle source.

To solve the problem a mathematical apparatus is made use of intended for solving the boundary problems in the case of the stationary kinetic equation /1/. The point of solving the problem is in the following:

a) The whole space area in question $\left(r \in [R_1, R_2\ ]\right)$ is divided in two areas: area "1" $\left(r \in [R_1, t\ ]\right)$ and area "2" $\left(r \in [t, R_2\ ]\right)$ where the point $r = t$ is a coordinate of particle sources. Since within each area the homogeneous kinetic equation holds true for areas "1" and "2" the boundary problem can be formulated and solved (the presence of source is represented by the appropriate boundary conditions).

b) Based on the general physical assumptions a distribution function for the whole area $\left(r \in [R_1, R_2\ ]\right)$ is written as combination of the solutions found. Postulate that this function is a solution to the boundary problem for the inhomogeneous kinetic equation for the point particle source and zero boundary conditions.

c) Operating on the general distribution function by the left side of the equation we will obtain the expression for the point source as the functions of coordinates and velocities.

1.1. Assume that $t = \tilde{r}$,i.e. $U(t) \geq U$ with $\left(r \in [R_1, R_2\ ]\right)$ (see Fig.1). In areas "1" and "2" the equation holds true

$$V \cdot \frac{\partial h_{1,2}}{\partial r} - \frac{dU}{dr} \cdot \frac{\partial h_{1,2}}{\partial V} = 0, \qquad (1)$$

where the functions h_1 and h_2 are distribution functions in areas "1" and "2" respectively.

By virtue of the conditions: $U(t) = U_t \geq U(r)$ the boundary conditions for the functions h_1 and h_2 have the form

$$h_1(R_1)\Big|_{v>0} = 0,\ h_1(t)\Big|_{v<0} = g\left(\frac{V^2}{2}, t\right);\quad h_2(t)\Big|_{v>0} = g\left(\frac{V^2}{2}, t\right),\ h_2(R_2)\Big|_{v<0} = 0, \qquad (2)$$

where g is an arbitrary function (source power).

The solutions to the boundary problems (1), (2) have the form (see /1/)

$$h_1 = \left[1 - H\left(V + \sqrt{2(U_t - U)}\right)\right] \cdot g\left(\frac{V^2}{2} + U - U_t, t\right); \qquad (3)$$

$$h_2 = H\left(V - \sqrt{2(U_t - U)}\right) \cdot g\left(\frac{V^2}{2} + U - U_t, t\right), \qquad (4)$$

where H is the Heavyside function.

Formally solutions (3) and (4) can be combined as follows

$$f = H(t - r) \cdot h_1 + H(r - t) \cdot h_2\,, \qquad (5)$$

The character of the problem in question permits drawing the conclusion that in the cited case the notion "particle source" is of spatial nature. The cited conclusion allows of introducing the following

point $r = t$ manifests itself in operating on the function (5) by the left side of the kinetic equation *only* when differentiating the function with respect to the coordinate "r".

Consequently we obtain:

$$L[f] = V\cdot\frac{\partial f}{\partial r} - \frac{dU}{dr}\cdot\frac{\partial f}{\partial V} = V\cdot\delta(t-r)\cdot(h_2 - h_1)\Big|_{r=t},$$

$$\left.\begin{array}{l} V>0 \rightarrow (h_2-h_1)\Big|_{r=t} = g\left(\dfrac{V^2}{2}, t\right) \\ V<0 \rightarrow (h_2-h_1)\Big|_{r=t} = -g\left(\dfrac{V^2}{2}, t\right) \end{array}\right\} = sign(V)\cdot g\left(\frac{V^2}{2}, t\right)$$

or

$$V\cdot\delta(t-r)\cdot(h_2-h_1)\Big|_{r=t} = |V|\cdot\delta(t-r)\cdot g\left(\frac{V^2}{2}, t\right).$$

Thus, one can contend that function (5) is a solution to the following boundary problem.

— kinetic equation
$$V\cdot\frac{\partial f}{\partial r} - \frac{dU}{dr}\cdot\frac{\partial f}{\partial V} = |V|\cdot\delta(t-r)\cdot g\left(\frac{V^2}{2}, t\right) \qquad (6)$$

— boundary condition
$$f(R_1)\Big|_{v>0} = 0, \quad f(R_2)\Big|_{v<0} = 0 \qquad (6.a)$$

Supplementary condition: $U_t = \max\limits_{R_1 \le r \le R_2}(U)$.

1.2. Consider the situation where the source and potential coordinates are not the same, i.e., the case where $t = r_1$ or $t = r_2$ (see Fig.1). The method of solving the appropriate boundary problem in this case is analogous to that applied to solving boundary problem (6). For the case $t < \tilde{r}$ the boundary conditions for areas "1" and "2" take the form

$$h_1(R_1)\Big|_{v>0} = 0, \quad h_1(t)\Big|_{v<0} = g\left(\frac{V^2}{2}, t\right) + h_2(t)\Big|_{v<0} \qquad (7)$$

$$h_2(t)\Big|_{v>0} = g\left(\frac{V^2}{2}, t\right), \quad h_2(R_2)\Big|_{v<0} = 0 \qquad (8)$$

The solution to the boundary problem (1), (8) in area "2" will be a function of the form (see /1/)

$$h_2 = H\left(V - sign(r-\tilde{r})\cdot\sqrt{2(\tilde{U}-U)}\right)\cdot g\left(\frac{V^2}{2} + U - U_t, t\right).$$

Consequently the boundary conditions for area "1" will have the form

$$h_1(t)\Big|_{v<0} = g\left(\frac{V^2}{2}, t\right) + h_2(t)\Big|_{v<0} = g\left(\frac{V^2}{2}, t\right)\cdot\left[1 + H\left(V + \sqrt{2(\tilde{U}-U_t)}\right)\right]$$

A function of the form will be the solution to the problem (1), (7) in area "1"

$$h_1 = \left[1 - H\left(V + \sqrt{2(U_t - U)}\right)\right]\cdot g\left(\frac{V^2}{2} + U - U_t, t\right) \times$$

$$\times\left[1 + H\left(V + \sqrt{2(\tilde{U}-U)}\right)\right],$$

where $\tilde{U}$ is maximum of the potential U over the entire interval $\left(r \in [R_1, R_2]\right)$. Further forming a function of the form (5) out of the functions h_1 and h_2 and substituting it in the left side of the kinetic equation we will obtain the same function as is the solution to the boundary problem (6). Similarly the appropriate expressions can be obtained for h_1 and h_2 in case $t = r_2$ (see Fig.1) and their combination as a function of the form (5) is a solution to the boundary problem (6).

Thus, in case of convex potential the boundary problem with a point source is described by equation (1) and with zero boundary conditions has the function (5) as a solution

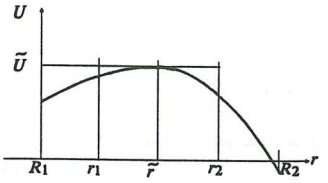

Fig.1

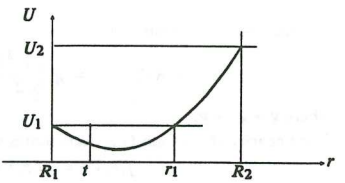

Fig.2

$$h_1 = \begin{cases} H\left(V - sign(r-\tilde{r})\cdot\sqrt{2(\tilde{U}-U)}\right)\cdot g\left(\frac{V^2}{2}+U-U_t,\,t\right), & t > \tilde{r} \\ \left[1 - H\left(V+\sqrt{2(U_t-U)}\right)\right]\cdot g\left(\frac{V^2}{2}+U-U_t,\,t\right)\times & \\ \times\left[1+H\left(V+\sqrt{2(\tilde{U}-U)}\right)\right], & t < \tilde{r}, \end{cases} \tag{9}$$

$$h_2\big|_{t>\tilde{r}} = h_1\big|_{t<\tilde{r}}, \quad h_2\big|_{t<\tilde{r}} = h_1\big|_{t>\tilde{r}}$$

1.3. Now assume that the particle source is in the potential well (see Fig.2). In this case the boundary conditions for areas "1" and "2" are written as

$$h_1(R_1)\big|_{v>0} = 0, \quad h_1(t)\big|_{v<0} = g\left(\frac{V^2}{2},\,t\right) + h_2(t)\big|_{v<0} \tag{10}$$

$$h_2(R_2)\big|_{v<0} = 0, \quad h_2(t)\big|_{v>0} = g\left(\frac{V^2}{2},\,t\right) + h_1(t)\big|_{v>0}$$

To solve the problem stated consider the following iterative process. At the first step of iteration assume that areas "1" and "2" are fully isolated from each other. The boundary conditions (10) are transformed into the form

$$h_1(R_1)\big|_{v>0} = 0, \quad h_1(t)\big|_{v<0} = g\left(\frac{V^2}{2},\,t\right);$$

$$h_2(R_2)\big|_{v<0} = 0, \quad h_2(t)\big|_{v>0} = g\left(\frac{V^2}{2},\,t\right)$$

By solving the boundary problem for the functions h_1 and h_2 with these boundary conditions find a first approximation of these functions. Then through expression (10) find a second approximation for the boundary conditions at the point t. By solving the boundary problem for h_1 and h_2 with a second approximation for the boundary conditions find a second approximation for the functions h_1 and h_2 etc.

The calculations based on this model showed that the problem with a point particle source being located in the potential well has no final solutions for the stationary formulation of boundary kinetic statement (in this case the distribution functions tends to infinity).

2. Solution to boundary kinetic problem for distributed source

The results obtained while analysing the problem on the point particle source permit presenting the function of the distributed particle source as

$$P(r,V) = |V|\cdot g\left(\frac{V^2}{2},\,r\right),$$

where g is an arbitrary function. The statement of the boundary kinetic problem has the form

— kinetic equation

$$V\cdot\frac{\partial f}{\partial r} - \frac{dU}{dr}\cdot\frac{\partial f}{\partial V} = |V|\cdot g\left(\frac{V^2}{2},\,r\right), \tag{11}$$

— boundary conditions

$$f(R_1)\Big|_{v>0} = g_1\left(\frac{V^2}{2}\right), f(R_2)\Big|_{v<0} = g_2\left(\frac{V^2}{2}\right), \qquad (11.a)$$

where $g \neq g_1 \neq g_2$.

The linearity of equation (11) necessitates seeking a solution to the equation in the form

$$f(r,V) = f_0(r,V) + f_1(r,V), \qquad (12)$$

where $f_0(r,V)$ is a solution to the homogeneous kinetic equation with boundary conditions (11a). The solution to this boundary problem is given in /1/; $f_1(r,V)$ is a solution to equation (11) with zero boundary conditions.

The function $f_1(r,V)$ can be presented as

$$f_1(r,V) = \int_{R_1}^{R_2} [H(t-r)\cdot h_1(t,r,V) + H(r-t)\cdot h_2(t,r,V)]\cdot dt, \qquad (13)$$

where the functions h_1 and h_2 conform to presentation (9).

Prove that function (13) is a solution to equation (11). Write the expression

$$L[f_1] = \int_{R_1}^{R_2} L[H(t-r)\cdot h_1(t,r,V) + H(r-t)\cdot h_2(t,r,V)]\cdot dt,$$

where "L" is a differential operator of the left side of the kinetic equation. The operator "L" affects the functions of "r" and "V" only. The function in the square brackets under integral is a solution to equation (6) with a point source at the point $r = t$. Consequently, we can write

$$L[f_1] = \int_{R_1}^{R_2} |V|\cdot g\left(\frac{V^2}{2} + U(r) - U(t), t\right)\cdot\delta(r-t)\cdot dt = |V|\cdot g\left(\frac{V^2}{2}, r\right).$$

The function (13) is thus shown to be a solution to equation (11). The function (13) satisfies the zero boundary conditions since they are satisfied by the functions h_1 and h_2. Thus we can assert that the solution to the boundary problem (11), (11a) has been found.

3. Discussion of the results obtained

Investigations carried out in the work permit drawing the following conclusions:

(1) a mathematical apparatus has been obtained which permits formulating (writing an explicit expression for the right side of the inhomogeneous kinetic equation) and finding a rigorously analytical solution (with accuracy to unknown "force" fields) to the boundary kinetic problem describing physical statement with a point and spatially distributed particle source inside the plasma region under consideration.

(2) it appeared that inside the potential well the solutions found admit of no existence of a particle source such as to "generate" the particles that remain inside the well. It turned out that a stationary problem describing the particle source inside a potential well can be formulated only when there is a particle "sink" inside the very well. This conclusion is quite evident and the fact that the result obtained was not postulated in advance while stating the problem but was obtained as a natural outcome of boundary kinetic statement is, in author's opinion, an indirect corroboration of adequacy of the results obtained.

(3) To completely solve the problems of constructing a completely closed mathematical apparatus in order to solve boundary problems with inhomogeneous kinetic equations it is necessary to exactly formulate and solve the boundary problem describing the particle "sinks".

/1/ Zhykharsky A.V. Physica Scripta. Vol.44, 606-616, 1991.

The Effect of Intense Pump Waves on Electrostatic Oscillations in an Ununiform Plasma

V. Demchenko
International Atomic Energy Agency
Wagramerstrasse 5, P.O. Box 100
A-1400 Vienna, Austria

Abstract. Equations describing parametric excitation of the potential waves in an ununiform plasma are derived. It is shown that such equations with an accuracy of redefinition of natural (basic) plasma frequency coincides with well-known equations describing parametric resonance in an uniform plasma. The natural frequencies of plasma waves could be obtained by solution of a boundary-value problem taking into account spatial distribution of plasma density.

1. Introduction. Although linear theory of parametric instabilities of uniform plasmas can be regarded to be developed [1,2], the study of such instabilities in a nonuniform plasma is still far from complete. Since in a real experimental conditions plasma ununiformity, as a rule, could play a significant role in all dynamical processes, it is of considerable practical interest to consider influence of strong high-frequency (pump) elertrical field on waves dispersion in an inhomogeneous plasma.

2. "Separation" method for equations describing parametric excitation of potential waves in an ununiform plasma. Let us consider uniform isotropic plasma with density gradient directed along z-axis. The pump electrical field is supposed to coincide with x -axis:

$$E_{xp} = \sum_{i=0}^{2} E_i \sin \omega_i t \quad , \qquad \omega_1 = \omega_0 + \Omega \, , \quad \omega_2 = \omega_0 - \Omega \, , \quad \omega_0 \gg \Omega$$

An initial set of equations can be written as follows:

$$\frac{\partial \vec{v}_a}{\partial t} + (\vec{v}_a \nabla)\vec{v}_a = \frac{e_a}{m_a}(\vec{E}_p - \nabla\varphi) \, , \quad \frac{\partial n_a}{\partial t} + \operatorname{div}(n_a \vec{v}_a) = 0 \, , \quad (1), (2)$$

$$\Delta\varphi = -4\pi \sum_a e_a n_a \, , \qquad (3)$$

where $n_a, \vec{v}_a$ - density and velocity of particles $(a = e, i)$, φ - electrostatic potential.

From Eq. (1) the electron quiver velocity is simply

$$\vec{v}_e = -\frac{e}{m_e} \sum_{i=0}^{2} \frac{E_i}{\omega_i} \cos \omega_i t$$

Perturbation of density $\tilde{n}_a = n - n_0(\vec{r})$, velocity $\tilde{\vec{v}}_a = \vec{v}_a - \vec{v}_a(t)$ as well as electrostatic potential, could be written in the form $\sim f(z,t)\exp(i\Phi), \Phi = k_x x + k_y y$.
Eqs. (1) and (2) could be combined to give

$$\frac{\partial^2 \tilde{v}_a}{\partial t^2} = \frac{e_a^2}{m_a^2} \exp(i A_a(t)) \, \hat{L}_1 \varphi \, , \qquad (4)$$

where $v_a = e_a \tilde{n}_a \exp(i A_a(t))$, $\hat{L}_1 \equiv \partial/\partial z\,(n_0(z)\,\partial/\partial z) - k^2 n_0(z)$,

$$A_a(t) = k_x \int_{-\infty}^{t} v_a(t')\,dt' = -\frac{e_a}{m_a} k_x \sum_{i=0}^{2} \frac{E_i}{\omega_i^2} \sin \omega_i t.$$

In new variables, Eq. (3) becomes

$$\hat{L}_2 \varphi = 4\pi \sum_a v_a \exp(-i A_a(t)), \quad \hat{L}_2 \equiv k^2 - \partial^2/\partial x^2 \qquad (5)$$

Now suppose $v_a(z,t) = v_{a1}(t)\, v_{a2}(z)$, $\varphi(z,t) = \varphi_1(t)\,\varphi_2(z)$, so that Eqs. (4) and (5) yields

$$\frac{\hat{L}_2 \varphi_2(z)}{\hat{L}_1 \varphi_1(z)} = \varphi, \qquad \varphi = -\frac{4\pi e^2}{m_e p^2}, \qquad (6)$$

p - unknown (separation) constant to be determined from the solution of boundary-value problem (6). For time-dependent functions $v_{e,i}(t)$ the following set of equations can be written:

$$\frac{\partial^2 v_{e1}}{\partial t^2} + p^2 \left\{ v_{e1} + v_{i1} \exp\left[i (A_e(t) - A_i(t)) \right] \right\} = 0, \qquad (7)$$

$$\frac{\partial^2 v_{i1}}{\partial t^2} + \frac{m_e}{m_i} p^2 \left\{ v_{i1} + v_{e1} \exp\left[-i (A_e(t) - A_i(t)) \right] \right\} = 0. \qquad (8)$$

Eqs. (7) and (8) with an accuracy of redefinition $p^2 \longrightarrow \omega_{pe}^2$, $(m_e/m_i)p^2 \longrightarrow \omega_{pi}^2$ coincides with system of equations describing parametric excitation of volumetric waves in an uniform plasma (see Ref. [1]).

3. Solution of "spatial" part of the problem. As an example, let us consider excitation of surface waves propagating along plasma cylinder of radius a ($\tilde{n}_a$, v_a, $\varphi \sim \exp[i(kz + m\varphi)]$. Eq. (6) becomes

$$\frac{1}{r} \frac{d}{dr} \left(\varepsilon(r)\, r \frac{d\varphi_2}{dr} \right) - \left(k^2 + \frac{m^2}{r^2} \right) \varepsilon(r) \varphi_2 = 0. \qquad (9)$$

Continuity of values $\varepsilon\, d\varphi_2/dr$ and φ_2 at $r = a$ yields

$$\varepsilon_0(p) + \eta_m(ka) = 0, \quad \varepsilon_0(p) \equiv \varepsilon(r \le a), \quad \eta_m(ka) = -\frac{I_m(ka)}{I_m'(ka)} \cdot \frac{K_m'(ka)}{K_m(ka)}. \qquad (10)$$

From Eq. (10), we have, in explicit form, expression for value p :

$$p \equiv \omega_{pe}^{*} = \omega_{pe}(a) \cdot \left(1 + \eta_m(ka)\right)^{1/2}. \tag{11}$$

4. Solution of time-dependent equations. Parametric excitation of volumetric waves in a homogeneous plasma has been investigated in [3]. Following this paper, let us introduce functions

$$\langle v_{e1} \rangle = \frac{\omega_0}{2\pi} \int_0^{2\pi/\omega_0} v_{e1}(t)\, dt = \sum_k \langle v_{e1} \rangle^{(k)} e^{-ik\omega t - ik\Omega t},$$

for which one could obtain the following set of equations:

$$\langle v_{e1} \rangle^{(m)} = - R_e^{(m)} \sum_k \langle v_{i1} \rangle^{(m+k)} A_{-k}, \tag{12}$$

$$\langle v_{i1} \rangle^{(m)} = - R_i^{(m)} \sum_k \langle v_{e1} \rangle^{(m+k)} A_k, \tag{13}$$

where $A_k = A_{-k} = \sum_{\ell} J_{-k-2\ell}(q_0)\, J_{k+\ell}(q_1)\, J_{\ell}(q_2)$,

$$q_i = \frac{e k_z E_i}{m_e \omega^2}, \quad R_e^{(m)} = \frac{p^2}{p^2 - (\omega + m\Omega)^2}, \quad R_i^{(m)} = \frac{(m_e/m_i)\, p^2}{(m_e/m_i) p^2 - (\omega + m\Omega)^2}.$$

From Eqs. (12) and (13) one can determine the dispersion equation in the form

$$\left(1 - R_e^{(0)} \sum_k A_k^2 R_i^{(k)}\right)\left(1 - R_e^{(-1)} \sum_k A_{-(k+1)} R_i^{(k)}\right) = R_e^{(0)} R_i^{(-1)} \left(\sum_k A_k A_{k+1} R_i^{(k)}\right)^2. \tag{14}$$

Eq. (14) predicts the parametric build-up of HF oscillations ($\omega \sim |p|$) at the frequency domain $\Omega \approx 2|p|/q$ (q-odd number).

For weak pump amplitude modulations ($E_1 = E_2 = \frac{\Delta}{2} E_0, \Delta \ll 1$) the growth rate may be written as

$$\gamma = \frac{1}{2}\left[f(p) + f(-p) + \frac{1}{\sqrt{2}} \left\{ \Delta''^2 + \Delta'^2 + 4|W|\, f(p) f(-p) + \left[\left(\Delta''^2 - \Delta'^2 + 4|W|\, f(p) f(-p)\right)^2 + 4(\Delta' \Delta'')^2 \right]^{1/2} \right\}^{1/2} \right], \tag{15}$$

where

$$\Delta' = g_1(p) - g_2(-p), \qquad \Delta'' = f(p) - f(-p),$$

$$f(p) = -\delta\varepsilon_e''(p)\left(\frac{\partial\varepsilon_e'(p)}{\partial\omega}\right)^{-1}, \quad g_1(p) = \left(\frac{\partial\delta\varepsilon_e'(p)}{\partial\omega}\right)^{-1}\sum_k A_k^2 R_i^{(k)},$$

$$g_2(p) = \left(\frac{\partial\delta\varepsilon_e'(p)}{\partial\omega}\right)^{-1}\sum_k A_{k+1}^2 R_i^{(k)}, \quad W = \frac{\left(\sum_k A_k A_{k+1} R_i^{(k)}\right)^2}{\delta\varepsilon_e''(p)\,\delta\varepsilon_e''(-p)}, \quad \delta\varepsilon_e'' = \frac{\omega_{pe}^2}{p^3}\nu_{ei},$$

ν_{ei} -electron - ion collision frequency.

From expression (15) one can get the condition for parametric build-up:

$$0 \le \Delta' < (|W|-1)\,(f(p) + f(-p))^{1/2} \tag{16}$$

and maximum value of the growth rate

$$\gamma_{max} = \frac{\omega}{2}\cdot\left(\frac{m_e}{m_i}\right)^{3/2}\cdot p\cdot\left(a_0 J_0(a_0) J_1(a_0)\right). \tag{17}$$

"Separation" constant p entering expressions (16) and (17) is determined by formula (11).

References

1. V.P. Silin, Parametric Effects of Intense Radiation on Plasmas (in Russian), Nauka, Moscow, 1973.

2. Advances in Plasma Physics, General Editors: A. Simon and W.B. Thompson, v. 6, New York, Wiley, 1976.

3. Yu. M. Aliev, D. Sunder, JETP (Russ), 1971, v. 61, p. 1057.

CONFORMAL MAGNETOSONIC WAVES

S.V. Bulanov* and F. Pegoraro**

* General Physics Institute of Russian Academy of Sciences, Moscow, Russia
** Dept. of Theoretical Physics, University of Turin, Turin, Italy

The propagation of magnetosonic and Alfvèn waves in an arbitrary planar current-free magnetic configuration is solved explicitly, with the help of a conformal transformation in the case of magnetosonic waves. The role of critical points of the magnetic configuration is discussed. The expressions of dimensionless parameters describing the relative role of nonlinear and dissipative effects near X-points are presented.

The problem of the propagation of MHD perturbations near the critical points of a magnetic configuration is related to the general problem of reconnection of magnetic field lines. X- and O-points represent a typical local behaviour of a nonuniform, locally two-dimensional configuration in the neighbourhood of a critical field line, while additional structures, such as Y-points, arise in the presence of current sheets. In the case of an X-point the propagation of small MHD perturbations leads to singularities of the electric current, which, in the nonlinear regime, correspond to the formation of current sheets either at the X-point or at the two separatrices. This current accumulation occurs because in these regions the group velocity of the perturbations tends to zero. It indicates that the wave dynamics becomes nonlinear and, in the presence of a finite electron resistivity, it leads to magnetic reconnection.

We consider two-dimensional MHD perturbations that propagate in a static plasma with uniform density ρ in a planar, current-free, magnetic configuration : $\mathbf{B}_o(x,y) = -\mathbf{e}_z \times \nabla \mathbf{A}_o(x,y)$. The equations governing small amplitude magnetosonic and Alfvèn waves in the absence of dissipation are

$$\frac{\partial^2 a}{\partial t^2} - \frac{(\nabla A_o)^2}{4\pi\rho}\,\Delta a = 0, \tag{1}$$

$$\frac{\partial^2 b}{\partial t^2} - \frac{(\mathbf{B}_o \cdot \nabla)^2}{4\pi\rho}\; b = 0, \tag{2}$$

where $a = a(x,y,t)$ and $b = b(x,y,t)$ are the z-components of the perturbed vector potential and magnetic field respectively. In a uniform magnetic field Eq.(1) reduces to $\omega^2 = |\mathbf{k}|^2 |\mathbf{c}_a|^2$, and Eq.(2) to $\omega^2 = (\mathbf{k}\cdot\mathbf{c}_a)^2$, with $\mathbf{c}_a = \mathbf{B}_o/(4\pi\rho)^{1/2}$ the Alfvèn velocity.

Since the background magnetic field is taken to be current free, $\Delta A_o = 0$, the unperturbed vector potential A_o is a harmonic function. In this case we can solve Eq.(1) by introducing a conformal mapping from the complex $\zeta = x + iy$ plane to the complex plane $w = u + iv$. Under the conformal mapping

$$w = w(\zeta) = \int^{\zeta} \frac{d\zeta}{A'(\zeta)}, \tag{3}$$

the Laplace operator Δ_ζ is changed into $|w'(\zeta)|^2\, \Delta_w = |A'|^{-2}\Delta_w$, where a prime denotes complex differentiation and the index denotes the variables with respect to which the Laplacian is taken. Then the magnetosonic wave equation (1) takes the simple Cartesian form

$$\frac{\partial^2 a}{\partial t^2} \; - \; \Delta_w a = 0, \tag{4}$$

where we have redefined t so as to include the factor $4\pi\rho$. The Alfvèn wave equation (2) can instead be rewritten in the form

$$\frac{\partial^2 b}{\partial t^2} \; - \left(|A'(\zeta)|^2 \, \frac{\partial}{\partial F_o} \right)^2 \; b = 0. \tag{5}$$

Here $A(\zeta)$ is an analytic function: its real part, $\Re A(\zeta)$, coincides with the unperturbed vector potential A_o, and its imaginary part is $F_o = \Im A(\zeta)$. The magnetic field $\mathbf{B}_o(x,y)$ can be written in terms of $B(\zeta) \equiv A'(\zeta)$ as $B_{ox} = -\Im B(\zeta)$, and $B_{oy} = -\Re B(\zeta)$.

Eq.(5) describes the propagation of Alfvèn waves along the field lines of the unperturbed magnetic field and its general solution $b = b(A_o, \theta)$ is an arbitrary function of

$$A_o = A_o(x,y), \quad \text{and} \quad \theta(x,y,t) = t \pm \int \frac{dF_o}{|A'|^2}. \tag{6}$$

Eq.(4) can be solved by separation of variables either in Cartesian coordinates in the $u - v$ plane, or in "cylindrical" coordinates $\varpi = (u^2 + v^2)^{1/2}$ and $\psi = \arctan u/v$. Solutions of the form $a = a(u \pm t)$ or $a = a(v \pm t)$ in w-plane correspond to waves that propagate in physical $x - y$ space respectively perpendicular or parallel to the field lines of the dual magnetic field whose complex vector potential is $w(\zeta)$ and is defined by $B^*(\zeta) \equiv 1/A'(\zeta) = 1/B(\zeta)$ (i.e. $\mathbf{B}^*_o(x,y) \equiv \left[-B_{ox}(x,y)\mathbf{e}_x + B_{oy}(x,y)\mathbf{e}_y \right] \left| B_o(x,y) \right|^{-2}$). For general propagating Cartesian solutions the complex wave vector $\kappa_\zeta \equiv k_x + ik_y$ in $x - y$ space [defined in terms of the logarithmic derivative of $a(x,y,t)$] is related to the complex wave vector κ_w in the ζ-plane by $\kappa_\zeta = i\kappa_w \; B^*(\zeta)$, $\kappa_w = -i\kappa_\zeta \; B(\zeta)$. This duality condition allows us, by interchanging $B(\zeta)$ with $B^*(\zeta)$, to relate, e.g., the propagation of magnetosonic waves around a current free X-point to that around an O-point with all the current concentrated at the singular point where $|B(\zeta)| \to \infty$ (current

line). If $B(\zeta) \to 0$ for $\zeta \to \zeta_o$, $w'(\zeta)$ and $B^*(\zeta) \to \infty$. Thus in the $x-y$ plane, both the wave vector and the amplitude of the perturbed magnetic field diverge if $a(w) \neq 0$ and $k_w \neq 0$ at $w = w(\zeta_o)$. Inversely, if $B(\zeta) \to \infty$ at $\zeta = \zeta_o$, the wave vector and the field amplitude in the $x - y$ plane vanish. Thus magnetic energy accumulates in the vicinity of an X-line and is reflected by an O-point with a current line. This also implies that dissipative effects are important in the former, but not in the latter case. Depending on the zeros and singularities of $A'(\zeta)$, the image of the $x - y$ plane under the conformal mapping $w(\zeta)$ can either be a subdomain of the w-plane, or it can require the definition of branch cuts in the w-plane, which has to be extended over different Riemann sheets. This requires a reexamination of the boundary conditions to be imposed in the w- and in the ζ-planes, and of the position and form of the radiation source terms.

In the case of a uniform magnetic field, $A(\zeta) = B_o\zeta$, the conformal transformation (3) is trivial: $w(\zeta) = \zeta/B_o$. In the neighbourhood of a current free X-point $A(\zeta) = h\zeta^2/2$, where h is the value of the field gradient, and the field lines are hyperbolae $\Re A$ = const. The conformal mapping is $w(\zeta) = h^{-1} \ln \zeta$ so that $u = h^{-1} \ln r$ and $v = h^{-1}\phi$, with r and ϕ the polar coordinates in the $x-y$ plane. The simplest Cartesian solutions in the w-plane correspond in the $x - y$ plane to cylindrical waves of the type $a = a(\ln r \pm ht)$ and to "rotating waves" $a = a(\phi \pm ht)$. Radially converging solutions take an infinite time to reach $r = 0$. The dual configuration is $B^*(\zeta) = 1/(h\zeta)$, and corresponds to the magnetic field near the O-point with a "current line" $c/(2\pi h)$ at the O-point. The conformal mapping is in this case $w(\zeta) = h\zeta^2/2$. Cartesian solutions in w-plane correspond in $x - y$ plane to perturbations propagating perpendicularly to a branch of an equilateral hyperbola. The phase velocity increases towards the O-point, where the wave number and the amplitude of the perturbed magnetic field tend to zero. Analogous solutions can be obtained for the case of a Y-point ($B(\zeta) \propto w(\zeta) \propto \zeta^{1/2}$) and its dual configuration ($B^*(\zeta) \propto \zeta^{-1/2}$), and for a current sheet between two Y-points $B(\zeta) = h(\zeta^2 - \zeta_o^2)^{1/2}$, $w(\zeta) = h^{-1}$ $\arcsin \zeta/\zeta_o$, where $h|\zeta_o|^2$ measures the total current in the sheet. In these configurations, perturbations reach the singular points in a finite time. Cartesian solutions of the form $a = a(v \pm t)$ with $v = \Im \arcsin \zeta/\zeta_o$ reach the current sheet simultaneously at $t = 0$ due to the non uniformity of the velocity of propagation. The magnetic field configuration given by $B(\zeta) = h(\zeta - \zeta_o^2/\zeta)$ corresponds to the configuration with two X-points at $\zeta = \pm\zeta_o$ and an O-point with a current line at $\zeta = 0$. The corresponding conformal mapping is $w(\zeta) = (1/2h)\ \ln(\zeta^2 - \zeta_o^2)$. The dual field is $B^*(\zeta) = \zeta/[h(\zeta^2 - \zeta_o^2)]$ with one X-point and two O-points with current lines. Perturbations propagate faster towards the center of the island in the direction

of the O-point with the current line, which they reach in a finite time, and are then deflected towards the X-points, where energy is accumulated.

Nonlinear effects are important when the wave amplitude becomes comparable to the unperturbed field $|B_o|$. Near the null points of $|B_o|$, the perturbed magnetic field of the magnetosonic waves tends to ∞ as $|\mathbf{b}_\perp| = |(\partial a/\partial t)w'| = |(\partial a/\partial t)||B_o|^{-1}$. Then, the characteristic nonlinear scale r_m is given by $|B_o(r_m)|^2 = |\partial a/\partial t|$. Analogously the relevant nonlinear scale r_a for Alfvèn waves can be obtained from $|B_o(r_a)| = |\mathbf{b}_\perp|$. Ohmic dissipation leads to damping of both Alfvèn and magnetosonic waves and to their reflection from the vicinity of the null points. The characteristic distance from the null points reached by a wave with frequency ω is $|B_o(r_\nu)|^2 \approx \omega\nu_m$, with ν_m the magnetic diffusion coefficient. The dimensionless ratio $L_m = [B_o(r_m)/B_o(r_\nu)]^2 = (\partial a/\partial t)/[(4\pi\rho)^{1/2}\nu_m\omega]$ characterizes the relative role of nonlinear and dissipative effects in the case of magnetosonic waves, and $L_a = [B_o(r_a)/B_o(r_\nu)]^2 = |\mathbf{b}_\perp|^2/(4\pi\rho\nu_m\omega)$ that of Alfvèn waves. Here we have reintroduced the factor $4\pi\rho$. If $L_m, L_a \gg 1$, current sheets will be formed in the vicinity of the null points.

To clarify the meaning of these dimensionless parameters we show, as an example, that in the Sweet-Parker model of forced reconnection L_m represents the square of the ratio between the width d and the length l of the current layer. Simple order of magnitude estimates based on the continuity, momentum balance and Ohm's equations give $d^2 \approx \nu_m/\Omega$ and $v_{in} \approx \Omega d$, where $\Omega \approx h/(4\pi\rho)^{1/2}$ is the Alfvèn frequency at an X-point with field gradient h, and v_{in} is the plasma inflow velocity. The length l is related to the total current I in the layer: $l^2 \approx I/(hc)$. Writing $I/c \approx J(ld/c) \approx cE(ld/\nu_m)$, where J is the current density in the layer and the electric field E is given by $E = -\partial a/c\partial t$, we obtain $L_m = (\omega l)/(\Omega d)$. We can interpret ω as the inverse of the reconnection time $l/v_{in} \approx l/(\Omega d)$' defined as the time it takes the plasma to cross the region of size l where the current density is significant. Then we find $L_m \approx (l/d)^2$.

S.V. Bulanov and S.I. Syrovatskii, Sov. J. Plasma Phys. **6**, 661-667 (1980).

S.V. Bulanov and F. Pegoraro "Conformal Magnetosonic Waves" to be published in Phys. Lett. **A** (1993)

Negative Energy Waves in a Magnetically Confined Guiding Center Plasma

G.N. Throumoulopoulos [1] and D. Pfirsch
Max-Planck-Institut für Plasmaphysik
EURATOM Association, D-8046 Garching, Germany

The conditions for the existence of negative-energy waves for electrostatic initial perturbations (which could be nonlinearly unstable and cause anomalous transport) are investigated for an equilibrium with space dependent, sheared magnetic field. The method of investigation consists in evaluating the general expression for the second-order wave energy derived by Pfirsch and Morrison [1] for the case of the Maxwell-drift kinetic theory, based on the Lagrangian formulation of the quiding center theory given by Littlejohn [2] and later regularized by Correa-Restrepo and Wimmel [3]. In Cartesian coordinates, the equilibrium magnetic field is given by $\boldsymbol{B}^{(0)} = B_x^{(0)}(y)\boldsymbol{e}_x + B_z^{(0)}(y)\boldsymbol{e}_z$, and the mean Lorentz force, acting along the y-axis, balances the force due to the pressure gradient; thus, the equilibrium condition $P^{(0)} + (B^{(0)})^2/8\pi =$ constant is satisfied. The guiding center drift velocity $\boldsymbol{v}_{g\nu}^{(0)}$ of any species ν possesses, in addition to the component $v_{g\nu\|}^{(0)} = q_4/g_\nu'$ parallel to the magnetic field, a perpendicular component due to the grad-B drift (q_4 is a velocity variable, the function $g_\nu(z)$ regularizes the theory, and the rest of the non-standard symbols are illustrated in Table 1). The equilibrium guiding center distribution function $f_{g\nu}^{(0)}$ is a function of y, y being a conserved quantity because the quiding centers move on a plane perpendicular to the y-axis, q_4 and the adiabatic invariant magnetic moment μ [$f_{g\nu}^{(0)}(y, q_4, \mu)$].

After a lengthy calculation, the second-order wave energy for the equilibria considered and for purely electrostatic initial perturbations can eventually be cast in the neat form

$$F^{(2)} = -S\sum_\nu \int dq_4 d\mu dy\, |G_\nu^{(1)}|^2\, \frac{B_\nu^{*(0)}}{m_\nu} \left(\boldsymbol{k}_{xz}\cdot \boldsymbol{v}_{g\nu}^{(0)}\right) \left(k_\| \frac{\partial f_{g\nu}^{(0)}}{\partial q_4} - k_\perp \frac{g_\nu'}{\omega_\nu^{*(0)}} \frac{\partial f_{g\nu}^{(0)}}{\partial y}\right),$$

where $G_\nu^{(1)}(y, q_4, \mu)$ is a first order function which is connected with the perturbations around the equilibrium state, and $\boldsymbol{k}_{xz}$, $k_\|$ and $k_\perp$ are, respectively, the wave vector lying on the x-z plane and its components parallel and perpendicular to $\boldsymbol{B}^{(0)}$. The following conditions for the existence of negative-energy waves, which need only be satisfied locally in y, q_4 and μ, obtain if the reference frame is one of minimum energy, i.e. if in it the center-of-mass velocity parallel to $\boldsymbol{B}^{(0)}$ vanishes. The conditions for oblique propagation ($k_\| \neq 0$) are substantially different from those for perpendicular propagation ($k_\| = 0$). The former case is thus discussed separately from the latter as follows.

[1] Permanent address: University of Ioannina, Department of Physics, Division of Theoretical Physics, GR 451 10 Ioannina, Greece.

Symbol	Meaning or Definition
S	normalization surface
v_0	constant velocity
z	q_4/v_0
g'_ν	dg_ν/dz
$B^{(0)}$	magnetic field modulus
$\boldsymbol{b}^{(0)}$	$\boldsymbol{B}^{(0)}/B^{(0)}$
$\boldsymbol{B}^{*(0)}_\nu$	$\boldsymbol{B}^{(0)}_\nu + (m_\nu c/e_\nu)v_0 g(z)\,\nabla\times\boldsymbol{b}^{(0)}$
$B^{*(0)}_\nu$	modulus of $\boldsymbol{B}^{*(0)}_\nu$
$\omega^{*(0)}_\nu$	$e_\nu B^{*(0)}_\nu/cm_\nu$

Table 1: Notation

1. Oblique waves ($k_\parallel \neq 0$) If any $f^{(0)}_{g\nu}(y, q_4, \mu)$ has the property $\frac{q_4}{g'_\nu}\frac{\partial f^{(0)}_{g\nu}}{\partial q_4} > 0$, negative-energy waves exist provided $\frac{k_\parallel}{k_\perp} < min(\Lambda_\nu, M_\nu)$ or $\frac{k_\parallel}{k_\perp} > max(\Lambda_\nu, M_\nu)$, where $\Lambda_\nu \equiv -\frac{4\pi g'_\nu \mu\, dP^{(0)}/dy}{m_\nu q_4 B^{(0)}\omega^{*(0)}_\nu}$ and $M_\nu \equiv \frac{g'_\nu \partial f^{(0)}_{g\nu}/\partial y}{\omega^{*(0)}_\nu \partial f^{(0)}_{g\nu}/\partial q_4}$. For particles with thermal velocities it holds $\Lambda_\nu \approx M_\nu \approx \frac{(r_{L\nu})_{th}}{L} \ll 1$, with $(r_{L\nu})_{th}$ the Larmor radius at thermal velocities and L the macroscopic scale length. No essential restriction is therefore imposed on the orientation or the magnitude of the wave vector $\boldsymbol{k}_{xz}$. The condition $\frac{q_4}{g'_\nu}\frac{\partial f^{(0)}_{g\nu}}{\partial q_4} > 0$ also obtains for a homogeneous magnetized plasma ($\boldsymbol{B}^{(0)}$ = constant), a result which was first derived by Pfirsch and Morrison [1]. In addition the same condition is valid for an inhomogeneous force-free equilibrium with sheared magnetic field of constant modulus, which can be described by taking $B^{(0)}_x = B^{(0)}\sin(\alpha x)$, $B^{(0)}_z = B^{(0)}\cos(\alpha x)$ [α^{-1} is the shear length, and $f^{(0)}_{g\nu} = f^{(0)}_{g\nu}(q_4, \mu)$]. The last result agrees with that obtained by Correa-Restrepo and Pfirsch [4], in the context of Maxwell-Vlasov theory.

If $\frac{q_4}{g'_\nu}\frac{\partial f^{(0)}_{g\nu}}{\partial q_4} < 0$, a condition which is more frequently satisfied, only waves for which the quantity $\frac{k_\parallel}{k_\perp}$ is restricted within the interval $[min(\Lambda_\nu, M_\nu), max(\Lambda_\nu M_\nu)]$ can possess negative energy. For particles with thermal velocities this condition implies that $\frac{k_\parallel}{k_\perp} \approx \frac{(r_{L\nu})_{th}}{L} \ll 1$. The possible waves are therefore nearly perpendicular.

2. Perpendicular waves ($k_\parallel = 0$) If $\frac{dP^{(0)}}{dy}\frac{\partial f^{(0)}_{g\nu}}{\partial y} < 0$, negative-energy waves exist for any wave number $k_\perp$, irrespective of the sign of the quantity $\frac{q_4}{g'_\nu}\frac{\partial f^{(0)}_{g\nu}}{\partial q_4}$. Since, according to the results of the present work, the most important negative-energy perturbations concern perpendicular waves, the last condition is further examined for tokamak-like and

stellarator-like equilibria. To simplify the notation, the superscript (0) will be suppressed in the following, on the understanding that all the quantities pertain to equilibrium.

2.1 Tokamak-like equilibria To describe an equilibrium of this kind, the space-dependent, shifted Maxwellian distribution function

$$f_{g\nu} \propto \exp\left[-\frac{\mu B(y) + 1/2 m_\nu (v_{g\nu\|} - V_\nu(y))^2}{\kappa T_\nu(y)}\right]$$

is used. The small parallel shift velocity $V_\nu(y)$ $[\frac{V_\nu}{(v_\nu)_{th}} \approx \frac{(r_{L\nu})_{th}}{L} \ll 1$, where $(v_\nu)_{th}$ stands for a thermal velocity] produces a net "toroidal current" (the coordinates x and z represent the poloidal and toroidal directions, respectively). In the case $\eta_\nu \geq 0$ for all ν, if $\eta_\nu > 2/3$ for at least one ν, negative-energy waves exist for any perpendicular wave number $k_\perp$, except $k_\perp = 0$. The existence of negative-energy waves is therefore related to the threshold value 2/3 of the quantity η_ν, a quantity which usually expresses the trigger for the temperature-gradient driven modes. This is lower than the critical value η_ν^c, which is determined in the framework of a linear stability analysis (for example, performing a linear kinetic stability analysis of the ion temperature-gradient mode, Dominguez and Rosenbluth [5] obtained a critical value $\eta_i^c \geq 1$). Accordingly, the value $\eta_\nu^{sc} = 2/3$ is subcritical and the possible existence of negative-energy waves below the instability threshold implies that self-sustained turbulence may be present in a linearly stable tokamak regime. This result agrees with numerical results obtained by Scott [6] as well as by Nordman, Pavlenko and Weiland [7] within the framework of a nonlinear collisional and a nonlinear collisionless fluid model, respectively.

Furthermore, the part of the phase space and, consequently, the fraction of the particles which are associated with negative-energy waves are determined. (Henceforth particles of this kind will be called active particles.) This is accomplished by using analytic tokamak-like solutions of the drift kinetic equilibrium equation for cold ions, which have the following characteristics: constant toroidal magnetic field, poloidal magnetic field of the form $B_x \propto \tanh\rho$ ($\rho = y/L$) and peaked pressure as well as current density profiles ($P, j_z \propto 1/\cosh^2\rho$). With the electron shift velocity profile appropriately chosen, the following three equilibria with typical η_e-values, compared with the subcritical value, are considered:

- $\eta_e = 1$ for any ρ. In this case both the density profile and the temperature profile are peaked (N_e, $T_e \propto 1/\cosh\rho$). Although the value of η_e is equal to the critical value for linear stability or probably a little lower, nearly one-third of the electrons that possess thermal velocities are active.

- $\eta_e \to \infty$ for any ρ. In this case the density profile is flat and the temperature profile is peaked ($T_e \propto 1/\cosh^2\rho$). All the electrons are now active, as expected, because η_e approaches an extremely large value.

- $\eta_e = 0$ for any ρ. Conversely, this equilibrium exhibits a flat temperature and a peaked density profile ($N_e \propto 1/\cosh^2\rho$). In this case it is shown that the plasma

has no negative-energy waves, as again expected, because η_e takes its lowest non-negative value well below the subcritical one.

For the equilibria considered the fraction of the active particles increases as one proceeds from the center ($\rho = 0$) to the edge ($\rho = 1$) This indicates that self-sustained turbulence exists to a higher degree in the edge region.

2.2 Stellarator-like shearless equilibria The distinguishing feature of these equilibria in comparison with the tokamak-like ones is that the net plasma current vanishes. The single toroidal component of the magnetic field exhibits a hollow profile ($B_z = (B_c^2 + B_s^2 \tanh^2 \rho)^{1/2}$, where B_c and B_s are constants) and the associated poloidal current density is an odd function of ρ ($j_x \propto \tanh\rho/\cosh^2\rho$). Thus, the current in the one half-space ($\rho > 0$) flows in the opposite direction to that in the other ($\rho < 0$). To derive equilibria of this kind, an appropriate distribution function is a y-dependent Maxwellian ($V_\nu \equiv 0$). By treating this distribution function, the condition $\frac{dP}{dy}\frac{\partial f_{g\nu}}{\partial y} < 0$ furnishes the same subcritical value $\eta_\nu^{sc} = 2/3$. Equilibria which exhibit electron density and temperature profiles identical to those of the tokamak-like ones discussed above are also examined. It is shown that the results of the tokamak-like equilibria that concern the fraction of the active particles are also valid in the stellarator-like regime. It therefore turns out that, as far as the existence of negative-energy waves is concerned, within the approximation considered in the present work the two confinement systems are equivalent.

ACKNOWLEDGMENTS

We would like to thank D. Correa-Restrepo and P.J. Morrison for useful discussions. One of the authors (G.N.T.) acknowledges the support by Commission of the European Communities, Fusion Program, Contract No. B/FUS*-913006.

References

[1] D. Pfirsch and P.J. Morrison, Phys. Fluids B **3**, 271 (1991).

[2] R.G. Littlejohn, J.Plasma Physics **29**, 111 (1983).

[3] D. Correa-Restrepo and H.K. Wimmel, Physica Scripta **32**, 552 (1985).

[4] D. Correa-Restrepo and D. Pfirsch, Phys. Rev. E **47**, 545(1993).

[5] R.R. Dominguez and M.N. Rosenbluth, Nucl. Fusion **29**, 844 (1989).

[6] B.D. Scott, Phys. Rev. Lett. **65**, 3289 (1990).

[7] H. Nordman, V. Pavlenko and J. Weiland, Phys. Fluids B **5**, 402 (1993).

PLASMA DIELECTRIC TENSOR IN A TOKAMAK

SATISH PURI
Max-Planck-Institut für Plasmaphysik, EURATOM Association,
Garching bei München, Germany

Periodic modulation in particles' parallel velocity in a tokamak gives rise to an infinite, discrete set of singularities in the rf induced plasma current: Both Landau and cyclotron damping involve a correspondingly infinite spectrum of resonances [1]. This behavior has led to the widespread misunderstanding that unless the particles were to possess an infinite phase memory, the collisional (or stochastic) dephasing processes would render such a model untenable. In this paper it is shown that in accord with the linear theory, the particle motion in the periodic geometry model is amnesic and that for plasmas of thermonuclear parameters, the collisional dephasing has no significant effect on collisionless damping. Dielectric tensor ϵ is strictly local in the zero-Larmor-radius limit; in a Maxwellian plasma dissipation is positive definite at every spatial location, not just as a flux-surface (or volume) average. Landau and cyclotron damping in an imhomogeneous magnetic field is given an alternative interpretation that avoids the misleading physical picture of indefinitely sustained resonant absorption. Errors in the existing cyclotron damping models involving collisional dephasing effects are pointed out.

1. Introduction

Using the Grishanov-Nekrasov [1, 2] formulation for the plasma dielectric tensor in a large-aspect-ratio tokamak, it has been shown that the lower-hybrid-current-drive spectral-gap anomaly may be resolved via the enhanced Landau damping of large-phase-velocity waves [3, 4]. Using steepest-descent and stationary-phase integration approach, it is possible to obtain both the real and imaginary parts of the dielectric-tensor components in the zero-Larmor-radius limit [4, 5].

The presence of resonant singularities arising from the periodic zero-order motion of the particles in the tokamak has led to the misunderstanding that unless the particles were to possess an infinite phase memory, collisional (or stochastic) effects would render such models untenable. Before attempting to present detailed results for the dielectric-tensor components in a tokamak, it is imperative to justify the Grishanov-Nekrasov model.

In this paper, it is shown that collisionless damping in an inhomogeneous magnetic field is a robust velocity-space diffusion process and is not significantly altered by collisional dephasing in a thermonuclear environment. Furthermore, in contradiction to presently exisitng results, it is shown that for a Maxwellian plasma in the zero-Larmor-radius limit, both Landau and cyclotron damping are strictly local entities and are positive definite at every point in space. A new interpretation for the collisionless Landau and cyclotron damping that avoids the misleading physical picture of an indefinitely sustained resonant interaction is presented.

2. Landau damping

In the straight geometry, the change in particle's velocity in the field of a longitudinal wave (turned on at $t = t_0$) may be expressed as

$$\Delta v = \int_{t_0}^{t} \frac{eE}{m} \cos(\alpha t + \varphi)\, dt = \frac{eE}{m} \frac{\sin(\alpha t + \varphi) - \sin(\alpha t_0 + \varphi)}{\alpha} ,$$

where $\alpha = kv - \omega$. After averaging $(\Delta v)^2$ over φ, velocity-space diffusivity may be expressed as

$$D(v) = \frac{<(\Delta v)^2>}{t - t_0} = \frac{\pi}{2} \left(\frac{eE}{m}\right)^2 \left[\frac{\sin^2 \beta(t - t_0)}{\pi \beta^2 (t - t_0)}\right] ,$$

where $\beta = \alpha/2$. For increasing $(t - t_0)$, the term in the square brackets gathers near $\beta = 0$, approaching the value $(t - t_0)\delta[\beta(t - t_0)]$ as $t - t_0 \to \infty$: Since $D(v)$ vanishes identically for $t - t_0 < 0$, this term may be approximated as $\delta(\alpha) \equiv \delta(kv - \omega)$, giving the well-known linear-theory result employed in quasi-linear analyses

$$D(v) = \frac{\pi}{2} \left(\frac{eE}{m}\right)^2 \delta(kv - \omega) . \tag{1}$$

Introduction of causality to obtain the time-independent $D(v)$ is reminiscent of Landau's initial-value solution of the Vlasov equation. The limit $t \to \infty$ used to obtain (1) is in keeping with the definition of diffusivity; in the linear theory, $D(v)$ is valid at all times after switching on the electric field. The associated diffusion flux $\phi(v) = -n_0 D(v)(\partial f/\partial v)$, where $f(v)$ is the velocity distribution function. The energy absorption rate becomes

$$\frac{\partial W}{\partial t} = \int mv\phi(v)\, dv = -\int \pi \omega_{pe}^2 v \left(\frac{1}{2}\epsilon_0 E^2\right) \frac{\partial f}{\partial v}\, \delta(kv - \omega)\, dv ,$$

where ϵ_0 is the dielectric permittivity of free space and ω_{pe} is the plasma frequency. Upon performing the integration, one obtains the Landau result

$$\frac{\partial W}{\partial t} = -\frac{\pi \omega_{pe}^2}{\omega} v_p^2 \left.\frac{\partial f}{\partial v}\right|_{v_p} W , \tag{2}$$

where $v_p = \omega/k$ is the wave phase velocity and W is the energy density.

In more complex magnetic-field configurations, modulations in particle's parallel velocity can lead to dramatic changes in Landau damping. Consider a paraxial particle in a straight, periodically varying magnetic field such that[1]

$$kvt = k\bar{v}t + \sigma \sin \omega_0 t ,$$

where $\bar{v}$ is the average velocity and ω_0 is the modulation (bounce) frequency. For this case

$$\Delta v = \int_{t_0}^{t} \frac{eE}{m} \cos(k\bar{v}t + \sigma \sin \omega_0 t - \omega t + \varphi)\, dt$$

[1]Arbitrarily complex velocity modulations may be similarly handled after Fourier decomposition.

and

$$D(\bar{v}) = \frac{\pi}{2}\left(\frac{eE}{m}\right)^2 \sum_{p=-\infty}^{\infty} J_p^2(\sigma)\,\delta(k\bar{v} - \omega + p\omega_0)\ . \tag{3}$$

The single resonance at $v = \omega/k$ is now split into an infinity of resonances located symmetrically around ω/k and spaced $\delta v = \omega_0/k$ apart. Since $\sum_{-\infty}^{\infty} J_p^2(\sigma) \equiv 1$, the combined strength of the resonances remains unchanged; the emergence of secondary resonances ($p \neq 0$) is inextricably bound up with the weakening of the primary resonance ($p = 0$). **If the secondary resonances occur where $\partial f/\partial v$ is larger than the corresponding slope at ω/k, there would be a net increase in Landau damping.**

3. Stochasticity effects

Collisions or irregularities in periodicity introduce random or pseudo-random variations in ω_0 and σ. For $\nu \ll \omega_0$, ω_0 would acquire a spread $\mathcal{O}(\nu)$ centered at the mean value $\bar{\omega}_0$. Approximating the spread in ω_0 by discrete Fourier spectrum gives[2]

$$kvt = k\bar{v}t + \sum_{l=-L}^{L} \sigma_l \sin\left(\bar{\omega}_0 t + \frac{l}{L}\nu t\right)\ ,$$

and

$$D(\bar{v}) = \frac{\pi}{2}\left(\frac{eE}{m}\right)^2 \prod_{l=-L}^{L}\left\{\sum_{p_l=-\infty}^{\infty} J_{p_l}^2(\sigma_l)\right\}\delta\left[k\bar{v} - \omega + \sum_{l=-L}^{L} p_l\left(\bar{\omega}_0 + \frac{l}{L}\nu\right)\right]\ , \tag{4}$$

where $\prod_{l=-L}^{L}$ is the product operator acting on the expression in the curly brackets while the summation indices p_l enter the argument of the δ function. Thus, collisions lead to further fine structure in $D(v)$ without materially altering Landau damping provided $\nu \ll \omega_0$. A direct intuitive grasp of this result follows from the fact that **for a Maxwellian distribution, collisions leave $f(v)$ and hence the linearized wave-particle energy exchange interactions (summed over the ensemble of particles) intact**; even as the absorption spreads in v.

The structure of (4) reveals that the total diffusivity, summed over all resonances, remains invariant for velocity modulation of arbitrary complexity; $D(v)$ gets simply redistributed over an ever finer mesh. This result of wide ranging generality, underscores the robust character of Landau damping, unperturbed by arbitrarily-random velocity fluctuations, slow compared to the fundamental period of particles' parallel velocity.

In (4) $\bar{\omega}_0 = 0$ corresponds to the uniform magnetic field case; collisions cause diffusivity to spread around $v = \omega/k$ by the amount $\Delta v \sim \nu/k$. In the absence of a significant change in the slope of the Maxwellian for the velocity shift Δv, collisions would not materially affect Landau damping.

---

[2]Inclusion of cosine terms in the Fourier spectrum can be treated similarly.

In the limit $L \to \infty$ in (4), the total diffusivity remains unaltered even though the discrete resonance spectrum merges into a continuum: Thus, spatially-inhomogeneous, non-periodic magnetic fields, too, can be treated in the manner of (4). Since the zero-order velocity is uniquely specified for all $\mathbf{x}$ (or t) by assigning derivatives (spatial or temporal) of v to all orders, **the resonance structure in (4) is equivalent to regarding v as an analytic function.** Landau damping is then seen as a function of particle's velocity and its derivatives rather than as a set of resonances. Since these derivatives are locally defined everywhere, the requirement of an indefinite phase memory in the particle's orbit disappears. **Hence, it is proposed that viewing Landau damping as dependent upon local velocity and its derivatives is a more valid physical interpretation than the resonant interaction model:** Landau damping continues to be a valid local entity even when no well-defined resonances exist in a non-periodic magnetic field.

4. Cyclotron damping

The foregoing considerations for Landau damping are equally applicable to cyclotron damping in a tokamak. Collisional effects are even less important because, unlike Landau damping, cyclotron damping involves a much broader segment of the particle population. Being a diffusivity effect, cyclotron damping, too, would be positive definite at every point (r, θ, φ) in the tokamak volume for a Maxwellian plasma in the zero-Larmor-radius limit. Grishanov-Nekrasov theory indeed yields positive definite damping everywhere, in contrast to the presently existing results [6] which might, at best, *fortuitously* become positive definite upon averaging over the magnetic surface. **The error in [6] stems from the neglect of higher-order velocity derivatives**; nor is the situation remedied by *ad hoc* introduction of collisional dephasing. As discussed in the previous section, **neglect of higher-order velocity derivatives is tantamount to disregarding valid resonant interactions.**

5. Conclusions

The Grishanov-Nekrasov [1] derivation of ϵ in a tokamak involving an infinite, discrete set of singularities retains its validity in the presence of stochastic dephasing effects; the collisionality contribution being negligible in plasmas of thermonuclear parameteres. Landau and cyclotron damping are local quantities depending only upon the local velocity and its derivatives; thus it is not imperative for the particles to remain in step with the wave for indefinite periods to validate the Grishanov-Nekrasov model. A derivation of ϵ that includes finite Larmor radius as well as drift terms and involves singular resonant interactions similar to those of Ref.[1] has recently been given by Lamalle [7].

References

[1] GRISHANOV, N. I., NEKRASOV, F. M., Fiz. Plasmy **16** (1990) 230.
[2] ELFIMOV, A. G., PURI, S., Nucl. Fusion **30** (1990) 1215.
[3] PURI, S., Europhys. Abstracts **16E** (1992) 241.
[4] PURI, S., Czech. J. Phys. **43** (1993) (to be published).
[5] PURI, S., Europhys. Abstracts **16E** (1992) 17.
[6] SMITHE, D., et al., Phys. Rev. Lett. **60** (1988) 801.
[7] LAMALLE, P. U., Phys. Letters A **175** (1993) 45.

Strongly nonlinear plasma waves

S.V.Vladimirov and V.S.Krivitsky*
Theory Department, General Physics Institute, 117942 Moscow, Russia

Recently a number of plasma particle accelerators schemes (for achieving high acceleration rates and high energies) has been proposed (see, e.g., a beat-wave acceleration scheme [1], a wake-field acceleration scheme [2], a laser wake-field acceleration scheme [3,4]). All these mechanisms imply the excitation of an intense longitudinal plasma wave, in which the effective acceleration is realized. The high amplitudes of the excited waves require the taking into account nonlinear effects. More often one restricts oneself in that case to the use of perturbation theory. But the use of a finite number of terms in the perturbation theory series is valid only for sufficiently small wave amplitudes. On the other hand, both from the point of view of the theoretical requirements for acceleration and of the corresponding experiments, the amplitudes of the excited longitudinal waves are rather large.

A theory taking into account exactly the nonlinearity of a one-dimensional plasma wave was already produced in the fifties [5-8]. However, this theory was based upon the equations of cold collisionless hydrodynamics (nonrelativistic [5] and relativistic [6-8], see also more recent papers [9,10]) so that the range of its applicability is limited to a plasma with a temperature $T = 0$. Moreover, the problem itself of the validity of the hydrodynamic approximation for nonlinear motion in a collisionless cold plasma is nontrivial. On the other hand, for arbitrary distributions with nonvanishing characteristic particle valocities (thermal, "two-temperature", etc. distributions) the hydrodynamic description is invalid (even in the linear limit when obtaining a valid dispersion one must introduce *ad hoc* an adiabatic index into the equations).

The considerations of Ref.11, based on kinetic theory, have shown that taking the particle velocity distribution into account introduces qualitatively new features into the description of a (one-dimensional) nonlinear plasma wave. In particular, they analyzed the possibility of the existence of particles trapped by the wave, and if their distribution is appropriate, any form of nonlinear waves can be obtained.

Here, we develop in detail and analyze methods which enable us to obtain exact nonlinear wave solutions for arbitrary particle distributions in the plasma. It is important that in principle some of these solutions cannot be obtained in the framework of the hydrodynamic approximation. In particular, we indicate the possibility of the existence of solitary nonlinear waves even in the case when the role played by the trapped particles is negligibly small.

We consider a plasma with an electron component which is described by the collisionless kinetic equation. The electric field is described by the Poisson equation.

---

* *Present address: Theor. Physik I, Ruhr-Universität-Bochum, D-44721 Bochum, Germany*

By solving these equations we can obtain the following equation which describes oscillations of the field of the wave

$$\frac{d^2}{dt^2}Z(\tau) = -\frac{\partial W(Z)}{\partial Z}, \tag{1}$$

where $Z = -e\phi/mu^2$, $\tau = \omega_{pe}(t - x/u)$, ϕ is the electrostatic potential ($E = -\partial\phi/\partial x$), m is the electron mass, u is the speed of the wave (we are interested in solutions $\propto (x - ut)$), and ω_{pe} is the electron plasma frequency. The "potential function" $W(Z)$ is

$$W(Z) = 1 + Z - \sqrt{1 + 2Z} \tag{2}$$

for a nonrelativistic ($u \ll c$, where c is the speed of light) wave propagating in a cold plasma (if only the electron contribution is considered). Taking the motion of the (cold) ions of mass M into account gives

$$W(Z) = 1 - \sqrt{1 + 2Z} - (\sqrt{1 - 2Zm/M} - 1)M/m. \tag{3}$$

The generalization of (2) into a relativistic case ($u \approx c$) is

$$W(Z) = (1 - u^2/c^2)^{-1}(1 + Z - \sqrt{1 + 2Z + Z^2u^2/c^2}. \tag{4}$$

Taking into account the electron thermal motion results in

$$W(Z) = 1 + Z - \sqrt{1 + 2Z} + [2 + (1 + 2Z)^{-3/2} - 3(1 + 2Z)^{-1/2}]v_T^2/2u^2, \tag{5}$$

here $v_T \ll u$ is the lectron thermal velocity $v_T = \sqrt{T/m}$.

The dependence of the wave field upon time is given in a general case by the elliptic functions. For the case of small amplitude the period P of the wave oscillations is

$$P \simeq 2\pi\sqrt{M/(m + M)}[1 - 15Cm/8(m + M)] \tag{6}$$

for the "potential" (3),

$$P \simeq 2\pi(1 + 3Cu^2/8c^2) \tag{7}$$

for the "potential" (4), and

$$P \simeq 2\pi/\sqrt{1 + 3v_T^2/u^2} - 15\pi Cv_T^2/u^2 \tag{8}$$

for the "potential" (5). Here, $C = U/n_0mu^2 \ll 1$, where U is the wave energy spatial density. The expressions (6)-(8) coincide with the known results obtained by using the perturbation theory up to the third order in the wave field.

The results (3)–(5) are obtained directly from the kinetic equation without using the series expansion in powers of the electric field. Indeed, the general solution of the

kinetic equation in our case (when the wave $E = E(t-x/u)$ propagates in x-direction) is

$$f = f_0(mu + m\sqrt{(v-u)^2 + 2e\phi/m}), \tag{9}$$

where f_0 is an arbitrary (smooth) function. In a difference from [11], we suppose the argument of the function (9) to be a momentum p but not an energy $V = m(v-u)^2/2 + e\phi$. This choice is better because the function upon energy would achieve the same value for different velocities v (corresponding to the same energy V). But such the restriction is unnecessary (this is evident in the special case $\phi = 0$: a solution of the "free" kinetic equation is arbitrary function $f(v)$ which generally should not obey the equality $f(v) = f(-v)$). Moreover, using the argument V instead of p in the non-perturbative consideration results in the absence of a "good" limit when $\phi \to 0$ (i.e. the "free" plasma state and the correct linear theory – see also [11]). It should be also mentioned that the function $\sqrt{(v-u)^2 + 2e\phi/m}$ in (9) can not be considered "algebraically", but analytically, as a corresponding branch of an analytical function of a complex argument.

The non-perturbative kinetic theory allows us to properly take into consideration all thermal effects without expansion in v_T^2/u^2. It also allows us to answer the question: what is $W(Z)$ for $Z \leq -1/2$ (in a nonrelativistic case)? The "potential" $W(Z)$ is ($Z < 0$)

$$W(Z) = Z - \frac{mu}{\sqrt{2\pi m T}} \int_0^Z dz \int_{-\infty}^{+\infty} d\xi \exp\left[-\frac{1 + \xi^2 - 2z + 2\sqrt{\xi^2 - 2z}}{2v_T^2}\right]. \tag{10}$$

We should take a principal value of an integral (10) due to the necessity of making a cut between two special points $\pm i\sqrt{2|z|}$ of the square root function in (10) in order to get a regular branch of the analytical function.

After some algebraic transformations we obtain for $W(Z)$ the following estimation

$$W(Z) \simeq Z + 1 + v_T^2/u^2 + O(1) \tag{11}$$

for the case $Z \to -\infty$. Thus the function $W(Z)$ (10) is smooth and reachs its maximum in the point $Z = Z_{\max} \simeq -1/2$ if the plasma temperature $T \neq 0$ (when $T \to +0$, the $Z_{\max} \to -1/2$). The function $W(Z)$ is continuously differentiable for $T \neq 0$; the discontinuity in the derivative dW/dZ as $T \to +0$ is connected with the appearance of a singularity of the exponential in the integrand (10):

$$\frac{u}{\sqrt{2\pi}v_T} \exp\left(-\frac{u^2y^2}{2v_T^2}\right) \longrightarrow \delta(y) \quad \text{if} \quad v_T \longrightarrow +0. \tag{12}$$

The "potential" $W(Z)$ allows soliton-like solutions of Eq. (1): the oscillation period P tends to infinity when $C = W(Z_{\max})$. Thus for any (even arbitrary small)

temperature T there does not occur the wave breaking, as in hydrodynamics, but the formation of a solitonlike state $Z(t - x/u)$. Of course, the problem of whether such a soliton is a "true soliton" goes beyond the scope of the present consideration. Taking ions into account does not change in principal this important statement, it should only be noted that for a case of electron-positron plasmas the solitonlike structures have different asimptotics in the limits $\tau \to \pm\infty$, therefore these are kink-like instead of single wave as in the case $M \gg m$).

The obtained results are based on the assumption of absence (or small number) of trapped particles. Generally, as was clarified in [11], it is possible to obtain an arbitrary "potential function" $W(Z)$ and hence an arbitrary type of the wave, if the proper distribution function of the trapped particles is chosen. Of course, there are always some particles trapped by the wave; but one should study the process of trapping in detail in order to know how many such particles are present in the system.

It seems to be rather natural to suppose that for the wave phase velocity $u \sim c$ (which is the most interesting case in the problem of particle acceleration) the number of the trapped particles should not be very large, because in the corresponding experiments the majority of plasma particles has velocities of the order of v_T which is much less c. But in general it is necessary to study the dynamics of the process of trapping, this problem is beyond the limits of the present consideration based on the assumption that all solutions depend upon the argument $t - x/u$.

Acknowledgements One of the authors (SVV) would like to thank the Humboldt Foundation for financial support, and M.Y.Yu for hospitality.

[1] T.Tajima, J.M.Dawson, Phys. Rev. Lett. **43**, 267 (1979)
[2] P.Chen *et al*, Phys. Rev. Lett. **54**, 693 (1984)
[3] P.Sprangle *et al*, Appl. Phys. Lett. **53**, 2146 (1988)
[4] V.N.Tsytovich, U. de Angelis, R.Bingham, Comments Plasma Phys. Contr. Fus. **12**, 249 (1989)
[5] A.I.Akhiezer, G.Y.Liubarski, Sov. Phys. Doklady **80**, 153 (1951) (*in Russian*)
[6] A.I.Akhiezer, R.V.Polovin, Sov. Phys. Doklady **102**, 919 (1955) (*in Russian*)
[7] A.I.Akhiezer, R.V.Polovin, Sov. Phys. JETP **30**, 915 (1956) (*in Russian*)
[8] V.N.Tsytovich, Sov. Phys. Doklady **142**, 63 (1963) (*in Russian*)
[9] P.K.Kaw, J.M.Dawson, Phys. Fluids **13**, 472 (1970)
[10] J.Noble, Phys. Rev. A **32**, 460 (1985)
[11] I.B.Berstein, J.M.Greene, M.D.Kruskal, Phys. Rev. **108**, 546 (1957)

On dissipative acceleration of coupled ion-sound and Langmuir solitons

S.V.Vladimirov , S.A.Boldyrev and V.N.Tsytovich*
Theory Department, General Physics Institute, 117942 Moscow, Russia
** Theor. Physik I, Ruhr-Universität-Bochum, D-44721 Bochum, Germany*

The problem of nonlinear coupling between Langmuir and ion-acoustic waves in plasmas was actively discussed [1-4]. We have to distinguish two limiting cases. The first is the case when the speed V_0 of the nonlinear wave and the intensity of the Langmuir field satisfy the inequality

$$(1 - V_0^2/V_s^2)^2 \gg |E^l|^2/n_0 T_e \sim m_e/m_i, \tag{1}$$

where $V_s = \sqrt{T_e/m_i}$ is the ion sound speed (we suppose $T_e \gg T_i$), $m_{e(i)}$ is the electron (ion) mass, $T_{e(i)}$ is the electron (ion) temperature and n_0 is the unperturbed plasma density. In this case the Zakharov equations can be used to describe the coupling. The second case takes place for stronger Langmuir fields

$$|E^l|^2/n_0 T_e \gg m_e/m_i, \tag{2}$$

and for the speed

$$|E^l|^2/n_0 T_e \geq (1 - V_0^2/V_s^2)^2 \gg m_e/m_i, \tag{3}$$

when the Zakharov equations cannot be used. In this case we have to take into account nonlinear as well as dispersive terms in the equation for a low-frequency potential.

Nonlinear equations for the Langmuir wave's amplitude and the ion-acoustic field potential with dispersive terms previously were obtained by using hydrodynamics only [2]. Here, we consider the exact kinetic description to correct the above system and to obtain new dissipative terms which describe Landau damping of the ion-sound waves as well as a nonlinear scattering of the Langmuir waves on plasma particles. In our approximations (1) and (3), the dissipative terms can be considered by using a standart perturbation procedure [3,5]. As we will see, the dissipative effects result in some amplitude reduction (in a quasi-soliton state which we will define below) as well as in acceleration of the coupled nonlinear wave.

Let us introduce dimensionless variables and functions

$$x' = \mu\omega_{pe}x/2V_s, \quad t' = t\mu\omega_{pe}/e, \quad \mu = 4m_e/3m_i \ll 1, \quad \Delta = 2(\omega_0 - \omega_{pe})/\mu\omega_{pe}, \tag{4}$$

$$e = E^l/\sqrt{4\pi n_0 T_e \mu}, \quad \Phi = -q_e\varphi^s/T_e, \quad E^s = -\partial_x\varphi^s, \tag{5}$$

where $\omega_{pe} = \sqrt{4\pi n_0 q_e^2/m_e}$ is the electron plasma frequency, $E^{l(s)}$ is the high frequency Langmuir (low frequncy ion-sound) field, φ^s is the potential of the low frequency field. Below we will omit the primes at the dimensionless variables x, t. After the kinetic calculation we obtain the following system of equations which generalize the system [2]

$$i\partial_t e + \partial_x^2 e + \Delta e = \frac{1}{\mu}\Phi e + \hat{N}(\Phi, e), \tag{6}$$

$$\partial_t \Phi + (1 + 3\frac{T_i}{T_e})\partial_x \Phi + \frac{1}{6}\mu\partial_x^3 \Phi + \frac{1}{2}\partial_x(\Phi^2) + \frac{1}{2}\mu\partial_x|e|^2 + \hat{D}(\Phi) = 0. \tag{7}$$

In this system, the operators $\tilde{N}$ and $\tilde{D}$ describe the dissipative effects. We have

$$\tilde{N}(\Phi, e) \equiv \frac{1}{\mu}e\delta\Phi = \frac{i}{\mu}e\int_{-\infty}^{+\infty}\frac{d\omega dk}{(2\pi)^2}\sqrt{\frac{3\pi\mu}{8}}\Phi_{\omega,k}\mathrm{sign}(k)\mathrm{e}^{-i\omega t+ikx}, \tag{8}$$

and

$$\tilde{D}(\Phi) = \int_{-\infty}^{+\infty}\frac{d\omega dk}{(2\pi)^2}\sqrt{\frac{\pi}{\mathrm{e}}}\frac{\omega^2}{|k|v_{Te}}\Phi_{\omega,k}\mathrm{e}^{-i\omega t+ikx}. \tag{9}$$

Let us firstly assume $\hat{N} = \hat{D} = 0$. Then we can find a solution of Eqs.(6),(7) in the form

$$\mu|e|^2 = \alpha_0 + \alpha_1\Phi + \alpha_2\Phi^2. \tag{10}$$

Thus we have for Φ a general solution in the form of a cnoidal wave [2]. For the solution close to a set of solitons (so-called quasi-soliton) we obtain

$$\Phi = a + 6\mu\eta^2\mathrm{cn}^2(\eta\xi, s), \tag{11}$$

where $\xi = x - V_0 t - x_0$. The parameter a can be derived from the conservation of number of particles: $\int_{-\infty}^{+\infty}\delta n^{(e,i)}d\xi = 0$, we have $\delta n^{(e)} \sim \Phi$, $\delta n^{(i)} \sim \Phi/V_0^2$ in the first approximation. Furthermore, we obtain

$$\alpha_0 = 6\mu\eta^2\left(8\frac{\mu\eta^2}{K} + \delta\alpha_1\right)\left(1 - \frac{1}{K}\right) - \frac{3}{4}(\delta\alpha_1)^2, \tag{12}$$

$$\alpha_1 = -8\mu\eta^2\left(1 - \frac{2}{K}\right) + \delta\alpha_1, \tag{13}$$

$$\alpha_2 = -\frac{4}{3}, \tag{14}$$

$$\Delta = -\eta^2 - 6\frac{\eta^2}{K} - \frac{3}{8}\frac{\delta\alpha_1}{\mu}, \tag{15}$$

$$\delta V \equiv 1 - V_0 = -3\frac{T_i}{T_e} + \mu\eta^2\left(\frac{10}{3} - \frac{6}{K}\right) - \frac{1}{2}\delta\alpha_1, \tag{16}$$

where $K = K(s) = \int_0^1 d\tau/\sqrt{(1-\tau^2)(1-s^2\tau^2)}$. Then from Eq.(10) one can find the field amplitude e which is proportional to

$$\exp\left(\frac{1}{2}iV_0x - \frac{1}{4}iV_0^2t + i\int d\xi\frac{M}{|e|^2} + i\theta\right),$$

$$M^2 = \mu\eta^6\left\{-27\delta\alpha_1^2 + 1440\frac{\mu\eta^2\delta\alpha_1}{K^2} + 0\left[\left(\mu\eta^2/K^2\right)^2\right]\right\}. \tag{17}$$

Five parameters η, K, $\delta\alpha_1$, x_0, θ are still free. To satisfy the conditions $\mu|e|^2 \geq 0$ and $M^2 \geq 0$, we have to choose

$$0 \leq \delta\alpha_1 \leq \frac{160}{3}\frac{\mu\eta^2}{K^2}. \tag{18}$$

Another restriction follows from the condition of a small variation (due to the damping effects) of the parameter $\delta\alpha_1$ with the soliton characteristic time $\tau \sim 1/\eta$. We have $\partial_t\delta\alpha_1 \ll \eta\delta\alpha_1$, this leads to sufficiently weak inequality on the nonlinear wave period $K \ll 500\eta$.

The system (6),(7) without dissipative terms admits a variational principle and conserves the number N and momentum P of the waves. In the first approximation we describe the nonlinear wave damping (if $K \gg 1$) as a slow time variation of free parameters η and $\delta\alpha_1$. To satisfy the condition of uniformity we have to put K/η =const (the distance between two quasi-solitons in the nonlinear wave is not changing with time). To describe the evolution of the parameters η and $\delta\alpha_1$ resulting from the dissipative processes, we consider the conservation equations for average quantities [4] in which we take into account the dissipative terms:

$$\frac{\partial\bar{N}}{\partial t} = 0, \tag{19}$$

$$\frac{\partial\bar{P}}{\partial t} = \bar{R}_P \equiv -\frac{1}{2K\mu^2}\int_{-2K}^{+2K}\Phi\hat{D}(\Phi)d\xi - \frac{1}{4K\mu}\int_{-2K}^{+2K}|e|^2[\partial_\xi(\delta\Phi)]d\xi. \tag{20}$$

The average quantities by definition are

$$\bar{A} \equiv \frac{1}{4K}\int_{-2K}^{+2K}Ad\xi. \tag{21}$$

The main dissipative effect is the linear Landau damping of the ion sound (the first term in the r.h.s. of (20)). It is wellknown (and worth stressing) that the main part of near-sonic momentum and energy is contained in the ion-acoustic field.

Let us substitute in Eqs.(19),(20) $N = |e|^2, P = i(e\partial_x e^* - e^*\partial_x e)/2 + \Phi^2/\mu^2$. The average forse $\bar{R}_P$ we calculate in the soliton approximation $K \gg 1$

$$\bar{R}_P = -\frac{1}{K\mu^2}\int_{-\infty}^{+\infty}\Phi^{(0)}\hat{D}\left(\Phi^{(0)}\right)d\xi - \frac{1}{2K\mu}\int_{-\infty}^{+\infty}|e^{(0)}|^2\left[\partial_\xi\left(\delta\Phi^{(0)}\right)\right]d\xi, \qquad (22)$$

where $\Phi^{(0)}$ and $e^{(0)}$ are solitary solutions of Eqs.(6),(7) without dissipative terms. Futher we will use the following formulae

$$\frac{2}{\mu^2}\int_{-\infty}^{+\infty}\Phi^{(0)}\hat{D}\left(\Phi^{(0)}\right)d\xi \simeq \frac{3456}{\pi^3}\sqrt{\frac{3\pi\mu}{8}}\eta^4\zeta(3), \qquad (23)$$

$$\frac{1}{\mu}\int_{-\infty}^{+\infty}|e^{(0)}|^2\left[\partial_\xi\left(\delta\Phi^{(0)}\right)\right]d\xi \simeq \frac{2688}{\pi^2}\sqrt{\frac{3\pi\mu}{8}}\mu\eta^4\zeta(3), \qquad (24)$$

where $\zeta(3) \simeq 1.202$. Finally, we obtain

$$\partial_t\left(\alpha_0 + \alpha_2\bar{\Phi}^2\right) = 0, \qquad (25)$$

$$\partial_t\delta\alpha_1 = \frac{96}{\pi^3 K}\sqrt{\frac{3\pi\mu}{8}}\mu\eta^3\zeta(3), \qquad (26)$$

$$\frac{\partial_t\eta}{\eta} = -\frac{12}{\pi^3}\sqrt{\frac{3\pi\mu}{8}}\eta\zeta(3). \qquad (27)$$

The rate of the change of the soliton velocity we find from Eq.(16)

$$\partial_t\delta V = \frac{20}{3}\mu\eta^2\frac{\partial_t\eta}{\eta} < 0, \qquad (28)$$

and we can see that the nonlinear wave is indeed accelerated, since $\delta V \equiv 1 - V_0$.

Our results demonstrate that the near-sonic quasi-soliton increases its velocity because of the dissipative effects, if the inequality (3) is valid. The amplitude of the nonlinear wave is decreased simultaneously. To describe the soliton damping, we have used the perturbation procedure which is not valid if $(1 - V_0^2/V_s^2)^2 \leq m_e/m_i$, or if the period of the nonlinear wave is sufficiently large, since the larger the period K, the smaller the interval (18) for changes of the $\delta\alpha_1$, and for the "pure" solitary wave ($K = \infty$) the perturbation theory is not valid. For the speed interval (1) one can use the Zakharov equations with dissipative terms, in this case both the velocity and the amplitude of the "usual" Langmuir soliton are decreased [5].

Acknowledgements One of the authors (SVV) would like to thank the Humboldt Foundation for financial support, and M.Y.Yu for hospitality.

[1] V.E.Zakharov, Sov. Phys. JETP **62**, 1745 (1972)
[2] K.Nishikava *et al*, Phys. Rev. Lett. **33**, 148 (1974)
[3] F.Kh.Khakimov and V.N.Tsytovich, Sov. Phys. JETP. **70**, 1785 (1976)
[4] G.B.Whitham, *Linear and Nonlinear Waves* (Wiley, N.Y., 1974)
[5] L.I.Rudakov and V.N.Tsytovich, Phys. Rep. **40C**, 1 (1978)

ON INFLUENCE OF THE PLASMA–MASER EFFECT ON EVOLUTION OF RESONANT WAVES

S.I.Popel*, S.V.Vladimirov** and M.Y.Yu**
*Institute for Dynamics of Geospheres,
Leninsky pr.38, bld.6, Moscow 117979, Russia
**Institute of Theoretical Physics 1, Ruhr University
Bochum, Germany

The evolution of waves in turbulent plasmas, in which a large number of degrees of freedom is excited, can often be determined by the nonlinear interactions of the waves. Among them the nonlinear interaction of resonant waves with the non–resonant ones can be important (see, e.g., /1,2/). The non–resonant waves are those for which both the Čerenkov resonance condition

$$\omega - \mathbf{k}\cdot\mathbf{v} = 0 \qquad (1)$$

and the scattering (off the second type of waves, namely the resonant waves) condition

$$\omega - \Omega - (\mathbf{k}-\mathbf{q})\cdot\mathbf{v} = 0 \qquad (2)$$

are not satisfied, while the resonant waves are those for which the condition (1) is satisfied. Here ω and Ω are the frequencies of the considered waves, $\mathbf{k}$ and $\mathbf{q}$ are the corresponding wavenumbers, and $\mathbf{v}$ is the velocity of a plasma particle. The effect of the nonlinear interactions of the resonant and non–resonant waves is called the plasma–maser effect (see, e.g., /2/).

In the present paper, we investigate the nonlinear evolution of the resonant waves accounting for their interaction with the non–resonant waves. We obtain a general expression for the nonlinear growth rate of the resonant waves.

The electron distribution function $f_{\mathbf{p}}$ satisfies the collisionless kinetic equation

$$\frac{\partial f_{\mathbf{p}}}{\partial t} + \mathbf{v}\cdot\frac{\partial f_{\mathbf{p}}}{\partial \mathbf{r}} + e\mathbf{E}\cdot\frac{\partial f_{\mathbf{p}}}{\partial \mathbf{p}} = 0 \qquad (3)$$

where the electron charge is $e=-|e|$. Let us define the regular part $\Phi_{\mathbf{p}}$ of the distribution function by

$$\Phi_{\mathbf{p}} = \langle f_{\mathbf{p}} \rangle, \qquad (4)$$

where the angular brackets $\langle\ \rangle$ denote averaging over a statistical ensemble. For the sake of simplicity, we assume that all fields are longitudinal. The electric field $\mathbf{E}$ is then governed by the Poisson's equation

$$\mathrm{div}\mathbf{E} = 4\pi e \int \delta f_{\mathbf{p}} d\mathbf{p}/(2\pi)^3. \qquad (5)$$

where $\delta f_{\mathbf{p}}$ is the fluctuating part of the distribution function. We shall represent it by an expansion in powers of the turbulent field $\mathbf{E}$:

$$\delta f_p = \sum_{l=1}^{\infty} \delta f_p^{(l)}, \tag{6}$$

where $\delta f_p^{(l)} \propto |E|^l$. We have normalized the distribution function f_p by

$$n = \int \frac{dp}{(2\pi)^3} f_p, \tag{7}$$

where n is the concentration of plasma electrons.

We now introduce the correlation function of the Fourier components of the electric fields by

$$\langle E_{\omega,k;i} E_{\omega',k';j} \rangle = |E_{\omega,k}|^2 \delta(\omega+\omega') \delta(k+k') k_i k_j / |k|^2, \tag{8}$$

where

$$E_{\omega,k} = \int E(t,r) \exp(i\omega t - ik\cdot r) dt dr/(2\pi)^4 = k E_{\omega,k}/|k|. \tag{9}$$

Here, for the frequency and wavenumber of the Fourier components of the resonant waves, we use the notations ω and k, while for those of the non–resonant waves we use Ω and q. The last factors in Eqs.(9) and (10) demonstrate the longitudinal character of the waves.

We are interested in the nonlinear contribution to the dielectric function (of the resonant waves) proportional to $|E_{\Omega,q}|^2 E_{\omega,k}$. This can come from the coupling $(\delta f_p^{(2)})^2$ as well as from $\delta f_p^{(3)}$. The contribution of the second order (in the fields) terms to the imaginary part of the nonlinear dielectric permittivity of the resonant waves is

$$\mathrm{Im}\delta\varepsilon^{pol}(\omega,k) = -\frac{16\pi^2 e^6}{|k|^2} \int \frac{d\Omega dq}{|q|^2} \frac{|E_{\Omega,q}|^2}{|k-q|^2 \varepsilon^L(\omega-\Omega,k-q)} \cdot$$

$$\mathrm{Im}[S(\omega,k;\Omega,q;\omega-\Omega,k-q)\cdot S(\omega-\Omega,k-q;\omega,k;-\Omega,-q)] \tag{10}$$

where the (symmetrized over the last two indices) second order plasma response is

$$S(\omega,k;\omega_1,k_1;\omega_2,k_2) = \int \frac{dp}{(2\pi)^3} \frac{1}{\omega - k\cdot v + i0} \left\{ \left[k_1 \cdot \frac{\partial}{\partial p}\right] \cdot \right.$$

$$\left. \frac{1}{\omega_2 - k_2\cdot v + i0} \left[k_2 \cdot \frac{\partial}{\partial p}\right] + \left[k_2 \cdot \frac{\partial}{\partial p}\right] \frac{1}{\omega_1 - k_1 \cdot v + i0} \left[k_1 \cdot \frac{\partial}{\partial p}\right] \right\} \Phi_p \tag{11}$$

In Eq.(11) only for the resonant waves the imaginary parts of the denominators are to be taken into account (the scattering condition (2) is not satisfied here).

The contribution of the resonant waves to the imaginary part of the nonlinear dielectric permittivity by the third order terms is

$$\mathrm{Im}\delta\varepsilon^{(3)}(\omega,k) = \mathrm{Im}\left\{ \frac{4\pi^2 e^4}{|k|^2} \int \frac{dp}{(2\pi)^3} \frac{d\Omega dq}{|q|^2} \frac{|E_{\Omega,q}|^2}{\omega - k\cdot v + i0} \cdot \right.$$

$$\left[\mathbf{q}\cdot\frac{\partial}{\partial \mathbf{p}}\right]\frac{1}{\omega-\Omega-(\mathbf{k}-\mathbf{q})\cdot\mathbf{v}}\left[\left[\mathbf{k}\cdot\frac{\partial}{\partial \mathbf{p}}\right]\frac{1}{\Omega-\mathbf{q}\cdot\mathbf{v}}\left[\mathbf{q}\cdot\frac{\partial}{\partial \mathbf{p}}\right]-\right.$$

$$\left.\left[\mathbf{q}\cdot\frac{\partial}{\partial \mathbf{p}}\right]\frac{1}{\omega-\mathbf{k}\cdot\mathbf{v}+i0}\left[\mathbf{k}\cdot\frac{\partial}{\partial \mathbf{p}}\right]\right]\Phi_P\Big\} \qquad (12)$$

We can simplify this equation by a standard method /2,3/. In particular, we expand the denominator $[\omega-\Omega-(\mathbf{k}-\mathbf{q})\cdot\mathbf{v}]^{-1}$ by $[\omega-\Omega-(\mathbf{k}-\mathbf{q})\cdot\mathbf{v}]^{-1} = -(\Omega-\mathbf{q}\cdot\mathbf{v})^{-1}\{1+[(\omega-\mathbf{k}\cdot\mathbf{v})/(\Omega-\mathbf{q}\cdot\mathbf{v})] + [(\omega-\mathbf{k}\cdot\mathbf{v})/(\Omega-\mathbf{q}\cdot\mathbf{v})]^2+\ldots\}$ and use the sign symmetry of Ω and $\mathbf{q}$. We have finally

$$\mathrm{Im}\delta\varepsilon^{(3)}(\omega,\mathbf{k}) = -\frac{2\pi^2e^4}{|\mathbf{k}|^2}\int\frac{d\mathbf{p}}{(2\pi)^3}\frac{d\Omega d\mathbf{q}}{|\mathbf{q}|^2}|E_{\Omega,\mathbf{q}}|^2\delta(\omega-\mathbf{k}\cdot\mathbf{v})\cdot$$

$$\left[\left[\mathbf{q}\cdot\frac{\partial}{\partial \mathbf{p}}\right]\frac{2}{(\Omega-\mathbf{q}\cdot\mathbf{v})}\left[\mathbf{k}\cdot\frac{\partial}{\partial \mathbf{p}}\right]\frac{1}{(\Omega-\mathbf{q}\cdot\mathbf{v})}\left[\mathbf{q}\cdot\frac{\partial}{\partial \mathbf{p}}\right]-\left[\mathbf{q}\cdot\frac{\partial}{\partial \mathbf{p}}\right]\frac{1}{(\Omega-\mathbf{q}\cdot\mathbf{v})^2}\cdot\right.$$

$$\left.\left[\mathbf{k}\cdot\frac{\partial}{\partial \mathbf{p}}\right]\left[\mathbf{q}\cdot\frac{\partial}{\partial \mathbf{p}}\right]+2\left[\frac{\mathbf{k}\cdot\mathbf{q}}{m_e}\right]^2\frac{2}{(\Omega-\mathbf{q}\cdot\mathbf{v})^4}\left[\mathbf{q}\cdot\frac{\partial}{\partial \mathbf{p}}\right]\Phi_P\right]. \qquad (13)$$

Using the expressions (10) and (13), one can easily obtain the corresponding rates describing the evolution of the resonant waves

$$\gamma_{\mathbf{k}}^{pl} = -\frac{(\mathrm{Im}\delta\varepsilon^{pol}(\omega,\mathbf{k})+\mathrm{Im}\delta\varepsilon^{(3)}(\omega,\mathbf{k}))}{\delta\varepsilon^{L}(\omega,\mathbf{k})/\partial\omega}\Big|_{\omega=\omega(\mathbf{k})}, \qquad (14)$$

where $\varepsilon^L(\omega,\mathbf{k})$ is the linear dielectric permittivity, $\omega(\mathbf{k})$ is the linear frequency (i.e., the solution of $\varepsilon^L(\omega,\mathbf{k})=0$) of the resonant waves.

When the constant particle distributions are maintained (i.e. the system is open), the contribution to the growth rate of the resonant waves caused by the plasma–maser mechanism is determined by the expression (14). If the particle distributions are not constant then the effects of nonstationarity of the system can be essential when describing the evolution of waves in plasmas (e.g. the contribution of the effects of nonstationarity to the growth rate of the non–resonant waves is of the order of the "direct third–order" contribution to the nonlinear growth rate of these waves (see /2,3/). However for the closed systems (in which the (slow) variation of the plasma parameters is governed by the well–known quasilinear equation (see, e.g., /4/)) the effects of the system's nonstationarity do not make a contribution to the plasma–maser mechanism for the evolution of the resonant waves (see /5/) in contrast to the situation which occurs when describing the evolution of the non–resonant waves (see /2,3/).

The plasma–maser effect can significantly influence the evolution of resonant waves. For example, such a situation can arise when the one–dimensional beam of fast electrons propagates through a plasma /6/ in the presence of the ion–sound waves. In this

case the resonant (with the beam particles) waves are the Langmuir ones, while the non–resonant waves are the ion–sound those. The plasma–maser effect can /6/, in particular, result in the stabilization of the beam instability for the beams with the distributions

$$\Phi_v^{(b)} = \begin{cases} A(v_0-v_1)^m[1-(v_0-v)^m/(v_0-v_1)^m], & \text{if } v_1 \le v \le v_0, \\ A(v_0-v_1)^m[1-(v-v_0)^n/(v_2-v_0)^n], & \text{if } v_0 \le v \le v_2, \\ 0 & \text{, if } v<v_1 \text{ or } v>v_2 \end{cases} \qquad (15)$$

(where $v=p/m_e$, $m_{e(i)}$ is the electron (ion) mass, $1<m<2$, $n>2$, and the constant $A(>0)$ is determined in the usual manner by normalization), when the following conditions are valid:

$$\frac{n_b}{n} << \left[\frac{v_0}{v_{Te}}\right]^2 \left[\frac{m_e}{m_i}\right]^{1/2} \left[\frac{q_s v_{Te}}{\omega_{pe}}\right]^3, \; 1 << \left[\frac{W_s}{n T_e}\right]\left[\frac{v_{Te}^4}{v_0^2 \Delta v^2}\right] \qquad (16)$$

Here n_b is the concentration of the beam particles, q_s and W_s are respectively the characteristic wavevector and the energy density of the ion–sound waves, ω_{pe} is the electron plasma frequency, T_e is the electron temperature, $v_{Te}=(T_e/m_e)^{1/2}$, $\Delta v=v_2-v_1$. When the conditions (16) are valid the effect of nonlinear interaction of the resonant and non–resonant waves dominates over that of quasilinear interaction.

In conclusion, the effect of the plasma–maser type nonlinear mechanism on the resonant waves can result in new phenomena which are absent in the more familiar nonlinearities, such as decays and/or induced scatterings, as well as quasilinear interactions.

One of the authors (S.V.Vladimirov) would like to thank the Alexander von Humboldt Foundation for a research fellowship.

/1/ Tsytovich V.N., Stenflo L., Wilhelmsson H. Phys. Scripta, **11**, 251 (1975).
/2/ Krivitsky V.S., Tsytovich V.N., Vladimirov S.V. Phys. Reports, **218**, 141 (1992).
/3/ Isakov S.B., Krivitsky V.S., Tsytovich V.N. Sov. Phys. JETP, **63**, 545 (1986).
/4/ Tsytovich V.N. Theory of Turbulent Plasma. N.Y.: Consultants Bureau, 1977.
/5/ Vladimirov S.V., Yu M.Y., Popel S.I. Contrib. Plasma Phys. **33**, 1 (1993).
/6/ Popel S.I., Vladimirov S.V., Yu M.Y. Phys. Scripta. **47**, 239 (1993).

ABOUT THE INFLUENCE OF THE HIGHEST NONLINEARITIES ON THE FINISH STAGE OF THE LANGMUIR COLLAPSE.

Gulenko V.V., Gushchin V.V.

Kharkov State University, 310077, Kharkov, Ukraine.

The paper presents a hamiltonian approach to description of nonlinear dynamics of strong Langmuir wave on plasma. Among the numerous reasons stimulating this activity note the following. First of all, a considerable interest to Langmuir wave is due to the problems of their collapse [1] and strong turbulence [2] as well as on connection with plasma methods of charged particles acceleration [3]. Secondly, the presented approach to our mind, is the most effective under derivation of equations, which in sequaence take into account high orders of nolinearity and dispersion in different continuous media and possesses the universality. This is extremely important under studies of nonlinear regimes with the tendences of singularity formation (self-focusing, collapse, e.t.c).

It is wirth pointing out that the use of hamiltonian formalism for description of classical nonlinear fields of different physical nature is a wide-spread procedure [4-5]. However, the absence of the reduction procedure of the interaction hamiltonians of different nature waves considerably restricted the possibilities of the formalism. To remove this shortcoming we desired the nonliear canonical transforms excluding non-significant (non-resonant) processes from the interaction hamiltonians in general form. The appearence of dynamical equations appears to be completely defined by dispersion laws of interacted waves. Selecting all possible three-wave, four-wave, e.t.c. wave processes where they take part, we define significant terms in interaction hamiltonian and thus, the equations. Without goving details present only the searched set of equations on impulse $(\vec{k},t)$ presentation

$$\frac{\partial a_k}{\partial t} + i\omega_k a_k = -i\frac{\delta\tilde{\mathcal{H}}_{int}}{\delta a_k^*};\quad \frac{\partial b_k}{\partial t} + i\Omega_k b_k = -i\frac{\delta\tilde{\mathcal{H}}_{int}}{\delta b_k^*};\quad \tilde{\mathcal{H}}_{int} = \tilde{\mathcal{H}}_3 + \tilde{\mathcal{H}}_4 + \tilde{\mathcal{H}}_5 \qquad (1)$$

$$\tilde{\mathcal{H}}_3 = \int d\vec{k}_{123}\left\{\left(b_1^* b_2 b_3 + \text{c.c.}\right)U^6_{123}\delta_{1-2-3} + s\left(b_1 a_2 a_3^* + \text{c.c.}\right)U^{10}_{123}\delta_{1+2-3}\right\} \qquad (2)$$

$$\tilde{\mathcal{H}}_4 = \int d\vec{k}_{1234}\left\{\tfrac{1}{2}a_1 a_2 a_3^* a_4^* V^9_{1234}\delta_{1+2-3-4} + \right. \qquad (3)$$

$$\left. + \left(a_1^* a_2 b_3 b_4 + \text{c.c.}\right)V^5_{1234}\delta_{1-2-3-4} + a_1 a_2^* b_3 b_4^* V^7_{1234}\delta_{1-2+3-4}\right\}$$

$$\tilde{\mathcal{H}}_5 = \int d\vec{k}_{12345\sigma}\left\{\tfrac{1}{3}a_1^* a_2^* a_3^* a_4 a_5 a_\sigma Q^4_{12345\sigma}\delta_{1+2+3-4-5-\sigma} + \ldots\right\} \qquad (4)$$

Here $a_k \equiv a(\vec{k},t), b_k \equiv b(\vec{k},t)$ are the complex amplitudes of HF and LF

waves respectively, $d\vec{k}_{123}\equiv d\vec{k}_1 d\vec{k}_2 d\vec{k}_3$, $\delta_{i\pm2\pm3}\equiv\delta(\vec{k}_i\pm\vec{k}_2\pm\vec{k}_3)$,..., $U^{(i)}_{123}\equiv U^{(i)}(\vec{k}_1,\vec{k}_2,\vec{k}_3)$, $V^{(i)}_{1234}\equiv V^{(i)}(\vec{k}_1,\vec{k}_2,\vec{k}_3,\vec{k}_4)$ e.t.c. are the matrix elements of i-th order. Here we present only the clear appearence of some of them which will be used further in the case $kr_{de}\ll(m/M)^{1/2}\equiv\mu^{1/2}$.

$$U^{10}_{123}=\frac{(4\pi)^{-3/2}\,c_s}{2(n_0M_i\omega_{pi})^{1/2}\mu^{1/4}}k_1\frac{\vec{k}_2\vec{k}_3}{k_2k_3};\quad \tilde{V}^{3}_{1234}=-\frac{(2\pi)^{-5}}{4\pi n_0T}\frac{(\vec{k}_1\vec{k}_3)}{k_1k_3}\frac{(\vec{k}_2\vec{k}_4)}{k_2k_4} \qquad (5)$$

$$Q^{4}_{123456}=\frac{(8\pi)^{-6}\,3}{2(n_0m)^2\mu\omega_{pe}}\frac{(\vec{k}_2\vec{k}_3)}{k_2k_3}\frac{(\vec{k}_4\vec{k}_5)}{k_4k_5}\frac{(\vec{k}_1\vec{k}_6)}{k_1k_6} \qquad (6)$$

where r_{de} is the Debye radius, c_s is the ion acoustic velocity, ω_p - is the Langmuir frequency, $\vec{k}$ is the wavevector.

The study of linear stage in the framework of (1) shows that under sertain conditions the higher order nonlinearities may influence on the initial stage of the modulational instability evolution. In spite of the formal coincidence of the increments one has to separate the regions with $kr_{de}\ll\mu^{1/2}$ and $kr_{de}\gg\mu^{1/2}$ where HF and LF waves are unstable respectively. Note that there is mutual transition of these instabilities under the variation of the parameters of the task.

Using the reverse Fourier transform it is not difficalt to write the set (1) on the coordinate $(\vec{r},t)$ representation

$$i\Delta\frac{\partial\psi}{\partial t}=-2\pi\omega_{pe}\frac{\delta\mathcal{H}}{\delta\psi^*};\qquad \frac{\partial n}{\partial t}=\frac{\delta\mathcal{H}}{\delta\Phi};\qquad \frac{\partial\Phi}{\partial t}=-\frac{\delta\mathcal{H}}{\delta n}; \qquad (7)$$

$$\mathcal{H}=\mathcal{H}_{zakh}+\mathcal{H}_{el.non}+\mathcal{H}_{ion.non}+\mathcal{H}_{disp}+\ldots$$

Here n,Φ is a calonically conjugated pair of variables, n is perturbation of plasma particles concentration, Φ is velocity potential of them, ψ is the electric field potential of wave. By straightforward variation in (7) one can obtain equations describing the nonlinear dynamics of Langmuir waves. In the framework of these equations it is possible to simultaneously take into account electron and ion nonlinearities, variation of dispertion e.t.c.

Restricting $\mathcal{H}$ by $\mathcal{H}_{zakh}$ in (7) we obtain the set of Zakharov equations [1] and if $\mathcal{H}=\mathcal{H}_{zakh}+\mathcal{H}_{el.non}$ the set of Kuznetsov equations [6]. The concrete appearence of hamiltonians in (7) is not presented here. Due to fact that the possibilities of analytical study of Zakharov equations are limited one has to use a computer simulation under the studies of the collapse problem. Extremely great volume of calculation demands the information about the caverna physics in a numerical model (the automodel character of collapsing, a caverna anisotropy e.t.c.). The "improved" equations which are impossible to be obtained out of the framework of hamiltonian formalism are necessary for making the model more precise.

It is necessary to point out that the appearence of equations (1,7) is sensitive to the decay process HF ⇒ HF'+LH (s=1 in (1) if the decay process takes place and s=0 if not). It is impossible, one can exclude $\mathscr{H}_3$ from (1) and this set is reduced to the following equation

$$\frac{\partial a_k}{\partial t} + i\omega_k a_k = -i\int d\vec{k}_{123} a_1 a_2 a_3^* V^3_{123k} \delta_{1+2-3-k} - \tag{8}$$

$$-i\int d\vec{k}_{12345} a_1 a_2 a_3 a_4^* a_5^* Q^4_{k12345} \delta_{1+2+3-4-5-k}$$

In the case $Q^{(4)}=0$ the equation (8) in $\vec{r}$ representation corresponds to NSE or to the equation of statistical approach [1]. The modulational instability has been considered before do lead in this approximation to formation of singulariry. The dynamica of the latter goes to supersonic stage under $W/nT > \mu$, $W \equiv k^2\psi^2/8\pi$. Show that the taking into account of $Q^{(4)}$ leads to a stabilization. Really, in this case

$$\mathscr{H} = \mathscr{H}_2 - \mathscr{H}_4 + \mathscr{H}_6 \tag{9}$$

when $\mathscr{H}_6=0$ the condition $\mathscr{H}<0$ leads to the collapse. Using the similary transforms in (9) which conserves the integral of particles number $N=\int |a_k|^2 d\vec{k}$, $a(\vec{k},t) \Rightarrow \lambda^{-d/2} a(\vec{k}/\lambda, t)$, d is the dimension of the space, it is not difficalt to obtain the following dependence $\mathscr{H}$ on λ

$$\mathscr{H}(\lambda) = \mathscr{H}_2(\vec{\xi})\lambda^2 - \mathscr{H}_4(\vec{\xi})\lambda^d + \mathscr{H}_6(\vec{\xi})\lambda^{2d} \tag{10}$$

where $\vec{\xi} \equiv \vec{k}/\lambda$. One can see the stabilized influence of higher nonlinearities under the increase of λ (collapse in impulse represantation corresponds to $k \Rightarrow \infty$). The exact proof of the fact of collapse is based on Talanov theorem [1] (virial theorem) and is realized only for NSE or for nonrealistic spherically symmetric case. The similar situation probably takes place in impulse represantation. The another proof [1] is based on the impossibility of the stationary state realization, started from $\mathscr{H}<0$. Acting analogously to [1,7] we obtain

$$\mathscr{H} = \frac{d-2}{4-d} p^2 N - \frac{2}{3} \frac{\mathscr{H}_6}{4-d} \tag{11}$$

looking for the statinary solutions in the form $a(\vec{k},t) = \exp(ip^2 t) A(\vec{k})$. For $\mathscr{H}_6=0$ we have a reduction to [1]. The analysis of (11) shows a possibility of stationar. Moreover, the coordinate representation of equation (8) has a soliton-like solution

$$\psi(x,\vec{r}_\perp,t) = \tilde{\psi}(\xi)\exp[i(\Omega t - \vec{\varkappa}\vec{r}_\perp)] \qquad \xi = x - Vt, \qquad \vec{\varkappa} = (0, \varkappa_y, \varkappa_x)$$

$$\psi(\xi)=\frac{(\alpha/\alpha_2)^{1/2}}{\left[ch^2\left(\xi\alpha^{1/2}/4r_{De}\right)-\frac{\alpha}{32\mu}\exp\left(\xi\alpha^{1/2}/2r_{De}\right)\right]}; \qquad (12)$$

$$\alpha\equiv 2\left[\frac{\Omega}{\omega}+\frac{i}{2}(\varkappa^2-\lambda^2)r_{De}^2\right] \quad ; \quad \alpha_2\equiv\frac{q^2}{8\pi n\,T}$$

which is redused to the ordinary soliton when $Q^{(4)}=0$. In the framework of Zakharov-Kuztetsov method [7] using the integral inequalities of Helder one can prove its stability.

The estimate

$$\omega\approx\frac{3}{2}\omega_{pe}k^2r_{De}^2\approx\omega_{pe}\frac{W}{n\overline{T}}\approx\frac{3}{512\mu}\omega_{pe}\left(\frac{W}{n\overline{T}}\right)^2. \qquad (13)$$

follows from (8) and shows that the ion nonlinearities become significant even for $W/nT<1$, $(kr_d)^2<1$ while the electron ones become significant only if $W/nT\approx(kr_d)^2\approx 1$.

The automodel solutions of the studied sets of equations play an important part in the collapse problem. When $Q^{(4)}=0$, the equation (8) allows the following automodel substitution

$$a(\vec{k},t)=(t-t_o)^{(\alpha-1)/2+i\lambda^2}P(\vec{\xi}); \qquad \vec{\xi}\equiv\vec{k}(t-t_o)^{1/2} \qquad (14)$$

where t_o is the time of the singulariry formation. It is importants to point out that the solution (14) corresponds to well-known automodel solutions of NSE and to the equations of static approximation [1]. It is not difficult to get assured in this using the reverse Fourier transform. However, when $Q^{(4)}\neq 0$ the equation (8) has no automodel solutions of the form (14). It is necessary to search another nontrivial symmerties of equation (8).

The given examples convictively enough demonstrate the significant part of higher nonlinearities on the dynamics of Langmuir collapse at nondecay (in respest to the process $l\to l'+s$) part of its spectrum. The analogous studies may be carried out in the region $kr_d\gtrsim\mu^{1/2}$.

[1].V.E.Zakharov, In:Osnovy fiziki plasmy (Sov.), 1984, v.2, p.79.
[2].V.D.Shapiro,V.I.Shevchenko, In:Osnovy fiziki plasmy (Sov.), 1984, v.2, p.119.
[3].Plasma Science,1987,v,PS-15,N2,Special issue.
[4].V.E.Zakharov,E.A.Kuznetsov. Sov.Sci.Rev.sec.C.1984,v.4,p.167.
[5].V.E.Zakharov,S.L.Musher,A.M.Rubenchik. Phys.Reports, 1985,v.129, N5,p.285.
[6].E.A.Kuznetsov. Fizika Plasmy, 1976,v.2,p.327.
[7].E.A.Kuznetsov,V.E.Zakharov,A.M.Rubenchik. Phys.Reports,1986, v.142, p.103.

Nonlinear Generation of the Fundamental Radiation in Plasmas

A. C.-L. CHIAN
Department of Applied Mathematics and Theoretical Physics
University of Cambridge
Silver Street, Cambridge, England CB3 9EW
and
F. B. RIZZATO
Instituto de Física
Universidade Federal do Rio Grande do Sul
Caixa Postal 15051
91501 - 970 Porto Alegre, RS, Brazil

Nonlinear generation of coherent electromagnetic radiation by intense Langmuir waves in the vicinity of the fundamental plasma frequency f_p is of current interest in space and laboratory plasmas. In a pioneer work, Lashmore-Davies [1] demonstrated that an efficient process for converting intense Langmuir waves into f_p electromagnetic radiation can be achieved by two counterstreaming Langmuir pump waves through an electromagnetic oscillating two-stream instability. Recently Chian & Alves [2], Akimoto [3] and Rizzato & Chian [4] extended the formalism of Lashmore-Davies in order to include mixed processes with induced modes which are purely electrostatic or electromagnetic.

In this paper we extend our previous analysis [4], in order to study the nonlinear interaction involving travelling electromagnetic pumps, low-frequency density fluctuations and high-frequency f_p modes which can be electrostatic-electromagnetic hybrids.

In the model, a high-frequency transverse wave ($\omega_o \approx f_p, \mathbf{k}_o$) which is incident from left to right along the $\mathbf{x}$ axis with polarization along the $\mathbf{y}$ axis, nonlinearly interacts with low-frequency density fluctuations and emits a secondary high frequency wave with wavevector lying on the $\mathbf{x}$ $\mathbf{y}$ plane. The wavevector $\mathbf{k}_{lf}$ of the low frequency fluctuations is assumed to be parallel to the $\mathbf{y}$ axis but otherwise arbitrary, from which is readily seen that depending on its magnitude, the high-frequency mode may be predominantly electrostatic ($k_{lf}^2 >> k_o^2$), electromagnetic ($k_{lf}^2 << k_o^2$) or a fully mixed mode ($k_{lf}^2 \sim k_o^2$).

The coupled set of equations describing this kind of coherent process, if Fourier analyzed, yields the following relationships for the relevant perturbed physical quantities [4]

$$[-2i\omega_p\partial_t - \delta_\omega - c^2\mathbf{k}\times\mathbf{k}\times + 3v_{th}^2\mathbf{k}(\mathbf{k}\cdot)]\,\delta\mathbf{E}(\mathbf{k}) = -\frac{\omega_p^2}{n_o}\int n(\mathbf{k}_1)\mathbf{E}_o(\mathbf{k}-\mathbf{k}_1)d\mathbf{k}_1 \qquad (1)$$

and

$$d_S n = \frac{-k^2\epsilon_o}{2m_i}\int[\mathbf{E}_o(\mathbf{k}-\mathbf{k}_1)\cdot\delta\mathbf{E}(-\mathbf{k}_1)^* + \mathbf{E}_o(\mathbf{k}_1-\mathbf{k})^*\cdot\delta\mathbf{E}(\mathbf{k}_1)]d\mathbf{k}_1 \qquad (2)$$

with $d_S \equiv \partial_t^2 + \omega_S^2$, $\omega_S^2 \equiv c_S^2k^2$, $n(\mathbf{k}) = n(-\mathbf{k})^*$ as the $\mathbf{k}$ - Fourier component of the density fluctuations $n(\mathbf{r},t)$ and $\delta\mathbf{E}(\mathbf{k})$ as the $\mathbf{k}$ - Fourier component of the high-frequency perturbed field $\mathbf{E}(\mathbf{r},t)$. Besides, in the above set of equations we introduce $\omega_p^2 = n_o e^2/m_e\epsilon_o$, e as the

electron charge, m_e as its mass $\delta_\omega \equiv \omega_o^2 - \omega_p^2$, n_o as the particle density and $c_S' = \sqrt{k_B T/m_i}$ as the velocity of ion-acoustic waves with k_B as the Boltzman constant, T as the electron temperature and m_i as the ion mass.

Now one splits the high-frequency field into its electromagnetic and electrostatic components as $\delta\mathbf{E}(\mathbf{k}) = \delta\mathbf{E}_L(\mathbf{k}) + \delta\mathbf{E}_T(\mathbf{k})$, where $\delta\mathbf{E}_L$ is parallel to $\mathbf{k}$ and $\delta\mathbf{E}_T$ is perpendicular to that quantity. With that, taking into consideration that $\nabla \times \nabla \times \mathbf{E}_L = 0$ and $\nabla \cdot \mathbf{E}_T = 0$, and making use of the assumed pump spectrum $\mathbf{E}_o(\mathbf{k}) = \hat{\mathbf{y}} E_o \delta(\mathbf{k} - \hat{\mathbf{x}} k_o)$ one can finally arrive at the following low-frequency nonlinear dispersion, heretofore referred as the full dispersion relation:

$$\omega^2 - \omega_{os}^2 f = -\omega_{os}^2 \hat{W} \frac{f^2}{1+f}\left[\frac{\epsilon(1+f)-1}{(\epsilon(1+f)-1)^2 - \omega^2} + \frac{1}{f^2 - \omega^2}\right], \tag{3}$$

where $\omega_{os}^2 = c_S^2 k_o^2/R^2$, $\hat{W} = \frac{\omega_p \epsilon_o E_o^2}{8 T n_o k_B R}$, $R = \frac{c^2 k_o^2}{2\omega_p}$, $\epsilon = \frac{v_{th}^2}{c^2} = \frac{2T}{m_e c^2}$, $f = \frac{k_1^2 f}{k_o^2}$, and where frequencies has been normalized to R.

Our basic interest in this paper is to analyze mixed instabilities involving electrostatic and electromagnetic effects simultaneously (hybrid modes). To do that, let us start with some limiting cases where those instabilities are decoupled into pure electromagnetic or electrostatic modes.

1. Electromagnetic Case ($f << 1$)

Pure electromagnetic cases basically takes place when the wavevector of the emitted high-frequency wave is almost parallel to the $\mathbf{x}$ axis, which means $f << 1$. If besides that one notes that any emitted electromagnetic wave would have a larger wavevector than $\mathbf{k}_o$ and consequently a larger frequency than ω_o as well, one concludes that the interaction process cannot be of the decay type. Thus, on disregarding electrostatic effects in the full dispersion relation and writing $\omega = i\Gamma$ (Γ real) to search for purely growing modes, one can obtain the instability range for this kind of mode in the form

$$0 << f << \hat{W}, \tag{4}$$

a relation that leads to conclude that the original instability is entirely situated in the electromagnetic domain ($f_{max} << 1$) only when $\hat{W} << 1$, a condition characterizing what could be called a weak pump regime. If $\hat{W}$ is arbitrarily large, the instability will probably contain some admixture of electrostatic effects. It is seen that this instability, also known as electromagnetic filamentational instability, takes place when smooth transverse perturbations of the original propagating electromagnetic mode start to develop in time [1].

2. Electrostatic Case ($f >> 1$)

Similarly to the electromagnetic case, let us assume that we are working in a region of large enough values of f such that for the moment, the electromagnetic contribution to the dispersion relation may be disregarded from the full dispersion relation. The electrostatic system so obtained turns out to be a little more involved than the electromagnetic one, because now one can identify two possible situations as the factor f is varied. Indeed it is not hard to verify that there is a critical value for f, f_{cr}, such that if $f > f_{cr}$ the linear frequency of the emitted electrostatic wave is larger than ω_o while for $f < f_{cr}$ it is smaller. This critical quantity f_{cr} may be evaluated from the condition of null electrostatic mismatch, $\delta_L = 0 \Rightarrow (\epsilon(1+f_{cr})-1)^2 = 0$ which yields

$$f_{cr} = \frac{1}{\epsilon} - 1 \approx \frac{1}{\epsilon}, \tag{5}$$

a quantity that is naturally large. If $f > f_{cr}$ the interaction dynamics is much similar to the previously studied electrostatic case. In this situation there is no possibility of decay and

what one really has is a purely growing density mode whose unstable f's are located in the range

$$f_{cr} < f < \frac{\hat{W}+1}{\epsilon}. \tag{6}$$

One sees that the range may be either narrow or wide, depending on the pump power.

On the other hand, when $f < f_{cr}$, the instability is of the decay type. In the weak pump regime mentioned above, the peak of the instability (f_{peak}) is located at the resonance defined by $(\epsilon(1+f_{peak})-1)^2 - \omega_{os}^2 f_{peak}$, which can be seen to yield small values of f only when ω_{os} satisfies $\omega_{os} << 1$, something that can always occur for not too small values of k_o, or specifically when

$$\frac{c_S^2}{c^2}\frac{\omega_p^2}{c^2 k_o^2} << 1$$

(recall that $c_S^2/c^2 << 1$). For large enough ω_{os}'s or small enough k_o's, the instability would have its peak located at too small values of f_{peak} for the electrostatic electromagnetic decoupling to be operative. In Fig.(1) we plot all the frequencies $\omega = \omega_r + i\Gamma$, ($\omega_r$ and Γ real) of the various modes participating of a weak pump regime where $\omega_{os} << 1$, considering $\hat{W} = 0.1$, $\omega_{os} = 0.05$ and $\epsilon = 0.01$. The three basic unstable modes are clearly seen: mode M_3 is the purely growing filamentational instability; mode $M_2 + M_4$ is the pure electrostatic decay instability that appear as a result of the fusion of modes M_2 and M_4 (we denote $M_5 = M_2 + M_4$), and mode M_7 is the purely growing electrostatic mode.

3. Mixed Modes

The first mixed mode one should quote here is precisely the decay one occurring for $\omega_{os} \sim 1$ already in the weak pump regime. Besides that instability one should analyze the behavior of the previous purely growing electromagnetic filamentational instability as the pump power is increased. In order to accomplish that, we replace ω with $i\Gamma$ (Γ real) in the full dispersion relation.

If f is much smaller than one the situation is of a purely growing electrostatic instability as before. However, for larger values of f, the situation is changed. In this case of purely growing modes, it is not hard to show that the effect of the electrostatic term is to curve downwards the function defined by the right hand side of the full dispersion relation as one approaches $\Gamma = 0$. It may occur that due to this curvature, two mutual intersections of the right and left (which is a straight line if considered a function of Γ^2) hand sides, become possible. The critical existence condition of these kind of situation is closely related to the intensity of the pump power. Indeed, it can be shown that two critical quantities $\hat{W}_*$ and f_* can be introduced as

$$f_* \approx 1 - \frac{3\epsilon}{2} \quad , \quad \hat{W}_* \approx \frac{2}{\epsilon} >> 1. \tag{7}$$

such that if $\hat{W}$ is larger than $\hat{W}_*$ there will be some value of f, larger than f_*, for which the two roots simultaneously appear.

The larger of the two roots goes into the electromagnetic filamentation for $f << 1$, but the smaller one represents a new unstable mode that does not occur neither for $f << 1$ nor too small values of $\hat{W}$.

In Fig.(2) we plot the frequencies of the modes occurring in the strong pump regime $\hat{W} >> 1$. Purely real modes M_1 and M_2 join to form an additional unstable mixed mode M_1+M_2 which a numerical analysis reveals to be present for $\hat{W} \gtrsim 1$. In that region of relatively small values of f one also notes the presence of the purely growing mode M_3 that goes into the electromagnetic filamentation for $f \to 0$. For larger values of f, again one can note the presence of the second purely growing mode $M_{3'}$ along with a junction point **J** where modes

M_3, $M_{3'}$ and M_5 (an extension of the former decay instability) join together. In contrast to the former regime, the decay instability M_5 may now be seen as formed by the fusion of the purely growing modes M_3 and $M_{3'}$. In the figure we use $\hat{W} = 5.0 \times 10^3$ in order to be well above the threshold $\hat{W}_*(\epsilon = 0.01) \sim 200.0$, and take $\omega_{os} = 1.0$.

Acknowledgments: We wish to express our acknowledgments to Cláudio M. Rizzato for the help with the figures. This work was partially supported by CNPq, CAPES and FINEP (Brazil).

A.C.-L.Chian's permanent address: INPE, Caixa Postal 515, 12201, São José dos Campos, SP, Brazil.

References

[1] C. N. Lashmore-Davies, Phys. Rev. Lett. **32**, 289 (1974) *and* Nuclear Fusion **15** (1975).

[2] A. C.-L. Chian and M. V. Alves, Astrophys. J. **330** L-77, (1988).

[3] K. Akimoto, Phys. Fluids **31**, 538 (1988).

[4] F. B. Rizzato and A. C.-L. Chian, Journal of Plasma Phys. **48**, 71 (1992).

[5] S. G. Thornhill and D. ter Haar, Phys. Rep. **43**, 43 (1978).

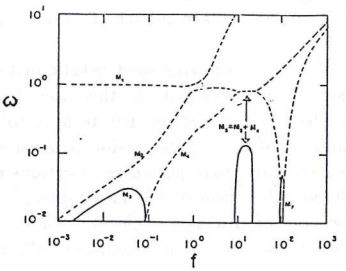

Fig.1- Frequency ($\omega = \omega_r(dotted) + i\Gamma(full)$, ω_r, Γ real) vs. f in the weak pump regime; $\hat{W} = 0.1$ and $\omega_{os} = 0.05$.

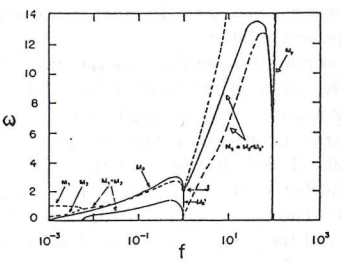

Fig.2-The same as in Fig.1, for the strong pump regime, $\hat{W} = 5.0 \times 10^3$ and $\omega_{os} = 1.0$.

ON THE INFLUENCE OF EXTERNAL PERIODIC FORCES ON NON-LINEAR LONGITUDINAL OSCILLATION IN THERMAL INHOMOGENEOUS PLASMA

I. A. El-Naggar
Physics Dept., Faculty of Education, Alex. University, Alex., Egypt.

In this case of a thermal plasma the system of initial fluid equations is of the form

$$\frac{dv}{dt} = \frac{e}{m}E - \nu_{col}\cdot v - \frac{1}{nm}\nabla P \,, \qquad (1)$$

$$\frac{dn}{dt} + \frac{\partial(nv)}{\partial x} = 0 \,, \qquad (2)$$

$$\frac{\partial E}{\partial x} = 4\pi e(n - n_0) \,, \qquad (3)$$

where $e<0$, $n_0 = n_0(x)$ is the ion equilibrium density which may be considered as stationary for high-frequency oscillations and ν_{col} is the effective frequency of electron-particle collisions. It is assumed to be small ($\nu_{col} < \omega_p$) and independent of the velocity. Here and later on d/dt is Lagrange (substantial) derivative. Taking into consideration that $n_0(x) \gg n$, one may write equation (1) as following

$$\frac{dv}{dt} = \frac{e}{m}E - \nu_{col}\cdot v - \frac{v_T^2}{\omega_p^2}\frac{\partial \omega_p^2}{\partial x} \,, \qquad (4)$$

where $\omega_p^2 = \sqrt{4\pi^2 e n_0/m}$ is the Langmuir frequency of plasma electrona For inhomogeneous plasma, this frequency depends on the displacement q . In order to solve the system one conveniently changes from Euler to Lagrange derivatives and considers the displacement of electron fluid element q from the position of equilibrium as a function of time and initial coordinates $x = x_0 + q(x_0, t)$. Following further a procedure described in El-Naggar, 1990 one obtains

$$\frac{d^3q}{dt^3} + \nu_{col}\frac{d^2q}{dt^2} + \omega_p^2\frac{dq}{dt} + v_T^2\frac{d}{dt}\left(\frac{1}{\omega_p^2}\frac{\partial \omega_p^2}{\partial x}\right) = \frac{e}{m}f(t). \qquad (5)$$

We consider the solution of equation (5) assuming that a monochromatic electromagnetic wave propagates in a plasma, so that

$$f(t) = f_0 \, Sin(\omega_{ex} t + \Phi_0) \,, \qquad (6)$$

where ω_{ex} is the external frequency, f_0 is the amplitude and Φ_0 is the initial phase of that wave. The case of thermal and weak non-homogeneous plasma, which is of greater interest from the physical point of view , will now be considered. Moreover, this paper is confined to the case of a basic subharmonic resonance ($\omega_{ex} = 2\omega_p$). Unstable oscillations can also develop at frequencies of $\omega_p = (\omega_{ex}/2)n$, where $n = 2, 3, \cdots$. But with arise in n , the resonance intensity (as well as the width

of the resonance range) decreases sharply. Consequently, in such plasma ω_p^2 may be expanded in a series involving the degrees of displacement q ,

$$\omega_p^2(q) = \omega_{p0}^2 + \alpha q + \beta q^2 + \gamma q^3 + \eta q^4 + \dots \qquad (7)$$

where, $\alpha \equiv (\partial\omega_p^2/\partial q)|_{q=q_{res}}$, $\beta \equiv \frac{1}{2}\partial^2\omega_p^2/\partial q^2|_{q=q_{res}}$, ...

Using equation (7), equation (5) is reduced to

$$\frac{d^2q}{dt^2} + 2\nu_{col}\frac{dq}{dt} + \bar{\omega}_p^2 q + \bar{\alpha} q^2 + \bar{\beta} q^3 = -\frac{eE_0}{m\omega_{ex}}\cos(\omega_{ex}t + \varphi_0), \qquad (8)$$

where, $\bar{\omega}_p^2 = \omega_{p0}^2 + v_T^2(2\beta - \alpha^2/\omega_{p0}^2)/\omega_{p0}^2$,

$\bar{\alpha} = \alpha/2 + 3v_T^2(\gamma - \alpha\beta/\omega_{p0}^2)/\omega_{p0}^2$,

$\bar{\beta} = \beta/3 + 2v_T^2(2\eta - \beta^2/\omega_{p0}^2 - 2\alpha\gamma/\omega_{p0}^2)/\omega_{p0}^2$.

Here it is noticed that the disappearance of the density inhomogeneity cancels the nonlinear effect due to thermal state. But the opposite is not true, unless under certain conditions as we shall see later on.

In the linear case (lst approximation) equation (8) has the following solution

$$\psi_1 = -\frac{\bar{F}}{3m\bar{\omega}_p^2}\cos(2\bar{\omega}_p t), \qquad (9)$$

where, $\bar{F} \equiv -eE_0/\omega_{ex}$,

i.e., oscillations with the frequency of an external high-frequency wave are excited in the plasma. It is clear that the contribution from the next order approximation, $\sim \psi_1 \cdot \psi_2$ is associated with a parametric-type resonance for the system being considered. Ignoring all non-linear resonance components it is easy to get the zone of instability as following

$$2\bar{\omega}_p\left[1 - \frac{h}{4} - \frac{3h^2}{64}\right] < \omega_{ex} < 2\bar{\omega}_p\left[1 + \frac{h}{4} + \frac{3h^2}{64}\right]$$

where, $h \equiv (2\bar{\alpha}\bar{F}/3m\bar{\omega}_p^4) \ll 1$.

It is important to observe that in inhomogeneous plasma the thermal state tends to cancel the mechanism of parametric excitation under the following condition

$$v_T^2 = \alpha\omega_{p0}^2/6(\alpha\beta/\omega_{p0}^2 - \gamma). \qquad (10)$$

But in cold plasma ($v_T \to 0$), the absence of parametric mechanism cannot be approached unless the density inhomogeneity itself disappears ($\alpha = 0$) (Demchenko & El-Naggar, 1971).

Taking into consideration all the nonlinear components one can get an equation for ψ_2 from equation (8) as follows

$$\frac{d^2\psi_2}{dt^2} + 2\nu_{col}\frac{d\psi_2}{dt} + \bar{\omega}_p^2\left[1 - h\cos(2\bar{\omega}_p t)\right]\psi_2 + \left[\bar{\alpha} - \frac{\bar{\beta}\bar{F}}{m\bar{\omega}_p^2}\cos(2\bar{\omega}_p t)\right]\psi_2^2 + \bar{\beta}\psi_2^3 = 0. \qquad (11)$$

The solution of equation (11), corresponding to the 1st approximation as suggested by Bogoliubov and Mitropoloskii, 1958 to the presence of the basic subharmonic resonance in the system considered, is found to be of the form

$$\psi_2 = a\cos\left(\frac{\omega_{ex}}{2}t+\theta\right) \quad , \psi = \frac{\omega_{ex}}{2}t+\theta, \tag{12}$$

where,

$$da/dt = hA_1(a,\theta), \tag{13}$$

$$d\theta/dt = \bar{\omega}_p - \omega_{ex}/2 + hB_1(a,\theta). \tag{14}$$

The magnitudes of A_1 and B_1 are determined from the following equations

$$A_1(a,\theta) = -\frac{1}{2\pi^2\omega_{ex}}\sum_{\sigma} e^{i2\sigma\theta}\int_0^{2\pi}\int_0^{2\pi} f_0(a,\omega_{ex}t,\psi)\,e^{-i2\sigma\theta}\sin\psi\,d\theta\,d\psi,$$

$$B_1(a,\theta) = -\frac{1}{2\pi^2 a\omega_{ex}}\sum_{\sigma} e^{i2\sigma\theta}\int_0^{2\pi}\int_0^{2\pi} f_0(a,\omega_{ex}t,\psi)\,e^{-i2\sigma\theta}\cos\psi\,d\theta\,d\psi$$

where, $f_0 = a\omega_{ex}\nu_{cl}\sin\psi + h\,a\,\bar{\omega}_p^2\cos(\omega_{ex}t)\cos\psi - \bar{\alpha}a^2\cos^2\psi + \frac{\bar{\beta}\bar{F}}{m\bar{\omega}_p^2}a^2\cos\psi\cos\omega_{ex}t\cos\psi + \bar{\beta}a^3\cos^3\psi$.

One may get from equations (13) & (14) the following

$$da/dt = -a\nu_{cl} - \frac{ah\bar{\omega}_p^2}{2\omega_{ex}}\sin 2\theta, \tag{15}$$

$$d\theta/dt = \bar{\omega}_p - \frac{\omega_{ex}}{2} + \frac{3\bar{\beta}a^2}{4\omega_{ex}} - \frac{h\bar{\omega}_p^2}{2\omega_{ex}}\cos 2\theta. \tag{16}$$

For stationary case equations (15) & (16) yield the relation between the amplitude a and the frequency of the external force ω_{ex}.

$$a^2 = \frac{8}{3\bar{\beta}}\left[\left(\frac{\omega_{ex}}{2}\right)^2 - \bar{\omega}_p^2 \pm \sqrt{h^2\bar{\omega}_p^4 - 4\omega_{ex}^2\nu_{cl}^2}\right]$$

With the help of this relationship one may construct a resonance curve as shown in Fig.(1)

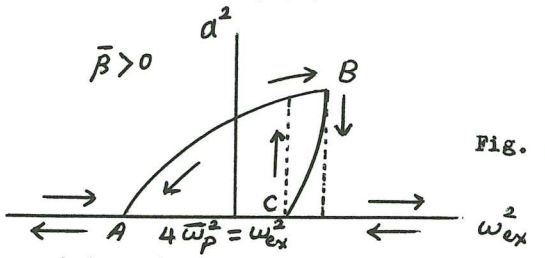

Fig. (1)

It is very interest to observe that a certain value of thermal velocity may cancel the nonlinear effect (which depends on both thermal and density inhomogeneity) and the amplitude of the oscillation increases infinitely. This

thermal condition is as follows ($\bar{\beta} = 0$)

$$v_T^2 \simeq \beta \omega_{p0}^4 / 6(\beta^2 + 2\alpha\gamma) \qquad (17)$$

It is easy to get the width of the parametric resonance zone (AC region) which equals to

$$\Delta = 2\sqrt{h^2 \bar{\omega}_p^4 - 16 \bar{\omega}_p^2 \nu_{cl}^2} \, .$$

One notes that the presence of collision reduces the interval inside which the parametric resonance arises. It is obvious that Δ will be real if the inequality

$$h > 4\nu_{cl} / \bar{\omega}_p \, ,$$

is satisfied. This inequality determines the minimum modulation percentage necessary for parametric resonance when collision is given. Again, it is found that under the thermal condition (10) the last inequality does not exist and the increment Δ will mot be real.

REFERENCES

Bogoliubov, N.N. and Mitropolskii, Y.A., 1958, Asympototic Methods of Non-linear Oscillation Theory, Gosizdat of Physics and Math. Literature, Moscow. (Translation : Hindustan Pub. Corpn., Delhi, 1961).

Demchenko, V.V. and El-Naggar, I.A., 1971, Plasma Physics, 13, 887 - 896.

El-Naggar, I.A., Feb. 21 - 28, 1990, Second Workshop on Plasma and Laser Technology, Cairo, 2, 113 - 118.

Contributed Papers Received During Printing

BIAS LIMITER EXPERIMENTS ON FT-2 TOKAMAK

V.O.Aleksandrov*, B.N.Budnikov, L.A.Esipov, E.R.Its,
S.I.Lashkul, A.D.Lebedev, I.E.Sakharov*, S.V.Shatalin*.

Ioffe Physico-Technical Institute,
St.Petersburg, 194021, Russia
*Technical University, St.Petersburg, Russia

The experiments on FT-2 tokamak (R=55 cm, a=6.5...7.7 cm, H=1.95 T, I=20 kA, t=40 ms) have been performed in order to study the influence of the drift flows in the poloidal limiter shadow upon the particle confinement in the plasma core. It is known [1,2] that the vertical drift of ions and electrons in a toroidal magnetic field and the boundary conditions on the poloidal limiter surface must cause the appearance of the poloidal electric field in the limiter shadow. Radial plasma drift $\vec{V}_d$ in this field can influence the particle confinement.

In our experiments two insulated movable segments of the poloidal limiter, Fig.1, have been differentially biased by the $\approx$ 250 V voltage at the 10-th ms after the origin of discharge current plateau. Before biasing the segments had been short-circuited forming an ordinary poloidal limiter. The polarity of electric field E was chosen so, that the drift $\vec{V}_d^* = c[\vec{E}\times\vec{H}]/H^2$ on the outboard side of the torus was directed opposite to the drift $\vec{V}_d$. We supposed that the suppression of the particle losses from the bulk plasma should take place in the presence on this drift. In order to obtain the magnetic field lines resting with both ends on the same segment, we limited plasma current by rather high value of the safety factor, q>4. In these conditions the electric field E should appear around the whole toroidal circumference of tokamak.

Plasma current, loop voltage, mean electron density, bolometric signal along the central chord, H_β and CIII lines emission are shown in Fig.2. Radiation losses profile have been measured by bolometer. These losses localized mainly on the plasma periphery. The calculated total radiation losses in

assumption of toroidal symmetry correspond to ohmic power input 45 kW before and 57 kW after biasing (for maximum plasma density). It should be pointed out that after biasing the radiation increases more significantly on the innerboard side of the torus. The electron temperature value, calculated from the power balance and conductivity, T_e=300 eV corresponds with the microwave FM-radiometer and soft X-ray measurements for Z_{eff}=1.6. The small decrease of microwave FM-radiometer and soft X-ray signals during biasing can testify to thereduction of T_e. In this case the calculated value of Z_{eff} remains constant. The increase of radiation losses ΔP_{rad} during biasing does not exceed $(\Delta n_e)^2$, i.e. we did not observe the additional impurity input.

Radial distributions of T_e and n_e in the limiter shadow had been measured by the movable four electrode probes for five values of poloidal angle (φ = 0^0, 30^0, 100^0, 130^0, 160^0). Fig 3 shows $T_e(r)$ and $n_e(r)$ on the 13-th ms after the begining of bias pulse for two angles, φ =$0^0$and φ =160^0. These distributions are rather complicated, but the tendency of the curves shift to the lower R side, i.e. in the drift V_d^* direction can be seen. Arrows indicate the profiles shift compared to that without biasing. The largest shift corresponds to φ =0^0. When the polarity of bias pulse changed the profiles shifts reversed.

Electron density profiles $n_e(r)$, illustrating the influence of the electric field E on bulk plasma characteristics, are shown on Fig.4. The significant (30%-40%) increase of the central electron density $n_e(0)$ during biasing can be seen, what, taking into account the constancy of particle sources, indicates the improvement of the particle confinement time.

So, the foregoing experimental data permits us to make the previous conclusion about the improvement of plasma confinement by the suppression of the particles drift in the limiter shadow region.

REFERENCES

1. Nedospasov A.V., Petrov V.G., Fidelman G.N. Plasma convection in the poloidal limiter shadow of a tokamak. Nuclear Fusion, 1985, vol.25,N.1, p.21-27.
2. Nedospasov A.V., Petrov V.G. Effect of anomalous transport on plasma convection in the poloidal limiter shadow of a tokamak. Nuclear Fusion, 1986, vol.26,N.11, p.1529-1536.
3. Levitskiy A.N., Sakharov I.E., Shatalin S.V., Four electrode probe for unhomogeneous plasma diagnostics, (in russ.), Pribory itechnica experimenta, 1992, N.5, p.153-157.

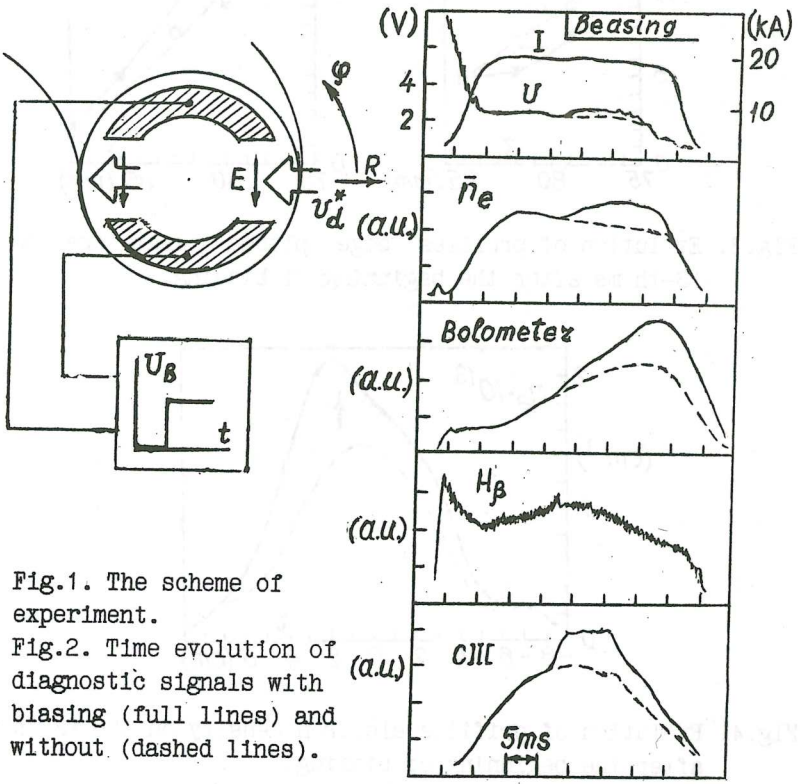

Fig.1. The scheme of experiment.
Fig.2. Time evolution of diagnostic signals with biasing (full lines) and without (dashed lines).

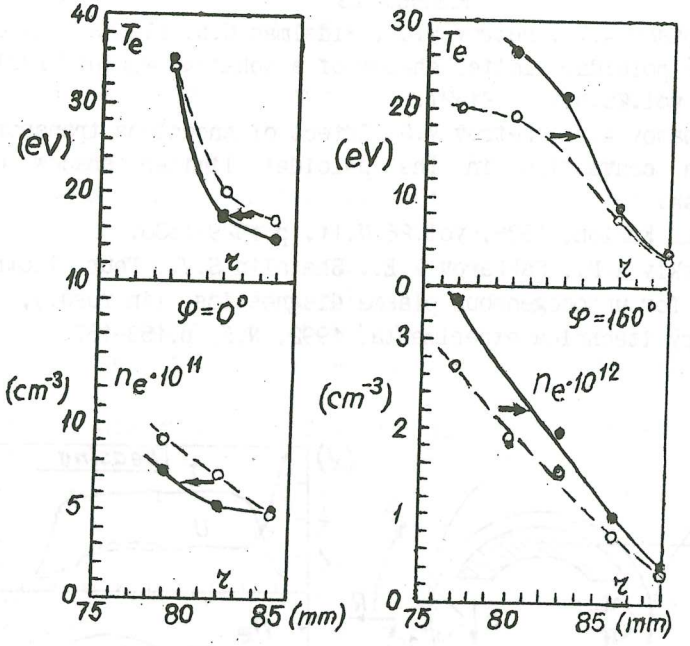

Fig.3. Evolution of profiles edge plasma parameters on the 13-th ms after the beginning of biasing.

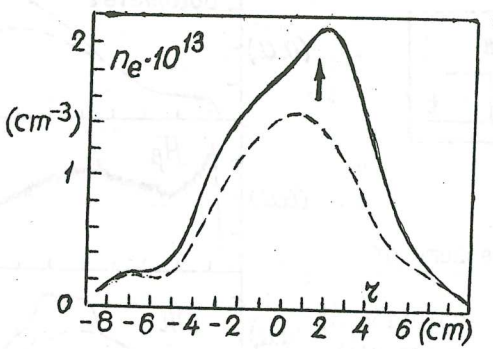

Fig.4. Evolution of prifiles electron density on the 13-th ms after the beginning of biasing.

OBSERVATION OF ENHANCED PLASMA CONFINEMENT AT FT-2 TOKAMAK AFTER THE LH PULSE HEATING.

V.O.Aleksandrov*, V.N.Budnikov, V.V.Dyachenko, L.A.Esipov, E.R.Its, S.I.Lashkul, A.D.Lebedev, K.A.Podushnikova, I.E.Sakharov*, S.V.Shatalin*, O.N.Sherbinin, A.Yu.Stepanov.

Ioffe Physico-Technical Institute,
St.Petersburg, 194021, Russia
* Technical University, St.Petersburg, Russia

The improved confinement regime was obtained at lower hybrid (LH) plasma heating in the FT-2 tokamak (R=55cm, a=8cm, B=2T, I=22kA), when RF driven current did not arise, but wave-particle interaction did exist and electron/ion heating was registered. The 3 ms RF power pulse was introduced into plasma from the lower field side at frequency 920 MHz and could be changed in the range 30...120kW. The LH waves in plasma were excited by the 2-waveguide grill operated out-of-phase with slowing factor 2...4 [1].

The improved confinement arose after the RF pulse [2]. The increased level of central density lasted up to the end of the discharge, Fig.1. The peripheral density in the shadow of the limiter decreased several times during the RF pulse and then recovered in several milliseconds after the RF pulse. The temperature and density profiles in the peripheral region measured by Langmuir probes are presented in Fig.2. Note that the increase of the electron temperature ΔT_e is independent of the RF power in the range 40...120kW and equal to 180eV. For less power the axial temperature continues to rise or keeps constant for 2 ms after the RF pulse. These data as well as the density increase Δn_e, the ion temperature increase ΔT_i and radiation losses P_{rad} are presented in Fig.3. It is worth to mention the ion temperature rise from 120eV up to 420eV for P_{RF}=120kW.

The change of energy content $\langle nT \rangle$ was determined by diamagnetic signal. It is significant that the latter was

conserved or even increased after the RF pulse, Fig.4. Taking into account the constant level of ohmic power ($P_{oh}\approx 85$kW) one can conclude about increase of energy life time τ_E in the post-heating phase. The calculations of the energy life time:

$$\tau_E = \frac{\int_V (n_e T_e + n_i T_i) dV}{I_p U_p - P_{rad} + P_{LH}}$$

have been made under conclusion $\partial\langle nT\rangle/\partial t \approx 0$ for ohmic regime and for the end of RF pulse. The calculation of τ_E from the diamagnetic signal coincides very well with calculations based on measured density and temperature profiles. We obtained that for P_{LH}=100kW τ_E decreases from 0.9 ms in ohmic heating to 0.6 ms at the end of RF pulse and in the post-heating phase increase up to 1.8...2.0 ms. The calculations by neoalcator scaling $\tau_{na}=7\times10^{-9} n_{13} a R_0^2 q$ [cm^{-3},cm] gives τ_{na}^{OH}=1.5ms and τ_{na}^{LH}=2ms. It should be mentioned that the increase of diamagnetic signal ΔV_{diam} during LH pulse corresponds to temperature measurements, shown in Fig.3, and the relation:

$$1.5H\Delta V_{diam} = \langle n_e \Delta T_E\rangle + \langle \Delta n_e T_e\rangle + \gamma_{OH}\langle n_e \Delta T_e\rangle,$$

where $\gamma_{OH}=(Z_i-Z_{eff})/(Z_i-1)$, Z_i=6, Z_{eff}^{OH}=2...3 is true. All three parts in the right side of the latter relation give approximately equal input in the diamagnetic signal.

Now we discuss the reason of the energy confinement improvement. The increase of T_e and accordingly $\sigma(r)\sim T_e^{3/2}$ causes the current chanal contraction, followed by its expansion after the RF pulse. Loop voltage characteristics V_p, as well as the suppression of MHD activity V_{MHD} in the post-heating phase during current chanal expansion, Fig.5, indicates on the existence of this processes. The hard X-ray signal X_h growths after RF pulse can also confirm our hypothesis about the approach of the current boundary to the limiter. Simulation of the poloidal magnetic field diffusion shows the enhancement of Z_{eff} during RF pulse from 2...3 to 3...4 and its decrease to the ohmic regime value in the post-heating phase. The contraction of the current chanal is

possibly responsible to the cooling and particle losses in the boundary plasma, what in its turn diminishes hydrogen (see H_β emission in Fig.5) and impurity fluxes from the walls. I.e. peripheral processes causes the improvement of plasma isolation especially in the post-heating phase, when the fast ions bombardment and the corresponding additional hydrogen fluxes from the limiter ceases.

Thus, the compatible ion and electron heating was carried out in tokamak plasma by LH waves. In the post-heating phase the essential enhancement in particle and energy confinement time was observed. This phenomenon was accompanied by typical processes in plasma periphery, which had been observed during transition to IOC and H-mode in various large tokamaks. The reason for this transition, as we suppose, is connected with the change in the current density profile, which follows the LH electron heating.

References:

[1] Budnikov V.N., Nuclear Fusion, 1991, v.31, N 4, p.611.
[2] Budnikov V.N. et al., Ioffe Inst. Preprint, N 1591, 1991.

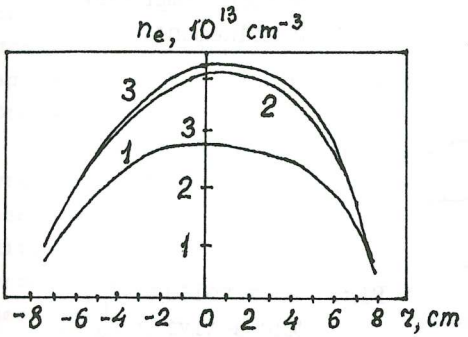

Fig.1 Plasma density profiles for different moments of discharge: 1 - OH, 2 - end of LH pulse, 3 - 1.5 ms in post-heating phase (PLH)

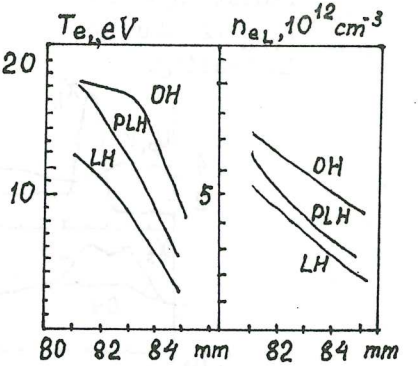

Fig.2 Electron temperature T_{eL} and electron density n_{eL} profiles in the limiter shadow region (80÷85mm).

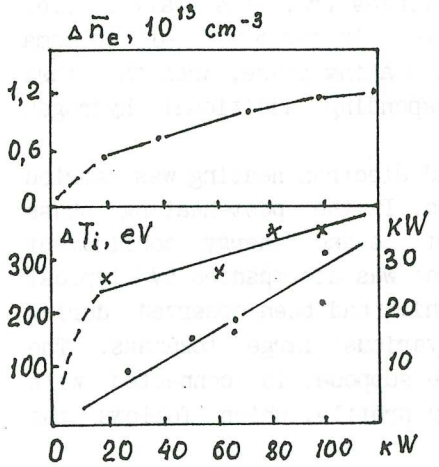

Fig.3 The increase of plasma density Δn_e, ion temperature ΔT_i (•) and radiation losses P_{rad} (x) during LH heating.

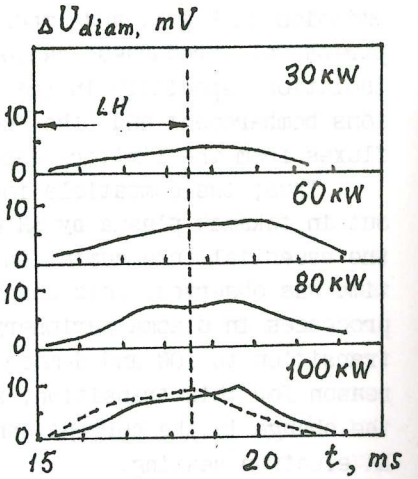

Fig.4 The diamagnetic signal in LH experiment for different P_{LH}. Dotted lines is the case without improved confinement.

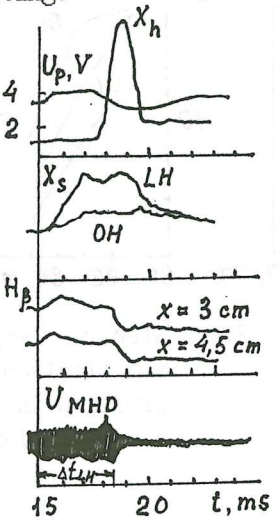

Fig.5 Loop voltage V_p, MHD activity V_{MHD}, soft X_s and hard V_h X-ray emission, H_β chord emission in LH experiment.

TRANSPORT STUDIES IN OHMIC H-MODE BEFORE AND AFTER BORONIZATION IN TUMAN-3

L.G.Askinazi, V.E.Golant, A.I.Kanaev*, V.A.Kornev, S.V.Lebedev, L.S.Levin, S.V.Mirnov**, K.A.Podushnikova, G.T.Razdobarin, V.V.Rozhdestvensky, A.I.Smirnov, A.S.Tukachinsky, V.M.Sharapov*, A.P.Zakharov*, S.P.Jaroshevich

A.F.Ioffe Phys.-Techn. Institute, Russian Academy of Sciences 194021, St.Petersburg, Russia
* Inst. of Phys. Chemistry, Russian Academy of Sciences, Moscow
** TRINITI, Troitsk, Moscow region

Transport analysis in Ohmic H-mode before boronization

In ordinary ohmic regime transition into improved confinement mode was found [1]. This Ohmic H-mode has typical signatures of the H-mode in bigger devices with powerful auxiliary heating: increase of the energy and particle content, suppression of the density fluctuations near the edge, drop of the D_α radiation. Transport analysis were performed for the regime with following plasma parameters: I_p = 0.115 MA, q^{cyl} = 2.45, $\bar{n}$ = (2-3.5) $10^{19} m^{-3}$. T_{e0} = 0.4-0.6 keV. $T_{i0} \simeq$ 0.12 keV.

Integration of the 1-D particle balance equation taking into account experimental density profile evolution showed that: (1) in the outer region (r=0.9a) D_e^{eff} drops by a factor of 7 after transition into H-mode, fig.1; (2) in the core region anomalous inward flux exceeds outward diffusion [2]. Steep gradient formation and boundary diffusion suppression are in agreement with a results obtained on ASDEX [3], DIII-D [4]. Decisive role of the convection was found also in [5].

Electron temperature profile evolution in the bulk plasma was measured by Thomson scattering technique. Edge T_e behavior was chosen to fit loop voltage derived from reducing of diffusion equation for poloidal field and measured U_p. This procedure gave also heat source radial distribution assuming neoclassical conductivity, Z_{eff} = 2.0 and validity of the Kadomtsev model [6] for internal disruptions. Effective thermaldiffusivity coefficient was obtained under the following assumptions: heat source distributed as j^2/σ, energy transfer from electrons to ions - collisional, radiative losses are negligible. In Fig.2 the temporal evolution of the χ_e^{eff} at r =

0.65a = 0.15m is shown. Observed sharp drop of χ_e^{eff} evidences suppression of the heat transport in the entire part of the plasma [2]. Taking into account convection term 5/2 $T_e\Gamma_n$ we found that improvement in the bulk energy confinement after transition is mainly due to the changes in thermal convection.

Boronization procedure and plasma performance after boronization

Boronization were performed using Helium Glow with Carborane ($C_2B_{10}H_{12}$) admixture [7] (partial pressure of Carborane is 5-30 %). In order to produce more uniform coating the vapor sources were placed in two toroidal positions. Solid Carborane begins to evaporate being heated up to 350-370 deg(K). During process metallic walls were baked up to 450 deg(K). Duration of the boronization procedure was 2 hours. After May 1992 procedure was repeated 3 times.

Best plasma performance was observed during two weeks after each boronization (200-300 shots). Then effect gradually decreased but didn't disappear after 3-4 months of operation. As a result of the boronization Oxygen and Carbon concentrations reduced by a factor of 4-8 and 2-3 respectively. Drop in the SXR intensity was about 10 times. Reduction of the impurity content allowed to reach higher densities in the boronized vessel. Fig.3 shows Hugill diagram for Tuman-3. Here open circles present ordinary ohmic regime and filled circles - Ohmic H-mode before boronization. Stars correspond to the Ohmic H-mode after boronization. In the last case highest density exceeds Greenwald limit ($2.7I_p/a^2$), Hugill parameter $q^{cyl}\bar{n}R/B_T$ ($10^{19}m^{-3}$,m,T) reaches 17.

Plasma resistance became by a factor of 1.5-2.0 less than before boronization. Resistance decrease couldn't be explained by Z_{eff} drop only. Taking into account bootstrap current we found reasonable agreement between measured and calculated resistance. Fraction of the I_{bs} is 17-20% I_p in Ohmic H-mode. We should mention that in spite of reduction of the input ohmic power after boronization electron temperature didn't change significantly. There was no noticeable difference between T_e profiles during Ohmic H-mode fig.4a and only small decrease in central T_e was observed in ordinary ohmic regime fig.4b.

Corresponding loop voltages for the shots with plasma current 0.115 MA are shown in fig.5. Data presented on figs.4&5 indicate enhancement of the confinement properties as a result of boronization. Energy confinement time as function of density is given on fig.6. Note that after wall coating τ_E became by a factor of 1.5-2.0 longer than before. Similar effect was observed in VH-mode on DIII-D [9]. τ_E values 13-15 ms exceed linear fit for ordinary ohmic confinement by a factor of 3-4 and Neo-Alcator scaling prediction by a factor of 4-6.

REFERENCES

1. T.Yu.Akatova, et al, Proc. XIII IAEA Conf. on Plasma Phys. and Contr. Nucl. Fusion Res., (Washington, 1990), v.1, p.509.
2. M.V.Andrejko, et al, Proc. XIV IAEA Conf. on Plasma Phys. and Contr. Nucl. Fusion Res., (Wurzburg, 1992), # CN-56/A-7-11.
3. F.W.Wagner, et al, Phys. Rev. Lett., 53 (1984), 1453.
4. K.H.Burrell, et al, Proc. XIII IAEA Conf. on Plasma Phys. and Contr. Nucl. Fusion Res., (Washington, 1990), v.1, p.123.
5. T.K.Kurki-Suonio, et al, Nuclear Fusion, v.32 (1992), p.133.
6. B.B.Kadomtsev, "Fizika plasmy" (in russ.), v.1 (1975), p.710.
7. E.A.Azizov, et al, Proc. 198th Eur. Conf. on Contr. Fusion and Plasma Physics, Innsbruck, 1992, V. 16C, part 1, p. 47.
8. "ITER Physics Design Guidelines: 1989", IAEA, Vienna, 1990.
9. G.L.Jackson, et al, Phys. Rev. Lett., 67 (1991), 3098.

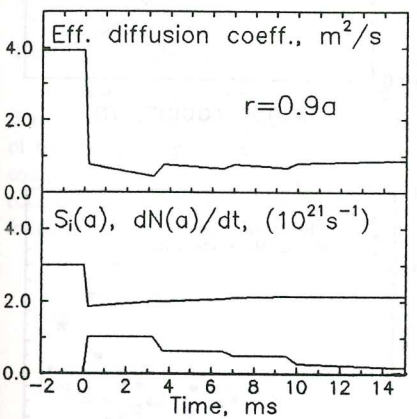

Fig.1 Evolutions of the effect. diffusion coefficient, ioniz. source and derivative of the number of particles through Ohmic H-mode.

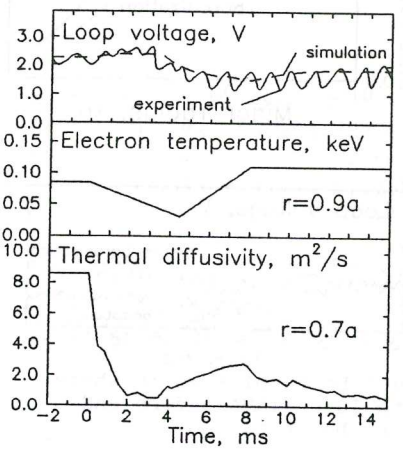

Fig.2 Evolutions of the simulated and measured loop voltages, boundary temperature and eff. thermaldiffusivity in Ohmic H-mode.

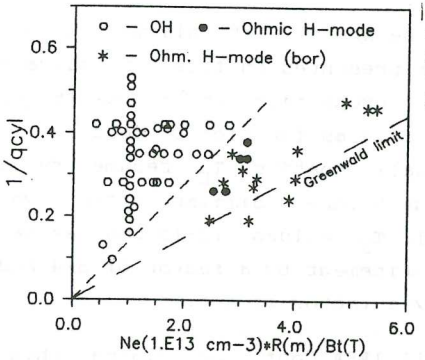

Fig.3 Hugill diagram for TUMAN-3 open circles – ordinary ohmic regime, filled circles and stars – Ohmic H-mode before and after boronization.

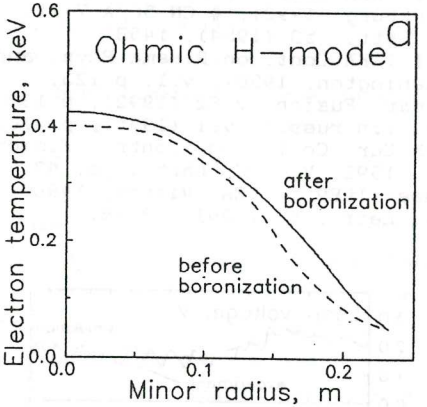

Fig.4 Electron temperature profiles in 0.115 MA Ohmic H-mode – a and ordinary ohmic regime – b.

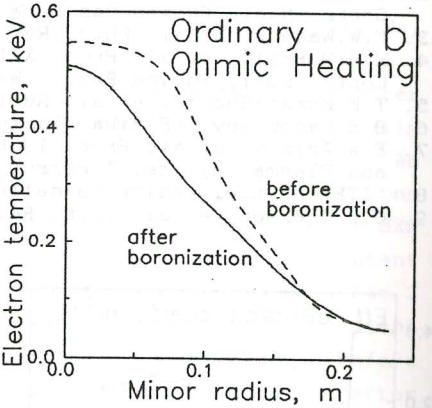

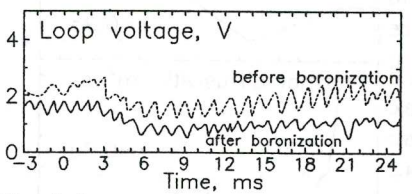

Fig.5 Loop voltages in shots with Ip=0.115MA before and after boronization.

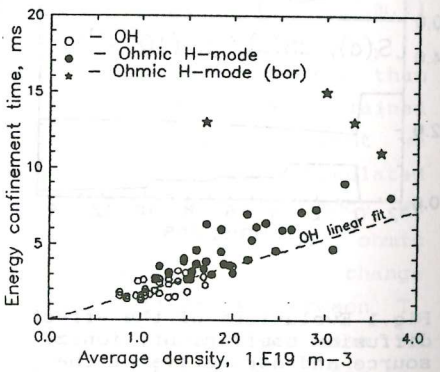

Fig.6 Energy confinement time vs. average density for different regimes.

RECENT RESULTS FROM THE ROTAMAK PROJECT

N. Donaldson, P. Euripides, I.R. Jones and S. Xu

School of Physical Sciences, Flinders University
G.P.O. Box 2100, Adelaide 5001, AUSTRALIA

The Rotamak

The Rotamak is a very simple magnetic configuration: it is a small aspect ratio, toroidal plasma current ring kept in horizontal and vertical equilibrium by a 'vertical' (tokamak terminology) magnetic field, in other words, a toroidal z-pinch. The unique feature that distinguishes it from other configurations is the fact that the toroidal current is driven in a steady, non-inductive manner by means of the application of a rotating magnetic field (RMF). By now, the possibility of using an RMF to drive steady plasma currents has been amply demonstrated and a straight forward description of the technique and its application in the Rotamak can be found, for example, in the review papers by Jones /1/ and the references contained therein. A description of the various components of a typical Rotamak device can also be found in these papers.

During the past 2-3 years Rotamak experiments have been undertaken using RF generators which are capable of operating at power levels of up to ten times those of previously available generators /2/. The purpose of this paper is to present some of the latest results obtained in high-powered experiments made with 10-litre and 50-litre spherical discharge vessels.

The 10-litre Rotamak Results

The toroidal plasma current, I_ϕ, which is ostensibly driven by the applied RMF produces a steady poloidal magnetic field; the *total* steady poloidal magnetic field is the sum of this component and the pre-determined vertical field. The radial variation of the z-component of the total poloidal field (B_z) in the equatorial ($z = 0$) plane (with the RMF rotating in planes of constant z) is shown in Fig. 1 (a) for two discharges having the following parameters:

	Case (i)	Case (ii)
Filling pressure of H_2 (mTorr)	8	8
Pre-determined vertical field, B_V (Gauss)	38.5	88.8
I_ϕ (amps)	2070	5590

In cylindrical coordinates, the toroidal current density is given by:

$$j_\phi = -\frac{1}{\mu_0}\frac{\partial B_z}{\partial r} + \frac{1}{\mu_0}\frac{\partial B_r}{\partial z}$$

An examination of the Solov'ev solution /3/ of the Grad-Shafranov equation for a spherical separatrix configuration shows that the $\partial B_r/\partial z$ term contributes only 20% to the total value of j_ϕ. We take advantage of this fact and obtain an acceptable estimate of j_ϕ by using the simplified version:

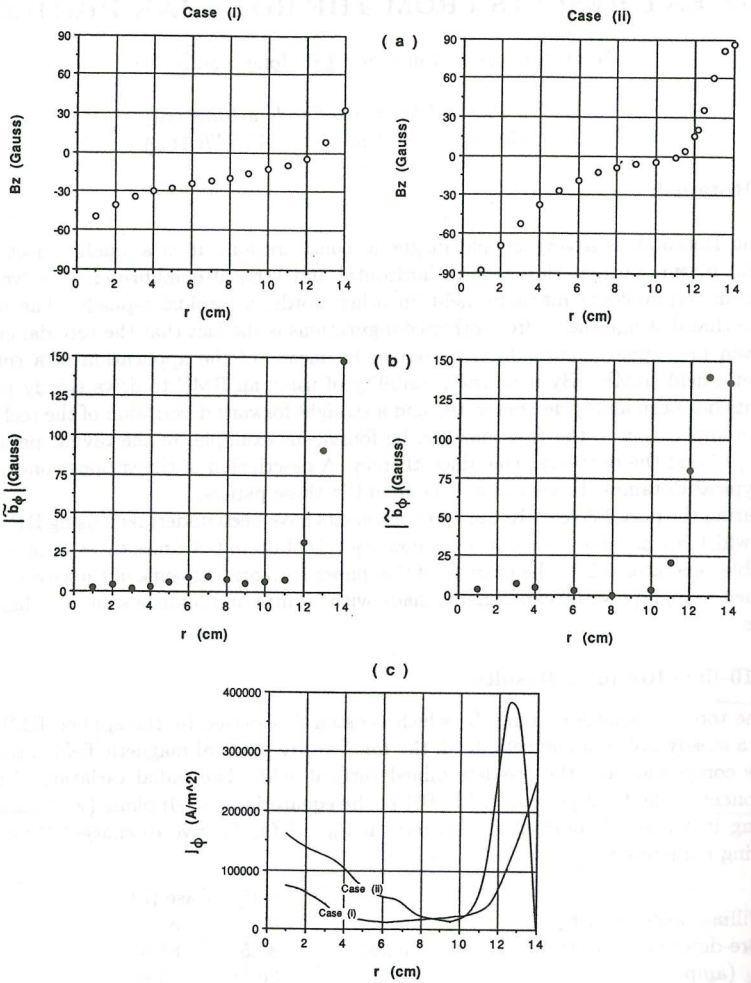

Fig. 1

$$j_\phi = -\frac{1}{\mu_0}\frac{\partial B_z}{\partial r}$$

The radial profiles of j_ϕ obtained in this manner for the two cases are shown in Fig. 1 (c). These graphs show that a major toroidal shell of current exists in the vicinity of the

discharge vessel wall. More interestingly, however, they show that a second toroidal belt of current is driven, in the same direction, in the interior region of the discharge, that is, in the region $r \leq 8$ cm. As the value of B_V and, hence, the total current I_ϕ is increased, the amount of current driven in this interior region also increases.

The measured radial variation of the amplitude of the toroidal component of the RMF, $| \tilde{b}_\phi |$, are shown in Fig. 1 (b) for the two cases under consideration. These show that the penetration of the RMF into the plasma is poor and, in particular, we note that $| \tilde{b}_\phi |$ is very small for $r \leq 10$ cm. This begs the question: What drives the toroidal plasma current in the interior region of the discharge if

- there is no steady induced toroidal electric field present in the Rotamak discharge,
- the RMF is small and the $< \tilde{j} \times \tilde{b} >$ current drive mechanism cannot be operative in that region?

A theoretical investigation by Auerbach and Condit /4/ sheds light on this question. They considered a Solov'ev compact torus equilibrium in which the emf necessary to drive the toroidal plasma current was supplied completely by the diffusion of the plasma across the steady poloidal field. We have repeated their calculations and in Fig. 2 (which complements Fig. 2 of the Auerbach and Condit paper) we show the flow lines of the diffusing plasma in the interior region which is of interest in the present context. Our interpretation of the experimental results is that the outer toroidal current ring is primarily driven by the applied RMF whilst the inner current ring is driven by the dynamo action of plasma transport across the poloidal magnetic field i.e. by the $\mathbf{v} \times \mathbf{B}_{\text{poloidal}}$ term in Ohm's law. We conclude that a substantial fraction of the driven toroidal current in high-powered Rotamak discharges is bootstrap current of this type.

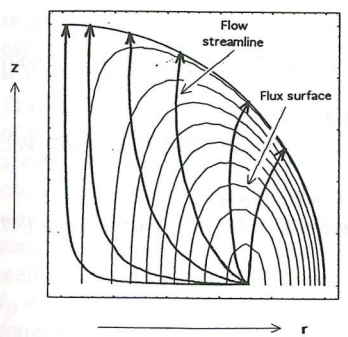

Fig. 2

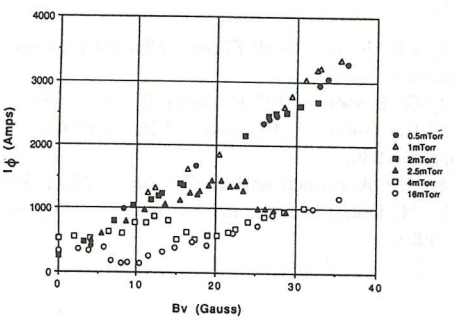

Fig. 3

The 50-litre Rotamak Results

Measurements made with the 10-litre discharge vessel showed that the total toroidal plasma current, I_ϕ, was primarily determined by the amplitude of the vertical field B_V and that I_ϕ varied linearly with B_V (see, for example, Donaldson *et al.* /5/).

For a spherical, axisymmetric, compact torus equilibrium, the Solov'ev solution predicts a linear relationship between I_ϕ and B_V, namely,:

$$\frac{I_\phi}{B_V} = \frac{5R}{\mu_0}, \tag{1}$$

where R is the radius of the spherical separatrix. This relationship was found to describe well the results obtained in the 10-litre experiment ($R = 0.14$ m).

Fig. 3 shows the (I_ϕ, B_V) measurements obtained in the 50-litre vessel experiment for a variety of filling pressures of hydrogen. The experimental points fall on two straight lines with a transition from one line to the other occurring for the higher filling pressures. Magnetic probe measurements showed that points corresponding to reversed compact torus configurations fell on the upper line while points on the lower line were associated with non-reversed (i.e. mirror) magnetic configurations.

The slope of the upper straight line is 91 amps/gauss. Substituting $R = 0.24$ m into the Solov'ev relationships yields

$$\frac{I_\phi}{B_V} = 95 \text{ amps/gauss}$$

which, again, is close to the observed value. This agreement does not necessarily imply that the observed compact torus equilibria are of the Solov'ev type; it is more likely the case that the relationship between I_ϕ, B_V and R encapsulated in equation (1) is relatively insensitive to the functional dependence of the pressure upon the flux function. For the moment, we consider equation (1) to be a convenient empirical recipe which relates I_ϕ, B_V and R.

/1/ I.R. Jones, *Small Plasma Physics Experiments II* (World Scientific, Singapore, 1990) pages 3-51.
/2/ G. Besson and G.R. Cottrell, Meas. Sci. Technol **2**, 581 (1991).
/3/ L.S. Solov'ev, *Reviews of Plasma Physics* (Consultants Bureau, New York, 1976) Vol. 6, page 239.
/4/ S.P. Auerbach and W.C. Condit, Nucl. Fusion **21**, 927 (1981).
/5/ N. Donaldson *et al. Europhysics Conference Abstracts* Vol. 16C, Part I, page 647 (1992).

STUDY OF PLASMA TURBULENCE IN THE T-10 AND TUMAN-3 TOKAMAKS BY REFLECTOMETER WITH CROSS-DETECTION.

V.V.Bulanin, D.O.Korneev, V.V.Dreval*

St.Petersburg Technical University, 195251, St.Petersburg, Russia
*Russian Sci. Center "Kurchatov Institute", 123182, Moscow, Russia

INTRODUCTION

During the last years phase reflectometry has been used on tokamak plasma experiments in an effort to measure both density profiles and fluctuation levels. In some of these experiments the phase ramping inconsistent with the cut off layer actual position was happened under the high level fluctuation conditions [1] - [3] This anomalously large phase changing named "phase run away" was just observed while using the quadrature (cross-detection) reflectometers [2], [3], where no one apparatus distortions could induce the phase runaway. Now there is a view that this event is a result of Doppler frequency shift associated with the poloidal rotation of the grating-like cut off layer surface [3]. In this work study of the phase runaway effect started previously in Tuman-3 with cross-detection reflectometer [3] was continued in T-10 tokamak experiments. Thus it became possible to compare the data obtained in two different installations. The alternative approach was developed in Tuman-3 while using the tangential microwave probing in a course of L-H transition when the phase runaway could be directly connected with the poloidal rotation of the plasma density waves.

MEASUREMENTS IN T-10 TOKAMAK

The experiments in the T-10 tokamak were performed with the O-mode cross-detection reflectometer. The similar single-antenna reflectometer has been used in the Tuman-3 and described in detail elsewhere [3]. The diagnostic layout is shown in Fig.1. The antenna of the 40*26 mm^2 aperture was used to probe the plasma along the minor radius by microwave at two fixed frequencies 18 and 24,3 GHz. The measurements were carried out during the electron cyclotron current drive experiments (I_p = 200-300 kA, B_t = 2.5 T). The time dependencies of the plasma current (I) and the ECR diagnostic signal (T) are shown in Fig.2 and Fig.3. Using sine and cosine signals the amplitude and phase of the reflected signal were computed separately. Some features of amplitude and phase spectra were similar to those of the Tuman-3. Namely the amplitude spectra were observed to be broader than the phase ones. The typical phase spectrum frequency band was about 5-10 KHz, as compared to the amplitude one of 100-300 KHz. The phase runaway effect which was found in the Tuman-3 was observed in the T-10 tokamak as well (see Fig.2 and Fig.3). The most value of the run away rate attributed to Doppler shift $f_p = 1/2\pi\, d\phi/dt$ is nearly 5-6 KHz as it seen from Figs.2 and 3. The incident frequency transition from 18 to 24.3 GHz was accompanied by larger phase run away. Note that minor radius dimension in phase units is 60π only. The phase run away rate and sign were happened to be connected with the discharge condition variation such as the current transition to the plateau phase (see Fig.3) or electron temperature uprise after gyrotron switching on (Fig.2). In some discharges the phase runaway rate seems to be dependent

on the cut off layer position. The cut off displacement to the last close flux surface (LCFS) with the plasma density growth causes the run away slowing down.

Both the T-10 and Tuman-3 experiments were arranged with the incident microwave beam directed nearly transversely to the LCFS. In this condition the phase runaway phenomena may be induced essentially by two reasons. The poloidal rotation of the grating- like cut off layer surface may produce the Doppler shift f_d provided the grating groove is asymmetrical [3]. The frequency f_d may be estimated as $f_d \simeq 2V_\theta \varphi / \lambda_o$ (here φ is blaze angle, V_θ is the velocity of plasma grating poloidal rotation, λ_o is the incident wave length in reflecting region). Another reason is connected with the possible deviation of the antenna axis from the normal direction [4]. This deviation may be caused by the magnetic surface small displacement. As is shown qualitatively in [4] in such a case the Doppler shift could be explained in the term of the first order diffraction on the plasma grating and f_d is determined by the formula written above (φ-diffraction angle). One can see that in both cases the phase run away contains the information on the poloidal rotation pattern in tokamak.

REFLECTOMETRY EXPERIMENTS IN TUMAN-3 WITH TANGENTIAL PROBING

The diagnostic schematic diagram of the Tuman-3 experiment is shown in Fig.1. Two antenna horns were used to transmit the O-mode microwaves under the angle of 50 with respect to the LCFS and to receive the reflected signals. In this condition accounting for the wave refraction process the back scattering grazing geometry approximation is valid and the Doppler frequency shift for large diffraction angel ($\varphi \simeq \pi/2$) is to be written as follows $f_d \simeq 2V_\theta / \lambda_o$. Two similar quadrature reflectometers have been used in Tuman-3 for simultaneous measurements of signals reflected back from the high and low magnetic field side regions.

The temporal development of the phase for the different incident frequencies are shown in Fig.4. The moment of the transition to ohmic H-mode induced by gas puffing is marked by arrow. Before the L-H transition the sign of phase runaway was consequent of the plasma grating rotation in the ion diamagnetic drift direction for both the inside and outside probing. Just after the L-H transition one readily observes the drastically change of the phase temporal variation in outside region (see Fig.4b). This effect could be accounted for the strong shear of the plasma wave rotation. This particular rotation pattern is in accordance with the scrape off layer plasma rotation pattern measured recently in the JFT-2M tokamak [5]. The actual shear radial position in the Tuman-3 may be determined after the ray tracing simulation which are going to be done. As for the inside probing the phase runaway shows the different rotation behavior which depends on discharge scenario (see Fig.4a and Fig.6). The phase run away sometimes was observed to remain constant (see Fig.4a) or to ramp in the L-H discharges (Fig.6). These variations however are less pronounced compared to the outside probing. This distinction may be connected with the difference of the radial position of the microwave reflection region. In other hand it could be referred to the actual poloidal asymmetries of the rotation pattern (see for example [6]).

The distinction between the amplitude oscillations was observed as well. Fig.5 shows the time dependence of the RMS amplitude averaged over frequency band above

200 KHz. Here the upper trace corresponds the inside probing. The amplitude suppression of the low magnetic field side after the L-H transition is well known [3]. The observed oscillation uprise with the inside probing demands more detail investigations. It may be for the displacement the reflecting region towards the antenna after the L-H transition.

REFERENCE

[1] A.C.C.Sips, Rijnhuizen Report 91-200 (1991).
[2] G.R.Hanson, Doctoral Thesis, Georgia Inst. of Techn., (1991)
[3] V.O.Aleksandrov et al.,19th Eur. Conf., Insbruck.1992,V1,p.111
[4] J.H.Irby and P.Stok, Rev. Sci. Inst., V61 (1990), 3052
[5] K.Ida et al., Phys. Fl.,V B4 (1992), 2552
[6] G.R. Tynan et al., Phys. Rev. Lett., V68 (1992), 3032

FIGURE CAPTIONS

Fig.1 Reflectometry diagnostic layout. ANT-antenna.
Fig.2 Time evolutions of plasma current (I), ECR diagnostic signal (T) and phase (Ph) in T-10 experiment F=18 GHz.
Fig.3 Temporal dependences of I, T and phase, F=24.3 GHz.
Fig.4 Phase run away in Tuman-3 a) inside probing, b) outside one.
Fig.5 Temporal dependences of RMS amplitudes.
Fig.6 Phase run away at inside probing (another series of shots).

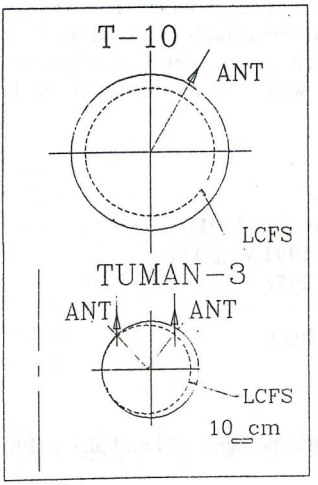

Fig. 1

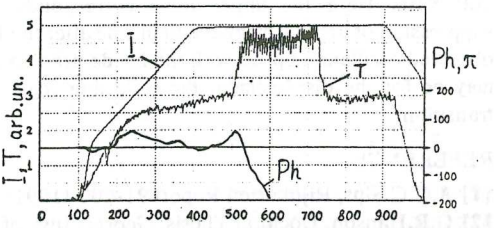

Fig. 2

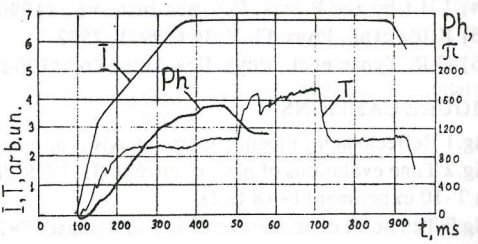

Fig. 3

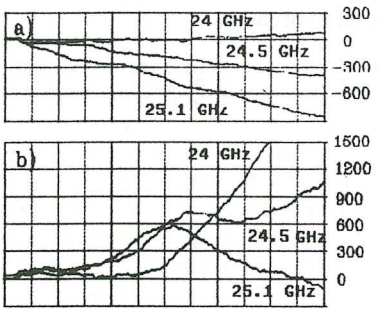

Fig. 4

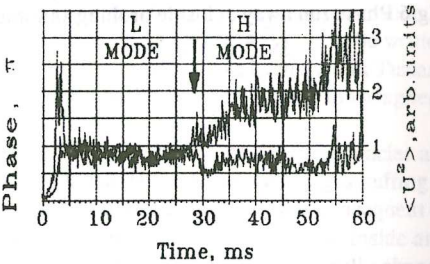

Fig.5

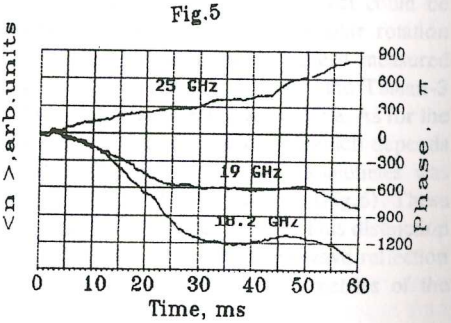

Fig. 6

X-Ray Vision Technique for Proton and Alpha-Particle Diagnostics

V.G.Kiptilyj,
Ioffe Physico-Technical Institute, 194021 S.Petersburg, Russia

Escaping proton and alpha-particle diagnostics based on the particle induced X-ray detection is proposed.

A diagnostic device, which mounted near the edge of the tokamak plasma, consist of a radiation shielded camera, inner target and a pipe to transfer the X-ray image. Unconfined particles penetrate into the camera through an entrance apertures closed by thin foil and interact with low-Z target atoms. Several kinds of the target (single element, complex, multi-layer) can be used for different diagnostic purposes.

The yield of X-rays produced by α-particle bombardment of thin target is

$$Y_x = F_\alpha * (N_A * \rho / A) * L * \sigma_I(E_\alpha) * \omega_K ,$$

F_α - the α-particle flux on the target, ($\alpha/cm^2 s$);
$N_A * \rho / A$ - the density of target atoms, ($atoms/cm^3$);
L - the thickness of target, (cm);
σ_I - the ionization cross-section, (cm^2);
ω_K - the fluorescence yield.

In the case of 1μm Mg target and E_α= 3.5 MeV the energetic losses of α-particles will be equal to ~ 130 keV and thin target approximation will be valid. Then

$$\sigma_I = 1.2\ 10^{-19}\ cm^2 ,$$
$$\omega_K = 0.0265 ,$$
$$E_{K\alpha} = 1.25\ keV .$$

If we suppose that

$$F_\alpha \sim 10^{11}\ \alpha/cm^2 s$$

then

$$Y_x \sim 1.3\ 10^9\ x/cm^2 s .$$

In the case of 1μm Si target :

$$\sigma_I = 4.34\ 10^{-21}\ cm^2\ ,$$
$$\omega_K = 0.047\ ,$$
$$E_{K\alpha} = 1.739\ keV$$

and

$$Y_x \sim 10^8\ x/cm^2 s\ .$$

As can see targets with lower Z may be used, too. The detector counting rate is

$$P_x = Y_x * S_t * (S_D/4\pi * R^2) * T_x * \varepsilon\ ,\ cps,$$

S_t, S_D - the square of target and detector (or mirror);
R - the target-detector distance;
T_x - the X-ray transmission;
ε the detector efficiency.

One can see that

$$S_t * (S_D/4\pi * R^2) * T_x * \varepsilon \sim 10^{-4} - 10^{-3}\ cm^2$$

is needed for time resolution of the diagnostics.

According to X-ray emission rate calculation the thin target yield of the Mg K_α-rays induced by 3.5-MeV alpha particles is 10^{-2} X-rays per particle. The yield factor is more higher in the case of protons. If escaping alpha-particle flux is more than $10^{11} cm^{-2} * s^{-1}$ and apertures of the order of 1 cm^2, the X-ray intensity would then be > $10^9\ s^{-1}$.

In general, the estimates indicate that this technique can be utilized. As to the X-ray detector system the research and development are needed to demonstrate feasibility of the diagnostics at high neutron and gamma-ray background.

For the calculation the following data have been used :
G.G.Johnson,Jr.,E.M.White. ASTM Data Series DS 46 (1970).
C.H.Rutledge,R.L.Watson. At.Data & Nucl.Data 12, 195(1973)
R.Woldseth,"X-Ray Energy Spectrometry" (Kevex Corp., Burlingame, California, 1973)

AUTHOR INDEX